

STUDY OF CEMENTITIOUS MATERIALS USING TRANSMISSION ELECTRON MICROSCOPY

THÈSE N^o 3759 (2007)

PRÉSENTÉE LE 23 MARS 2007

À LA FACULTÉ DES SCIENCES ET TECHNIQUES DE L'INGÉNIEUR
Laboratoire des matériaux de construction
SECTION DE SCIENCE ET GÉNIE DES MATÉRIAUX

ÉCOLE POLYTECHNIQUE FÉDÉRALE DE LAUSANNE

POUR L'OBTENTION DU GRADE DE DOCTEUR ÈS SCIENCES

PAR

Prakash Chandra MATHUR

B. Tech. in Civil Engineering, Indian Institute of Technology Delhi, Inde
et de nationalité indienne

acceptée sur proposition du jury:

Prof. H. J. Mathieu, président du jury
Prof. K. Scrivener, directrice de thèse
Dr B. Lothenbach, rapporteur
Prof. D. E. Macphee, rapporteur
Prof. P. Stadelmann, rapporteur



ÉCOLE POLYTECHNIQUE
FÉDÉRALE DE LAUSANNE

Lausanne, EPFL

2007

*To,
My Father–Mother and Sister
without whom nothing would have been possible*

Acknowledgments

I take this opportunity to present my regards and gratitude to Professor K.L. Scrivener for giving me the opportunity to pursue this doctorate, for her patient guidance, generously providing me with the salary for the past one year, and for her deft remarks on the pre-final drafts of this thesis which considerably helped the presented work in achieving its final form.

My sincerest respects and gratitude to Professor P.A. Stadelmann for *all* his teachings, encouragement and advice which together helped me to propel forward and gave me strength to not give up on several difficult occasions. Indeed, it has been a memorable privilege and honour to be his student these last five years.

I am indebted to Ms. D. Laub for her guidance in the TEM specimen preparation process and for her patience in answering my never ending questions. Without her presence, it might not have been possible to learn this method, which has been the backbone of my thesis.

Very many special thanks to Dr. E. Gallucci for his honest encouragement and the numerous important discussions I had with him regarding my work.

Special thanks to Shashank and Cyrill for their help in computer related challenges and to Shashank, Julien, Patrick, Rodrigo and Xingyu for their useful remarks on the thesis presentation; big thanks to Patrick and Julien for correcting (rewriting) the abstract in French.

I am grateful to Professors D.E. Macphee, P.A. Stadelmann, H.J. Mathieu, K.L. Scrivener and Dr. B. Lothenbach for presiding over the thesis defence and their essential feedback.

I wish to acknowledge the time and efforts of: Dr. S. Gradečak for introducing me to the practicalities of TEM; Drs. T. Füllman and G. LeSaoût for their assistance in X-ray diffraction; Dr. M. Cantoni for his kind help with the CM300 TEM and INCA; Ms. F. Bobard for preparing the TEM specimens using FIB and the Swiss National Foundation for funding this project.

Abstract

An important mode of hydration of Ordinary Portland cement (OPC) is via the formation of a shell of hydration products around cement grains. It has been shown so far that shells form not only in OPC but also around C_3A grains in a mixture of alite, C_3A and $C\bar{S}$ and in more restricted form in pure alite. The shells are believed to be hollow and limited information of the chemistry of the phases that constitute the shells is known so far. From the work done in this thesis some crucial knowledge has been gained on this subject. It is shown that shells are not empty but filled with C-S-H which appears to have a lower density than the rest of the hydration products. At early ages, in all observed instances shells are seen to form only around polyphase grains. Further, the shells form only around the silicate part of the grain at all observed ages. The cement grains are seen to have uneven reactivity and the hydration seems to follow a reaction front, leaving striations $\sim 1 \mu\text{m}$ on the grains. The Ca:Si ratio of all the C-S-H in the matrix is almost the same (about 2) for all ages.

The work done on novel mix binders involving OPC with minor additions of CAC and $C\bar{S}$ shows that the chemistry of the hydration products remain almost the same with these additions. The amount of expansion in the mixes depends on the added sulfate content, however, the effects of the time of demoulding of the mixes on the expansion are more drastic. This leaves many open questions concerning the phenomenon of expansion in cements.

In expanded heat cured Portland cement pastes, fine ettringite needles are seen to grow from an adjacent monosulfate plate. The work seems to confirm the theory of crystallization pressures and their destructive nature.

Keywords: OPC, Early age hydration, Mixed binders, DEF, TEM

Version abrégée

Un mode important concernant l'hydratation des Ciments Portland Ordinaire (OPC) est celui de la formation d'une coquille par les produits d'hydratation autour des grains de ciment. Il a été montré jusqu'à présent que ces coquilles ne se formaient pas exclusivement dans les systèmes OPC, mais également autour des grains de C_3A dans un mélange d'alite, C_3A et $C\bar{S}$ et dans une moindre mesure dans l'alite pure. Il était admis que ces coquilles étaient vides et seules quelques informations restreintes étaient connues quant à la composition chimique des phases qui les composaient. Il a été montré durant cette thèse, que ces coquilles ne sont pas vides mais remplies de C-S-H possédant apparemment une densité plus faible que le reste des produits. Dans tous les cas étudiés à jeune âge, les coquilles semblent se former uniquement autour des grains polyphasés. De plus, ces coquilles ne se forment qu'autour de la partie siliceuse des grains de ciment à tous les âges étudiés. Il a été observé que la réactivité des grains de ciment s'avère préférentielle et l'hydratation laisse des stries $\sim 1 \mu\text{m}$ sur les grains.

Les études faites sur mélange ternaire, comprenant un OPC en présence d'adjonction mineures de CAC et de $C\bar{S}$, ont montré que la composition chimique des produits d'hydratation restent essentiellement la même en présence de ces additions. Même si l'expansion dans ces mélanges dépend de la teneur en sulfate ajoutée, les effets liés au temps de démoulage sont plus drastiques, laissant dès lors l'explication de ce phénomène ouverte.

Lors de cures à haute température de pâte de ciment Portland, la croissance de fines aiguilles d'ettringite à partir de plaquettes de monosulfate adjacentes a pu être observée. Ces travaux semblent dès lors confirmer la théorie des pressions de cristallisation. *Mots-clés*: OPC, Hydratation à jeunes âges, mélanges ternaires, MET

Glossary

Abbreviations in cement chemistry

A	:	Al ₂ O ₃	C	:	CaO	\bar{C}	:	CO ₂
F	:	Fe ₂ O ₃	H	:	H ₂ O	K	:	K ₂ O
M	:	MgO	N	:	Na ₂ O	P	:	P ₂ O ₅
S	:	SiO ₂	\bar{S}	:	SO ₃	T	:	TiO ₂

ADF	Annular Dark Field (detector)
AFm	[{Ca ₂ (Al, Fe)(OH) ₆ · X · xH ₂ O}], where X denotes one formula unit of a singly charged anion, or half a formula unit of a doubly charged anion
AFt	[{Ca ₃ (Al, Fe)(OH) ₆ · 12H ₂ O} ₂ · X ₃ · xH ₂ O}], where X represents one formulae unit of a doubly charged, or, with reservations, two formulae unit of a singly charged anion
BF	Bright Field (image)
BSE	Backscattered Electron
CRT	Cathode Ray Tube
CAC	Calcium Aluminate Cement
C-S-H	Calcium Silicate Hydrate (poorly crystalline or amorphous of variable composition)
DEF	Delayed Ettringite Formation
DF	Dark Field (image)
DTA	Differential Thermal Analysis
EDS	Energy Dispersive Spectroscopy
EELS	Electron Energy Loss Spectroscopy
ESCA	Electron Spectroscopy for Chemical Analysis

Continued on next page

FEG	Field Emission Gun
FIB	Focussed Ion Beam
Fp	Flimsy product
HAADF	High Angle Annular Dark Field (detector)
Ip	Inner product
NMR	Nuclear Magnetic Resonance
OPC	Ordinary Portland cement
Op	Outer product
Q-phase	C_3A_2M , $C_{20}A_{13}M_3S_3$
RH	Relative Humidity
SEM	Scanning Electron Microscop(e,y)
SE	Secondary Electron
STEM	Scanning Transmission Electron Microscop(e,y)
TEM	Transmission Electron Microscop(e,y)
TG	Thermogravimetry
TMS	Trimethylsilylation
XRD	X-Ray Diffraction

Contents

Acknowledgments	i
Abstract	iii
Abstract (in French)	v
Glossary	vii
1 Introduction	1
2 Materials and characterization techniques	5
2.1 Materials used	6
2.2 Calorimetry	7
2.3 Rietveld X-ray diffraction	8
2.4 Electron microscopy	10
2.5 Terms used in imaging	10
2.5.1 Contrast and brightness	10
2.5.2 Image resolution	11
2.6 Interaction of electrons with matter	12

2.6.1	Various kinds of electron scattering	12
2.6.2	Interaction cross-section	14
2.7	Chemical analysis	15
2.7.1	Spatial resolution	17
2.8	SEM	18
2.8.1	Secondary electrons (SE)	19
2.8.2	Backscattered electrons (BSE)	19
2.8.3	Chemical analysis	20
2.9	Transmission Electron Microscope	20
2.9.1	Concept of contrast in TEM	21
2.9.2	Bright and dark field imaging	21
2.10	Scanning Transmission Electron Microscope	24
2.10.1	Z-contrast	26
2.11	Comparison between dark-field modes of TEM and STEM	27
2.12	Comparison of X-ray microanalysis among SEM, TEM and STEM	29
2.13	TEM specimen preparation techniques	30
2.13.1	Mechanical polishing	30
2.13.2	Focussed Ion Beam	31
3	Literature review of the hydration of Portland cement	35
3.1	Introduction	35
3.2	The anhydrous phases of cement	36
3.3	Calcium silicate hydrate (C-S-H)	37

3.3.1	Morphological classification	37
3.3.2	The atomic structure	39
3.3.3	Silicate polymerisation	41
3.3.4	Presence of aluminium	43
3.3.5	Sorption of sulfate ions	45
3.3.6	Chemical composition of C-S-H	45
3.3.7	Ca:Si ratio at early ages	46
3.4	AFt phases	47
3.4.1	Crystal structure	48
3.4.2	Solid state substitution of aluminium by iron	48
3.5	AFm phases	49
3.5.1	Crystal structure	49
3.5.2	Solid state substitution of aluminium by iron	50
3.6	Hydration of tricalcium silicate	50
3.7	Hydration of tricalcium aluminate in the presence of calcium sulfate	55
3.8	Hydration of the ferrite phase	56
3.9	Role of calcium sulfate at ambient temperature	57
3.10	Hydration of Ordinary Portland Cement (OPC)	58
3.11	Shell formation	59
3.12	Review of the work done on hydration of cement using TEM	63
3.12.1	Fine intermixing of hydration products	64
3.13	Key questions	65

4	Study of early OPC hydration by TEM	67
4.1	Introduction	67
4.2	Shell formation	67
4.2.1	Ca:Si ratio of C-S-H	74
4.2.2	Morphology of C-S-H	80
4.2.3	Specimen prepared using Focussed Ion Beam	88
4.3	Early hydration product	89
4.4	Growth of portlandite	97
4.5	Summary	97
4.6	Role of aluminates	99
4.6.1	Role of sulfates	99
4.7	Role of ferrites	105
4.8	Hydrated phases at nano-scale	110
5	Study of the microstructure and phenomenological study of expansion in OPC, CAC, C\bar{S} blends	111
5.1	Literature review of the development of the microstructure . .	111
5.1.1	Hydration of pure CAC cements	111
5.1.2	Mixture of OPC and CAC	112
5.1.3	CAC+C \bar{S}	113
5.1.4	Ternary blends	114
5.2	Introduction to the work done	114
5.3	Ternary mix M2	115
5.3.1	Ca:Si ratios	116

5.3.2	Role of aluminates	122
5.3.3	Role of ferrites	124
5.4	Expansion in ternary mixes	128
5.5	Literature review of the expansion in sulfoaluminate cements .	129
5.5.1	The crystal growth theory	129
5.5.2	The swelling theory	135
5.6	Work done	137
5.6.1	Mix design	137
5.6.2	Curing regimes	137
5.6.3	Experimental techniques	138
5.7	Results	140
5.7.1	Expansion and heat of hydration	140
5.7.2	XRD	148
5.7.3	SEM studies	151
5.8	Discussion	155
6	Heat induced internal sulfate attack (DEF)	157
6.1	Introduction	157
6.2	Literature review on delayed ettringite formation	158
6.3	Work done	160
6.3.1	Cement bar preparation	160
6.3.2	Curing regime	160
6.3.3	Expansion profiles	160
6.3.4	Observations using TEM	160

6.4	Discussion	165
7	Conclusions and future work	167
7.1	Ordinary Portland cement (at ambient temperature)	167
7.2	Blended cements involving OPC, CAC and $C\bar{S}$	169
7.2.1	Microstructural study	169
7.2.2	Phenomenon of expansion in ternary mixes	170
7.3	Expansion in heat-cured cement pastes (DEF)	170
7.4	Future work	171
A	Binary mixes of OPC, CAC and CAC, $C\bar{S}$	173
A.1	F15 (CAC: $C\bar{S}$)	173
A.2	B2 (CAC: $C\bar{S}$)	177
A.2.1	Discussion	179
B	Effect of specimen thickness on chemical analysis	181
B.1	Introduction	181
B.2	Work done	182
	Bibliography	184
	Index	207

List of Figures

2.1	Signals generated due to electron-matter interaction	13
2.2	Categorizing the electron scattering phenomenon	14
2.3	Energy-well of iron atom	16
2.4	Electron beam spreading while interacting with a specimen . .	18
2.5	Figure of an SEM	19
2.6	Ray diagram of image formation in a TEM	22
2.7	Dark and bright field image formation in a conventional TEM	24
2.8	Sketch of the operation of image formation in a Scanning TEM	25
2.9	Dark and bright field image formation in a scanning TEM . .	27
2.10	Dark field imaging in TEM and STEM	28
2.11	Charging of a cement sample in the Focussed Ion Beam	31
2.12	TEM specimen preparation using Focussed Ion Beam	33
3.1	Structure of Tobermorite	41
3.2	Structure of dreierketten	42
3.3	Structure of dreierketten with Al substitution	43
3.4	Crystal structure of ettringite.	48

3.5	Crystal structure of monosulfate.	49
3.6	Calorimetric curve of the hydration of C_3S	51
3.7	Microstructural development of a cement grain (few hours) . .	60
3.8	Hollow shells in alite pastes	62
4.1	OPC: shell formation around grains at various ages	69
4.2	Preferential reactivity of grains having shells	70
4.3	Shell formation in grains of different shapes and sizes	71
4.4	Beginning of shell formation (6 hours)	72
4.5	Shell formation around a polyphase grain (10 hours)	73
4.6	A sketch showing the formation of shell around a cement grain	74
4.7	Images showing that shells are not empty but filled with C-S-H	75
4.8	Shell formation, C-S-H and ridges on grains.	76
4.9	OPC 24 h: growth of ettringite	77
4.10	Final state of the shell (24 hours)	78
4.11	Ca:Si ratios of C-S-H in various regions of the microstructure .	81
4.12	Particulate morphology of C-S-H	82
4.13	OPC 24 hours: C-S-H within the shell	83
4.14	Foil-like morphology of shell	84
4.15	Morphology of shell and outer product	85
4.16	Morphology of outer product	86
4.17	Morphology of shell and C-S-H nearby	87
4.18	Specimen prepared using Focussed Ion Beam	89
4.19	Partial reaction of grains at 2 hours	91

4.20	Coating of variable thickness around cement grains (2 hours)	92
4.21	Hydration products deposited away from the grains at 2 hours	93
4.22	Ridges on grains and ettringite on silicate and interstitial phases	94
4.23	Gypsum adjacent and away from the shell (6 hours)	95
4.24	Growth of portlandite around the setting time of cement paste	96
4.25	OPC: Distribution of aluminium from 8–12 hours	100
4.26	OPC: Distribution of aluminium from 18–48 hours	101
4.27	S:Si ratio in various regions (OPC)	102
4.28	OPC: distribution of sulfates at 2 hours of hydration	103
4.29	Ettringite occasionally seen till 18 hours	104
4.30	Flurry of ettringite at 24 hours	104
4.31	OPC 24 hours: partially reacted C ₄ AF grain	106
4.32	OPC 48 h: formation of monosulfate	107
4.33	Phases at nano-scale	110
5.1	Ternary mix M2: heat of hydration along with expansion	115
5.2	Comparing the shell formation in OPC and M2.	117
5.3	M2, 16 hours: hydration product within the shell	118
5.4	The shell of hydrates in M2	119
5.5	M2, 16 hours, acicular shape C-S-H	120
5.6	M2, 16 h: C-S-H within the shell	121
5.7	Ca:Si ratios of C-S-H in M2	122
5.8	M2, 16 hours, distribution of aluminium	123
5.9	\bar{S} :Si ratios in M2	124

5.10	M2: Formation of ettringite	126
5.11	Al gel in M2 along with ettringite) and monosulfate.	127
5.12	Formulations of the studied binder systems	138
5.13	Expansion in ternary mixes as a function of added gypsum	140
5.14	High expansion in mixes with OPC as the major component	141
5.15	Composition of the ternary mixes for curing at 100% RH	142
5.16	Amount of expansion at 100% RH	142
5.17	Heat of hydration of expansive ternary mixes	143
5.18	Heat of hydration and expansion curves	143
5.19	Composition of the ternary mixes for curing under water.	145
5.20	Expansion curves of initial samples cured under water	146
5.21	Expansion curves of further samples cured under water	147
5.22	XRD patterns of ternary mixes cured under water	149
5.23	XRD patterns of ternary mixes cured under water (remaining)	150
5.24	Distribution of ettringite (by EDS) in the ternary mixes	152
5.25	Distribution of ettringite (SEM images) in the ternary mixes	153
5.26	Shell formation around OPC grains in expansive ternary mixes	154
6.1	DEF samples: heat curing regime	161
6.2	Expansion curve for the heat cured cement bars	161
6.3	DEF: abundant presence of monosulfate	162
6.4	DEF: High magnification images show fine ettringite	163
6.5	DEF: C ₄ AF grain with Ca, Al and Fe rich product around	164
6.6	DEF sample: ettringite seen in different shapes	164

A.1	Typical low-magnification image of F15 at 14 days	174
A.2	Comparing the morphologies of C-S-H in OPC and F15	176
A.3	TEM images of the binary mix (CAC, $\text{C}\bar{\text{S}}$) at 1 day	177
A.4	Monosulfate around calcium sulfate grain in B2 at 7 days	178
A.5	Alumina gel in CAC, $\text{C}\bar{\text{S}}$ mix	180
B.1	Effect on EDS analysis due to specimen thickness	182
B.2	Variation of Ca:Si ratios in pure alite with specimen thickness	183

List of Tables

2.1	Quantitative phase analysis of the OPC used	6
2.2	Chemical analysis of Secar 51 and Fondu	7
2.3	Mineralogical composition of Secar 51 and Fondu	7
3.1	Different types of C-S-H	38
3.2	Various types of C-S-H and their appearance under EM's . . .	39
4.1	Number of points to calculate Ca:Si ratios in OPC	79
4.2	OPC: solid-state substitution of iron in ettringite	108
4.3	OPC: solid-state substitution of iron in monosulfate	108
4.4	Number of points having iron and the Fe/Ca ratios in OPC . .	109
5.1	Composition of the ternary mix (M2) studied using TEM . . .	115
5.2	Number of points to calculate Ca:Si ratios in M2	118
5.3	Number of points having iron and the Fe/Ca ratios in M2 . .	125
5.4	Solid-state substitution of iron in ettringite (M2)	128
5.5	Solid-state substitution of iron in monosulfate (M2)	128

Chapter 1

Introduction

Concrete is known to be one of the most widely used material in the world, second only to water in terms of consumption. The present worldwide consumption of concrete is estimated to be of the order of 10 billion tonnes yearly [135].

Concrete is made of various components, viz., stones, aggregates and gravel. Although, all of these components have high physical strength, which is of paramount importance to concrete, none has the ability to bind them together. It is this critical need that is met by cement, in the presence of water, making it an invaluable component of concrete. Thus, to study and research a material as indispensable as cement seems fascinating and appropriate.

Considering the high consumption of cement, it is obvious that any engineering property, viz strength, durability, mass-transport properties, conductivity, etc, associated with it would be of immense importance and interest. Like for any other material, the mechanical and engineering properties associated with concrete at the macroscopic level are governed by the chemical phenomenon occurring at the micron and sub-micron level. It is this chemistry of cement during its early hydration that is the focus of this thesis.

Ordinary Portland cement or OPC is the most commonly used cement for

most commercial purposes. However, recently novel cementitious materials involving blends of OPC, calcium aluminate cement (CAC) and calcium sulfates (CS) have come into limelight and are proving to be of much commercial viability. Several key questions remain in the hydration of OPC and these novel mix binders, although latter are much more poorly understood than the former.

This thesis describes the hydration of OPC and mix binders during early ages. While in the case of OPC the focus of attention has been on the phenomenon of shell formation, the associated chemistry and the role played by aluminate and ferrite phases, the work done on mix binders is more to do with the phenomenon of expansion in these mixes at early ages. However, some results are presented to show the effects of minor additions of CAC and CS on OPC. The important aspect of the expansion in heat-cured mortars is also addressed.

Chapter 2 describes the various techniques used to characterize and understand the various phenomenons in these cementitious materials. Since Transmission Electron Microscopy (TEM) is the principal investigative technique used, the major part of the chapter is devoted to conceptually illustrate the principals involved in TEM.

Chapter 3 is a comprehensive illustration of the work done by various researchers in the field of early age hydration of cements and the phenomenon of shell formation. The chapter concludes with a list of key question that have been addressed in this study.

Chapter 4 is the main chapter of this thesis. It presents the results obtained in the hydration of Portland cement, with considerable efforts been made to further understand the phenomenon of shell formation. This involves studying the distribution of various phases and understanding the underlying chemistry involved. The shells are seen as thin compact sheets and are shown to be not empty, but filled with C-S-H. The Ca:Si ratio of all the C-S-H at all ages is about 2. There are ridges seen on the surface of cement grains, about $1\mu\text{m}$ deep by 1 day, believed to

be due to the uneven reaction of the surface with water. The various morphologies of C-S-H seen in different regions are also discussed.

Aluminium is observed to be well distributed in the matrix either in the form of clearly visible ettringite rods (confirmed by chemical analysis), or, in several instances, observed to be present on C-S-H. However for the latter it is not clear whether it is present as ettringite, finely intermixed with C-S-H or is absorbed in it along with sulfate. Ettringite is seen to be present both on silicate and interstitial phases showing that it forms via through-solution mechanism. The ferrites are seen to be least reactive. However iron is not totally absent, but present in limited amounts in the matrix. The solid-state substitution of aluminium by iron in ettringite and monosulfate phases is seen to commence at about 18 hours.

Sulfur is seen to be well distributed in the matrix. It is seen as ettringite and absorbed on C-S-H around silicate, interstitial phases and in the matrix at all ages. Until 18 hours, the maximum concentration of sulfur is seen to be on the shell, however at 24 hours it drops to a minimum on the shell. This is explained by the flurry of ettringite growth at 24 hours seen growing from the shell towards the grain. This indicates of the second burst of the hydration of aluminate phases and involves the consumption of sulfate absorbed on the shell.

A TEM specimen of Portland cement hydrated till 2 hours shows ettringite and calcium-siliceous products (most likely along with finely intermixed ettringite) around both silicate and interstitial phases. The coatings are relatively thicker on the silicate than on the interstitial phases.

Chapter 5 introduces the subject of mixed binders involving Portland cement, calcium aluminate cements and calcium sulfate. It presents the results of the study made on the microstructure of ternary blends involving OPC, CAC and $\bar{C}\bar{S}$ using TEM. It is seen that the Ca:Si ratios of C-S-H in the mix is only marginally higher than in pure OPC while the \bar{S} :Si ratios follow the same trend.

The other part of the chapter deals with the phenomenon of expansion in the ternary mixes. It begins by the literature review of the work done in the field of expansion in sulfoaluminate cements, involving the major theories of expansion. Then the results obtained are presented which show that when the samples are cured in 100% RH, the amount of expansion increases with an increase in added gypsum in the mix. However when cured under water the amount of expansion is seen to be much higher and dependent on the time of demoulding of the mix, irrespective of the amount of sulfur. Calorimetry results show that there is little link between the amount of expansion and the heat of hydration. XRD results also show the presence of ettringite before, at and after the main hydration peak. The amount of ettringite, estimated from the XRD patterns, is seen to increase with age along with the presence of hemihydrate in some compositions. The distribution of ettringite is revealed by SEM studies which show ettringite to be largely present around CAC grains. The results on the dependence of expansion on demoulding time apparently indicate towards the swelling of hydrates. This study leaves several open questions and reveals the complexity of the phenomenon of expansion in cementitious materials.

Chapter 6 is a brief chapter which deals with the important aspect of delayed ettringite formation (DEF) in heat cured Portland cement pastes. This work strengthens the now widely accepted theory that expansion occurs as a result of crystallization pressures developed due to the delayed formation of ettringite in heat cured cements/mortars.

Chapter 7 concludes the thesis with a point-wise summary of the results obtained in the hydration of OPC, the phenomenon of expansion in ternary mix binders and DEF

Chapter 2

Materials and characterization techniques

The understanding of cement hydration is strongly dependent on the available technology. The more sensitive the calorimeter, the more accurate the monitoring of heat evolution from hydrating cement; the more powerful a microscope better will be its output. The need for several techniques arises due to the presence of many different types of hydration products occurring in varying composition, sizes. their intermixing from micron to sub-micron level, and due to other property variations such as bulk *vs* surface properties. Over the past century wide ranging techniques, from classic chemical titration techniques to modern synchrotron 3D imaging, have been used. In this project, however, the stress has been on ‘seeing’ (imaging) the cement microstructure and obtaining accurate chemical information (EDS chemical analysis) using electron microscopy. To this end, transmission electron microscopy (TEM) is the main technique used which is supplemented with scanning electron microscopy (SEM), X-ray diffraction (XRD) and Calorimetry.

Table 2.1: Quantitative phase analysis of the OPC used in this thesis, using Rietveld X-ray diffraction. All values are given in weight%. Values lower than 0.5 are doubtful and should be considered as 0. The Rietveld analysis calculates always to 100 wt.%. Expected errors: phases less than 3 wt.% : ± 0.4 %; phases 10–20 wt.% : ± 1 %; phases > 20 wt.% : ± 2 %.

Phase analysis of the studied Portland cement		
Phases	Formula	Weight%
Alite	C_3S	62.5
Belite	C_2S	16.4
Aluminate	C_3A (cubic)	7.5
Aluminate	C_3A (orthorhombic)	1.8
Ferrite	C_4AF	3.2
Gypsum	$CaSO_4 \cdot 2H_2O$	2.3
Hemihydrate	$CaSO_4 \cdot 0.5H_2O$	1.8
Anhydrite	$CaSO_4$	1.1
Lime	CaO	0.0
Periclase	MgO	0.5
Portlandite	$Ca(OH)_2$	0.0
Calcite	$CaCO_3$	2.0
Arcanite	K_2SO_4	0.9

2.1 Materials used

The Portland cement used throughout in this study is the *CEM I 52.5N*. Its quantitative phase analysis as obtained using Rietveld X-ray analysis is presented in Table 2.1. For the study of pure OPC a w/c ratio of 0.35 was used. In all instances, 100 g of dry cement was taken and mixed with demineralized water using an electric blender for several minutes (5–7 minutes) until an even consistency was achieved. The hydration of all samples was stopped using freeze drying.

Regarding the study on mix binders, involving Portland Cement, Calcium

Table 2.2: Chemical analysis (weight %) of the CAC cements (Secar 51 and Fondu) [123]

Chemical analysis of Secar 51 and Fondu									
	CaO	SiO ₂	Al ₂ O ₃	Fe ₂ O ₃	K ₂ O	Na ₂ O	TiO ₂	MgO	SO ₃
<i>Secar 51</i>	37.48	5.07	52.41	1.12	0.19	0.11	2.51	0.51	< 0.05
<i>Fondu</i>	37.44	4.65	39.15	15.50	< 0.01	0.08	1.87	0.92	< 0.05

Table 2.3: Mineralogical composition of Secar 51 and Fondu [123]

Mineralogical composition of Secar 51 and Fondu								
<i>Secar 51</i>	CA (main phase)	C ₂ AS	Q-phase	CT	MgAl ₂ O ₄			
<i>Fondu</i>	CA (main phase)	C ₂ AS	C ₁₂ A ₇	C ₂ S	C ₄ AF	Q-phase	CT	MgAl ₂ O ₄ (spinel)

aluminate cements (CAC) and calcium sulfate, two kinds of CAC cements were used, namely Secar 51 and Fondu, provided by *Lafarge Aluminates*. Their chemical analysis and phase composition is presented in Tables 2.2 and 2.3 respectively. The preparation of mixes and various curing regimes in the studies of expansion due to delayed ettringite formation and expansion in ternary mixes are presented in the respective chapters.

2.2 Calorimetry

This method is used to observe the heat evolution of hydrating cement with time. The equipment used is a eight-channel isothermal heat conduction calorimeter operating in milliwatt range. All eight calorimetric channels are mounted together to form a single heat-sink block housed in a temperature controlled air thermostat. Each calorimetric channel is constructed in twin

configuration with one side for the sample and the other side for a static reference.

Each calorimeter operates using the heat flow principal. Heat created by any physical or chemical reaction in the sample will flow rapidly to its surroundings. Within each calorimetric channel, there are two Seebeck heat flow sensors, one under the sample and one under the reference. The main route for heat exchange between the sample and its surrounding is through the heat flow sensor. The flow of heat, caused by the temperature gradient across the sensor, creates a voltage signal proportional to heat flow. The twin configuration of sample and reference within a channel allows the heat flow from the active sample to be compared directly with the heat flow from the active sample to be compared directly with the heat flow from the inert reference. The voltage difference is an expression of the overall rate of heat production in the sample.

In this study, mixture of cement and water in a known quantity is introduced in the chamber and the heat evolved from the mixture is read on the computer control. The output is divided by the weight of cement paste to get the heat evolved per unit weight as a function of time. No reference material is used in the reference slot. Thus, essentially, comparative heat curves of various mixtures are obtained without the need of using any reference material.

It is a quick and powerful technique to obtain the heat evolution plots which provide important information on the rate of reaction of the cement paste.

2.3 Rietveld X-ray diffraction

In 1913-1914, the work of W.H.Bragg and his son W.L.Bragg founded a new branch of science of the greatest importance and significance, the analysis of crystal structure by means of X-rays. They found out that a plane of atoms in a crystal with inter atomic spacing of d will reflect an incoming X-rays of wavelength λ at an angle θ , such that

$$\lambda = 2d \cdot \sin(\theta) \quad (2.1)$$

Thus by measuring λ at a known wavelength of X-rays, d of the particular crystal can be found, thus identifying the crystal. This fundamental discovery gave the father-son duo the noble prize in physics in 1915 and made X-ray diffraction as one of the most widely used techniques for the characterization of crystalline solids.

It is a non-destructive technique and specimen preparation merely involves crushing or slicing the bulk samples. This idea of identifying crystals works fine with single crystals, but there is an overlap of spectrums when it comes to identifying multi-crystal materials. In 1969, H.M. Rietveld derived the mathematical relationships to refine neutron diffraction data [170], which was later adapted for X-ray diffraction.

Rietveld analysis is a powerful technique for obtaining the relative amounts of individual phases of a mixture, such as cement. However, a good knowledge of crystallography and the development of a refinement strategy with synthetic phase mixtures are essential to obtain reliable results. The Rietveld technique allows quantification of OPC pastes [183] and qualitative identification of phases of hydrated binary/ternary mixes of OPC with calcium aluminate cements and gypsum [73].

In this thesis, X-Ray Diffraction (XRD) data were collected using a 'PANalytical XPert Pro MPD' diffractometer employing the CuK_α radiation at an operating voltage of 40 KV and current of 50 mA. The samples were scanned between 7° and 60° (continuous scan) with the XCellerator detector. For all hydrated samples, XRD patterns were recorded of slices removed from the bulk specimens. The phase identification was achieved by comparing the X-ray pattern obtained with an international recognized database (JCPDS) containing references patterns for more than 70000 phases.

2.4 Electron microscopy

Modern day electron microscopy (EM) techniques are powerful tools to investigate any complex material. Their multi-purpose approach makes them all the more interesting for researchers worldwide. On one hand where Scanning Electron Microscope (SEM) is relatively easy to use with automatic sample polishing machines at disposal, Transmission Electron Microscopes (TEM's) are more complicated and training intensive machines, often with specimen preparation as the bottle-neck factor. They, however, serve different purposes and prove most effective when used in conjunction with each other.

Whereas SEM is generally used to see the larger picture of a material and identifying the possible interesting areas, TEM is used to study more specific regions of a material. With a large variation of particle size distribution in hydrated cements, imaging in SEM can start from a few hundred times magnification and go up to few thousand times. From there on, TEM can take over to start looking at specific phases or areas starting from few thousand times magnification to up to about 170,000 times. Seeing the phases clearly above about 150–170 thousand times get difficult due to the amorphous nature of cement hydrates. For this reason atomic scale resolution is not possible in these materials.

In order to understand and appreciate the various results from EM's it is best to illustrate some fundamental underlying principals of physics.

2.5 Terms used in imaging

2.5.1 Contrast and brightness

Contrast (C) can be quantitatively described in terms of the intensities (I_1 and I_2) of two adjacent areas

$$C = \frac{I_2 - I_1}{I_2 + I_1} \quad (2.2)$$

Intensity (I) on the other hand is simply the number per unit area (density) of electrons hitting the imaging region in an electron microscope.

$$I = \text{total number of electrons/area}$$

Thus we can have *bright* or *dark* intensity but *strong* or *weak* contrast. It is interesting to know that normal human eyes can not detect intensity changes $< 5\%$. Thus, to be able to see an image properly the contrast should be certainly $> 5\%$ and ideally $> 10\%$.

2.5.2 Image resolution

Resolution of any imaging instrument refers to its ability to clearly view two separate imaging objects present in the same view-field. For instances, a normal human eye *cannot* clearly resolve two points that are less than 0.1–0.2 mm apart, meaning that if the distance between two points is less than 0.1 mm, the eyes will not be able to see them as two separate objects, but as one. Thus, any instrument that can show images revealing detail finer than 0.1 mm can be termed as a ‘microscope’. Resolution (δ) was first quantified by Lord Rayleigh for light microscopes and is defined as follows:

$$\delta = \frac{0.61 \cdot \lambda}{\mu \cdot \sin \beta} \quad (2.3)$$

Where, λ is the wavelength of radiation, μ the refractive index of the viewing medium, and β is the semi-angle of collection of the magnifying lens. ($\mu \cdot \sin \beta$) is often referred to as the numerical aperture of a microscope. For a light microscope, the wavelength of green light in the middle of the visible spectrum is about 550 nm, whereas for a 200 KeV transmission electron microscope, the wavelength of electrons is about 3 pm. Although the theoretical

resolution limit in TEM is not achieved in practice due to the inability to create *perfect* electronic lenses, still the practically achieved resolution limit of modern TEM's ($\sim 2 \text{ \AA}$) is about 1000 times better than that of optical microscopes (300 nm), good enough to clearly image atom columns of crystals.

2.6 Interaction of electrons with matter

It is useful to know that when any matter in general is bombarded with electrons, it results in the generation of several different kind of *signals*, ranging from visible light photon emission to X-ray generation (Figure 2.1). Some of these signals are used for the formation of image in SEM and some are used in TEM. Still others are used to obtain other useful information about the material, such as X-rays for chemical analysis. This is further explained in the following sections.

2.6.1 Various kinds of electron scattering

Consider this: sometimes when a window pane is new or extremely clean, onlookers think the pane is not there, or in other words it appears invisible. The reason why that happens is because the photons of light almost do not interact with the glass pane but instead almost fully transmits through. This tells us that anything with which light does not interact at all becomes, in effect, invisible. Similarly, a thin foil through which electrons totally pass through without any interaction appears invisible. It is in this context that we need to look at the phenomenon of scattering and diffraction of electrons from an atom.

Scattering of electrons reveals their dual-nature. They can be treated as particles, which either loose some of their energy after interaction with the 'target' atom (*inelastic scattering*) or may not loose any energy after the interaction (*elastic scattering*). Simultaneously they can exhibit their wave-

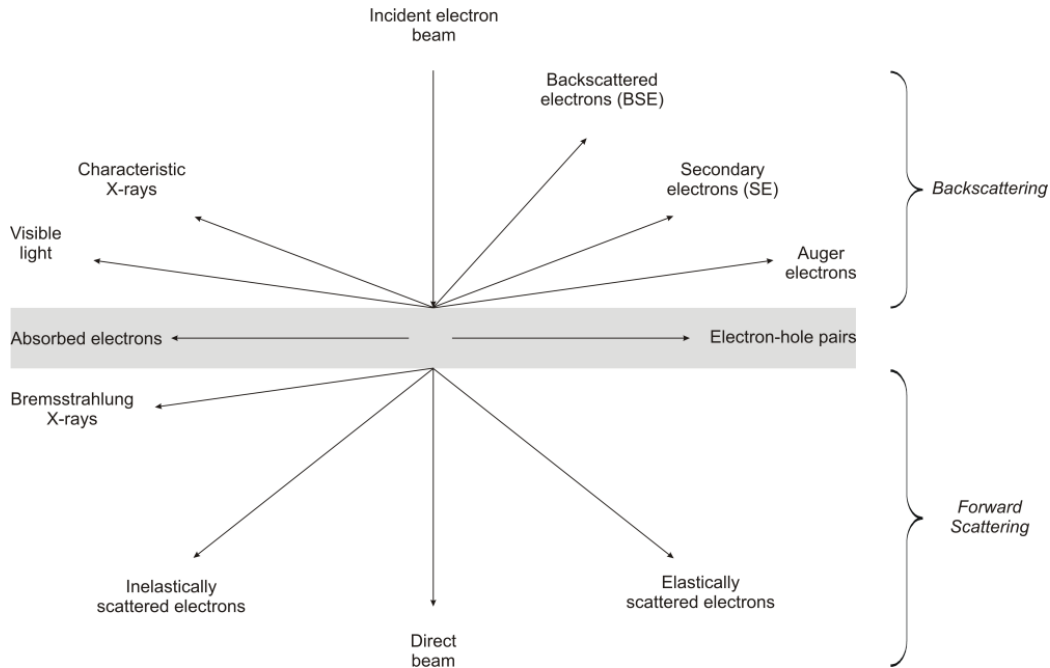


Figure 2.1: Signals generated when a thin specimen is bombarded with a high-energy electron beam. BSE and SE are generally used in a SEM, while electrons scattered in the forward direction are used for image formation or diffraction pattern in a TEM. Characteristic X-rays are used for chemical analysis in both techniques (*Figure adapted from [211, page 7]*)

nature by continuing their phase relationship (*coherent scattering*) or totally losing their phase relationship after interaction (*incoherent scattering*). This is depicted in Figure 2.2. Interestingly, these distinctions are related, since elastic electrons are usually coherent and inelastic electrons are usually incoherent [212, chapter 2]. Some useful facts about these various kinds of interactions are listed as follows:

- Elastic scattering is usually coherent, if the specimen is thin and crystalline.
- Elastic scattering usually occurs at relatively low angles ($1-10^\circ$) in the forward direction.
- At higher angles ($> 10^\circ$) elastic scattering becomes more incoherent

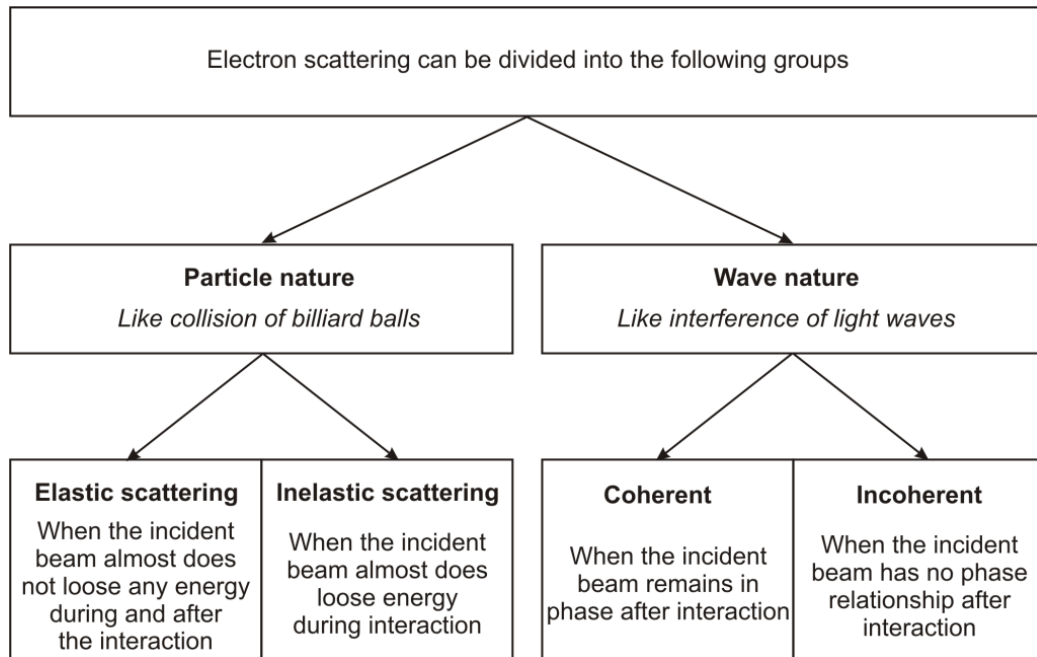


Figure 2.2: Categorizing the electron scattering phenomenon

- Inelastic scattering is almost always incoherent and occurs at relatively low angles ($< 1^\circ$) in the forward direction.
- As the specimen gets thicker, less electron are forward scattered and more are backscattered.

2.6.2 Interaction cross-section

There is one more crucial concept in this context, called interaction cross section of an atom. The existence of nucleus and the first mathematical conceptualization of electron nucleus (matter) interaction was made by E. Rutherford and named Rutherford scattering. Later the atom interaction cross section for electron was mathematized by Hall [97] and Heidenreich [99] and was aptly explained by R.E. Peierls with the following analogy [211, Chapter 2]:

“If I throw a ball at a glass window one square foot in area, there may be one chance in ten that the window will break and nine chances in ten that the ball will just bounce. In the physicist’s language this particular window, for a ball thrown in this particular way, has a disintegration (inelastic!) cross-section of 0.1 square feet and an elastic cross section of 0.9 square feet”

Indeed, the cross-section is not a physical area, but when divided by the actual area of the atom it represents a probability that a scattering event will occur.

Scattering events per unit distance (Q_T) that the electron travels through the specimen can be given as:

$$Q_T = \frac{N_0 \cdot \sigma_T \cdot \rho}{A} \quad (2.4)$$

Thus the probability of scattering events when electrons pass through a specimen of thickness t will be given by:

$$Q_T \cdot t = \frac{N_0 \cdot \sigma_T \cdot (\rho \cdot t)}{A} \quad (2.5)$$

where N_0 is the Avogadro’s number (atoms/mole), σ_T the total scattering cross section for the isolated atom, and A is the atomic weight (g/mole) of the atoms in the specimen which has density ρ . The product of ρ and t is called the ‘mass-thickness’ of the specimen and is the primary source of contrast while imaging an amorphous material (e.g. hydrated cement) in a TEM.

2.7 Chemical analysis

The basic concept of chemical analysis in an electron microscope is illustrated in Figure 2.3 and described as follows. In this example, interaction of a K-level electron of iron atom (heaviest element present in Ordinary Portland cement) is shown.

An incoming electron interacts with an electron of one of the energy levels of the atom. The incoming electron during this *inelastic interaction* gives most of its energy to the interacting electron. If this energy is more than the binding energy

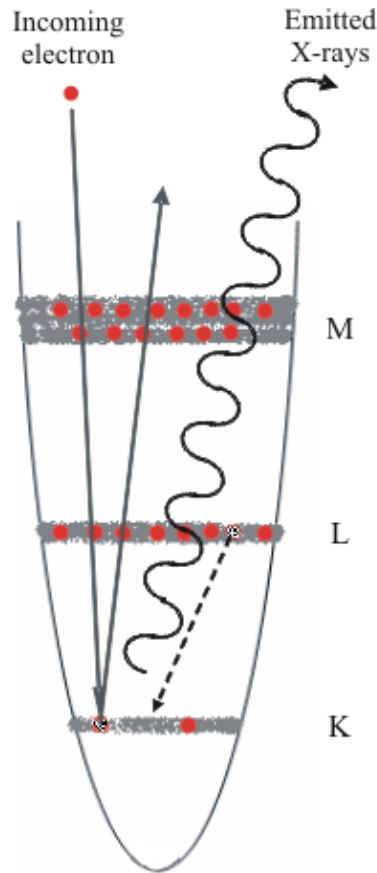


Figure 2.3: Representation of the *energy-well* of an iron atom. Red circles represent electrons. *Graphics adaptation: lecture notes, Prof. P.A. Stadelmann, Center of Electron Microscopy, EPFL*

of the K-level electron, latter is released from the influence of the nucleus and with sufficient energy (the energy of the incoming electron should be ~ 1.6 times the ionization energy of the atom for it to do so) it rests in one of the higher empty energy levels. This creates a void or a *hole* at the K-level. This hole can be filled by the transition of one of the electrons present in one of the higher energy levels. In this example an electron from the L levels is shown to fall down and fill the void. However, the energy of this electron is different after falling than before. This causes an energy difference in the atom which is released in the form of X-rays. Since energy levels are discrete, these X-rays have *characteristic* energy corresponding to a particular energy level of a particular atom, and are henceforth

called characteristic X-rays.

In an EM, these characteristic X-rays are collected by X-ray detectors which digitally process them to give an energy spectrum showing the relative amounts of obtained X-rays, and thus the relative amount of corresponding elements detected. It is however possible that the energy values of the X rays corresponding to different energy lines of different elements may overlap. If two or more such elements are present in the specimen, it is not possible to obtain any qualitative or quantitative information on the chemistry of the specimen. E.g. M line of gold, L line of molybdenum (Mo) and K line of sulfur overlap each other. This is why Mo grid, a very common grid should never be used to support TEM cement specimens. Fortunately, no such element combination is present in cements.

2.7.1 Spatial resolution

Spatial resolution of X-ray microanalysis can be defined as the smallest distance (R) between two volumes from which independent X-rays microanalysis can be obtained. The volume from which X-rays are emitted is called the *analysis volume* and R are governed by the beam-specimen interaction volume. This interaction volume is a function of the incident beam diameter d and the beam spreading b caused by elastic scatter of the beam within the specimen (Figure 2.4). It is believed that b depends on atomic number (Z), atomic weight (A), beam energy (E_0), specimen thickness (t) and density (ρ) such that [213, Chapter 36]:

$$b = 7.21 \times 10^5 \left(\frac{Z \cdot t}{E_0} \right) \sqrt{\left(\frac{\rho \cdot t}{A} \right)} \quad (2.6)$$

The formal definition of the X-ray spatial resolution is given by the following equation

$$R = \frac{d + R_{max}}{2} \quad (2.7)$$

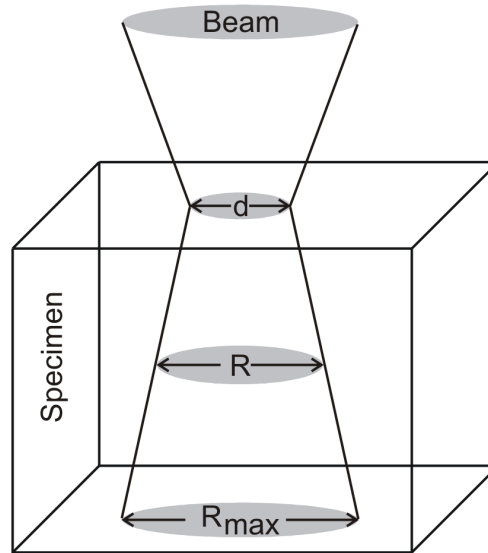


Figure 2.4: Schematic diagram of how the combination of incident beam size d and beam spreading through the foil combine to define the spatial resolution of X-ray microanalysis in a thin foil (*Adapted from [213, page 625]*)

where,

$$R_{max} = \sqrt{b^2 + d^2} \quad (2.8)$$

Note: Spatial resolution is not to be confused with image resolution

2.8 SEM

Scanning electron microscope is used to image and analyse bulk specimens. In a SEM, an electron probe, 2–10 nm in diameter, is scanned over a region of the specimen. The different signals that result from the electron-specimen interaction are collected to form images and obtain chemical analysis. Figure 2.5 shows the signals generally utilized in a SEM.

There are two principal imaging modes in a SEM which are briefly described as follows:

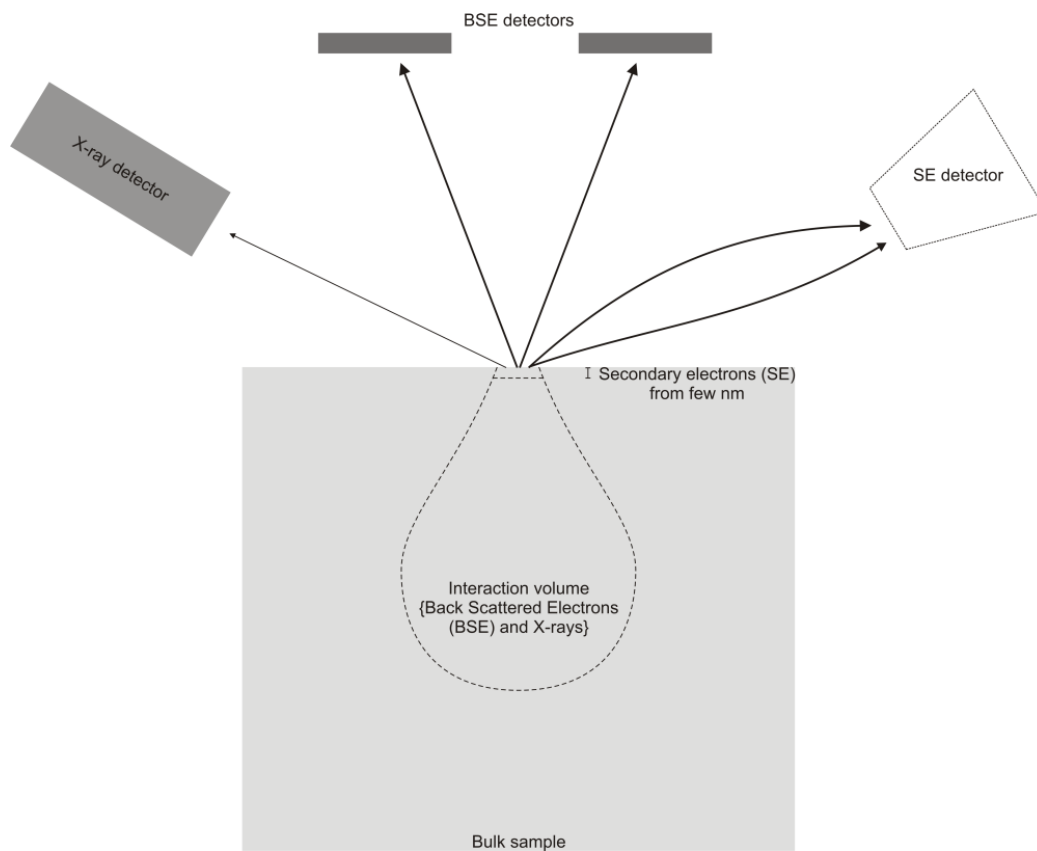


Figure 2.5: showing an SEM along with the signals used in this thesis to study the bulk specimen

2.8.1 Secondary electrons (SE)

They are electrons in the specimen that are ejected by the beam electrons. They can leave the specimen only from a very thin surface layer of the order of a few nanometers, thus providing the best image resolution and also revealing the surface topography. This is why SE mode is used to study fractured surfaces and not polished specimens since they have almost no topography.

2.8.2 Backscattered electrons (BSE)

These are electron with higher energy range than SE and consequently have much greater information depth (0.1–1 μ m).The amount of backscattered electrons is

indicated by the backscattering coefficient η , which depends on the average atomic number (Z) of an interacting phase as follows [162, page 143]:

$$\eta = A + B \cdot Z + C \cdot Z^2 + D \cdot Z^3 \quad (2.9)$$

where, A, B, C and D are constants whose values depends on parameters such as operating voltage, specimen thickness, specimen density, etc.

Thus higher the average atomic number of a phase, the higher the number of generated BSE, and brighter the phase will appear on the screen. A careful look at it reveals that BSE mode employs the same Z-contrast (see section 2.10.1, page 26) mode as used in HAADF-STEM.

2.8.3 Chemical analysis

It is known that the energy of an incoming electron should be ~ 1.6 times the ionization energy of the atom, for it to ionize the atom and consequently emit characteristic X-rays. The heaviest element in hydrated cement is iron. The ionization energy of its K-energy electrons is ~ 6.4 KeV, so the operating voltage of an SEM should be at least $6.4 \times 1.6 \approx 11$ KeV.

The interaction of electron with bulk matter results in the excitation of matter of few μm^3 in volume. This generally results in the excitation of X-rays from this volume, raising the possibility of identifying multiple phases and not the phase on which the probe had been placed.

In the present work, a Philips Quanta 200 SEM with PGT energy dispersive X-Ray analyser was used at an operating voltage of 15 KeV.

2.9 Transmission Electron Microscope

Transmission electron microscope is a powerful electron microscope in which electrons diffract through a ‘thin’ specimen (~ 100 nm thin) to form an image in transmission mode. With TEM one can achieve high magnifications (upto 170,000 times for amorphous material like cement) and high spatial resolution (2\AA) images.

Since the specimen has to be extremely thin the interaction volume of electrons and sample is of the order of beam diameter (few nm), providing standardless and accurate quantitative chemical analysis. Obtaining images although seemingly straightforward can be tricky. Amongst other things, imaging includes the concepts of ‘bright’ and ‘dark’ field and different kinds of contrasts, as will be illustrated in the following sections.

In a TEM, usually a thermionic electron gun is used, which emits electrons in a fixed columnar fashion which are bombarded on the specimen. Since the exposed region of the sample is constantly bombarded with electrons, these ‘static beam’ TEM’s are best used for beam insensitive specimens, especially for investigating crystals using various techniques of diffraction. Figure 2.6 is a ray diagram illustrating the image formation in a TEM.

2.9.1 Concept of contrast in TEM

Amount of electron scattering depends on the density and thickness of the specimen [see equation 2.5, page 15]. Thus thicker or higher Z areas of the specimen will scatter more electrons off axis than thinner or lighter (lower mass) areas.

2.9.2 Bright and dark field imaging

In bright field imaging both the scattered and unscattered electrons from the specimen are collected and contribute to image formation. In the dark-field imaging only the diffracted electrons contribute to image formation. The advantage of latter is that there is no background signal in the image. This is illustrated in Figure 2.7 on page 24. The beam referred to as signal is the slightly diffracted electron beam, whereas the one called as background is the undiffracted beam. Since the background beam had no interaction with the specimen, it has a larger number of electrons per unit area than the signal. Hence, the background electrons form the brightest part of the image, ‘signal’ forms relatively darker region and the electron diffracted still at higher angles (due to higher density or greater thickness) are completely blocked by the objective aperture and the corresponding region does not impinge any electrons on the imaging plates or screen, thus forming the darkest part of the image. This infact is the concept of *mass-thickness contrast*.

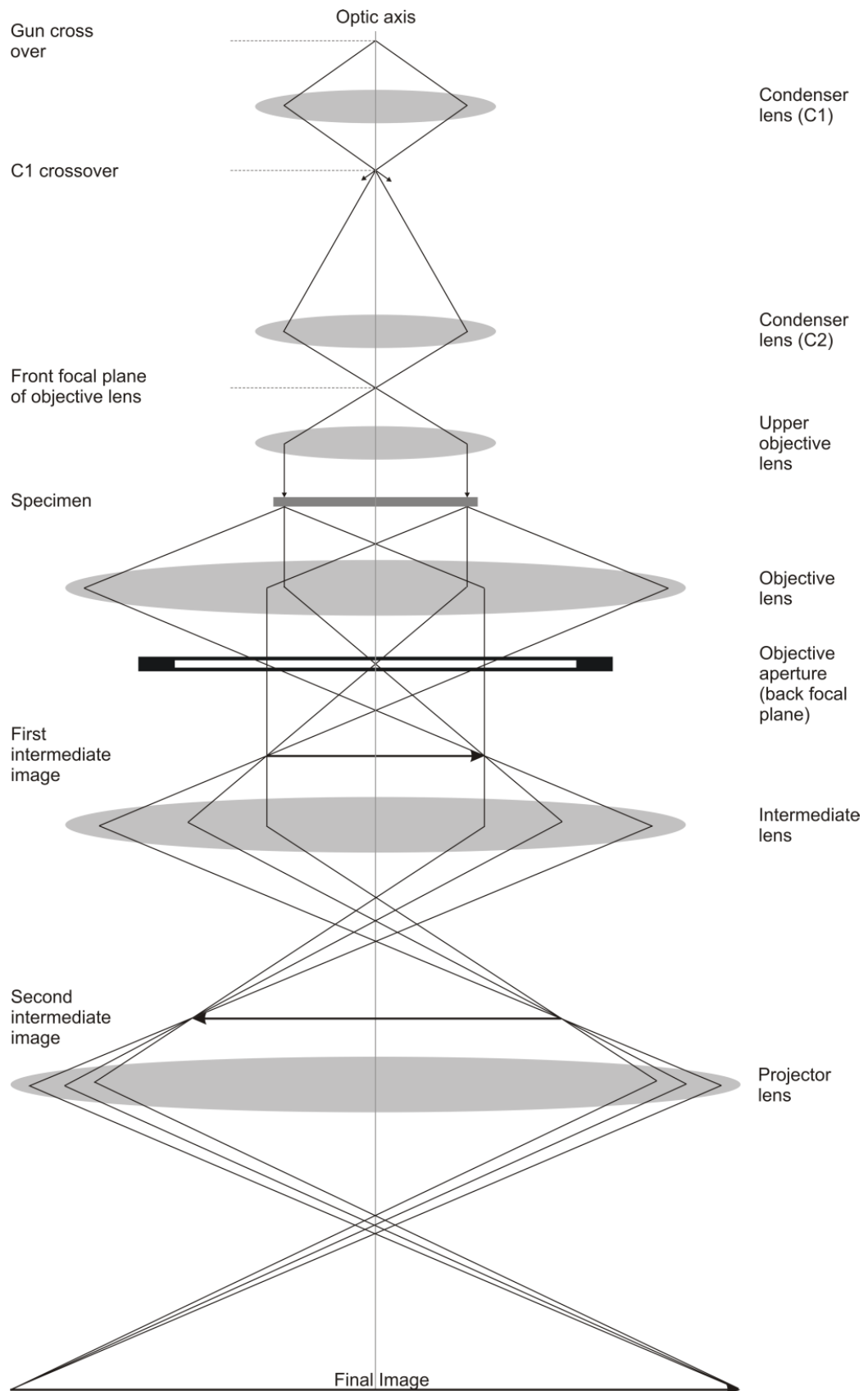


Figure 2.6: Ray diagram of image formation in a transmission electron microscope (*Adapted from [211, Chapter 9]*)

Now this concept can be used to form either bright field images, by filtering electrons scattered at high angles (angles greater than the aperture size), or can be used to form dark-field images by filtering the undiffracted beam and using only scattered electrons as the signal for image formation. In section 2.10.1 on page 26 an important sub-category of mass-thickness contrast called *Z-contrast* will be discussed.

A different kind of contrast is called *diffraction contrast*. It is applicable only while imaging crystals. Crystalline materials strongly diffract electrons, like X-rays, at specific angles called Bragg angles. Generally the diffraction angle between primary and diffracted beams is larger than the objective aperture. This means that the Bragg-diffracted beams are halted by the objective aperture in the BF mode and do not contribute to the image intensity. The image intensity thus becomes equal to the primary beam. On the other hand dark field image is formed by allowing only Bragg diffracted beam to pass through the objective diaphragm. Thus, only those specimen areas that contribute to the selected Bragg-diffraction spots appear bright.

These concepts of contrast are interestingly not exclusive to TEM, but are often used in our daily life, perhaps rather unknowingly. For instance, let us divert our attention for a moment to the event of watching a movie in a cinema hall. Start of the movie is preceded by several trailers and commercials. It is worthwhile pondering the differences in the *ambience* before and during the movie. During the pre-movie period, the screen is lit up with graphic images just like it is while the movie is on, the difference however been that the lights in the hall before the start of the movie are generally switched on while during the movie they are religiously switched off. Why?

The answer lies in the fact that when the lights are switched off (during the movie), *only* the illumination from the screen falls on our eyes, without any *dilution* from other light sources, but when the lights are switched on, photons both from the screen and from the several lights present in the hall are together striking our retinas. This in effect dilutes the ‘signal’ from the screen. Or in other words, the idea of switching off the light and thus making the *field* around the screen *dark*, while the movie is running is not to dilute the *principal signal* (movie) with any *background signal* (noise). Indeed the event of watching a movie while the ambient lights are switched off can be termed as watching the movie in ‘dark-field’ mode,

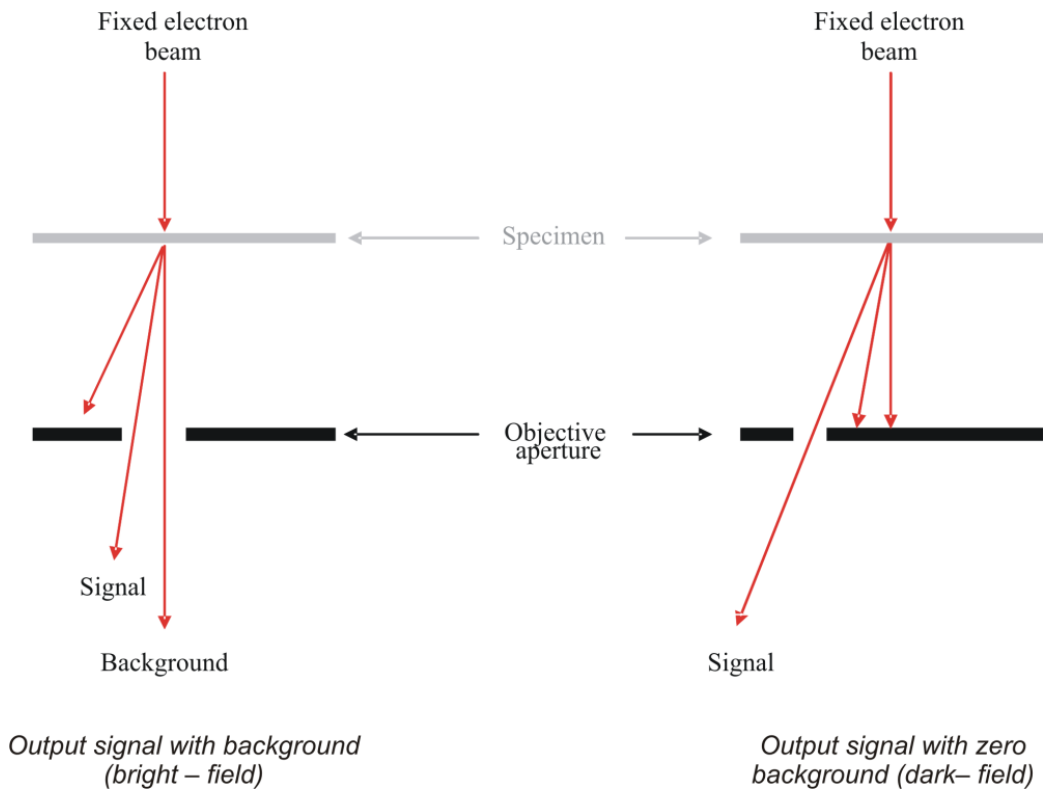


Figure 2.7: Dark and bright field image formation in a conventional TEM

whereas the period where commercials are on along with the background signals, can be called ‘bright field’ mode. Infact the bright field mode not only reduces the brightness and contrast of the images, but also their resolution. This is the reason why the audience would not ‘feel’ appropriate to the watch the movie with lights switched on!

A similar reasoning can be given to explain as to why the fireworks are usually done in the nights and not during the bright afternoons.

2.10 Scanning Transmission Electron Microscope

A STEM is a particular kind of a TEM where instead of having a fixed column of incident electrons, a pencil of electrons is rastered (like in a SEM) on the sample

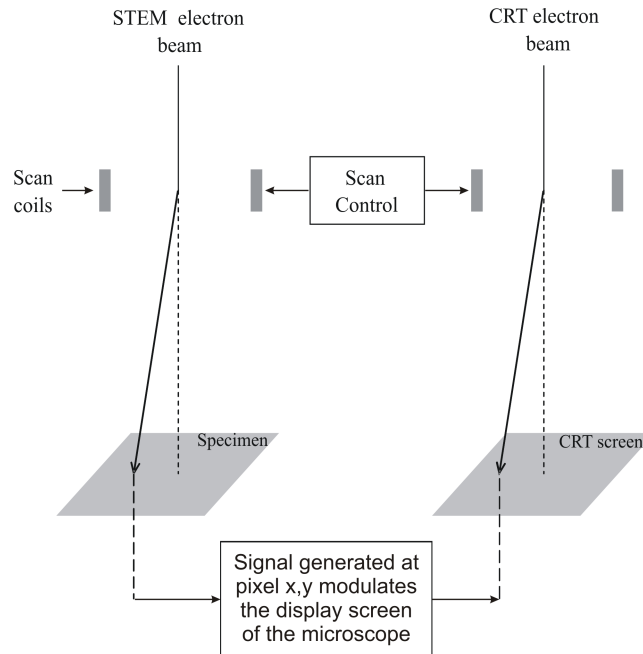


Figure 2.8: Sketch of the operation of image formation in a Scanning TEM. (Adapted from [211, page 145])

surface. Further, instead of an objective aperture a bright-field or a dark-field image detector is used to form the image. The signal generated at any point on the specimen is detected, amplified and a proportional signal is displayed at an equivalent point on the display screen of the microscope. The image is acquired over several seconds (Figure 2.8). Since no part of the specimen is constantly exposed to the electron beam, it significantly reduces any beam damage to the sample. Generally, STEM are fitted with EDS analyser at a high take off angle for efficient collection of the X-rays, and Electron Energy Loss Spectrometers (EELS) [213, Chapter 38]. STEM's are ideally suited for analytical work and are often termed as analytical electron microscopes (AEM), and for advanced diffraction work such as convergent beam diffraction (CBD) [212, Chapter 21].

Imaging in bright and dark field is achieved using respectively bright field (BF) detectors and dark field (DF) detectors (Figure 2.9). There are two types of DF detectors, one called annular dark field (ADF) detectors which collects electrons scattered at $> 10\text{--}50$ mrad and high angle annular dark field (HAADF) detector, which collectors electrons scattered at angles > 50 mrad.

2.10.1 Z-contrast

Z-contrast is a sub category of mass-thickness contrast (section 2.9.2, page 21) and is brought to use when a sample has phases of varying mass and/or density.

Contrast obtained in HAADF images is called Z-contrast, since the detector collects scattered electron from wide angles, corresponding to large variation of Z values of the phases in the specimen (assuming the changes in thickness are negligible). Since the contrast is very large and the background signal is totally absent the quality of images is very high. It is useful for imaging thick specimens (up to few hundred μm) as well. The scattering angle of electrons from thicker specimens will be large and majority of such electrons will not be detected by ADF detector, but will be easily collected by HAADF detector.

Cement's microstructure is composed of phases of various densities ranging from anhydrous phases to low-density C-S-H. Thus the annular distribution of diffracted electrons is large. In order to see and distinguish all the features clearly it is ideal to collect all the diffracted electrons, including the high angle ones, with the exclusion of the undeviated incident beam. These requirements are perfectly met by HAADF detector which provides the highest quality of images for hydrated cement, both in terms of contrast and resolution.

In the light of these facts, one can conclude the following:

- BF mode is not convenient for specimens with very small mass-thickness such as DNA molecules or virus particles or low-density C-S-H [161].
- DF imaging is advantageous if structures with high and low mass-thickness are to be imaged simultaneously, viz, early age OPC, where low-density C-S-H (small mass-thickness) is seen growing around alite (relatively higher mass-thickness) (page 76).

Most of the work is done on the HF2000 Field Emission Gun [211, Chapter 5] Scanning Transmission Electron Microscope (FEG-STEM) fitted with an EDS analyser at a high take off angle for efficient collection of the X-rays. This helped in making the analysis without tilting the specimen. The operating voltage was 200 KeV and the current at the sample surface was estimated to be about 1 nA.

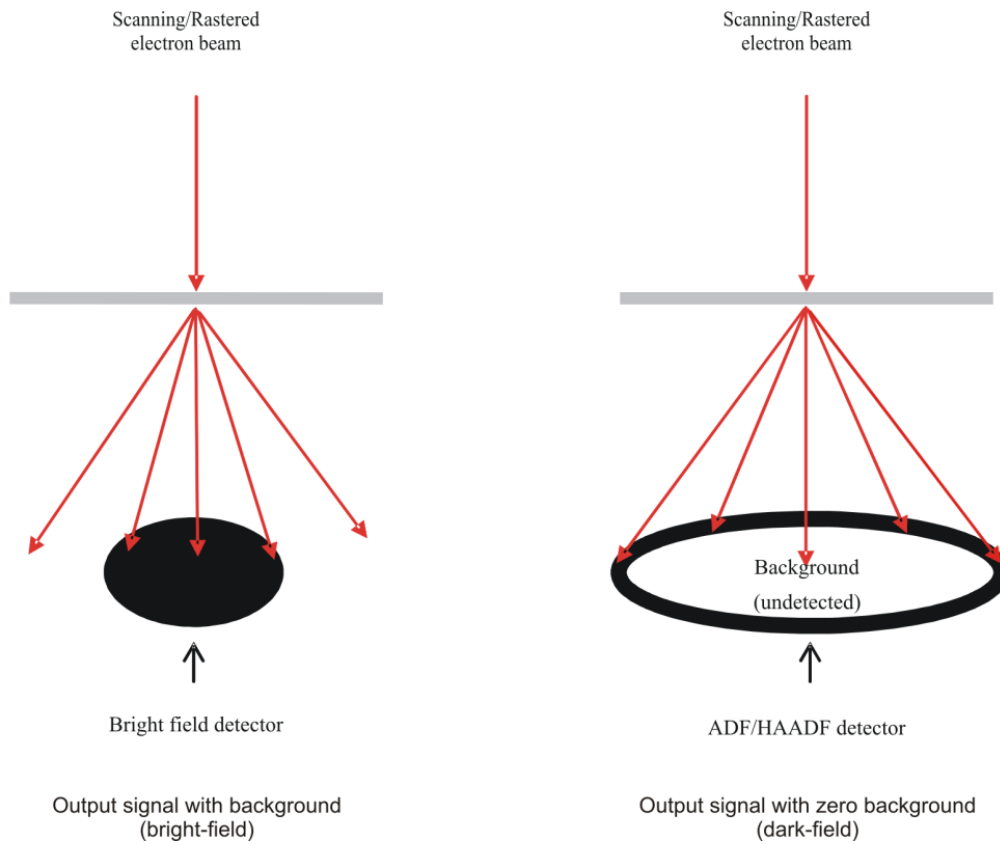


Figure 2.9: Dark and bright field image formation in a scanning TEM

STEM gives more leverage in obtaining high magnification images without any beam damage. Most of the images were acquired in the dark-field mode, with the help of a high angle annular detector fitted in the microscope. Chemical mapping was carried out in CM300 (FEG-STEM) at an operating voltage of 300 KeV while tilting the samples to $\sim 10^\circ$.

2.11 Comparison between dark-field modes of TEM and STEM

It could be argued that since DF mode of a STEM is so widely used, the same mode can also be used in a TEM. This indeed can be done, but only for crystalline materials. It is to be kept in perspective that crystalline materials diffract elec-

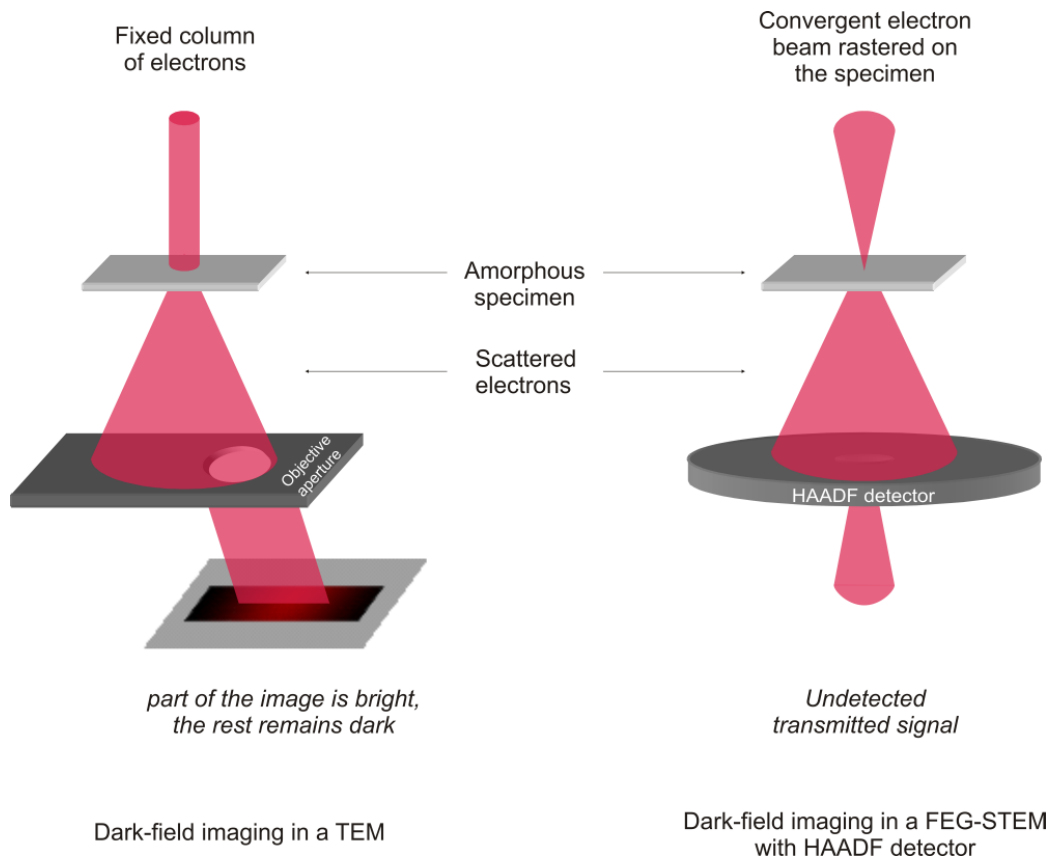


Figure 2.10: Dark field imaging in a TEM and STEM fitted with HAADF detector

trons at specific angles called Bragg angle and to collect those diffracted electrons, using an objective diaphragm, is rather easy. However an amorphous material like hydrated cement scatters electrons in a wide angular range, and any attempts to collect those scattered electrons will result in the formation of an image which would be an overlap of dark and bright modes. On the other hand, annular dark field detectors collect scattered electrons from almost all possible solid angles, thus showing all the phases in one mode (dark field). Let us look at the Figure 2.10 to understand it further.

In the image on the left in Figure 2.10, the objective aperture has been placed to collect diffracted electrons. However, the specimen being amorphous scatters electrons at angle ranges larger than the aperture. In order to show the diffracting phase of the specimen bright, all the electrons scattered from the phase should be

collected. However only a part of those electrons could be collected. This then results in some parts of the phase appearing bright and the other dark, causing a mixture of bright and dark field modes.

The arrangement in the image on the right in Figure 2.10 removes this problem. The dark field detector simultaneously collects most of the scattered electrons, letting go only of undeviated electrons and those that have undergone very slight diffraction (that's why the name, high angle annular dark field detector). Thus, a scattering phase is fully visible as the bright part of the image, whereas the holes of the specimen, through which electron pass undeviated appears dark. The specimen contrast is obtained by the varying Z values of the phases (assuming uniform specimen thickness). The higher the Z value, larger the angle of scatter and more the collection of electrons by the detector, thus brighter that part of the specimen appears on the image.

Rule of Thumb: In BF mode the dark part of the image corresponds to matter in the specimen and the bright parts are vacuum. In DF mode, the roles are reversed and bright parts show the sample and black parts are vacuum

Generally speaking Z-contrast images from HAADF detectors have the best resolution and overall quality. This is especially true for hydrated cement pastes.

2.12 Comparison of X-ray microanalysis among SEM, TEM and STEM

Increasing the accelerating voltage, when using *thin specimens* (TEM), decreases the total beam-specimen interaction volume, thus giving a more localized X-ray signal source and a higher spatial resolution. Conversely, with *bulk samples* (SEM), increasing the voltage increases the interaction volume.

In a TEM the electron beam is a column of diameter d whereas in FEG-STEM the electron beam is a point having much smaller d . Thus the beam spreading (proportional to R_{max}) and the R in equation(2.7) are much larger in TEM's than in FEG-STEM's. Larger R amounts to relatively poorer spatial resolution in TEM.

2.13 TEM specimen preparation techniques

2.13.1 Mechanical polishing

It is often said that the success of TEM technique is dependent largely on the quality of sample preparation, which is found to be a difficult task considering the brittle nature of hydrated cement samples. At early ages (< 1 day) specimens have practically no strength and need extreme care during the preparation.

In this context, a mechanical polishing method called tripod method was used to prepare cross-sectional TEM specimens. This process is mostly mechanical and was first developed by J.S. Klepeis and co-workers in the IBM's laboratories, USA [118]. After some practice the polishing process is been fine tuned for hydrated cements and is summarized as follows:

First, a sample is resin impregnated to provide some structural strength. Then a cylindrical disk about 1 mm thick and 2.5 mm in diameter is taken out from the centre of the bulk sample. The disk is subsequently polished down to a thickness of about $10\mu\text{m}$ on which a slotted grid is glued, as a means to handle the specimen. Finally the sample is ion milled (argon ions) at 2–2.2 KeV until electron transparency is achieved—interference coloured fringes are seen under an optical microscope. Thereafter, samples are coated with few nanometers thin layer of carbon to make them electrically conducting to avoid damage due to charge accumulation.

It needs to be emphasized that due to the brittle and extreme delicate nature of young hydrated cement pastes, in one case non-set cement of 2 hours old, is an extremely difficult process, requiring some degree of skill and persistence. Even slight human error while polishing, especially during the second side polishing, can result in poor surface finish that may take several weeks to smoothen out by ion milling and subsequent thinning to the required degree; and in some baffling instances may result in breaking of the sample, rendering itself useless.



Figure 2.11: Charging of a cement sample in Focussed Ion Beam

Problem of differential thinning

One thing inevitable in this method is the differential thinning of a material like cement. The hardness of the clinker phases like alite etc. is much more than the hardness of hydration products. Thus in a unit milling time, the amount of region occupied by hydration products is thinned more than the clinker phases. Consequently, the chemical analysis values of alite for instance sometimes show higher calcium content than expected (Ca/Si ratio comes out to be slightly more than 3). This is because the characteristic X-rays of silica, an element lighter than calcium, are easily absorbed. The only way to achieve a uniform thickness of all the phases is to employ Focussed Ion Beam (FIB) technique as illustrated in the next section.

2.13.2 Focussed Ion Beam

Focussed Ion Beam [192] is a technique similar to the SEM, with the distinction that a beam of excited ions are used instead of the conventional electron beam. The ion beam can be used to vaporise material from the sample surface and is capable of micro-machining trenches, troughs and remove layers etc. to reveal sections or surfaces of interest for imaging. In the case of dual beam instruments that have the capability of focussing both ion and electron beams onto the same region of

the sample, the prospect of sample preparation in-situ and under vacuum becomes a reality. Certain materials are reactive or oxidise easily which makes preparation by conventional methods impossible. FIB also creates the possibility of preparing materials that are too soft for conventional preparation such as cements hydrated for few hours.

Conventional FIB preparation of bulk cement proved futile due to excessive charge accumulation, as illustrated in Figure 2.11. After some deliberations, the *H-bar* method was found to be most suitable for cements. It involves two chief steps. First, the mechanical polishing of the sample to $\sim 30\mu\text{m}$ with the tripod and gluing the sample on a gold grid specially designed for FIB. Second, machining and thinning of the exposed edge of the sample with Ga^{2+} ions. This involves milling an area few microns in size, along the exposed edge, down to about 100 nm. These steps are graphically depicted in Figure 2.12. Before milling however, the sample is coated with gold to make it conducting. Since the exposed edge is about $30\mu\text{m}$, the charging effects are minimized but not completely eradicated and the operator has to take extreme precautions in order to avoid crumbling of the specimen while preparing. Eventually the whole specimen is carbon coated and the thinned part is ready for observation in a TEM.

The main advantage of sample preparation in FIB is that we get uniform thickness of the thinned part, and the problem of differential milling, as mentioned in the mechanical polishing method, is solved. However, the major disadvantage is the small achievable dimensions of the thinned part ($\sim 20\mu\text{m}$ a side), which is generally of the order of cement grain size.

Subsequent to successful completion of the TEM theoretical and practical training programs, all the work done on various TEM's and the results presented in this thesis are done fully and independently by myself (except the sample preparation using FIB) with no outside help or assistance whatsoever.

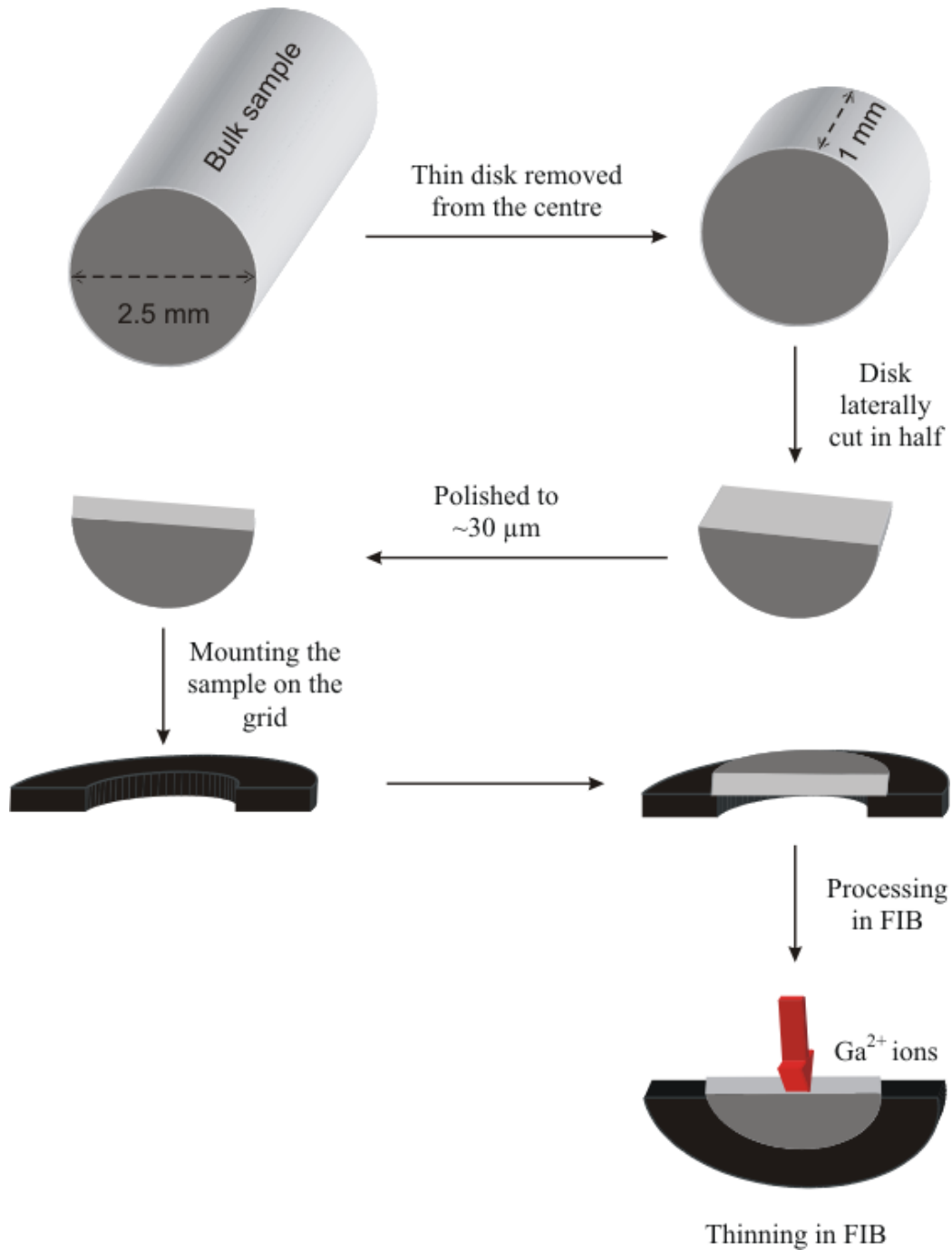


Figure 2.12: H-Bar method used for preparing TEM specimens of hydrated cements using Focused Ion Beam (FIB)

Chapter 3

Literature review of the hydration of Portland cement

3.1 Introduction

Hydration may be described as a reaction of an anhydrous compound with water giving new compounds, called hydrates. In cement chemistry hydration is understood to be the reaction of non-hydrated cement or one of its constituents with water, associated with both chemical and physico-mechanical changes of the system, in particular with setting and hardening.

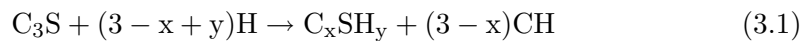
In the case of hydration of Portland cement, the chemical reactions with water are responsible for the setting and hardening of mortar and concrete. Since the processes of setting and hardening are of great significance to the practical viability of cement, the underlying chemistry of these processes must be understood. However, this is not an easy task because cement is a complex mixture of several compounds. Due to the complexity of the hydration of Portland cement, it makes good sense to discuss first the hydration of the individual compounds which constitute the Portland cement clinker.

3.2 The anhydrous phases of cement

Cement clinker is composed of the following phases. These phases with their basic reactions in the cement system are presented as follows:

Alite

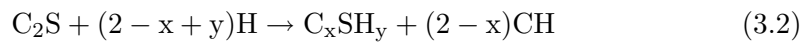
Alite refers to the impure form of tricalcium silicate ($3\text{CaO} \cdot \text{SiO}_2$, abbreviated to C_3S) which is doped with other ions present in the original raw mix.



C_xSH_y is an amorphous phase and forms the bulk of hardened cement pastes. More information about this phase is presented in greater detail in section 3.3. CH refers to $\text{Ca}(\text{OH})_2$ which forms as relatively large crystalline masses in between the cement gains in mature pastes.

Belite

Belite is the impure form of dicalcium silicate ($2\text{CaO} \cdot \text{SiO}_2$, abbreviated to C_2S). It has a lower reactivity than alite.



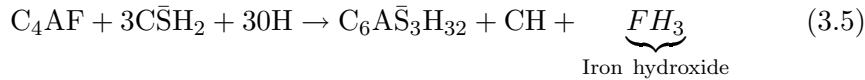
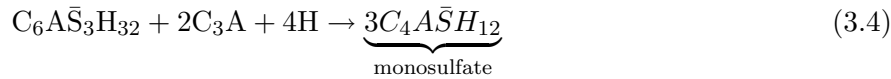
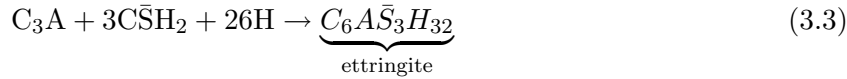
Tricalcium aluminate

It is an aluminate rich phase ($3\text{CaO} \cdot \text{Al}_2\text{O}_3$, abbreviated to C_3A) known to be the most reactive of the phases present in Portland cement and has a significant influence on its early hydration and rheology.

The ferrite phase

There exists a solid-solution series called the ferrite phase, having the general formula $\text{Ca}_4\text{Fe}_{(2-x)}\text{Al}_x\text{O}_{10}$, where $0 < x < 1.4$. C_4AF is not a stoichiometric compound, but just one point in the series where $x = 1.0$. Many cements have a ferrite phase with a composition close to that of C_4AF , this is the reason why it is the most common composition studied.

Gypsum is added to control the setting. The ideal reactions of the interstitial phases with gypsum are presented below [2].



3.3 Calcium silicate hydrate (C-S-H)

The exothermic reaction (3.1) is marked by the formation of two hydrations products, namely, calcium silicate hydrate, an amorphous phase of variable composition, hence usually written as C-S-H, which implies a non-specific stoichiometry; and crystalline calcium hydroxide ($\text{Ca}(\text{OH})_2$, abbreviated to CH), often referred to as portlandite.

3.3.1 Morphological classification

C-S-H can be divided into two major categories, viz. ‘outer’ and ‘inner’ product (Table 3.1).

C-S-H formed in the pore space outside the boundary of its parent grain is called

Table 3.1: Different types of C-S-H along with their various characteristics and associated terminologies

Microstructural designation	Time of formation	Relative density	Designated terms
Outer	Early	Low	Undifferentiated or Groundmass
Inner	Late	High	Phenograins

the *outer* product. As it is produced in the early stages of hydration during the main heat peak, it is also called the *early* product. Since it forms rapidly into the free pore space and thus contains significant microporosity, the term *low density* is also associated with it. Further, due to the presence of several fine anhydrous phases, it is not possible to know precisely if it lies within or outside the boundary of those grains — thus the terms *undifferentiated* or *groundmass*.

On similar lines, C-S-H formed within the original boundaries of the grain is called the *inner* product. Since it forms after the formation of the outer product, during the slow continuing reaction of the grains, it is also called the *late* product. It forms compactly in a space efficient manner, unlike the outer product, due to limited free space available. It is believed to have a higher elastic modulus [47] and lower microporosity than the outer product, thus referred to as the *high density* product. It is also called as *phenograins* since the form of this inner product replicates the positions of the cement grains.

This classification of the two types of C-S-H can be further supplemented by their respective morphologies which do not remain the same but undergo several physical changes and are visible under electron microscopes. Two major classifications based on apparent morphological changes during the course of hydration have been proposed. The one by Diamond [61] in which he observed hydrated Portland cement samples using Scanning Electron Microscopy (SEM) and the second by Jennings and co-workers in which they observed hydrated samples using a Transmission Electron Microscopy (TEM) [109]. They are illustrated in Table 3.2

Table 3.2: Correlation between the various types of C-S-H and with their appearance under different electron microscopes. The morphology descriptor, e.g. Type X, is accompanied in the table by a description of the main morphological feature.

Microstructural designation(s)	Morphological designations		Time of formation [section 3.6]
	SEM appearance [61]	TEM appearance [109]	
Outer product (Op), Groundmass, or, Early product	Type II ^c , reticulated	Type E, globular	During the induction period
	Type I, acicular	Type O, foil-like	First few days
		Type 1, acicular	Dried form of Type O
Inner product (Ip) or Phenograins or Late products	Type III, indeterminate	Type 3, fibrous	First 2-3 weeks
	Type IV, spherical	Type 4, indeterminate	Weeks to months

3.3.2 The atomic structure

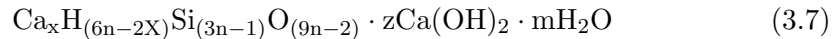
Knowledge of the atomic structure of C-S-H is vital as it is the most abundant hydrated phase present in cement pastes and is believed to play a key role in strength development and other important physical properties of cement. However, the aim of this thesis is not to try and add information to an already vast amount of literature devoted to understanding the true atomic structure of C-S-H. Thus, without omitting vital details, the following brief summary is presented.

Taylor mentioned [205, Chapter5] that since no long-range order exists in the structure of C-S-H, terms such as crystal chemistry or crystal structure are inapplicable to the material as a whole and suggested the term nanostructure as an appropriate term to describe the structure at this level. Due to its amorphous nature no present day technique is capable of showing the precise arrangement of atoms of C-S-H.

A frequent approach [71, 84, 85] has been to consider C-S-H as essentially two-component solid-solution system composed of calcium hydroxide and a calcium

silicate hydrate of low Ca/Si ratio, often an established crystalline calcium silicate hydrate, such as jennite ($C_9S_6H_{11}$, compositionally similar to C-S-H), and 1.4 nm tobermorite ($C_5S_6H_9$ approximately, where 1.4 nm refers to the thickness of the elementary layer in the structure; belongs to the tobermorite group which includes all the calcium silicate hydrate which are directly important in cement hydration, see Figure 3.1).

Consistent with this compositional approach, Kantro and co-workers [115] proposed that tobermorite-type layers are sandwiched between CH layers, while Birchall and Thomas [21] suggested that finite silicate units are attached to short calcium hydroxide-like sheets. This solid solution like approach seemed to be strengthened by evidence from chemical extraction methods as reported by Stade and Wieker [188], who found that CH could be leached from high Ca/Si ratio C-S-H gels, whereas very little could be removed from C-S-H with low initial ratios, indicating a possible limiting value of extractable Ca^{2+} and OH^- . Richardson and Groves [167] proposed a generalized model for the C-S-H and expressed the general formula as



This model was extended to cement pastes by allowing the possibility of various ionic substitutions [168] and seems to be implicitly based on altered 1.4 nm tobermorite. Taylor, however, suggested [202] that C-S-H gel most likely contains elements of both 1.4 nm tobermorite and jennite structures, in which the infinite chains of dreierketten are degraded by omission of some bridging tetrahedral. Chemical analysis [194] and NMR spectroscopy [86, 167] shows that the organization of the silica is in the form of linear chains of silicate tetrahedral of variable length, which most probably represents fragments of dreierketten (Figure 3.2). This seems to confirm the hypothesis that C-S-H gel contains structural elements of the layer structure of tobermorite.

Jennings proposed [108] a model in which he mentions of the two types of C-S-H, namely, high density (HD) and low-density (LD). Both types were said to be made of basic building blocks that form into globules that have two possible packing arrangements, one of the arrangements causes the formation of HD and the other of LD C-S-H. Nonat proposed [144] a surface reaction thermodynamic

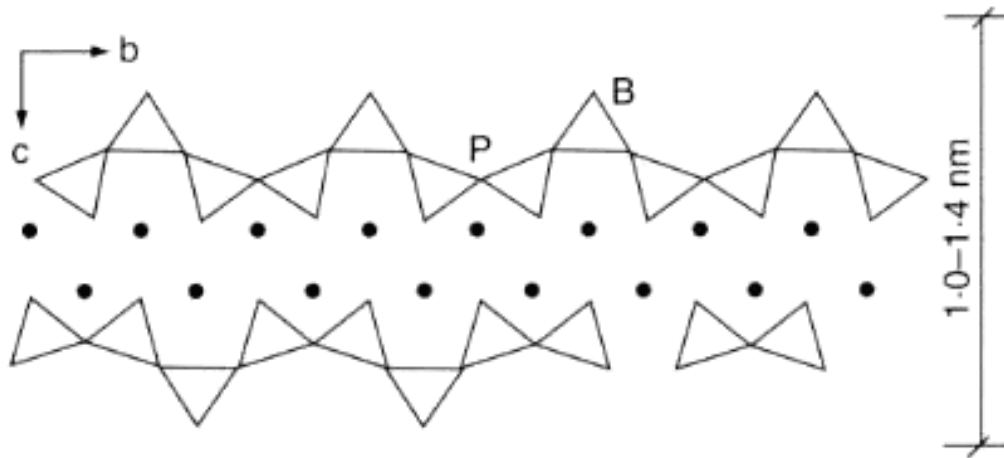


Figure 3.1: Single layer of tobermorite structure. Variable c lattice spacing could be reduced to 1.0 nm by strong drying or can have a maximum value of 1.4 nm. (●) represent Ca^{2+} ions which are coordinated to unshared oxygen atoms in the paired tetrahedral (P) which are linked by bridging tetrahedral (B) (Figure reproduced from [32, page 109])

model which takes into account the structure and the morphological properties of C-S-H. It was discussed to predict and correlate the chemical and structural evolution of C-S-H with solution chemistry. Gauffinet and co-workers [80] using atomic force microscopy state that C-S-H is an assembly of oriented nanoparticles with dimensions of few tens of nanometers.

3.3.3 Silicate polymerisation

The understanding of the polymerization of the silicate anion of the C-S-H structure sheds light on important topics such as the interactions of C-S-H with other hydrated phases, such as absorption of aluminium, and the variation of Ca/Si ratios in different cements and with age.

Generally, nuclear magnetic resonance (NMR) and chemical methods, such as the study of the kinetics of the reaction with molybdate or more commonly used technique of characterization of trimethylsilyl (TMS) derivatives, are employed to study the degree of polymerisation.

While chemical methods suggest [60, 199] that no tetrahedron (called monomer,

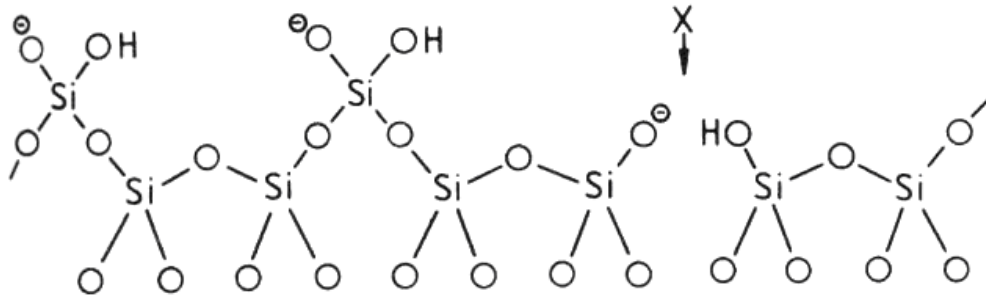


Figure 3.2: Silicate chain of the type present in tobermorite and jennite (dreierkette). The tetrahedra in the lower row are described as paired and those in the upper row as bridging. X refers to a missing bridging tetrahedron. (Figure reproduced from [202]).

SiO_4) is present within the first few hours, NMR studies [39, 172] seem to suggest that there is little monomer present which begin to decrease after a few hours. Results from both methods indicate that dimers (two attached tetrahedron, Si_2O_7) are the main constituent present within the first few hours and are later accompanied by single chains or rings of higher order polymerised silicates, called polymer. However, octomers or larger species were not found even in mature pastes [23, 39, 172, 216]. Brough and co-workers [23] concluded from their NMR data that polymerisation occurs by linking of a single tetrahedron to the dimers, converting them to higher order polymers. This seems to confirm the earlier postulate of Taylor [202], who using similar techniques hypothesized the structure of a polymerised silicate (Figure 3.2). The proposed structure shows the presence of two types of silicate tetrahedra, bridging and paired. Further, each bridging tetrahedron is shared by two paired tetrahedra; thus the presence of one bridging tetrahedron in the structure amounts to a pentamer (four paired and one bridging tetrahedra). This was further explained by stating that with the partial or complete absence of bridging tetrahedra in the structure the theoretically infinite chain is split into fragments containing 2, 5, 8, $(3n - 1)$ tetrahedra.

Various researchers have attempted to relate the degree of polymerisation with the Ca/Si ratio. Some authors [44, 89] reported an increase in polymerisation with decreasing Ca/Si ratios, however, others found no significant change in polymerisation in C-S-H with Ca/Si > 1.2 [127] or > 1.3 [46].

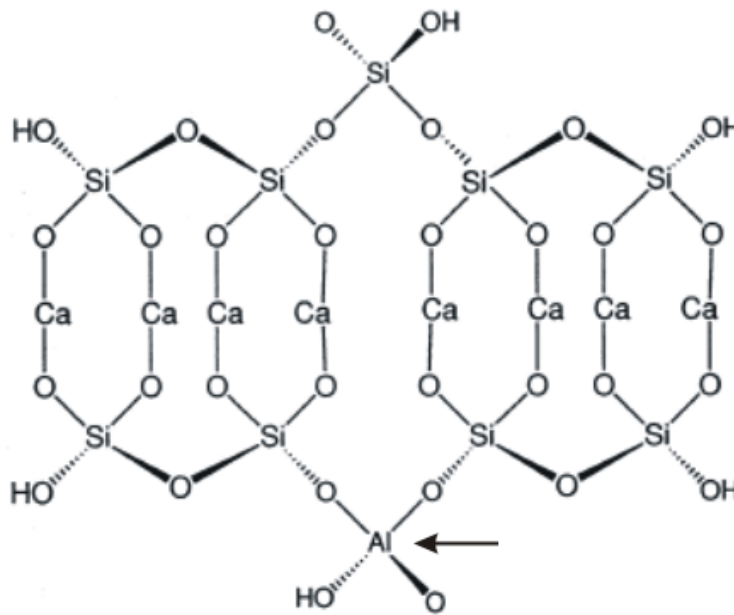


Figure 3.3: A single layer in the crystal structure for a 14 Å tobermorite. The top part shows a pentameric silicate chain of the “dreierkette” based models for the C-S-H phase. Al is shown (indicated by the arrow) to be incorporated in the bridging site of the silicate chain. Interlayer water molecules and Ca^{2+} ions are not included in this representation. (Figure reproduced from [4]).

3.3.4 Presence of aluminium

In order to study the interaction of Al^{3+} and Fe^{3+} ion with C-S-H, some authors studied mixtures of artificially prepared C-S-H or C_3S with aluminate and ferrite rich sources. Using DTA [111, 112], XRD and solution chemistry methods [33, 48], it was concluded that the ions were substituted in C-S-H and that one in six silicon atom could be substituted.

Studies using NMR and EELS have shown that this substitution is essentially limited to silicon sites of bridging tetrahedral [29, 164, 168, 169]. Experimentally the maximum level is about 0.26 [68], although the maximum theoretical level is expected to be about 0.33. TEM microanalysis seems to suggest that outer product C-S-H has a higher Al/Ca ratio compared to the inner C-S-H [169].

Recent studies [4–6, 195] confirm that Al in 4-coordination (Al[4]) occurs on the bridging tetrahedra of the dreierkette (Figure 3.3). However it was also found [4, 195]

that Al can also occur in 5- (Al[5]) and 6- (Al[6]) coordination in C-S-H. Andersen et. al. [4] in their study of hydration of white Portland cement with water and in a solution of NaAlO₂, using NMR, suggest that Al[5] most likely results from Al³⁺ substituting for Ca²⁺ ions in the interlayer of C-S-H. This possibility seems to be strengthened by the findings of Sun et. al. [195] who, in their study of Al-substituted C-S-H samples using XRD and NMR, found strong evidence of the presence of a significant amounts of Al in the interlayer. It was further shown that in XRD the positions of the (hk0) peaks, which are primarily controlled by the central Ca-O sheet of the drierkette, do not change with an increase in Al concentration, thus excluding the possibility of Al occupancy of the Ca-O sheet. In confirmation with the previous studies, their NMR results showed Al[4] to be largely present on the bridging tetrahedron and no significant presence was found on the paired tetrahedra. This experimental evidence was further justified with the following arguments: (1) It is noted that the two non-bridging oxygen atoms pointing into the interlayer are less constrained than those of the non-bridging oxygens of the pairing tetrahedra, which are coordinated to the calcium atoms of the constrained central Ca-layer. Now since Al[4]-O bonds are about 0.1 Å longer than Si-O bonds, the Al[4] substituted tetrahedron will have more space to fit into at the bridging than at the paired sites. (2) There is also the question of charge balance when Al[4]³⁺ substitutes Si⁴⁺. If Al[4] were to substitute the paired tetrahedra, then the only location for additional positive charge on nearest neighbor positions will be in the main layer (Ca-O sheet) and Al³⁺ for Ca²⁺ substitution there would provide this charge. This Ca substitution by Al is ruled out by the XRD data as explained earlier (no change in (hk0) peaks). However, the non-bridging oxygens of the bridging tetrahedra, that are surface sites or on the walls of the interlayer space, can be coordinated to additional charge balancing alkali cations (e.g. H⁺ to form OH⁻ groups).

Since most of the above mentioned studies were carried out on mature pastes and not always on OPC, in this thesis chemical analysis using TEM is employed to identify the presence of aluminium in C-S-H at early ages of hydration of OPC and to understand the form in which it may be present.

3.3.5 Sorption of sulfate ions

Unlike aluminate or ferrite ions, sulfate ions are not expected to substitute for silicon in C-S-H, as the $\bar{S} - O - Si$ bonds are likely to be easily hydrolysed. Instead sulfate ions are believed to be adsorbed [53, 146] and this adsorption was found to be reversible [64]. Barbarulo and co-workers [8] found that the capacity of C-S-H to bind sulfate seems depend on its Ca/Si values and is independent of temperature. This seems to strengthen the findings of Bentur [19] who reported that beyond 50% hydration of C_3S (in mixtures of pure C_3S and gypsum) the C/S ratio tends to increase with increase in gypsum content. Barbarulo and co-workers further reported that when ettringite and C-S-H are placed together in solution, ettringite dissolves partly and the released sulfate is bound to the C-S-H. With rise in temperature ettringite solubility increases resulting in an increased concentration of sulfate ions in solution, which subsequently gets adsorbed on the C-S-H. Thus, temperature seems to have an indirect effect on the binding capacity of C-S-H with respect to sulphur in the presence of ettringite.

3.3.6 Chemical composition of C-S-H

C-S-H in cement is known to adsorb considerable quantities of impure oxides to form solid solutions [49, 111]. It has been estimated [49] that nearly half of total sulfate, alumina and iron present in the cement is found in C-S-H rather than in AFt and AFm phases. The composition of C-S-H gel is therefore quite variable depending on the extent of substitution. Chemical analysis using SEM [22, 61, 159] and TEM [164, 165, 169, 203, 204, 209] show a large variability of composition from point to point and particle to particle. Inner product is known to have a relatively constant composition, suggesting a pure C-S-H phase [203, 204] free of any foreign ions. Outer products analyses tend to lie along lines between Ip and hydrate phases such as AFm, AFt and CH. This suggests that in Op, C-S-H gel is mixed with other phases. According to these studies C-S-H has compositional ratios of Ca/Si ~ 1.7 – 2.1 , Ca/Al ~ 20 – 30 , Ca/ \bar{S} ~ 25 . The microanalyses indicate that most chemical species are distributed widely throughout the matrix.

3.3.7 Ca:Si ratio at early ages

The question of Ca/Si ratio in solution at early ages (few minutes) is important and likely to give vital information on the dissolution of C_3S . The Ca/Si ratio in solution at early ages is reported to be strongly depend on w/c [130], and time. Electron Spectroscopy for Chemical Analysis or ESCA was thought to be a powerful tool in finding the Ca/Si ratios and other important information on the chemistry of the first hydration products. This high-vacuum technique measures the composition to a depth of only $\sim 10 \text{ \AA}$, but averaged over a large area, while changes in binding energy can also be detected by measuring the energy shift of ESCA peaks. However, in order to measure Ca/Si of initial hydration product, they should represent a continuous C-S-H layer whose thickness exceeds the depth that ESCA can measure. In the case of partial surface coverage, which is the case within first few minutes of hydration, the precipitated superficial phase would have a lower Ca/Si value than actually observed.

Few authors [132,160,189,210] have attempted to analyse the surface of C_3S after very short periods of immersion in water. It was found that the binding energy of some oxygen atoms increases slightly after wetting and also that even fresh anhydrous C_3S samples show signs of surface hydration (which had to be removed by sputtering). The apparent Ca/Si ratio versus hydration time curves show an initial dip to about 2.0–2.5 from 3.0 of the non-hydrated material within a few seconds, followed by a brief increase to about 2.7–2.8, followed again (after about 1 min) by a slower but steady decrease, to values < 2.0 . This decrease can readily be explained on the assumption of a steadily increasing thickness of a low Ca/Si hydrated layer. Thus ESCA work supports the concept that a fairly uniform coating of some kind (with, $Ca/Si \ll 3$) develops within the first 10 min. However, at very short times the thickness of the hydrate layer formed at the surface is likely to be $< 10 \text{ \AA}$, thus the data (high Ca/Si values) obtained by this method at this stage may not reflect the exact composition of the hydrated material, but are likely to be influenced by the underlying C_3S grain.

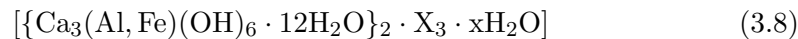
Yet another technique called Secondary Neutrals Mass Spectroscopy (SNMS), in which the composition of a surface region only about three atomic layers thick can be analysed, can be used to investigate the chemistry of very early age hydration products. Using this method, the formation of a hydrate layer with a very low

Ca/Si molar ratio was observed in the initial period of hydration with excess water [50].

SEM studies show the rapid precipitation of a few isolated globular particles which is completed within the first minute [189]. After that, the surface becomes progressively damaged by selective pitting on certain crystal faces [81, 132, 145]. The initial surface hydrate layer detected by ESCA can be expected to be fairly homogenous and uniform in thickness over the surface, so as not to be visible by SEM. At later stages, more evolved morphologies are observed; such as thin flakes or foils of C-S-H which are seen to develop and grow rapidly at the surface forming honeycomb-like structures [81, 132, 145] or an oriented fish scale morphology [79]. Similar morphologies have been detected by TEM observations in a ‘wet-cell’. In the TEM studies of Henderson and Bailey [101] the initial surface hydrates were found to have a wide range of CaO/SiO₂ compositions, consistent with rapid and variable rate of dissolution of Ca²⁺ ions from only specific reactive surface sites. The very early surface hydrates appear disordered on a 1 nm scale. At later ages these become heterogeneous, with more structurally ordered sheer-like fragments and regions developing within the disordered regions. At 30 minutes hydrates observed within the first 10 and 40 nm of the surface have compositions ranging from anhydrous silica up to Ca/Si = 1.2

3.4 AFt phases

They are characterized by the following general formula:



where X represents one formulae unit of a doubly charged, or, with reservations, two formulae unit of a singly charged anion; and $x \leq 2$ [205, Chapter 6].

Ettringite $\{\text{X} \rightarrow \text{SO}_4^{2-}\}$ is the most important AFt phase, since a phase of or near this composition is formed during the early hydration of cements. It generally forms as thin prismatic crystals of hexagonal cross-section, with high (> 10) aspect ratios.

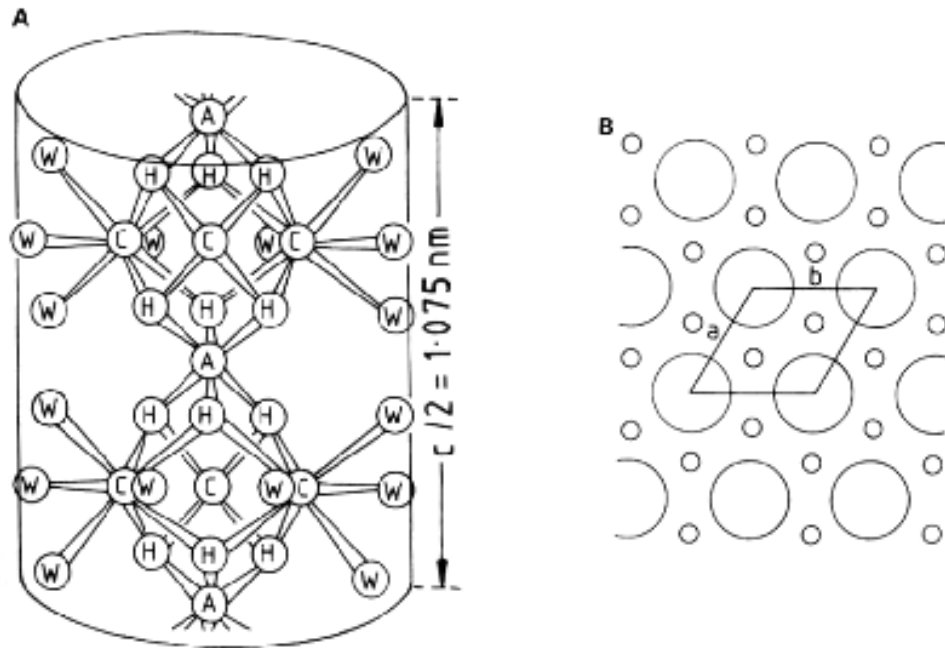


Figure 3.4: Crystal structure of ettringite. *Left*: Part of a single column in $(1\bar{1}20)$ projection; A \rightarrow Al, C \rightarrow Ca, H \rightarrow O of an OH, W \rightarrow O of an H_2O molecule. *Right*: Projection on the ab -plane, showing columns (large circles) and channels (small circles which indicate sulphate ion positions); the unit cell, with $a = 1.123$ nm. (Figure reproduced from [205, page 167])

3.4.1 Crystal structure

The crystal structure of ettringite is based on close-packed columns of composition $[\text{Ca}_3\text{Al}(\text{OH})_6 \cdot 24\text{H}_2\text{O}]^{3+}$ running parallel to the long (c) axis of the crystals. In the channels between the columns are charge balancing SO_4^{2-} and additional molecules (Figure 3.4).

3.4.2 Solid state substitution of aluminium by iron

Studies have shown that SO_4^{2-} can be partly or fully replaced by OH^- [137, 154], CO_3^{2-} [154], CrO_4^{2-} [18, 31] ions. Solid solutions of ettringite with Fe^{3+} , Mn^{3+} , Ti^{3+} , Cr^{3+} in place of Al^{3+} have also been reported [17, 31, 193]. In the above reported cations, iron is the chief element present in Portland cement. However,

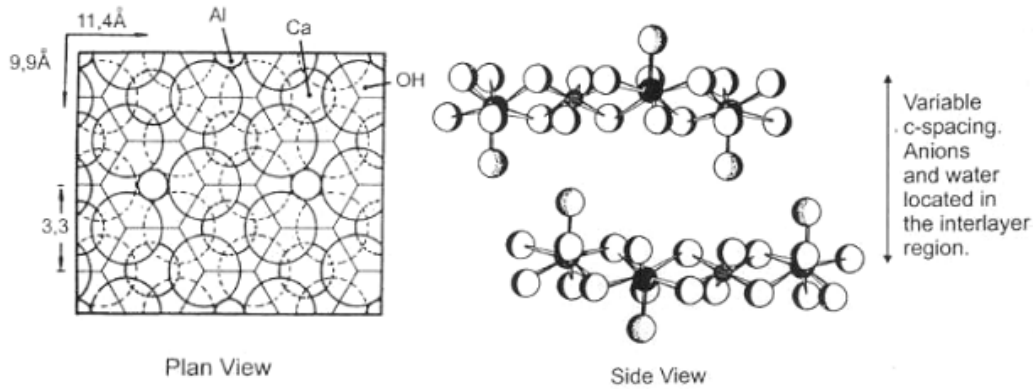
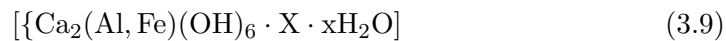


Figure 3.5: Crystal structure of AFm. In side view filled circles are Ca^{2+} , hatched circles Al^{3+} , and open circles OH^- (Figure reproduced from [78, page 106]).

very little work has been done to identify when and how much aluminate in AFt is replaced by iron. It is believed that an investigation in this direction could help to identify the degree of hydration of the ferrite phase and its consequences on the reactions mechanisms.

3.5 AFm phases

They are characterized by the following general formula:



where X denotes one formula unit of a singly charged anion, or half a formula unit of a doubly charged anion. The range of anions that can occupy the X sites is relatively more than for AFt, prominent amongst which are SO_4^{2-} , OH^- , CO_3^{2-} .

3.5.1 Crystal structure

Monosulfate or monosulfoaluminate $\{\text{X} \rightarrow \text{SO}_4^{2-}\}$ is a common AFm phase found in Portland cements hydrated under normal conditions. There are no accurate methods for determining AFm phases in cement pastes mainly due to the low

degree of its crystallinity. Determination of AFm phase by quantitative X-Ray diffraction is only semi-quantitative [148].

3.5.2 Solid state substitution of aluminium by iron

Iron analogues of AFm phases have been reported in the literature. [120, 176]. C_4FH_{13} has been obtained by many investigators [173, 176] and is known to form a continuous series of solid-solutions with C_4AH_{13} [176]. There are several anions which are reported to substitute for sulfate in monosulfate.

This study attempts to give an estimate on the amount of solid state substitution between Al and Fe in ettringite and monosulfate phases and on the time at which the substitution begins. Further, the question of Al, Fe substitution in C-S-H within few hours of hydration, if any, is addressed.

3.6 Hydration of tricalcium silicate

Tricalcium silicate is the main and the most important constituent of Portland cement, which to a great extent controls its setting and hardening. It is widely recognized that there are some differences between the hydration kinetics of C_3S and Portland cement mainly due to the interactions with the other reacting compounds. Nevertheless, these differences can be considered to be perturbations on the C_3S -water system, which do not greatly change the fundamental reaction mechanisms. Thus studies of pure C_3S -water mixtures have given valuable insights into the hydration of Portland cement, although there continues to be considerable difference of opinion amongst the authors concerning the mechanism of hydration [76, 106, 129, 185, 203, 206].

Stage 0 is the initial fast reaction, where, upon contact with water, calcium, oxide and silicate ions in the surface layers of the anhydrous phase pass rapidly into solution, presumably as simple hydrated ionic species [78]. Initially the Ca_{aq}/Si_{aq} molar ratio is 3 : 1, indicating a congruent dissolution of C_3S [147]. However, seconds after mixing, relatively high silicate concentrations are observed which are found to decrease quickly to low values [198, 217]. Ca^{2+} concentration, however, continues to increase [12, 27, 55, 197, 206, 215, 217]. This step appears to be a

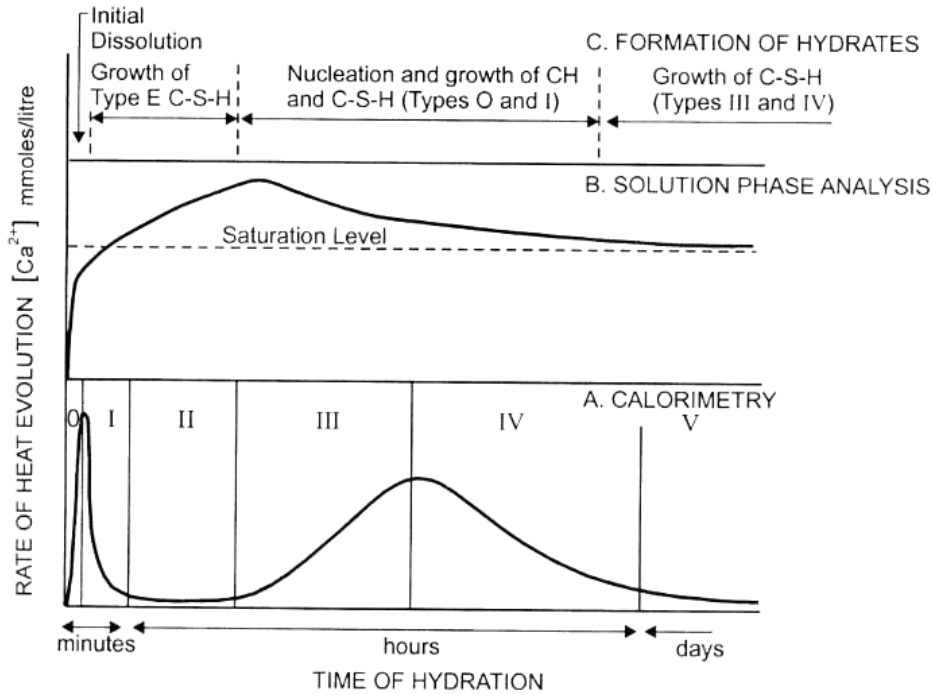
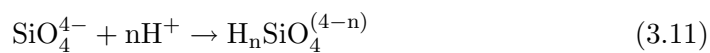


Figure 3.6: Schematic representation of changes during the hydration of C_3S pastes ($w/c < 1.0$) (Figure reproduced from [78, page 106]).

protonolysis of the silicate and oxygen ions at the C_3S surface, followed by a congruent dissolution of the material [12,55,90]. The O^{2-} ions present originally in the C_3S lattice enter the liquid phase as OH^- ions and SiO_4^{4-} ions as barely dissociated H_4SiO_4 . These steps can be expressed by the following chemical equations:



Damidot and Nonat [58] used dilute solutions to lengthen the early reaction period and resolve them clearly. However, even at high w/c the initial dissolution rate is not properly resolved by calorimetry. This proves that the dissolution of C_3S is strongly inhibited at all times after the first rapid dissolution.

Once the mean concentrations of calcium and silica in the solution reach a critical

solubility product, called *maximum supersolubility* [9, 11, 13, 131], nucleation and precipitation of an initial product occurs. It is this transition that appears to terminate the initial fast reaction, since the surface of C_3S becomes altered in such a way as to be less reactive. This marks the onset of the first deceleration period—**stage I**. Some researchers proposed the concept of the *superficially hydrolysed* layer, C_3S_{sh} [10, 131] which is a charge-separated transition state on the surface that is expected to occur if the first step in the hydrolysis is protonation of O^{2-} , SiO_4^{4-} to give OH^- and $H_3SiO_4^-$ respectively. This results in a protonated C_3S surface, with a net positive charge. Some authors do not seem to agree with this concept [78] and recent work shows the surface charge of C_3S in dilute suspension to be negative [141], rather than positive. Solubility studies based on very dilute suspensions [57] seem to indicate the presence of a so called associated path, on which the calcium and silica concentrations decrease from the curve of maximum supersolubility to a curve for a slightly lower solubility product. It was believed that this associated path is the solubility curve of a C-S-H *coating* which forms on the surface of C_3S as proposed by Jennings [107]. Gartner [77] proposed that this coating is in a metastable state and it would exist in some kind of pseudo-equilibrium with the solution during this period. This is in line with the results obtained by Groves [87] who examined thin sections of cement clinker in TEM and reported the presence of hydrate gel coatings around alite even after 5 minutes of immersing the clinker in water. Thus one school of thought believes in the existence of a protective coating of C-S-H. However, there exists another school of thought which disagrees with the concept of a protective coating of C-S-H around C_3S grains. Further, it is argued that C-S-H nucleates around C_3S according to the phenomenon of homogeneous nucleation [75]; that it forms as agglomerates of nanoparticles and grows either parallel or perpendicular to the tricalcium silicate surface, and whose rate of growth depends only on the lime concentration of the solution [82].

In the presented work, attempt is been made to directly observe in a TEM the presence or absence of a coating on cement grains.

The plateau in the idealized heat evolution curve (Figure 3.6) is called the induction or dormant period and represents the **stage II**. It, however, does not tantamount to ceasing of the chemical reaction. It has been shown [28] that there is no true induction period, but merely a period of slow reaction rate and consequently low

heat evolution. Calcium and hydroxyl ion concentration continues to increase and exceeds the theoretical saturation level of portlandite. C-S-H continues to develop on the C_3S surface [206], but the total degree of hydration by the beginning of hydration period (Stage III) is only 0.1–1%. A maximum saturation factor (defined as the ionic activity product for the relevant solid, divided by its value at saturation) of well over two with respect to portlandite is reached before it begins to crystallize at a significant rate. At about the same time as the crystallization of CH begins [217], a new C-S-H morphology (Type 0) can often be observed [109]. It is interesting to note the often close correlation between the onset of the acceleration period, the formation of crystalline CH, and the formation of the above mentioned new type of C-S-H. This led some researchers to believe that it was the rapid removal of CH from solution at that point that drove the renewed acceleration of the reaction [217]. This was later found to be untrue; instead addition of crystalline CH often retarded the onset of the acceleration period (stage III). High concentration of silica was thought to poison the growth of CH [198, 217] and it was expected that a renewed growth of CH would only occur either when the silica concentrations fall to very low levels or CH supersaturation becomes much higher.

Along with the crystallization of portlandite theory, there was another theory based on the growth of C-S-H [191]. This theory said that it was the nucleation and growth of a more stable form of C-S-H that caused the acceleration. Some reports [107] seem to agree with this theory. Others [76] postulated how the conversion of the metastable surface coating [C-S-H(m)] to a more stable form of C-S-H [C-S-H(s)] by a nucleation and growth process could give rise to the observed reaction kinetics of stages II and III. It was further suggested that the initial number of nuclei of C-S-H(s) is directly proportional to the total amount of C-S-H(m) precipitated during stage I. This helps to explain as to why there is no true induction period. The argument of the C-S-H(s) nuclei seems to be strengthened by findings, where the addition of artificially prepared C-S-H in C_3S solution shorten the apparent induction period, resulting in very early transition from the first deceleration (stage I) to the acceleration period (stage III) [76]. The study on dilute suspensions show that the rate of formation of C-S-H increases well before the onset of rapid CH crystallization. Damidot and Nonat [56, 57] proposed a theory, similar to that by Gartner and Gaidis [76], to explain this result. They also mention two types of C-S-H which they called C-S-H(SI) and C-S-H(SII),

stable at CH concentrations below and above about 20mM respectively. C-S-H(SI) is said to be the initially formed product, which becomes metastable and gives way to the nucleation and growth of C-S-H(SII). It is the conversion which controls the kinetics. The dissimilarities between the theories of Damidot/Nonat and Gartner/Gaidis lie in the details of the structure and composition of the two types of C-S-H. Despite these differences, Damidot and Nonat mention an interesting point which is worth noting. They stress the need in their model for a high lime concentration in solution, close to that of CH saturation, for the onset of a phase transition from C-S-H(SI) to C-S-H(SII), at the same time as permitting an acceleration period in overall hydration. This way, their theory seems to form a correlation between the ‘CH nucleation’ and ‘C-S-H nucleation’ theories.

Within first few hours of hydration **stage III** or the acceleration period begins, by which time less than 1% of C_3S is hydrated. However, by the end of this stage, typically at about 5–10 hours, almost 30% of C_3S is consumed. In a study using very dilute suspension [79], in which the CH concentration in the liquid phase is initially adjusted to a desired value and then kept fairly constant, C_3S hydration profiles were observed to be sigmoidal and considerably dependent on initial CH concentration in the solution. This indicated a growth process starting from a relatively small number of nuclei formed at the very beginning. It was further found that at low CH concentrations ($[CH]$), C-S-H precipitation, indicating hydration of C_3S , occurs earlier and at lower degree of hydration, while at higher $[CH]$ it occurs later and at higher degree of hydration. It was proposed that this could be due to the changes in morphologies of C-S-H with the change in $[CH]$. Further, computer modeling studies [145] were done to estimate any possible changes in size of C-S-H, with varying $[CH]$. It was concluded that the apparent early end of the acceleration period was due to the preferentially laminar growth of the C-S-H parallel to the C_3S surface which led to earlier onset of diffusion control. This dilute suspension study clearly demonstrated that the kinetic curve is similar in shape for a wide range of $[CH]$, whereas only the actual values of rate with degree of hydration change.

Electron microscopy [109] and atomic force microscopy [80] studies on **stage IV** show that a dense layer of C-S-H forms around the hydrating C_3S grains at around the onset of this stage. This dense layer is believed to bring into effect the diffusion controlled hydration process which retards the fast dissolution of C_3S , thus causing

this second deceleration period. [78]

The final slow reaction (**stage V**) is marked with the growth of portlandite crystals and densification of C-S-H, without having any major fundamental differences in mechanisms from stage IV. CH crystals continue to grow larger, filling large water-filled voids, often engulfing zones of C-S-H and hydrating C_3S , thereby limiting their potential for complete hydration. C-S-H, on the other hand, continues to densify due to limited empty space available. It has been suggested [209] that the hydration at this stage is at least partially *pseudomorphic* and this seems to be confirmed by the finds of alite like relics in the microscopic observations [22, 26]. Based on the estimates, it appears likely that this stage involves a small migration of calcium and silicon ions, which consequently seem to prove the hypothesis that the rate limiting process is the process of diffusion, possibly of one of these ions through the hydrating coating. Further there is evidence that Ca^{2+} is the more mobile of the two species [78]. It is important to note that since there is a growing overlap of the hydrating coatings of neighbouring grains there is much less empty pore space. This means that the atoms have to travel a larger effective diffusion distance from the point of their obvious origin, the grains, and the water filled pore space in which C-S-H and CH get deposited.

3.7 Hydration of tricalcium aluminate in the presence of calcium sulfate

Studies [42, 177, 190] using calorimetry, electron microscopy, XRD and TG have shown that this reaction occurs in three stages, two of which are strongly exothermic.

The first stage is characterized by a peak in the heat evolution curve during the first 30 minutes. Minard [140] shows that this first peak is due to the formation of AFm. This is followed by the second stage, which is a period of steady heat evolution whose duration increases in the presence of $CaSO_4$ or K_2SO_4 [187]. This is possibly due to steady ettringite formation, most likely by a diffusion process. The third stage is marked by a peak typically occurring at 24–48h, in which C_3A and ettringite reacts further and AFm phases are formed. The ideal reactions are

given in equations 3.3 and 3.4 on page 37

Ettringite forms as long as sulphate ions are available for reaction. Once the gypsum is consumed, ettringite reacts to form monosulfoaluminate. Since ettringite is usually detected at the surface of the C_3A , rather than on the gypsum particles, some researchers [177] have proposed that ettringite forms a continuous coating on the reacting C_3A surface which impedes the diffusion of other ions, thus slowing down the reaction and resulting in an induction period. Induction period is found to lengthen by increasing the gypsum content and the kinetics of ettringite formation indicates diffusion control [26,155]. When the liquid phase of the hydrating system becomes deficient in Ca^{2+} and SO_4^{2-} ; the protective coating is disrupted, which results in the renewed hydration of C_3A to form AFm phases.

Skalny and co-workers [187,197] mention that C_3A , upon contact with water, dissolves incongruently, leaving an aluminum-rich layer on the surface. Calcium ions adsorb on this surface, giving a positive charge to the surface. The formation of such a structure appears to minimize the active dissolution sites, resulting in a decrease of the dissolution rate of C_3A . In the presence of $CaSO_4$ or K_2SO_4 the dissolution was found to impede further. From their dissolution and electrokinetic data they concluded that the negatively charged sulfate ions adsorb on the positively charged C_3A particles, resulting in further reduction of the dissolution sites — a conclusion reported earlier [69], which would otherwise be available for hydroxyl ions to catalyze the dissolution. $CaCl_2$ or $NaCl$ did not influence the positive surface charge significantly. This led them to conclude that the observed effects of calcium and potassium sulfates are a result of the specific actions of the sulfate ions.

Colleparidi et al. [42] disagree with the above conclusion because Na_2SO_4 does not have the same retarding effect as gypsum.

3.8 Hydration of the ferrite phase

The reactivity of the ferrite phase is known to decrease as the iron content increases [24,143]. Nevertheless, the hydration products of phases in the series are essentially similar to those formed from C_3A under comparable conditions [36, 43, 103, 158, 173, 200]

When gypsum is present, the hydration sequence for the ferrite phase is the same as for C_3A (equations 3.5 and 3.6 on page 37). Iron substituted AFt first forms and later converts to AFm when gypsum is exhausted. An amorphous phase, presumably aluminum-substituted $Fe(OH)_3$ is also formed. Disproportionation of iron between the crystalline and amorphous phases is observed here too, and could be attributed to the low mobility of iron. The formation of iron rich pseudomorphs of the original C_4AF grain has been observed both in pure systems [72] and in Portland cement [181]. Some researchers have concluded that C_2AH_8 or alumina gel precedes the formation of AFt in the C_4AF –gypsum system and the early AFt contains little or no Fe^{3+} [25]. It has been reported that conversion of ettringite to AFm phases could occur even in the presence of gypsum and also at very low w/c ratios and higher temperatures. Thus it is believed that in such cases AFm phases did not necessarily result from reactions involving ettringite [158].

Due to similarities in the hydration of C_3A and C_4AF , they could be expected to compete for gypsum during the course of hydration of Portland cement. Some authors have studied the hydration of mixture of C_4AF , gypsum with varying additions of C_3A [103]. It was observed that the reaction of C_3A and ettringite to AFm occurred sooner, depending on the amount of C_3A added. Ettringite is formed more rapidly indicating that C_3A competes more efficiently for sulfate ions. Once depletion of gypsum occurs, which happens earlier in the presence of C_3A , C_4AF reacts to form monosulphoaluminate.

3.9 Role of calcium sulfate at ambient temperature

Addition of calcium sulfates to clinker is one of the most important technological parameters in the manufacture of Portland cement. They are added (about 5 wt.%) to control the rapid reaction of C_3A hydration (*control of set*). They also influence volume stability and play an important role in the acceleration of alite hydration in cement [19, 49, 104, 105, 126], thus influencing the rate of strength development and volume stability. During the acceleration of cement hydration (stage III) calcium sulfate dissolves and the SO_4^{2-} ion concentration begins to decline due to the formation of ettringite and sulfate adsorption on C-S-H.

It is believed that the course of early reaction is dependent more on the rate at which ionic species are made available at the cement surface, rather than on the amount of sources providing sulfate and aluminate ions. For CaSO_4 the rate at which Ca^{2+} and SO_4^{2-} ions are made available for reaction would depend, in addition to the amount, on the physical and chemical form (order of rate of dissolution: hemihydrate > gypsum > anhydrite), particle size distribution and spatial distribution in the hydrating matrix. Tang and Gartner [201] have shown that intergrinding of gypsum is much more effective in achieving a particular property than addition by blending. This is probably because the inter-particle spacing between calcium sulfate and other species is reduced more in intergrinding than in blending, rendering the sulfate more easily accessible to other phases during hydration.

It is suggested that the presence of C_3A and soluble sulfates extends the acceleration period [7] but soon after the diffusion process begins, the rates become slower than in the C_3S system. Generally in Portland cements enough sulfate is present to extend the period of low reactivity of C_3A well beyond the first day, thus very little C_3A hydration occurs by the setting time of OPC (~ 6 hours). However, this expected period of low reactivity of C_3A is found to be considerably shortened, thus causing the C_3A hydration to renew much earlier than expected. Kanare and Gartner [114] have, in an attempt to explain this, interestingly suggested that it was necessary to assume that calcium sulfate was ‘significantly adsorbed or, possibly, physically entrapped’ by the C-S-H and could not be available to retard the C_3A hydration for the expected period of time.

Thus it is evident that several aspects of calcium sulfate in cement hydration are known. However, its role in the hydration of interstitial phases, and thus of cement, during the early hours, needs to be further understood

3.10 Hydration of Ordinary Portland Cement (OPC)

The practical viability of cement as a construction material is due to its abilities of the existence of a period of workability, then setting, hardening and strength

development. The setting process is the consequence of a change from a concentrated suspension of flocculated particles to a viscoelastic solid skeleton capable of supporting an applied stress, and can be monitored by rheological measurements. The continued development of the solid-skeleton is called hardening — a physico-chemical process, which leads to the development of mechanical properties.

This versatile nature of cement paste is due to a series of chemical reactions between the clinker phases and the added gypsum in presence of water. However, as learned in the preceding sections, the hydration processes of individual clinker phases are rather complex in themselves. Thus, it is to be expected that the hydration of their chemical mixture, in the form of cement, is even more complex. However, the general principals are the same: the dissolution of anhydrous phases leads to the precipitation of much less soluble products, typically colloidal and micro-crystalline hydrates that form the hardened paste.

3.11 Shell formation

In order to establish the structure-property relationships of cement based materials, it is essential to understand and appreciate the architecture of the microstructure of the cement paste. In this context, one of the most prominent features of the microstructure of Portland cement is the precipitation of the hydration products in a separated *shell* like manner around the reacting cement grains. Such grains are named after the discoverer as Hadley grains [95] and are further illustrated as follows.

In the 1970's, Hadley observed in fractured cement samples the presence of hollowed shell of hydration products. The youngest specimens examined were one day old, which had marked presence of the shells. It was further observed that by 3 days, there was no appreciable filling of the void between the shell and the grain, instead the hollowing out process seemed to continue from 1 to 3 day old samples. The appearance of hollow shells was clearly seen in 14 day old cement pastes and finally, even in specimens 28 days old, Hadley found the presence the hollow-shell grains. Interestingly, the shells were seen to have acicular crystals, projecting into the empty space inside the shell. These crystals were thought to be ettringite and were about 1 μm long, suggesting that the shell was not originally entirely hollow

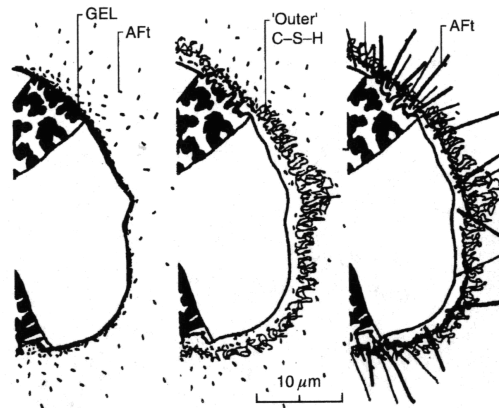


Figure 3.7: Summary of microstructural development around a cement particle showing development and fitting in of a shell, *from left*: 10 minutes, 10 hours, 18 hours (*Figure reproduced from [180]*).

and a gap of at least this size existed between the shell and the unhydrated core.

Interestingly, prior to these investigations, SEM micrographs from various studies [128, 214] of fractured cement samples showed the presence of hydrated shells. However, they were often interpreted, incorrectly, as places where residual unhydrated cores have been pulled out during fracturing of the specimen.

It is sometimes suggested that the major cement phases may be considered to hydrate independently. This may be true in later stages of hydration when limited amounts of free water remain, in the early stages significant interaction has been found [180, 184]. This is to be expected since most cement particles larger than about $3\text{--}5\ \mu\text{m}$ are polymineralic, the distribution of the interstitial phases is particularly wide, and that initially at least through-solution processes predominate. Scrivener and Pratt [184] studied a mixture of monomineralic grains of C_3S , C_3A and hemihydrate. They reported, at one day of hydration, close contact between the C_3S grains and hydration product but gaps up to $10\ \mu\text{m}$ between C_3A grains and their hydration shells. This difference in behaviour between cement and a mixture of individual constituents indicates that the hydration process is affected by the distribution of the anhydrous phases within the cement grains. An additional factor not present in studies of the pure phases is the extensive and varied level of solid solution occurring in commercial clinkers [205, Chapter 4].

Scrivener [180] made use of a combination of several electron microscopy techniques, from wet-cell TEM to backscattered SEM imaging, to observe the hydration process from few minutes to several days and presented the Figure 3.7 (only partially reproduced) as a description of the development of microstructure. It shows the formation of alumina gel around a poly-mineralic cement grain and nucleation of short AFt rods formed due to the reaction of C_3A with $CaSO_4$, within the first few minutes. Shell formation was attributed to the growth of outer product C-S-H on AFt rod network leaving a gap of few μm between grain surface and the shell. Longer rods of ettringite are subsequently formed due to the further hydration (called secondary hydration) of C_3A . C_3S also continues to react further, forming the inner product C-S-H within the shell.

Hadley et al. studied [96] the systems of alite, alite with minor gypsum additions, and a mixture containing alite, gypsum and C_3A . They report that the hollow-shell formation is not restricted to cement per se, but occurs to some very limited extent with alite alone, and certainly with alite-gypsum and alite-gypsum- C_3A mixtures.

This claim seems to be further strengthened by the findings of Kjellsen and Justnes [117], who report the presence of hollow shells in alite and C_3S at 24 hours. These shells seem to form only in grains $< 5 \mu m$, unlike in Portland cement where even larger grains have shells around them. There was also contact between shell and remnant C_3S cores. Despite the apparent restriction of grain size for the formation of shells, these reported observations seem to challenge the previous claims [157, 206] that C_3S alone does not hydrates so as to leave Hadley grains.

Kjellsen and Justnes further claim that the hollow shell features are all filled with epoxy resin, used as part of specimen preparation, thus they have not formed from material being pulled out during specimen polishing. It is apparently not clear on the secondary electron images [Figure 3.8, *right*], which reveal the surface topography, that the empty part of the shell is fully filled with resin. Nevertheless there seems to be a small separation between the shell and alite in some instances [Figure 3.8, *left*].

Despite the apparent existence of separated or hollow shells in alite, one should bear in mind the fact that the microstructure of Portland cement paste is more complex, containing several hydration products, absent in alite hydration, inter-mixed at micron and sub micron scale. Thus the mechanisms of shell formation

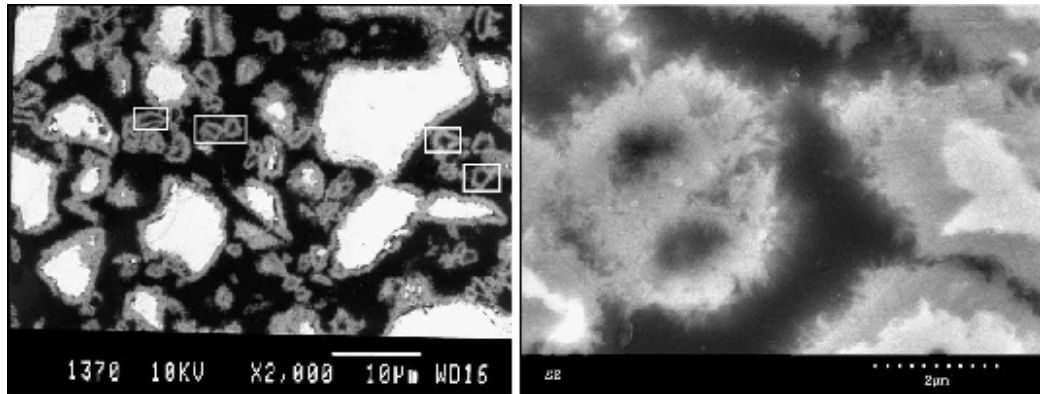


Figure 3.8: SEM images of alite and C_3S showing hollow shells. *Left*: SEM backscattered electron images of alite. *Right*: Secondary electron image of C_3S paste hydrated for 24 hours (*Images reproduced from [117]*).

in alite and OPC may be similar, but may also have important differences.

Recently, some researchers [98] have made use of 3D laser scanning confocal microscopy (LSCM), an optical microscopy technique, to obtain three-dimensional imaging of hollow shell cement grains and showed that hollow shells are connected to hardened cement paste capillary pores by channels, supporting molecular transport. However the formation of these channels was neither directly observed nor understood. It was said that they could be either naturally occurring or damage induced.

It needs to be stressed that all the work done in the past on shell formation is qualitative in nature and relies mainly on the obtained images. This is unlike, for instance, the efforts been made to unravel the atomic structure of C-S-H, which is believed to be the most important phase in cement hydration. However, similar to the nature of the hydration products, the mode of hydration — formation of a shell in the case of cements — of any chemical product is also important and should be investigated in detail. There is a need to learn more about the chemistry of the hydration products which may constitute the shell and other related microstructural features. In the presented work this is achieved using transmission electron microscopy which provides accurate quantitative chemical analysis and high resolution, high magnification imaging. This potentially provides the possibility to learn more about those aspects of the microstructure which were

either earlier thought to be less significant or completely unknown. The overall approach should help resolve some questions, if not fully explain the reasons for the phenomenon of the formation of shell around hydrating cement grains.

3.12 Review of the work done on hydration of cement using TEM

The technique of TEM often raises suspicion on the representativity of the results, given the fact that a small region—less than 1 mm—is observable in one sample. This, though possibly true, comes with a huge advantage of being able to look at single grains, their hydration phases and how they bond with each other. This is particularly useful as it is known that particles in cement pastes resist separation and dispersion even at early ages, making the study of individual particles using any other technique rather difficult. Image acquisition using TEM usually yields images of much higher magnification and resolution than is achievable by any other current technique. Accurate chemical analysis, from a region merely few nanometers across, is also easily obtained.

The potential of TEM was realized as early as 1960's when Schwiete and Niel [178] used carbon replica method to study cement hydration. They claimed that the first hydration product of Portland cement (within minutes) is ettringite. The bulk of initial work, however, was done on crushed and dispersed samples [74, 121, 122] which helped in giving an idea on the chemical composition of the hydration products but it was not possible to observe the microstructure development. Lachowski et. al. [122] studied pastes of Portland cement and clinkers using TEM and found significant variations in the composition of all the chief phases, except portlandite, in all the pastes. It is interesting to learn that at 1 day the average C/S values of the clinker samples was found to be 2.3 and 2.7, whereas that of cement was 1.9, although the range of variation of C/S values was not presented, nor was there any attempt made to explain this difference in cement and clinker values. Wide variation in atom ratios of the chief cement phases was also reported by Taylor and co-workers [208]. Dalgeish et. al. [54] prepared ion-thinned OPC samples of up to 18 hours and did some qualitative chemical analysis. The formation of shell around cement grain was reported, which was credited as partially

hollow Hadley grain. Scrivener [180] ion thinned hydrated cement samples down to 2 hours to look at the microstructure and reported the phenomenon of shell formation although no chemical analysis could have been performed. Groves et. al. [88] looked at ion-thinned mature C_3S pastes and reported quantitative chemical analysis. Thereafter, Rodger [171] also used ion-thinned samples to look in TEM. The first comprehensive study on OPC using TEM was done by Richardson et. al. [165, 166, 169] and useful insight was obtained in the evolution of the microstructure and the chemical composition of various phases and regions. The samples observed were 1 day or older and it was not possible to prepare electron transparent samples less than 1 day old.

3.12.1 Fine intermixing of hydration products

Sub-micron scale phase mixtures are readily observed by TEM. As in C_3S pastes, Ip has a compact, fine-scale and homogeneous morphology, with pores $\leq 10\text{nm}$. Mg is never detected in TEM analysis of Op [165] and remains in the Ip, thus it can be used as a chemical marker for that region. AFm particles present in the Ip have a similar appearance in the TEM and, as both phases are poorly crystalline and electron-beam sensitive, they are only differentiated from one another by X-ray microanalysis. CH is also observed in the Ip region. The inner product region thus consists of C-S-H with small amounts of all of the major phases (i.e. AFt, AFm, CH) and some minor phases; a Mg, Al-rich phase (hydrotalcite-like), and an Fe-rich phase (a poorly crystalline hydrogarnet precursor). The bonding between Ip and Op C-S-H is generally excellent, with an often poorly defined interface [169]. The Op region contains four major phases; C-S-H, CH, AFm and AFt. Of these, the C-S-H and CH are by far the most abundant. AFt typically occurs as massive crystals, often many micrometers in length. Bonding with Op C-S-H is generally good. AFm is present in mature pastes as large irregular plates similar to those of CH. AFt occurs as thin hexagonal prism needles of up to $10\ \mu\text{m}$ in length. The morphology of the C-S-H in hardened OPC is very similar to that in C_3A pastes: where it forms in large pore spaces, it exhibits *coarse fibrillar* morphology; in smaller spaces, it retains a directional aspect but forms in a more space-efficient manner (*fine fibrillar*).

3.13 Key questions

In this study ion-thinned samples down to 2 hours were successfully prepared and studied in a TEM. For the first time, images have been acquired in the dark field mode that has significantly improved the image quality in terms of resolution and contrast, even at higher magnifications. It gives a clearer view of the fine intermixing of hydration products. This has been complimented with quantitative element mapping and highly accurate chemical analysis, giving interesting insights into the early age microstructure. The following issues of the hydration of Portland cement during early ages (2–48 hours) have been addressed:

- Understanding the phenomenon of shell formation. This includes identifying any marked characteristics of the grains, if any, around which the shell forms.
- Observing shell at high magnifications to see whether they are empty as believed so far.
- Detailed and accurate chemical analysis using TEM of the hydration products in the various regions of the microstructure.
- To observe whether there is a coating of hydration products present around the grains at very young ages (2 hours).
- To help understand the cause of setting which typically occurs around 6 hours.
- To understand the role played by aluminate and ferrite phases, both in conjunction with shell formation and development of the microstructure in general.
- To observe the distribution of sulfates in various hydrating regions of the matrix.
- To observe the solid-state substitution of iron in AFt and AFm phases. This involves reporting the time about which the substitution begins and the amount of iron that substitutes aluminium in those phases.

Chapter 4

Study of early OPC hydration by TEM

4.1 Introduction

This chapter presents the findings on the hydration of Ordinary Portland Cement from 2 hours up to 48 hours of hydration. It begins with the description of the observed phenomenon of shell formation and related microstructure, then presents its observed evolution and development with time along with the associated chemistry, as found by using EDS analysis in TEM. Thereafter, the observations of the interstitial and sulfate phases are presented.

4.2 Shell formation

The phenomenon of shell formation around cement grains as reported in the past was observed. The earliest time at which a distinct shell is seen is 6 hours. No shells are observed at 2 hours.

By 6 hours shells are present around many grains. They are seen to form either partially or fully around the grains and are connected with other parts of the hydrating matrix through C-S-H. The grains having shells around them are randomly

distributed in the matrix in the same manner as the grains without any shells. A sequence of images showing the shells at various times is shown in Figure 4.1.

In conjunction with shell formation around various grains, it is also noted that the phenomenon of shell formation does not depend on grain size. However for several of the grains it appears that some parts of a shell surrounded grain react more than the other parts of the same grain (Figure 4.2). This indicates the preferential reactivity of the grains. Although shells are noted to form around grains of various shapes and sizes (Figures 4.3), closer observation indicates that in all instances it forms approximately at a fixed distance from the grain surface and can thus be imagined as a 3D surface which approximately has the original shape of the grain it encloses.

Element mapping done for samples up to 10 hours reveals that in all observed instances the shell is formed *only* around polyphase grains. Further the shell forms *only* around the silicate part of the grain and not the alumino-ferrite part. This latter observation of shell formation only around silicate part of the grains is consistently noted for *all* the observed ages (Figures 4.2a, 4.4, 4.5 and 4.6). At 6 hours, the inception of shell formation is observed as well (Figure 4.4) which occurs around the silicate part of the grain.

Magnified views of the shell (Figure 4.7) reveal that unlike believed in the past, the shells are not empty but are filled with a *flimsy* C-S-H rich product which connects the shell and the grain surface. Due to a lower grey level of this flimsy product it is likely to have a lower density than the shell or the C-S-H outside the shell. Secondly, these images reveal ridges on the surface of grains which are nearly $0.6 \mu\text{m}$ deep at 12 (Figure 4.8) hours and $1 \mu\text{m}$ by 24 hours. This indicates preferential reaction along certain planes and it appears that the reaction of cement grains proceeds by the inward movement of a reaction front.

At 24 hours, several ettringite needles are seen growing from the shell inwards (Figure 4.9). This seems to indicate of the renewal of the reaction of the aluminate phase, which showed the first burst of reaction within first few hours in the form of short ettringite needles. This observation of the apparent second burst of aluminates at 24 hours is discussed in greater detail in later sections (section 4.3). At the same age several belite particles are seen present within the shell which were most likely to have been left over due to their slow reaction rate (Figure 4.10).

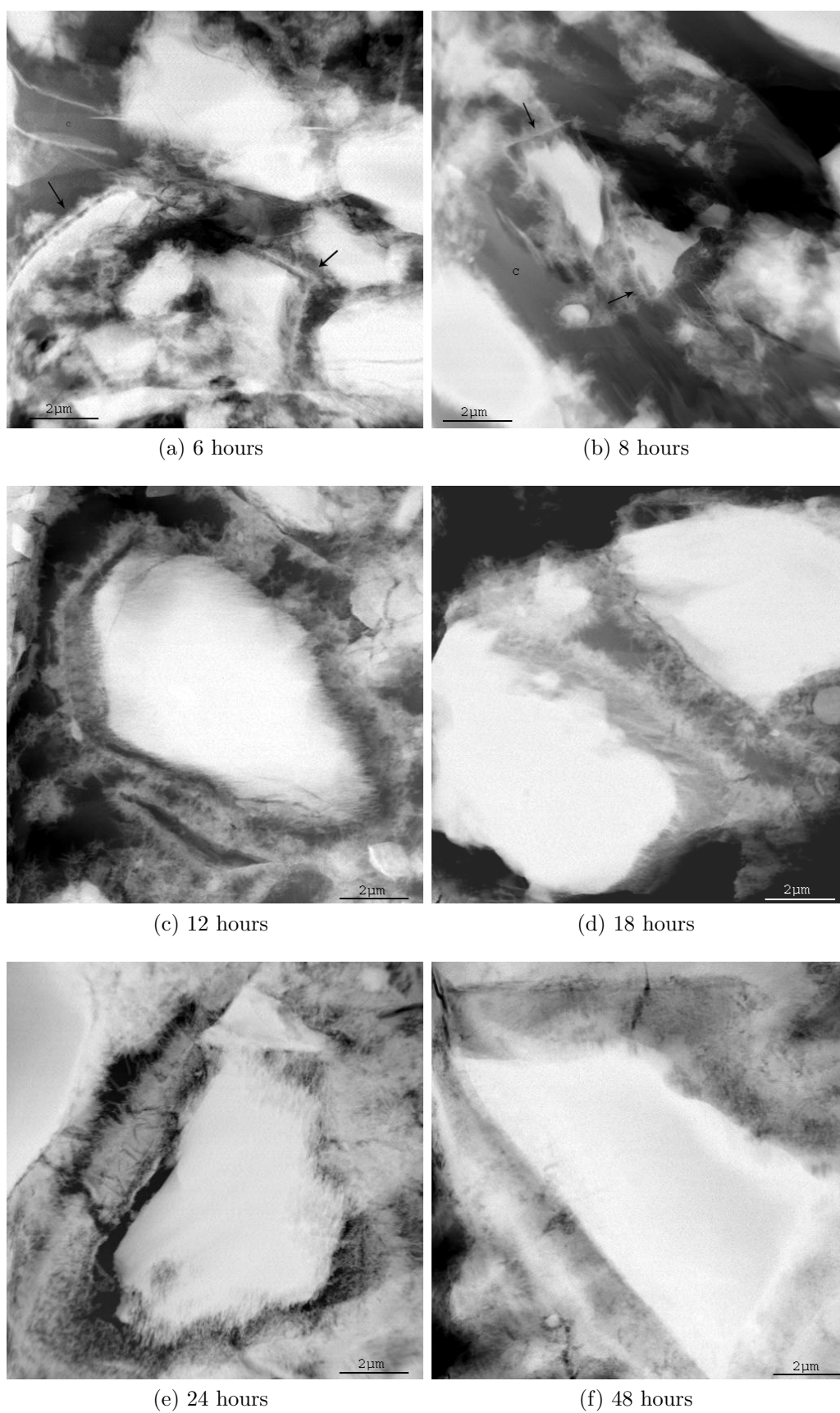


Figure 4.1: Dark-field TEM images: shell formation around grains at various ages (C → carbon-coating)

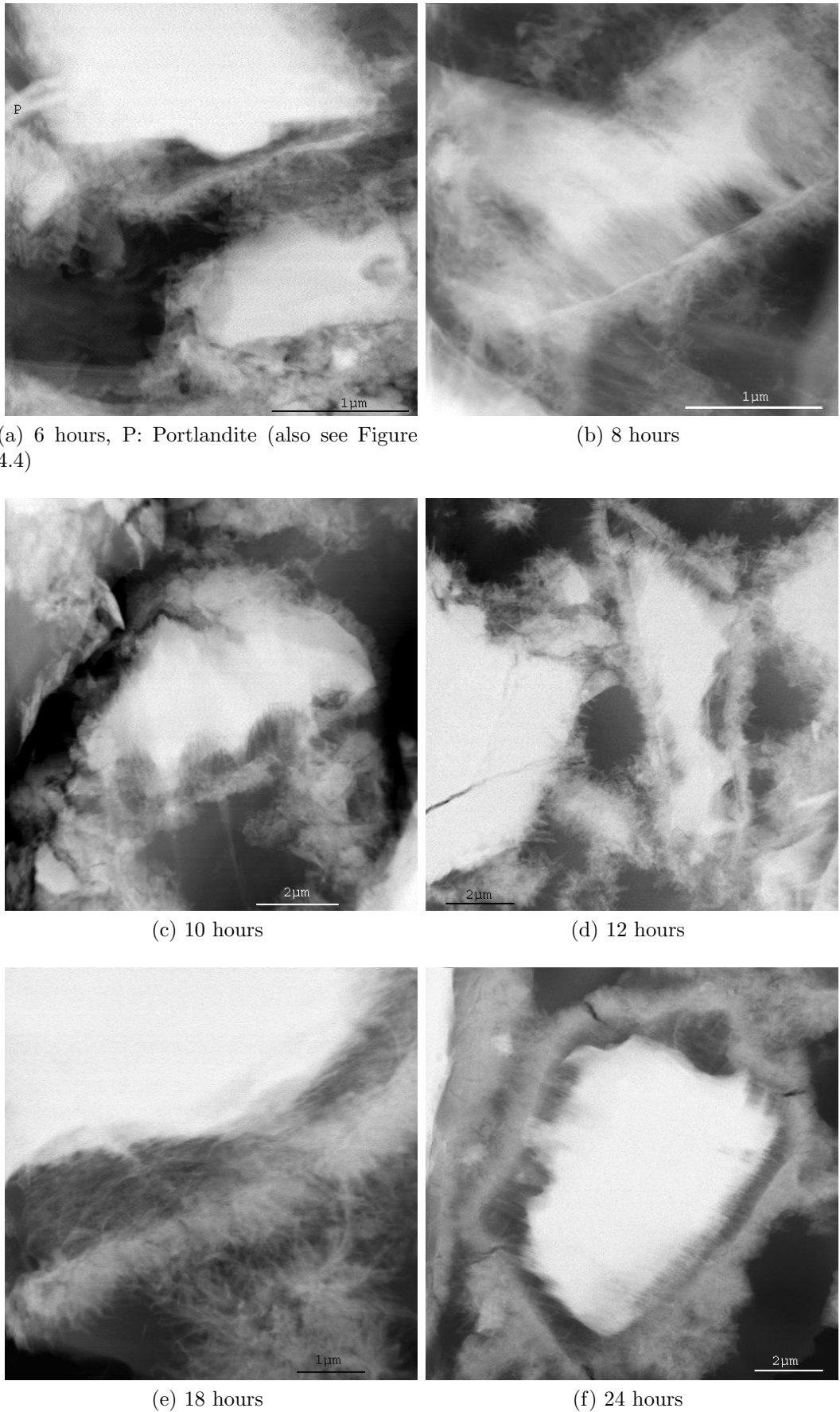
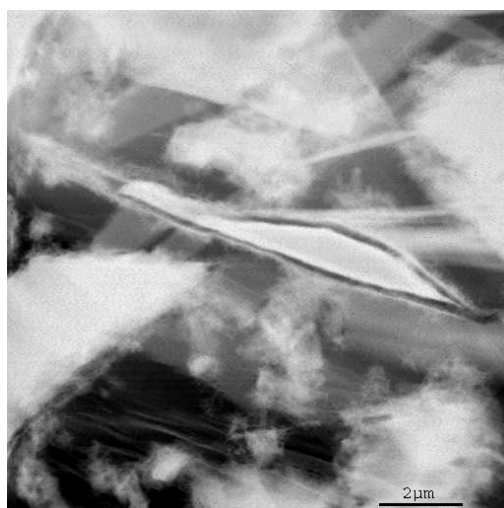


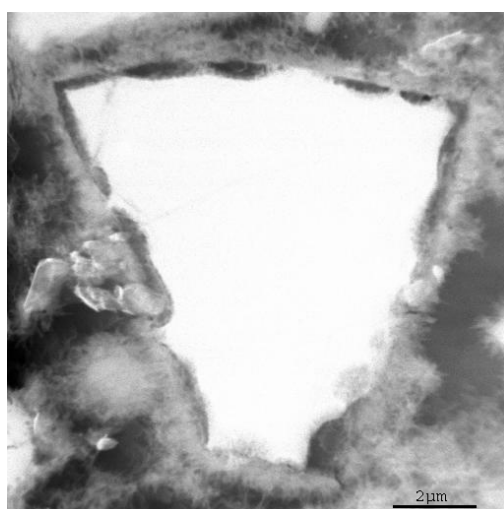
Figure 4.2: Preferential reactivity of grains having shells



(a) 6 hours

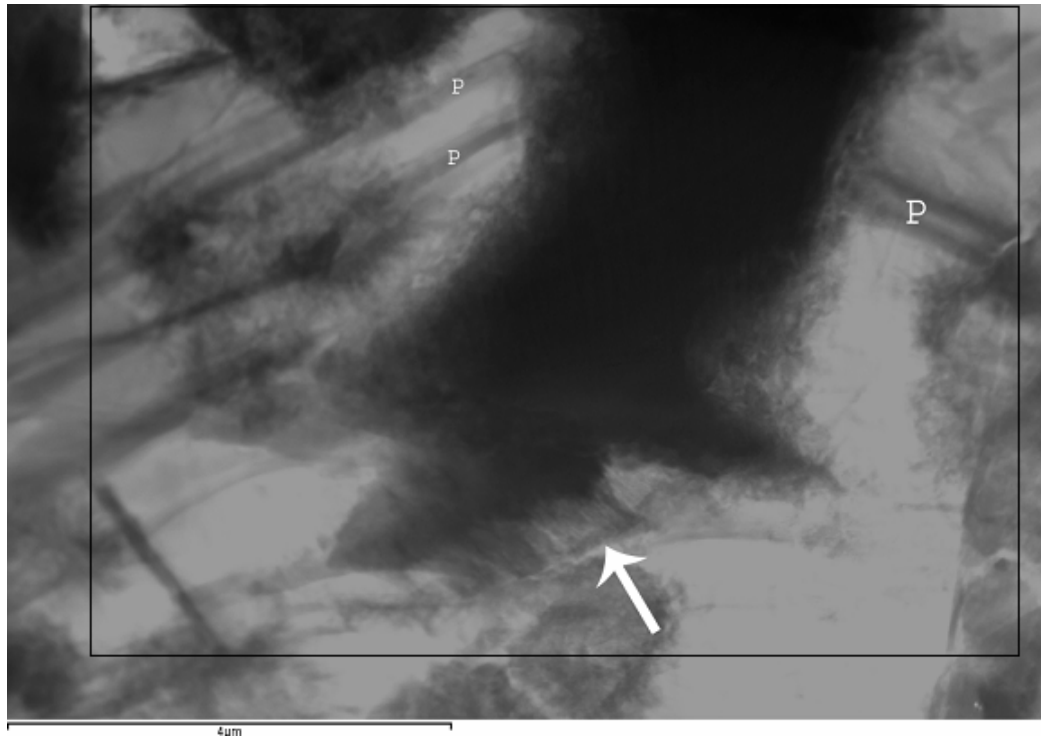


(b) 8 hours

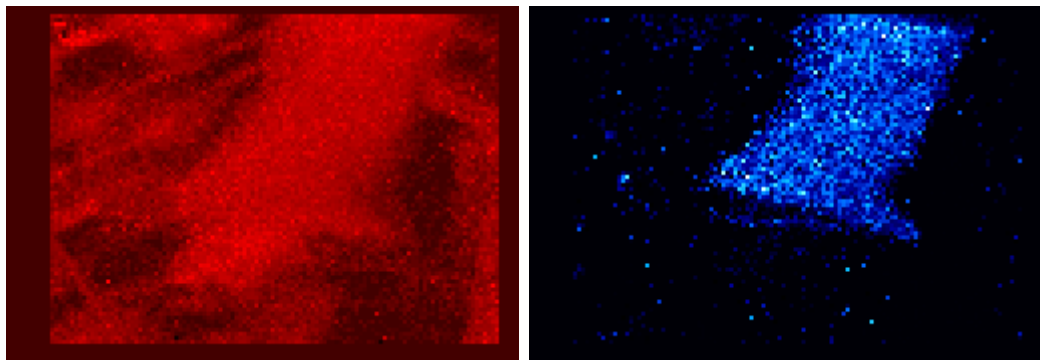


(c) 12 hours

Figure 4.3: Shell formation in grains of different shapes and sizes

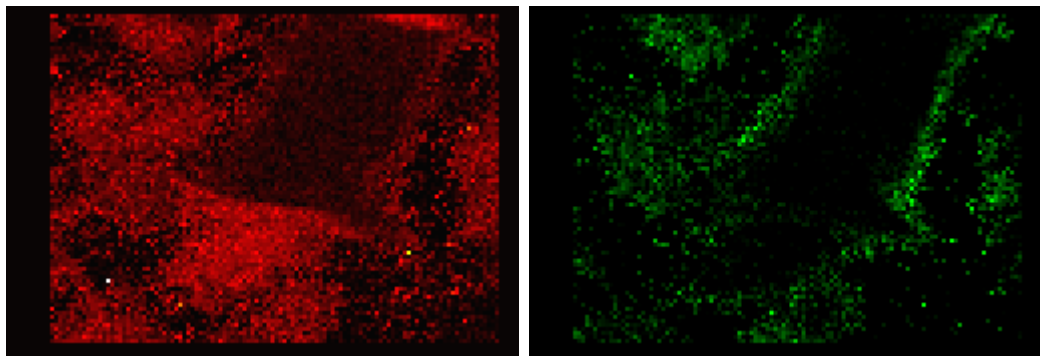


(a) Bright field (inverse contrast) STEM image (P→ Portlandite, box indicates the mapped region)



(b) Ca

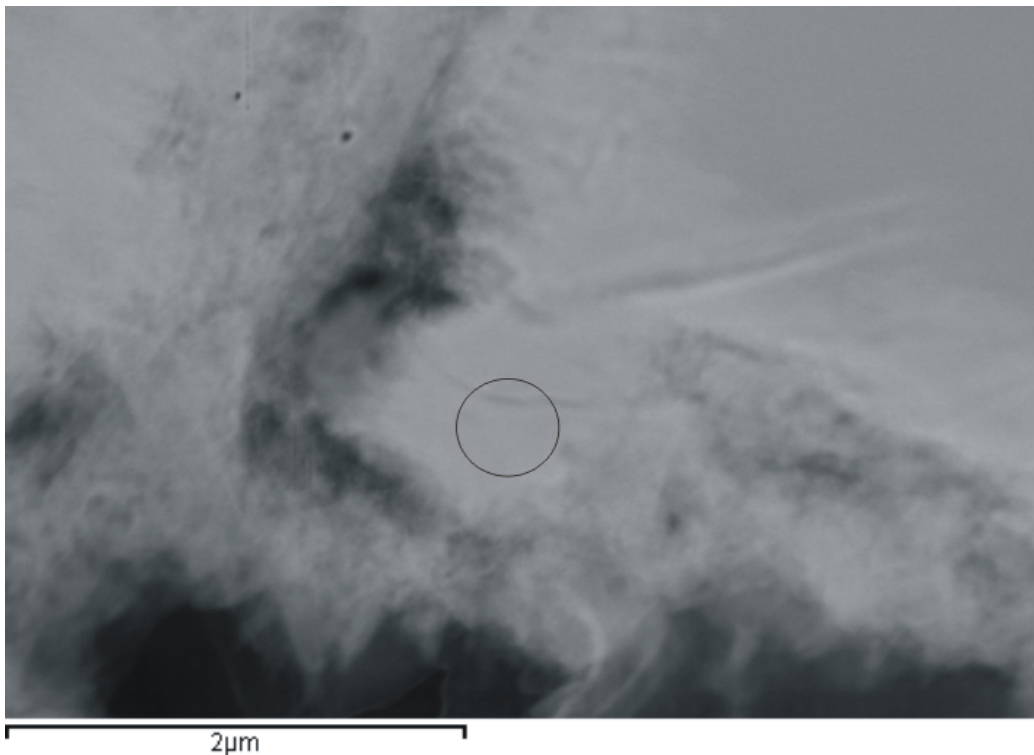
(c) Fe



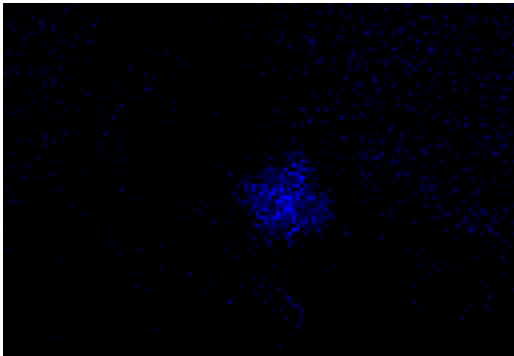
(d) Si

(e) S

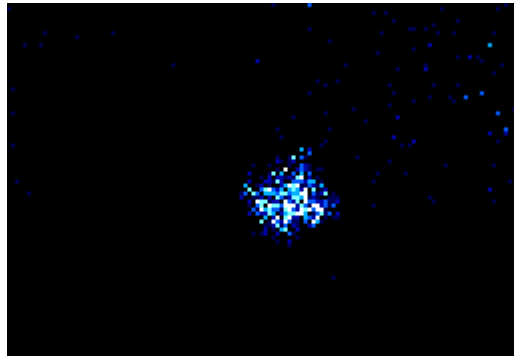
Figure 4.4: OPC 6 hours: *quantitative maps (atomic%)* showing the inception of shell formation (Figure 4.4a, marked by the arrow), rich presence of sulfur around the interstitial phase and growth of CH nearby. The remaining part of the grain, as can be seen from mapping results, is silicate with a distinct shell around and is shown in Figure 4.2a



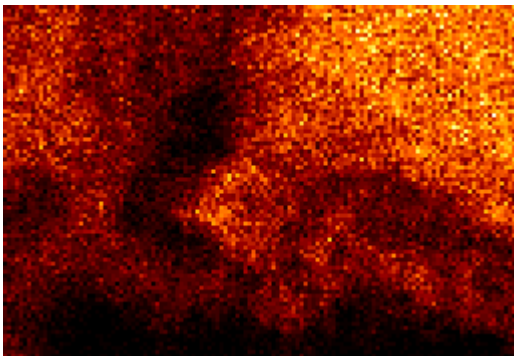
(a) Dark field STEM image (circled region is the interstitial part)



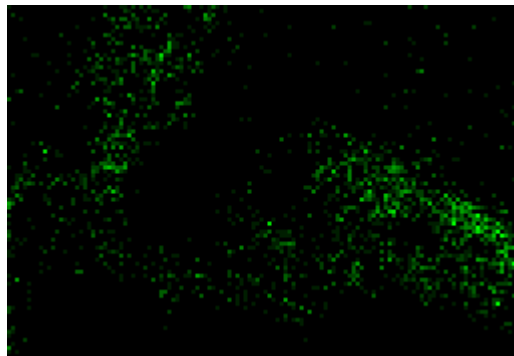
(b) Al



(c) Fe



(d) Si



(e) S

Figure 4.5: Mapping (qualitative) of OPC 10 hours showing the formation of shell in a polyphase grain. The gap is present only around the silicate part and not the alumino-ferrite part of the grain (map of Ca is omitted for brevity.)

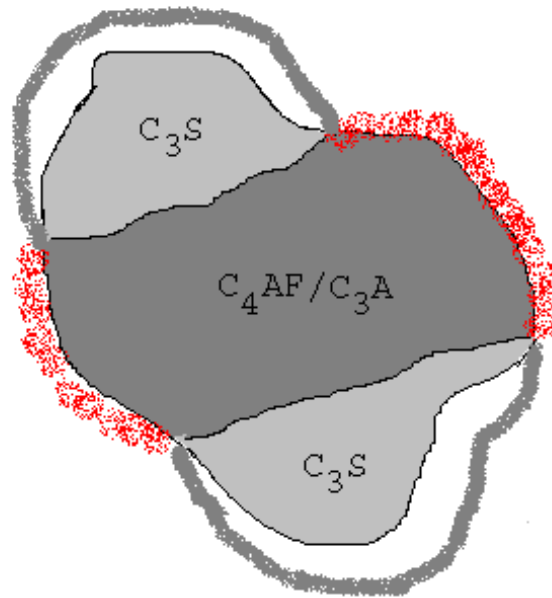


Figure 4.6: A diagram showing the formation of shell around a cement grain. In all observed instances at early ages (till 10 hours) shell is noted to form only around polyphase grains. Further, for all observed instance and for all ages shell is formed only around the silicate part of the grains.

In between 24 and 48 hours radical change occurs in the microstructure. The shell does not fill in progressively from one side but over the whole area. This gives to the formation of inner and outer product C-S-H (Figure 4.1f, page 69). In some instances, the belites are also seen at this age embedded within the shell (Figure 4.12d).

4.2.1 Ca:Si ratio of C-S-H

The fact that shell is seen to form only around the silicate part of the grain and in all observed cases shells are formed only around polyphase grains highlights the importance of knowing the chemistry of the system.

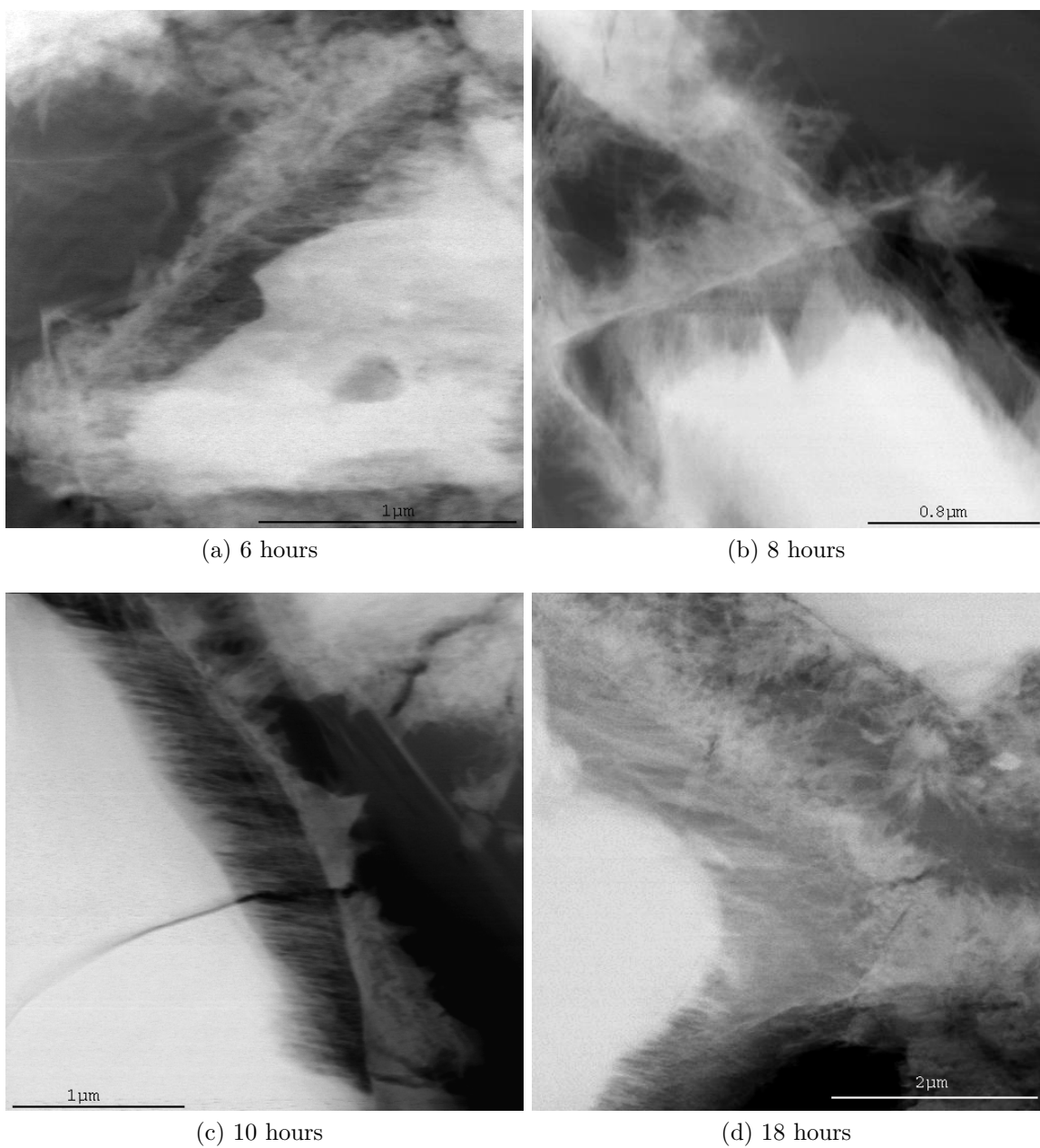


Figure 4.7: Higher magnification images reveal that the shells are not empty but filled with a C-S-H rich product

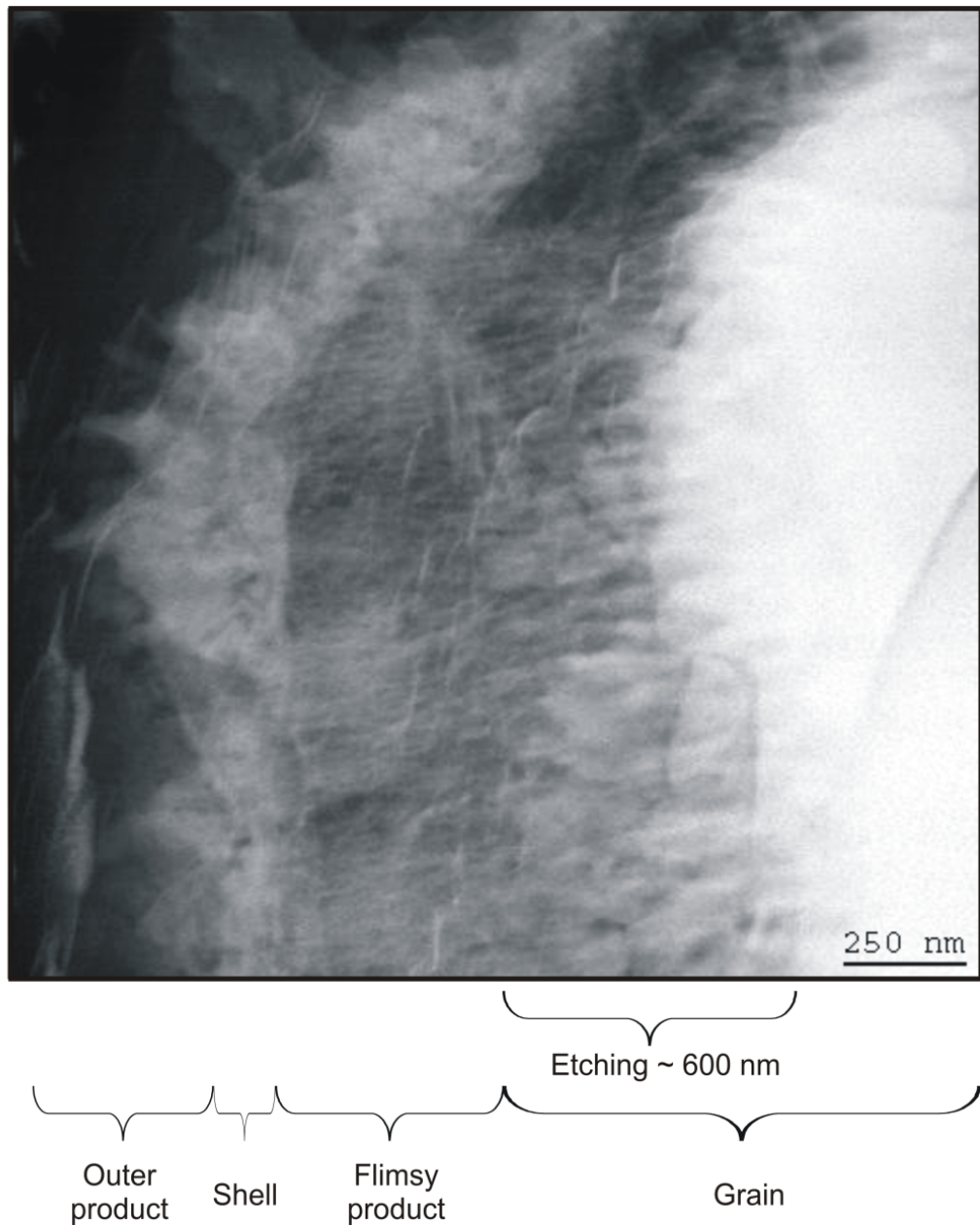


Figure 4.8: TEM image of OPC 12 hours showing the various regions of the hydration matrix, namely, flimsy C-S-H, shell and the outer product. The cement grain has ridges on its surface, possibly indicating preferential reactivity along certain crystal planes. Alite is the chief calcium silicate phase seen to exhibit this behaviour.

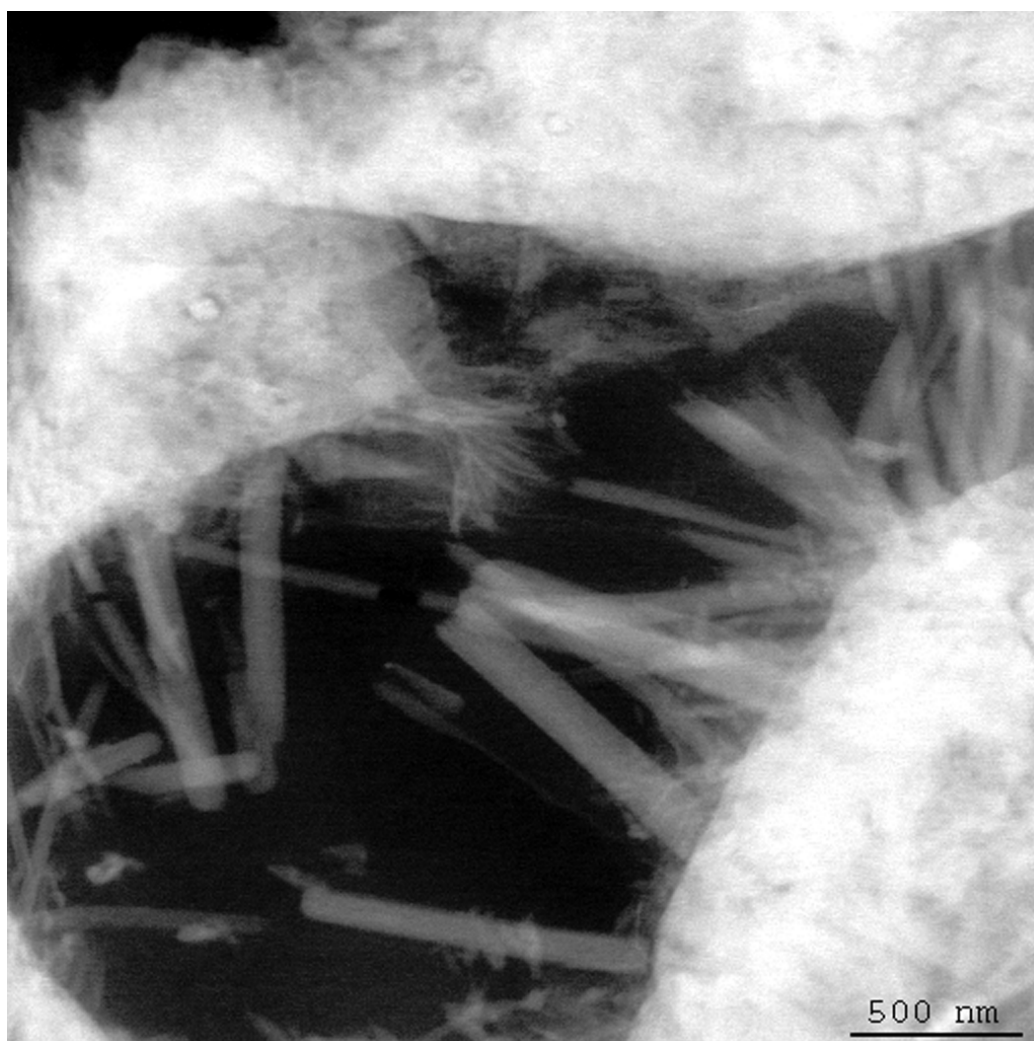


Figure 4.9: OPC 24 hours: growth of ettringite needles from the shell towards its core.

It was studied whether shell, flimsy product and the hydration products outside the shell had different chemical compositions. In order to understand the chemistry of these products a detailed quantitative chemical analysis using energy dispersive spectroscopy was carried out in TEM.

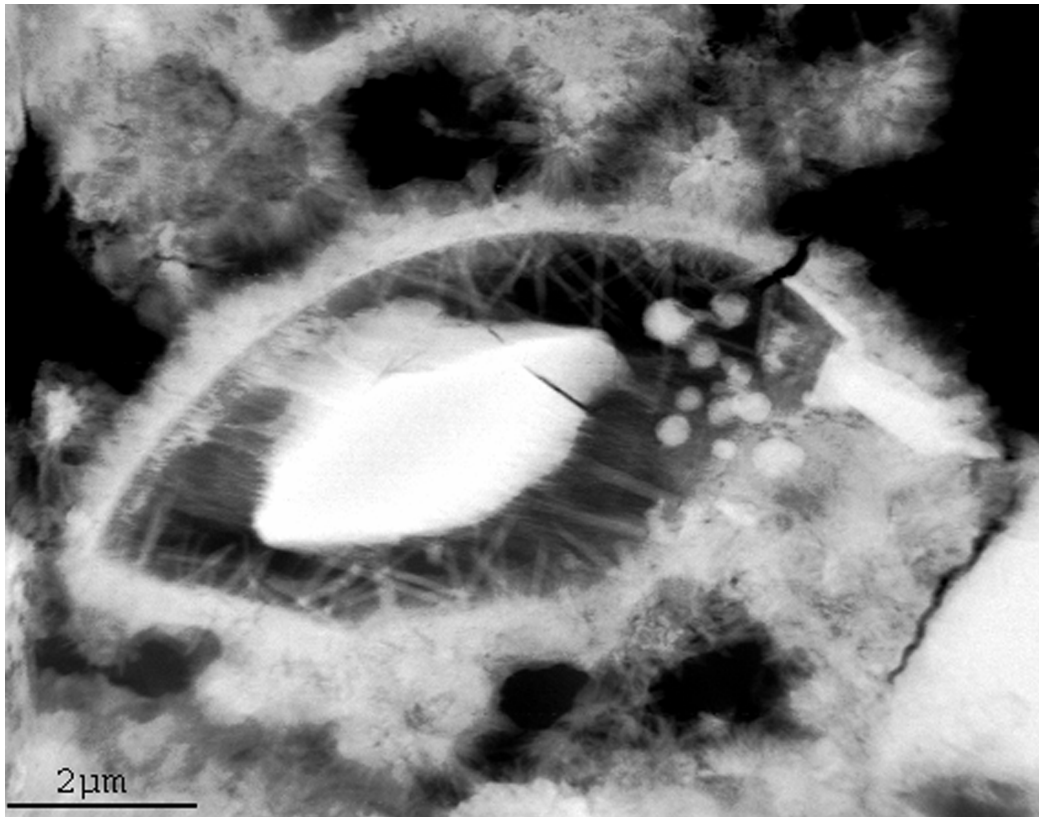


Figure 4.10: Final state of the shell with ettringite needles along with presence of belites at 24 hours

Problems in obtaining chemical analysis in TEM

Obtaining chemical analysis was found to be anything but trivial. Upon putting the microprobe (~ 2 nm) on the specimen, most of the hydration products, especially ettringite, were found to be highly prone to beam damage, as mentioned elsewhere [169], often resulting in high loss of calcium, besides possible loss of other elements as well. Use of cryogenic specimen holder (liquid nitrogen operating temperature) was found to be useless, unlike anticipated in the past [54], suggesting that more than the heat imparted on the sample by the beam, it was the high energy of electrons that caused the *knock-on* damage [211, page 63] to the sample. The damage was in the form of material loss at the exposed points and resulted in formation of holes. To avoid this, the desired feature of the microstructure was magnified to several hundred thousand times, such that it covered the whole

Table 4.1: showing the total number of points taken to calculate Ca/Si ratio in various regions and the number of points among them which have sulfur

Number of points taken to calculate Ca/Si ratios						
Age (h)	Within shell (Fp)		Shell		Outer product (Op)	
	points having sulfur	total points	points having sulfur	total points	points having sulfur	total points
6	13	14	05	05	013	013
8	18	20	11	11	094	101
10	14	20	14	14	031	031
12	06	18	11	13	011	021
18	09	13	16	16	042	045
24	11	24	25	27	017	019
48	03	17	02	06	014	036

of the observation screen and then a small area (10–20 nm a side) in the center was rastered while giving some defocus to the beam. This completely avoided the material loss and gave sensible analysis.

Results

Despite having a high spatial resolution of the order of 10–20 nm², often presence of Al, Fe and sulfur was found in C-S-H. This shows either the fine intermixing of C-S-H with Al and/or Fe rich hydration products at ‘nano’ scale or absorption of these ion on C-S-H. Due to the simultaneous presence of several ions, the obtained chemical analysis becomes complicated and difficult to interpret. Thus it is important to carefully break down these results into meaningful subcategories to obtain a full and clear picture of the complicated chemistry of hydrating cement.

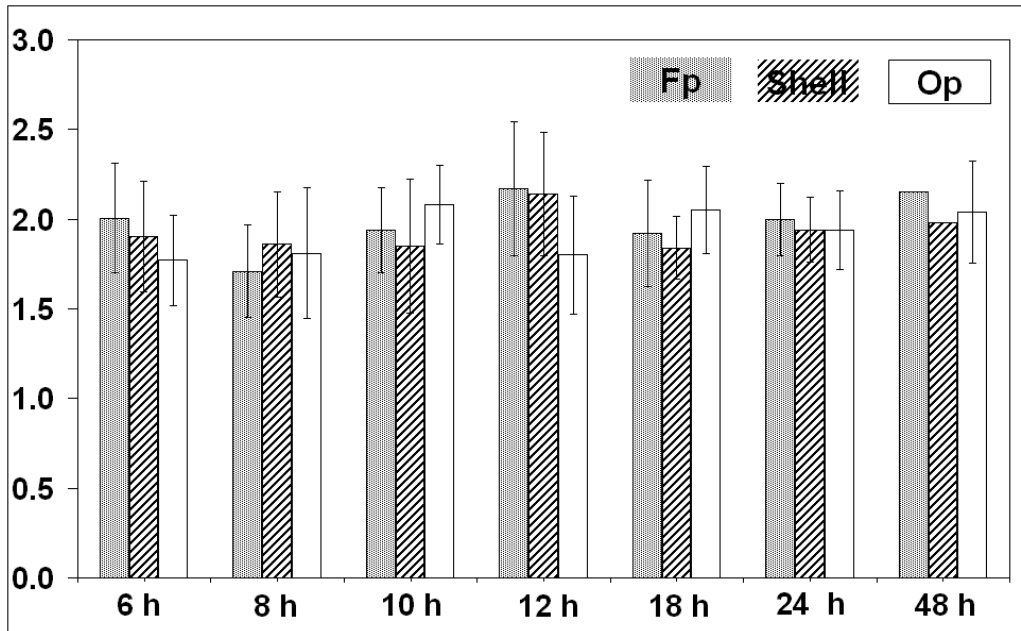
Since C-S-H is the major hydration product, it is important to find out its Ca:Si ratio and if it shows significant variations in different regions. In order to estimate the Ca:Si ratio of C-S-H free of any other phase the following steps were taken. Among the several analysis points taken on each sample, only those points were

taken into consideration whose location on the various regions was certain. Points which had presence of aluminium and/or iron in them were excluded from the analysis, since it is not evident if aluminium is absorbed on C-S-H or is present as finely intermixed ettringite. A detailed analysis of aluminium and iron is presented in later sections, which shows that aluminium is in fact present as ettringite and should not be included in the analysis of Ca:Si ratios. Additionally, either due to the certain parts of the sample being too thick or due to fine intermixing of portlandite, few points had a Ca/Si ratio > 3 . All such points were also excluded from the calculations. Finally, only those points were taken into consideration which had Ca and Si in them along with the presence or absence of sulfur. Sulfate is believed to be absorbed on C-S-H and it is thought that this absorption entails the coupled uptake of Ca^{2+} and SO_4^{2-} ions to preserve electrical neutrality. Thus for every mole of sulfate on C-S-H one mole of calcium is present as well. It means that the ratio $(\text{Ca} - \bar{\text{S}})/\text{Si}$ is the Ca/Si ratio of “pure” C-S-H. This model for sulfate absorption is suggested by the findings of Famy et. al. [65] who in their study of expansion in heat cured mortars found that a decrease in S/Ca ratios of C-S-H was associated with an increase in the Si/Ca ratios. Calcium from the C-S-H was found to release in approximately the same amounts as SO_4^{2-} , suggesting that sorbed SO_4^{2-} is balanced by an equal amount of sorbed Ca^{2+} in the C-S-H.

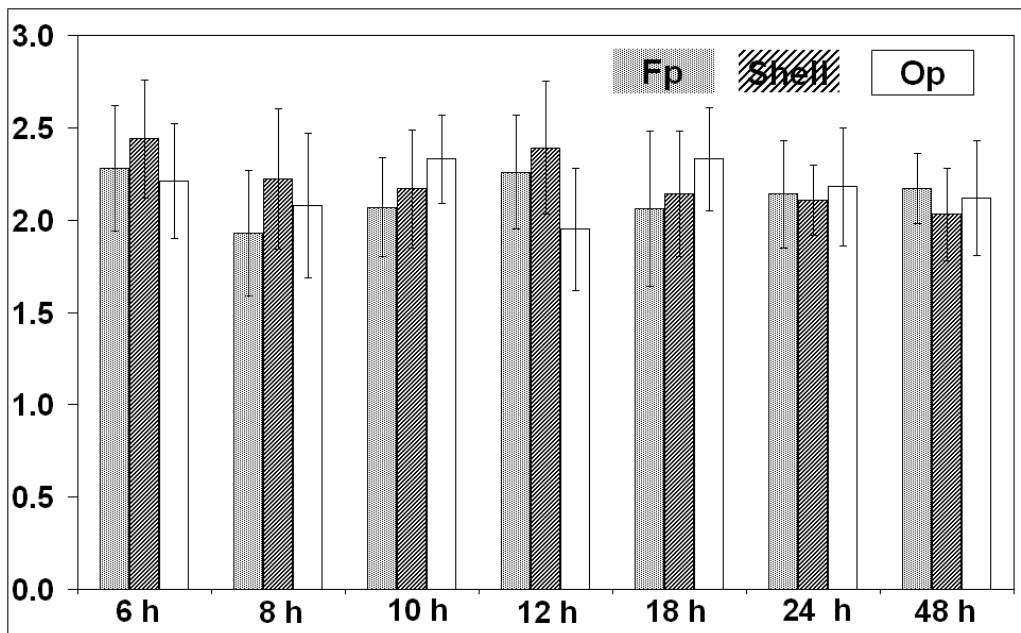
From this study, the final number of analysis points for calculation of Ca:Si ratios are presented in Table 4.1 and the distribution of Ca:Si of the various regions at the observed ages is presented in Figure 4.11a. It shows a near constant Ca:Si ratio of about 2 for all regions and for all observed ages. The Ca:Si ratio of 1 day old sample is found to be in the same range as reported by Richardson and Groves [169]. $(\text{Ca} - \bar{\text{S}})/\text{Si}$ ratio of all the C-S-H points in all the regions across all observed ages is found to be 1.94 ± 0.32 , (*number of points: 484*). For the sake of comparison, the Ca/Si ratios without removing sulfate is also presented (Figure 4.11b). It shows a higher Ca/Si ratio than expected in cement pastes, which is believed to be due to intimate mixing of sulfate.

4.2.2 Morphology of C-S-H

In this section the morphology of C-S-H in different regions is discussed.



(a) Average $(\text{Ca} - \bar{S})/\text{Si}$ ratios of different regions. The sulfate is assumed to be absorbed as Ca^{2+} and SO_4^{2-} on C-S-H



(b) Ca/Si ratios of different regions. The sulfate which is assumed to be absorbed as Ca^{2+} and SO_4^{2-} on C-S-H is **not** removed in the calculations

Figure 4.11: Ca:Si ratios of C-S-H in various regions with and without removing the absorbed sulfate. Fp refers to the ‘flimsy product’ within the shell and ‘Outer product’ Op refers to the product formed outside the shell or that attached to the grain without forming a shell (see Figure 4.8 on page 76).

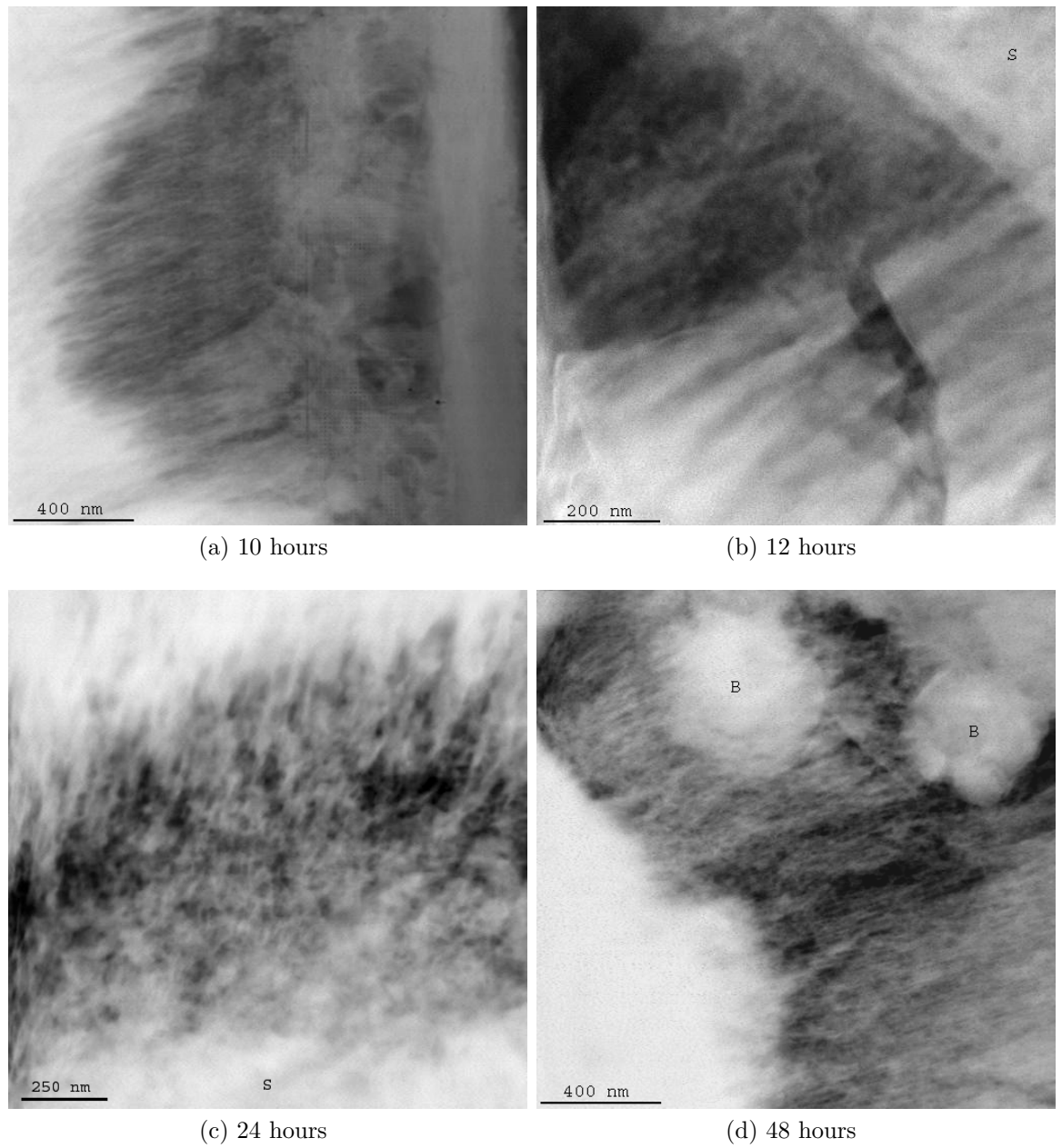


Figure 4.12: Particulate morphology of C-S-H seen close to the grain surface (S: shell, B: belite)

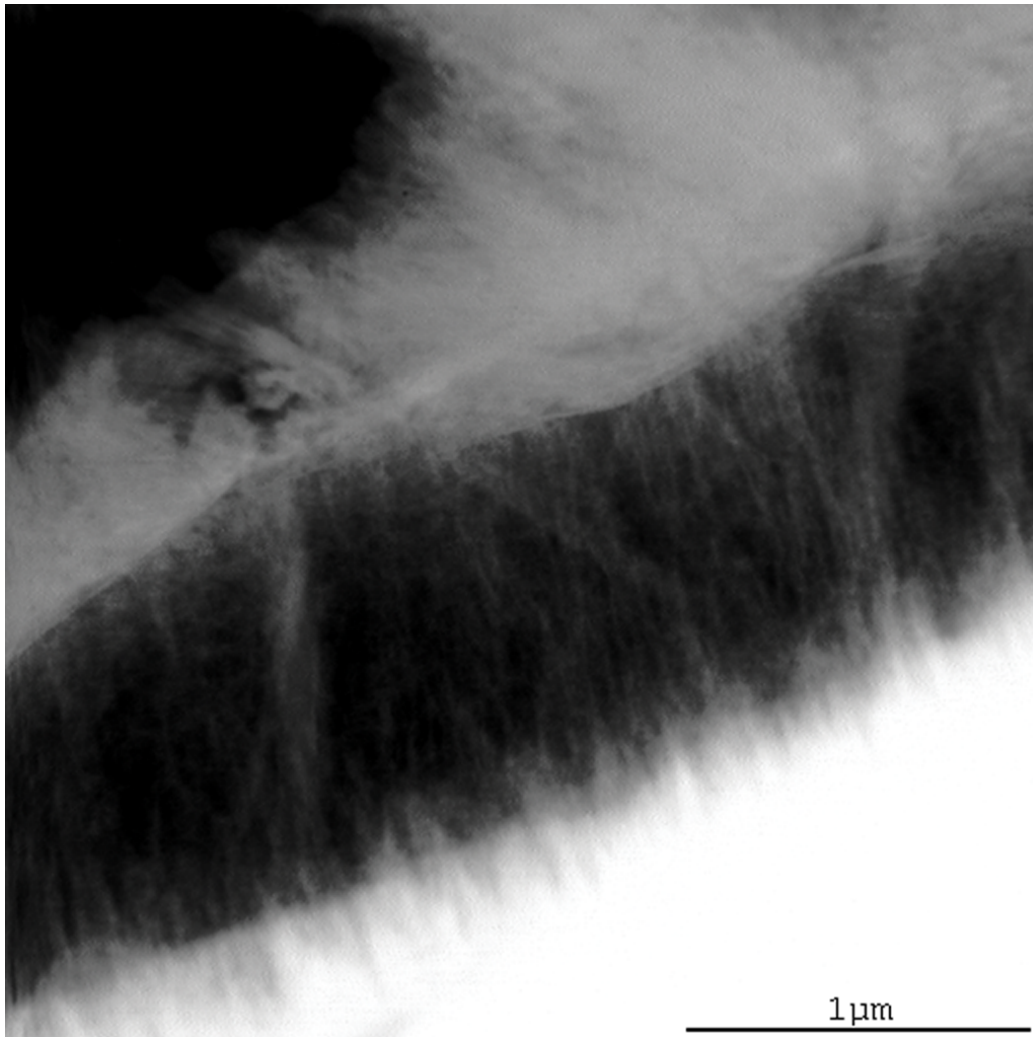


Figure 4.13: OPC 24 hours: fibrous nature of C-S-H within the shell, along with particulate C-S-H

Inside the shell

The C-S-H within the shell is ‘flimsy’ or insubstantial with less product per unit volume than in other regions. This product has a striated or sheet-like appearance which appears to be related to the uneven reaction of the alite phase. At higher magnifications the striations appear to be speckled or particulate with dimensions of 20–30 nm.

It is thought unlikely that these particles are a result of specimen damage because

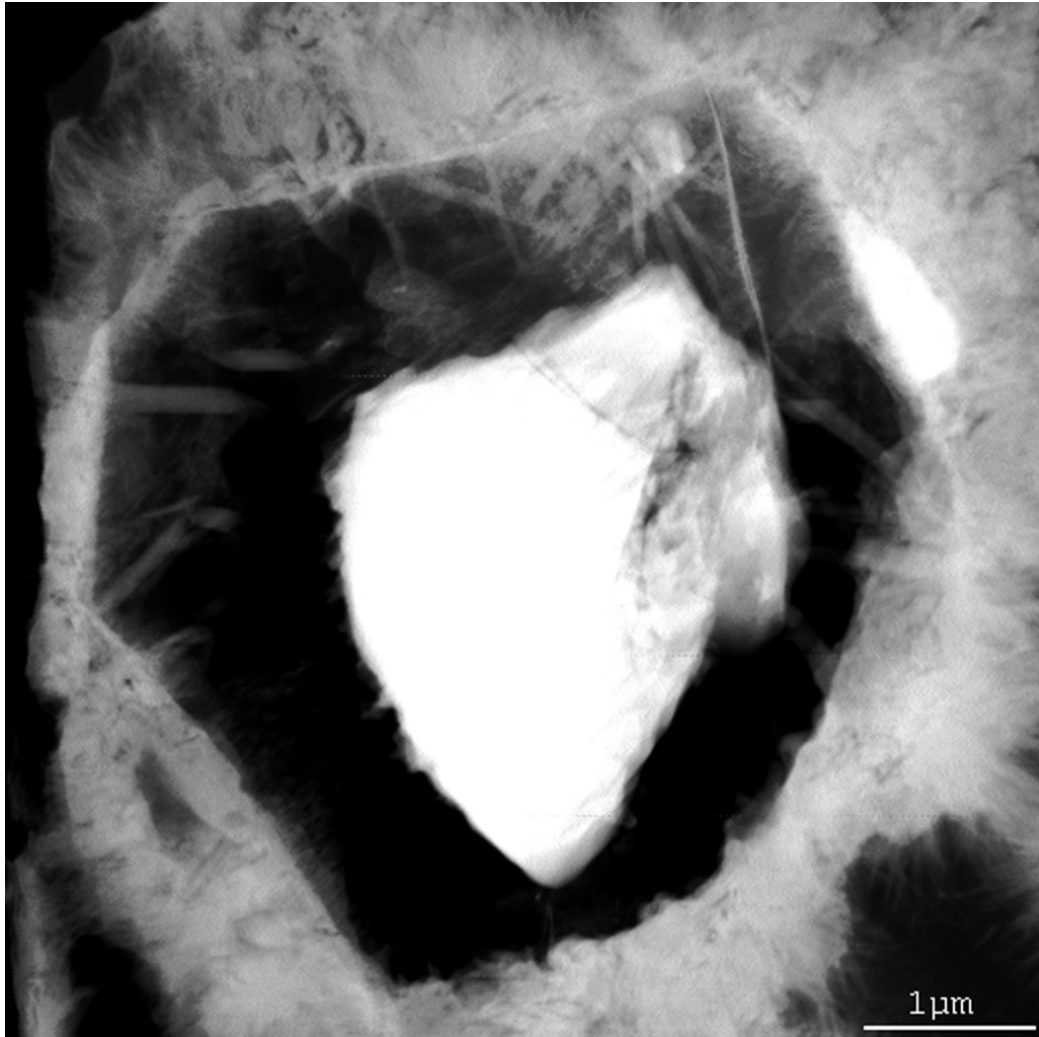


Figure 4.14: A well spread out foil like morphology of the shell at 24 hours.

had this been the case, these fine particles should have been observed in other regions of different specimens as well, which is not the case. Theoretically, it is possible that they may be present in the shell or outer product but may not be seen due to the consolidated nature of latter. In this context it is interesting to note that Gauffinet and co-workers using atomic force microscopy [80] reported that C-S-H is an assembly of oriented nanoparticles with dimensions of few tens of nanometers.

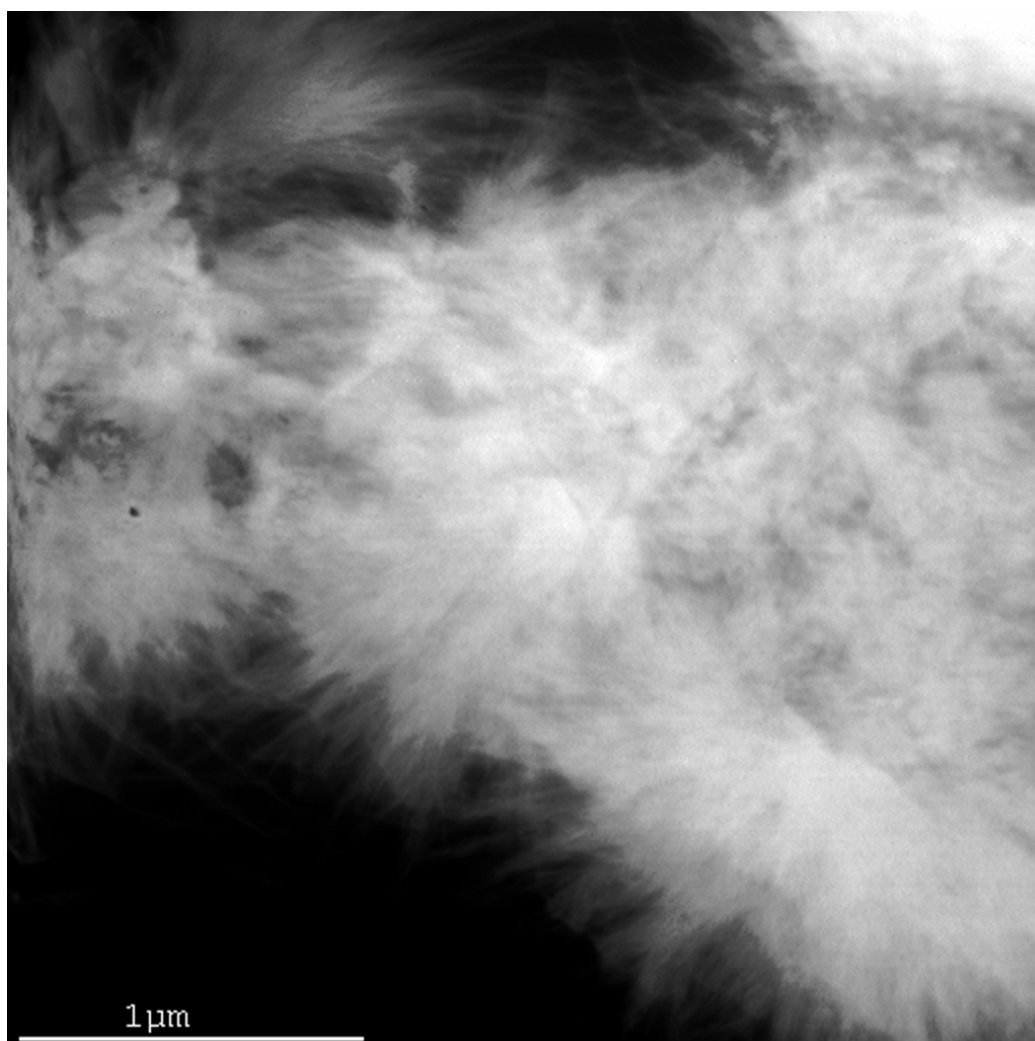


Figure 4.15: OPC 24 hours: dense morphology of the outer product along with fibrous C-S-H at the edges.

Shell

The shell is relatively dense and compact, thus appears as a layer (Figure 4.14) which is rather thin within first few hours with an increase in its thickness with time.

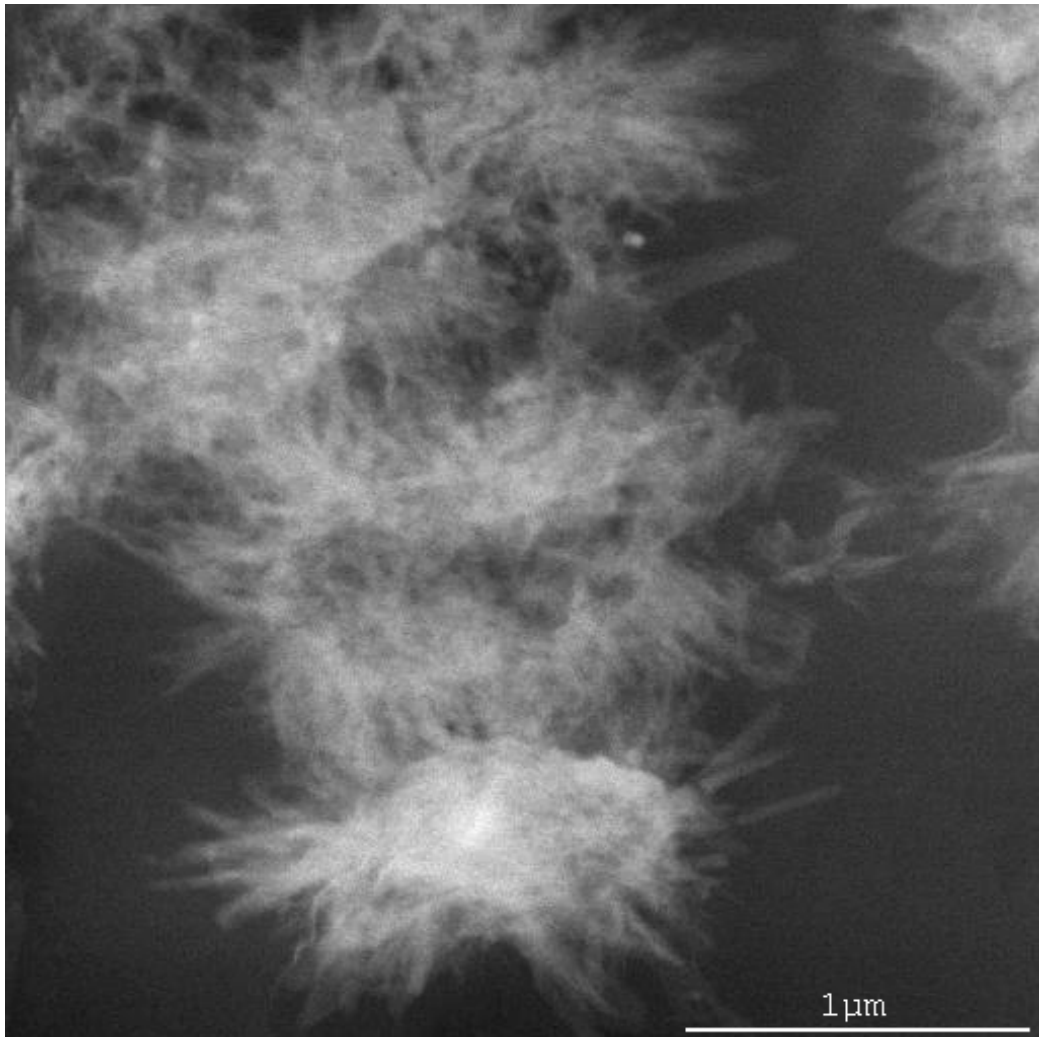


Figure 4.16: OPC 12 hours: crumpled foil morphology of C-S-H in the outer product with fibrous and needle shape C-S-H the edges.

Outside the shell

The maximum variability in terms of shapes of C-S-H is seen between the C-S-H that constitutes shell/flimsy-product and that seen in the matrix outside the shell. In several instances C-S-H attached to the shell and growing outwards is seen in a more 'individual' form in the shape of a fibre or a needle with large gaps between individual C-S-H (Figure 4.17). The C-S-H lying in the matrix outside the shells are rather more compact and cluster like and invariably have the fibrous

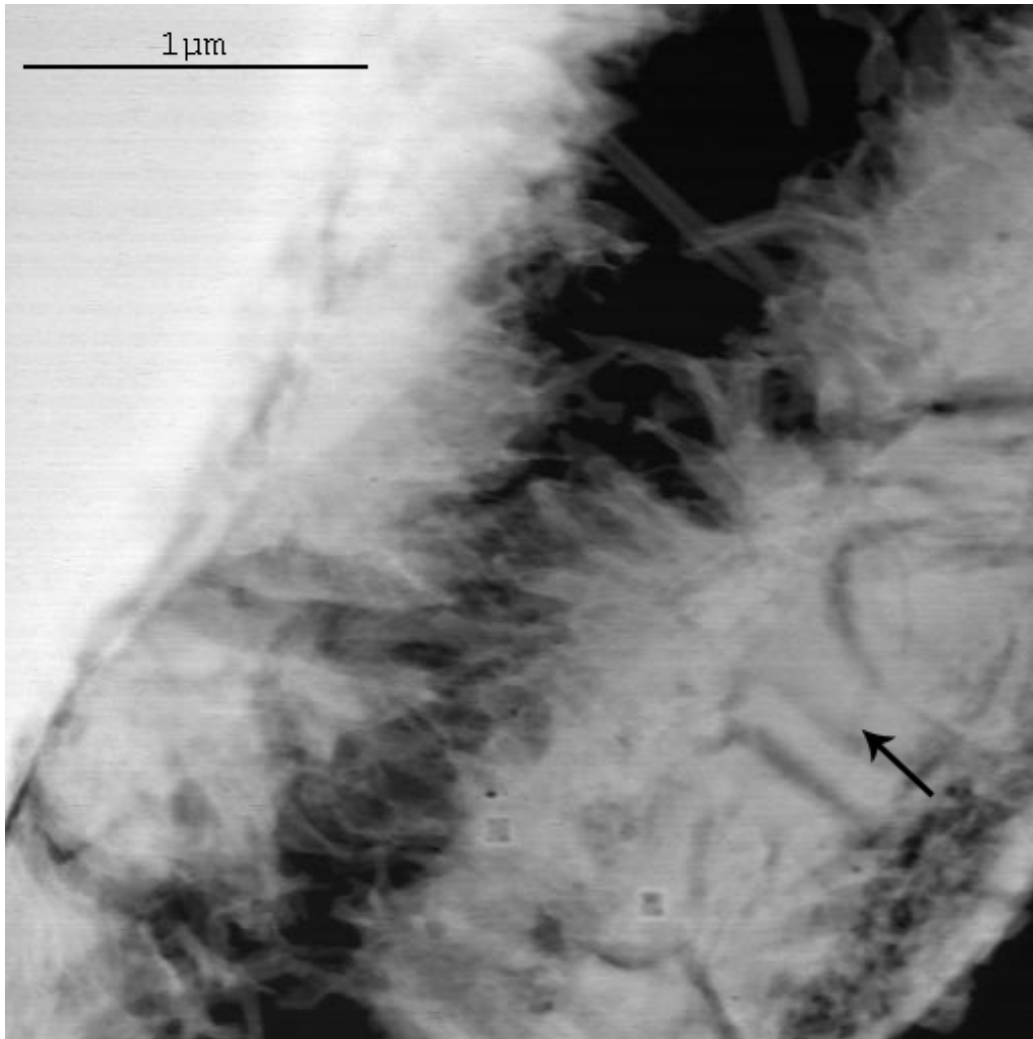


Figure 4.17: OPC 24 hours: dense morphology of the shell (indicated by the arrow) along with fibrous C-S-H at the edges.

and needle shape morphology of C-S-H at their edges (Figure 4.15). It is evident that outer product C-S-H is denser than the flimsy product within the shell but less dense than the shell itself. In several instances clusters of C-S-H are seen in the outer product which appear foil-like but not very compact (Figure 4.16). This is why such hydration products have been referred to as a 'crumpled foil' in the literature.

Discussion

These differences in morphologies could possibly be attributed to the ionic concentration of the pore solution that may favor the growth of a certain shape of C-S-H. For instance, if, due to whatever reasons, the pore solution has a variation of calcium and silicate ions then different points could witness the growth of a morphologically dissimilar C-S-H, unlike if the pore solution is homogenous in terms of ionic concentration. These events are likely to get accentuated or restrained depending on the availability of free space for C-S-H to grow.

With time the free pore space decreases with an increase in the amount of hydration products. This makes them to interface more with each other rather than grow in individual clusters or groups. A decrease in free space to grow also makes the hydration products compact and they then appear as a single mass spread out in the matrix around hydrating grains. This helps the whole matrix to become compact and would be significantly responsible for providing mechanical strength to cement.

4.2.3 Specimen prepared using Focussed Ion Beam

One sample was prepared using Focussed Ion Beam (FIB). This was done to check the effect of specimen preparation on the microstructure. The same microstructural features are seen in the samples prepared using different techniques. Figure 4.18 show the presence of shell and the preferential reactivity of the cement grains.

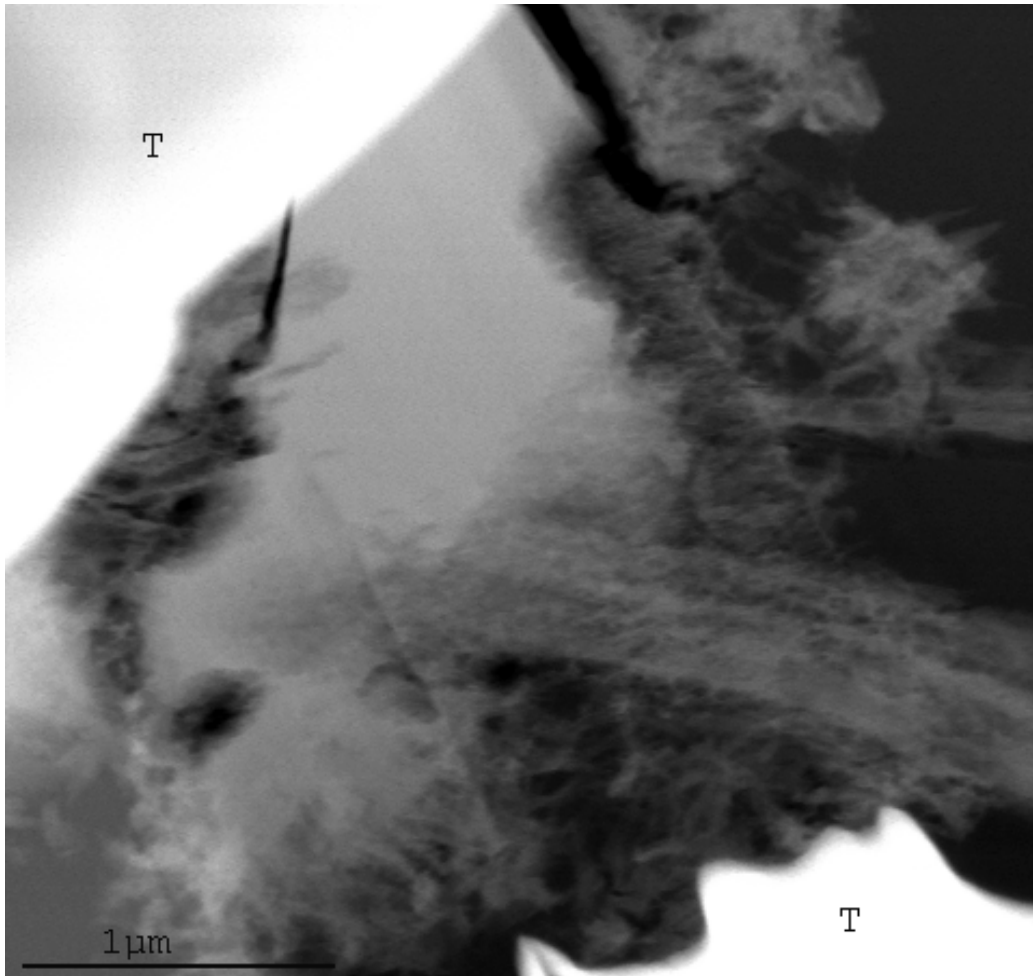


Figure 4.18: OPC 6 hours: specimen prepared using Focussed Ion Beam shows the same microstructural features as the one prepared by mechanical polishing (T → thick part of the specimen)

4.3 Early hydration product

In SEM studies of the OPC sample hydrated for 2 hours a limited amount of hydration product is visible along with ‘clean’ grain surfaces. Such grain parts seem to have not reacted at all.

TEM studies reveal the same trend but are able to provide a closer look at the grain surface due to the higher image magnification and resolution available. While parts of the grains (Figure 4.19) have unreacted surfaces, some parts of nearly all

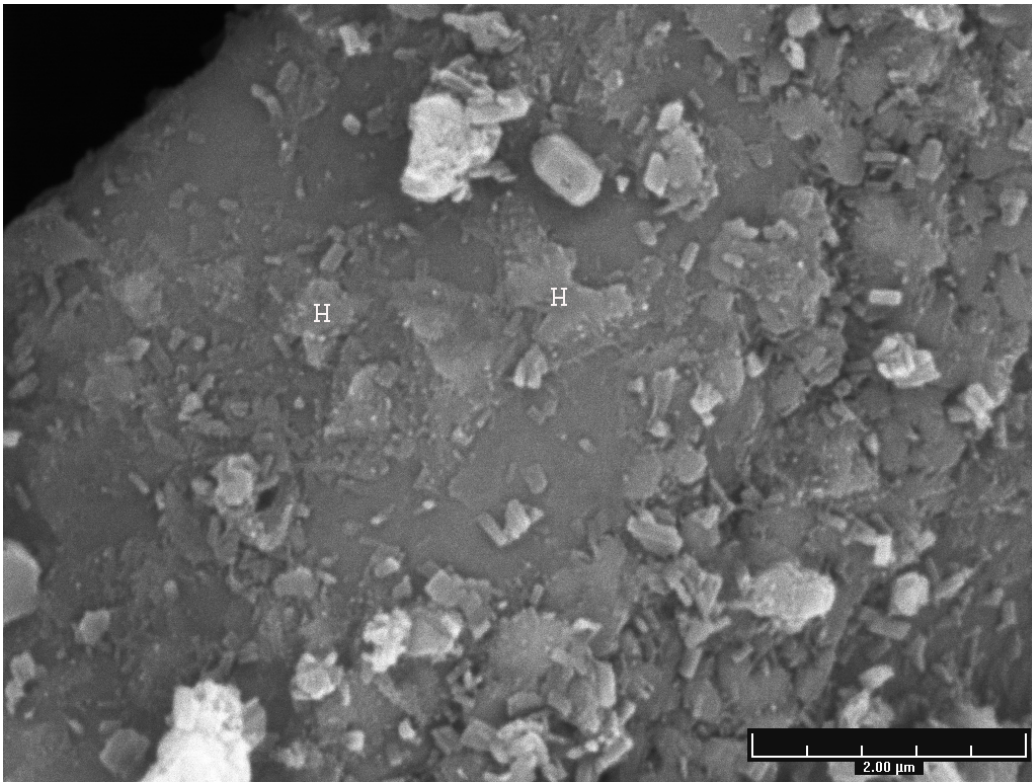
grains show the presence of hydration products around them. These products are mainly ettringite and C-S-H with a significant presence of sulfur and a near total absence of aluminium or iron in them.

These calcium-silicious products are often seen as a layer around the grains and have variable thickness (Figure 4.20), from few nanometers to ~ 100 nm. It can not be concluded, however, whether or not they inhibit the hydration of the grains it covers or are ‘protective’ in nature. These layers are present both on the silicate¹ and alumino-ferrite grains. However the layer is thicker on the silicates than on the interstitial phases. This is due to limited reaction of the latter and relatively more reaction of the former. There are relatively rich depositions of C-S-H around their parent grains, the silicates, and only a small deposited amount of C-S-H around foreign phases. It indicates the precipitation of products due to the through-solution mechanisms, although it may be operational only over a short-distance, which may be estimated by noting the distance over which hydration products are spread ($\sim 0.7 \mu\text{m}$ from the grain). This is further strengthened by the fact that ettringite is seen deposited both on the alumino-ferrites, which are its parent grains from the point of providing the requisite ions, and on silicate. This can only occur via the through-solution mechanism.

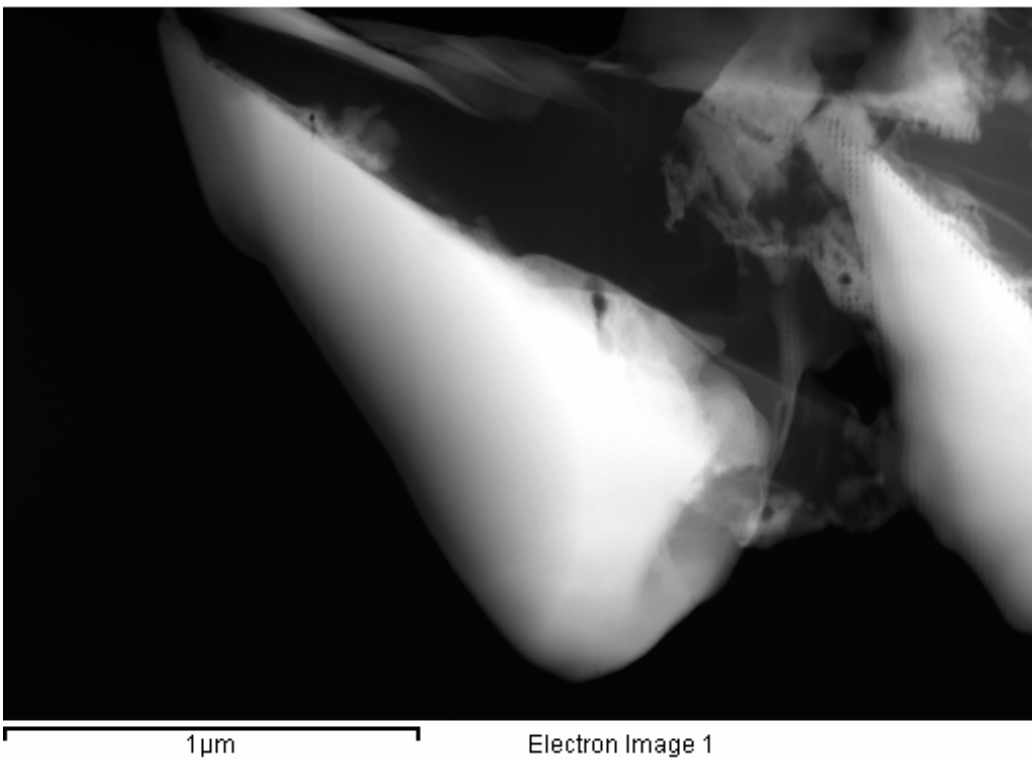
In some cases however C-S-H is seen to have also deposited slightly away from the grain surfaces in the free pore space. This is shown in the sequence of images in Figure 4.21. It is seen that there is diversity in the morphology and compactness of the C-S-H. Figure 4.21b shows the presence of platey clusters of C-S-H. The grain surface is seen to be striated in some cases at 2 hours. It is not an artifact due to specimen preparation but a mode of reaction as is illustrated in fracture surface of cement pastes (Figure 4.22).

Besides the presence of hydration products, large unreacted gypsum particles are also seen in the matrix up to 6 hours but not thereafter. In some instance gypsum is seen adjacent to the shell while in other cases it is present away from the shell (Figure 4.23). A detailed analysis of sulfates is presented later in the chapter.

¹All silicate grains are noted to have a small amount (about 1 at. wt.%) of aluminium in them

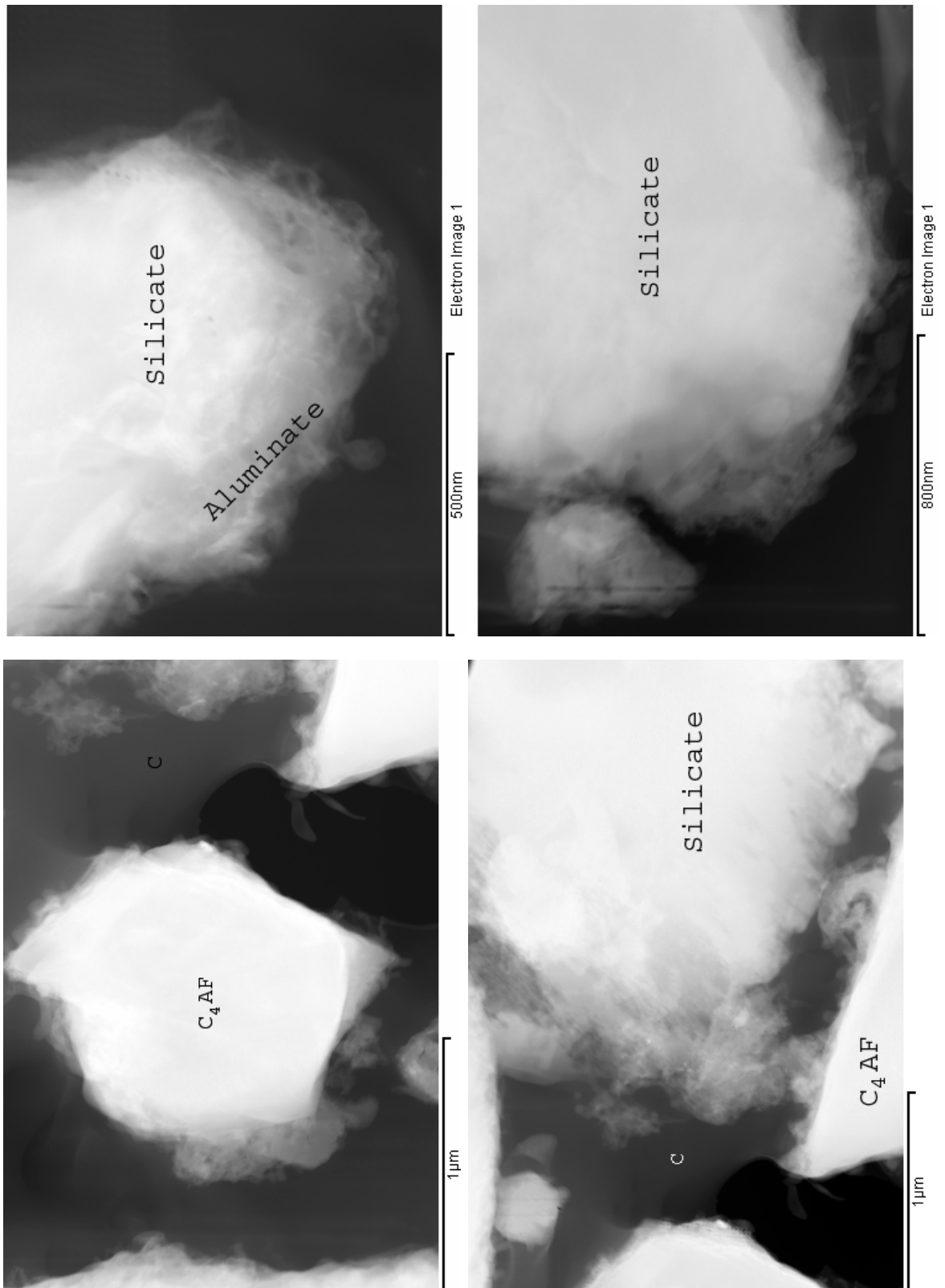


(a) SEM image of the fracture surface of OPC 2 hours



(b) TEM image in cross-section of OPC 2 hours (EDS mapping shows the two grains in view to be **silicates**)

Figure 4.19: OPC 2 hours: limited calcium-silicious products (H) along with short ettringite needles (seen in SEM). Some parts of the grains seem to have not reacted at all



(d) Sulfur mapping of C₄AF grain is shown in Figure 4.28d

Figure 4.20: OPC 2 hours: C-S-H rich product as a layer of variable thickness around cement grains. Identity of phases as seen in element mapping. (C → carbon-coating)

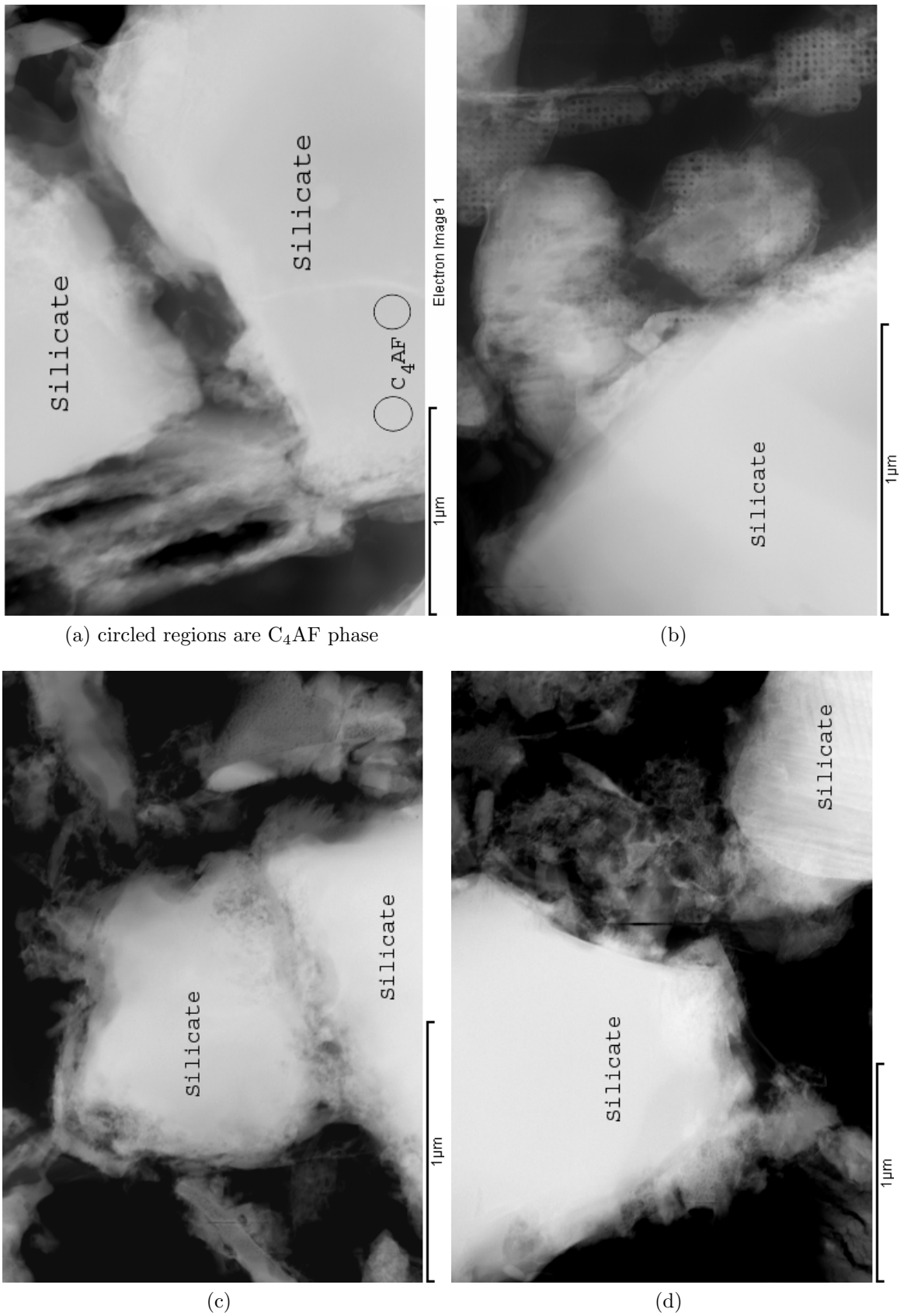
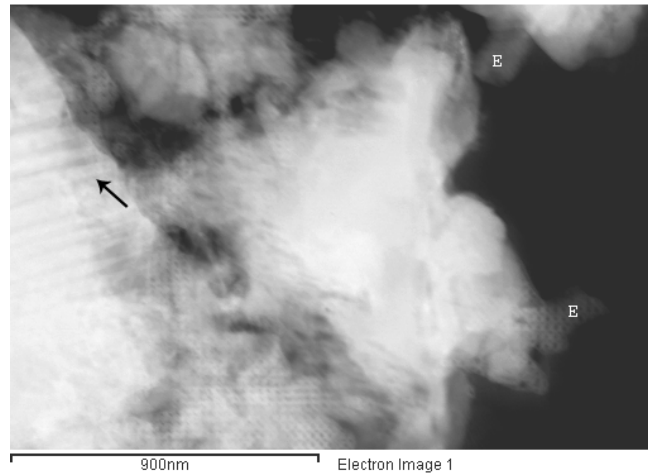
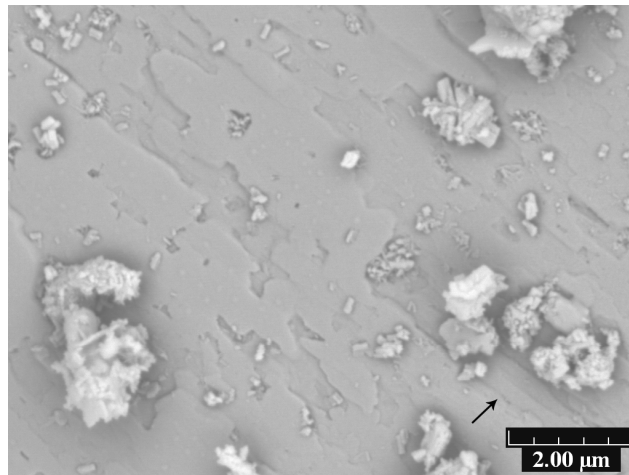


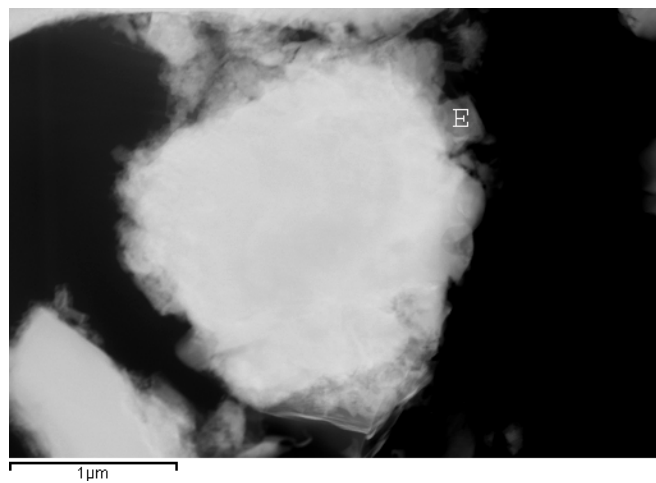
Figure 4.21: Hydration products are also seen to have also deposited slightly far away from the grains at 2 hours



(a) TEM image (2 hours): striations on grain surface and ettringite (E) on silicate phases

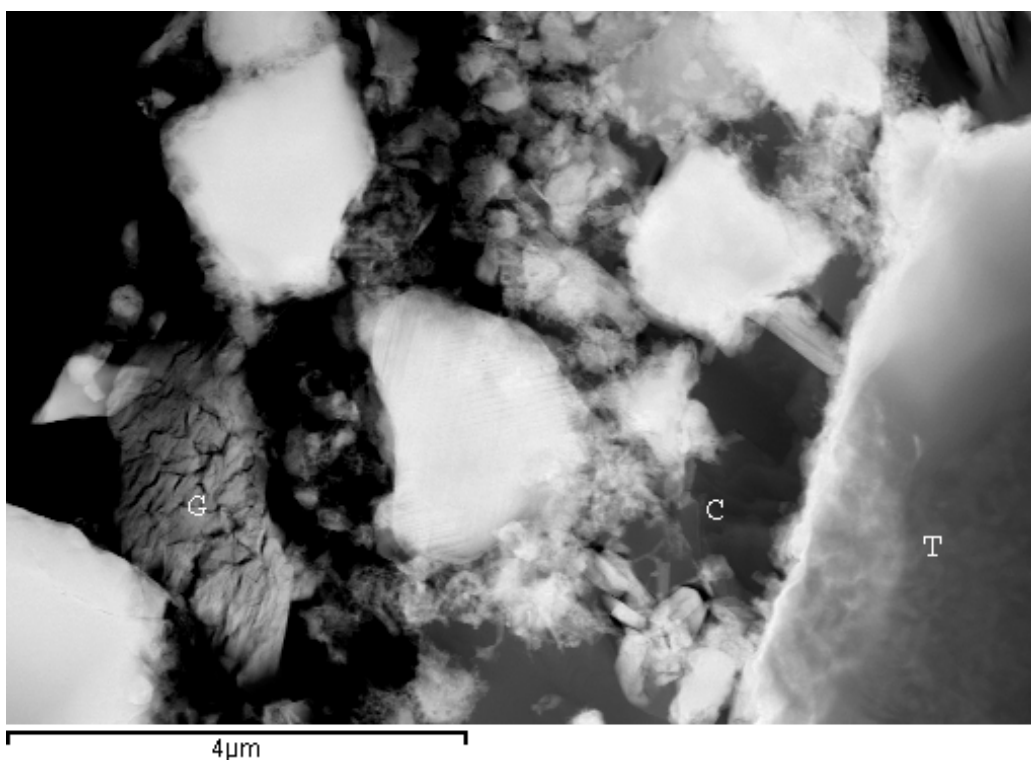


(b) SEM image of OPC 3 hours showing striations

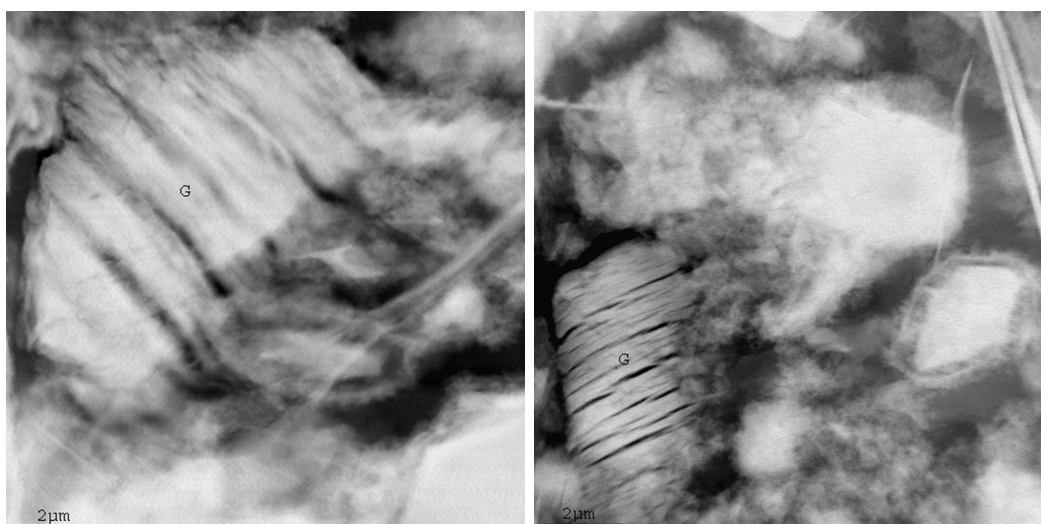


(c) TEM images of OPC 2 hours showing ettringite rods on alumino-ferrite phase

Figure 4.22: OPC 2 hours: striations on the grain surface and growth of ettringite both on the silicate and interstitial phases (phase identification of the grains is done by chemical analysis)

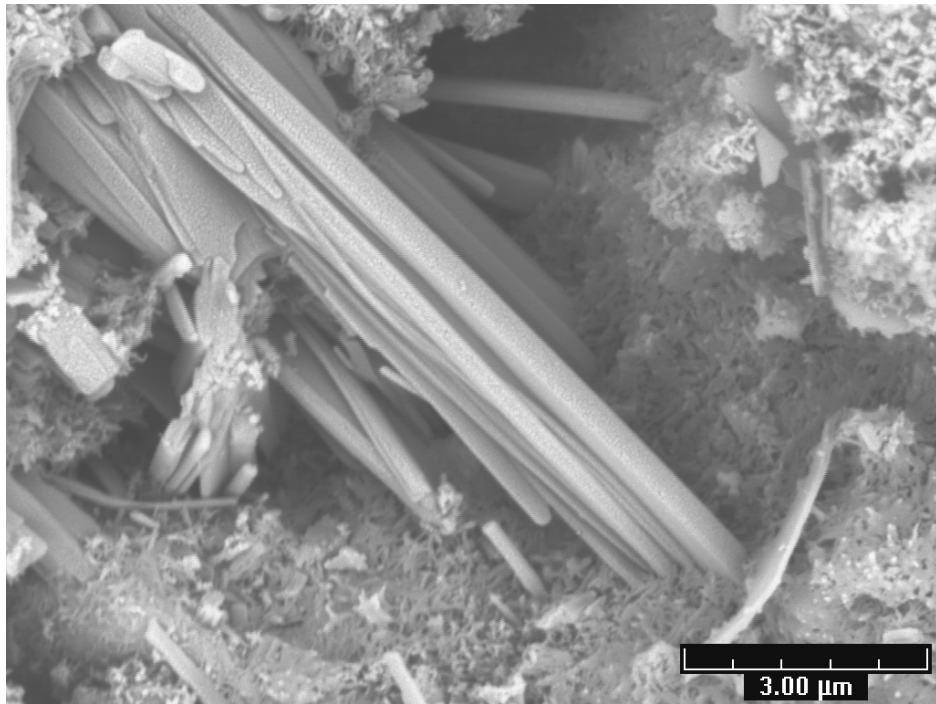


(a) OPC 2 hours

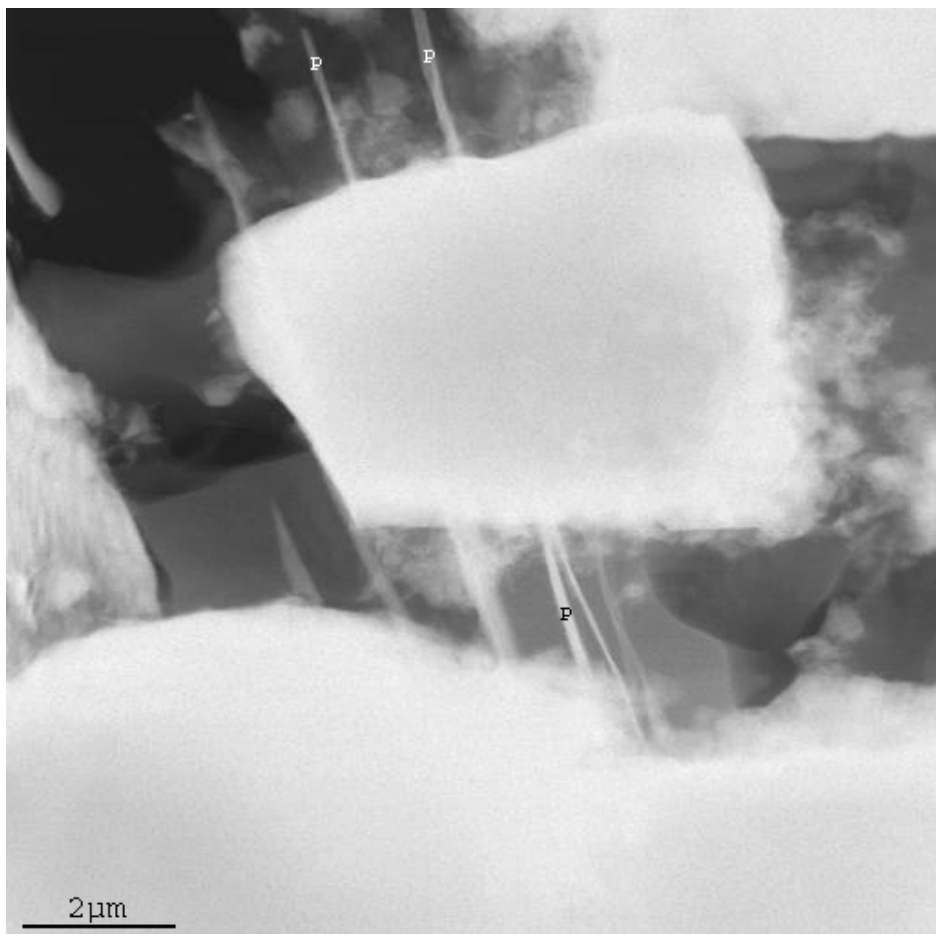


(b) OPC 6 hours: gypsum near a shell (c) OPC 6 hours: gypsum away from shell

Figure 4.23: Presence of gypsum (G) up to 6 hours; 'C' and 'T' respectively refer to carbon coating and the thick part of the sample



(a) SEM (portlandite plates at 5 hours)



(b) TEM (6 hours)

Figure 4.24: Growth of portlandite plates (P) around the setting time of cement paste, connecting various grains.

4.4 Growth of portlandite

Another significant observation is the growth of portlandites (Figure 4.24). They are first seen at 5 hours growing in the matrix as long and thin platelets and seem to connect various grains along their path of growth. It is likely that their growth in this manner may limit the freedom of movement of the connected grains. This likely influence on the mobility of the grains may at least partially aid in the setting of cement paste, which typically occurs around 6 hours.

4.5 Summary

2 hours

- Large ($\sim 3 \mu\text{m}$) particles of calcium sulfate are seen in the matrix.
- Hydration products (C-S-H and ettringite) are present.
- Ettringite is seen growing both on aluminates and silicate phases, indicating the mechanism of its formation as through-solution.
- Generally, a layer of C-S-H around the cement grain is present although from the present work, it can not be concluded whether or not the coating inhibits the hydration of the grain it covers.
- There is diversity in the morphology and compactness of C-S-H.
- There are striations present on the cement grains, seen both in TEM and SEM.

6 hours

- Distinct formation of a shell around grains seen.
- The shell is not empty but filled with a flimsy C-S-H.
- The gap between the shell and the grain surface is about 250 nm.

- First indication of portlandite plates. They are invariably seen passing around the aluminat and ferrite phases. SEM images on fracture surface show portlandite at 5 hours but not before.
- Large particles of calcium sulfate are seen in the matrix; in some cases adjacent to the shell.
- Some parts of the cement grains react more than the other parts.

8 hours

- The pore space begins to be filled with C-S-H.
- Portlandite plates several tens of microns in length are seen across the matrix.
- Nearly all grains have shells around them. The gap width is in the range 60–500 nm.

12 hours

- Various morphologies of C-S-H are seen.
- Significant filling of the pore space.

24 hours

- The shell is seen in its final form with gap up to 2.5 μm .
- The product between the grains and the shell is either not present or is extremely flimsy.
- Several ettringite needles are seen growing from the shell towards the grain.

48 hours

- Inner and outer products are distinctly seen. The bonding between the two is excellent.

- The inner product is compact and dense (low porosity), whereas the outer product is fibrous and much less compact (high porosity).

4.6 Role of aluminates

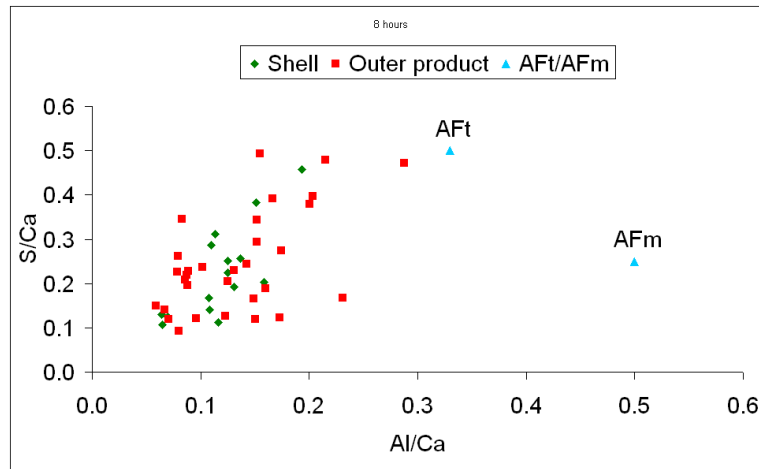
Aluminate phases are known to react within the first few hours and their reaction is seen in the form of precipitation of small ettringite rods. In the work done, imaging and chemical analysis show the presence of short ettringite rods as early as 2 hours. However, an attempt was made to learn whether aluminate is also present absorbed on C-S-H.

Various analysis points on C-S-H revealed the presence of aluminium in them. Some of these points have the presence of both aluminium and iron. All such analysis points have been excluded for this study and are dealt with separately in section 4.7 and shown in Table 5.3 on page 125.

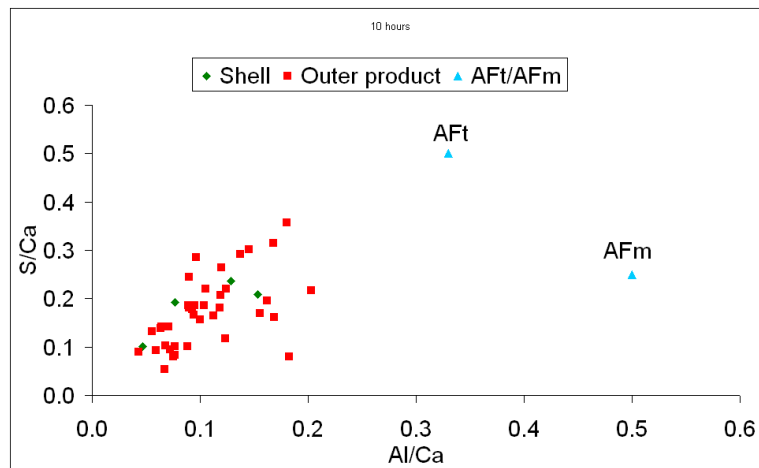
The points with only aluminium but no iron in them were taken and graphs of S/Ca versus Al/Ca at all observed ages were plotted (Figures 4.25 and 4.26). Most of the points seem to lie on the tie-line joining 'pure' C-S-H (no absorption or substitution of any ions) and ettringite. This might suggest that aluminium is present as ettringite finely intermixed with C-S-H. However, an alternate possibility could be that some or all of the aluminium has substituted the bridging sites or is present as 5- (Al[5]) or 6- (Al[6]) fold coordination in the interlayer [195], and the sulfate is adsorbed on the surface of C-S-H in a ratio corresponding to ettringite.

4.6.1 Role of sulfates

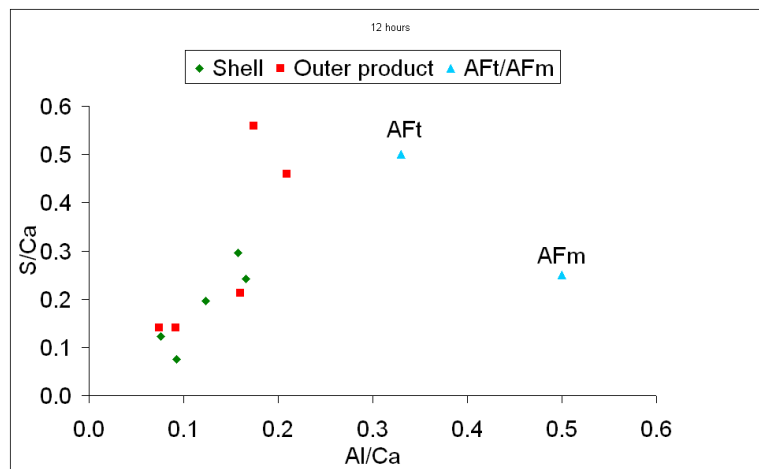
Sulfate is found to be well distributed in the hydrating matrix, present as ettringite and absorbed on C-S-H. While Figure 4.28 of OPC hydrated till 2 hours shows sulfur present around silicate, interstitial phases and on C-S-H, Figure 4.22a (page 94) also of OPC at 2 hours of hydration shows sulfur present in the form of short ettringite rods. In this context, it is observed that whereas until 18 hours ettringite is seen occasionally in TEM samples, at 24 hours there is a flurry of ettringite needles which are noted to grow from the shells inwards, towards their cores (pages 77, 78 and 104). This indicates the *second burst* of hydration of aluminate phase.



(a) 8 hours

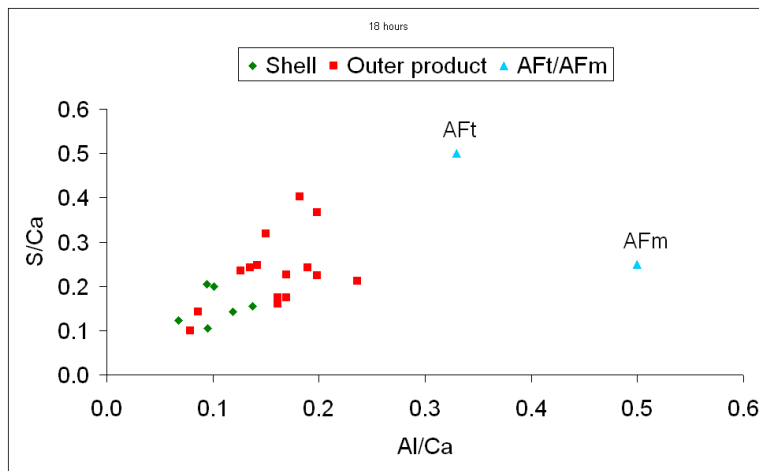


(b) 10 hours

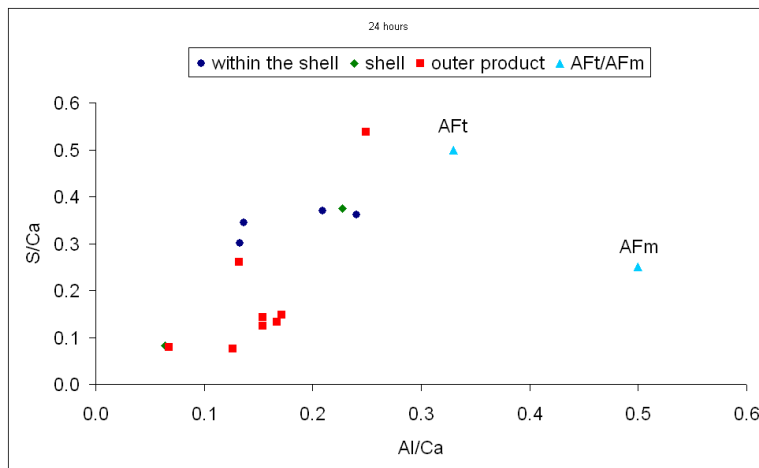


(c) 12 hours

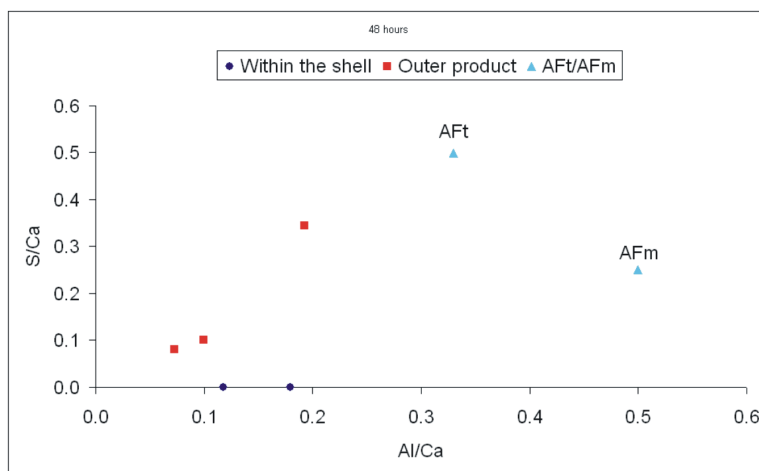
Figure 4.25: OPC: Distribution of aluminium in the various regions of the hydrating matrix from 8–12 hours. Most of the aluminium and sulfate seem to be present in the ratio corresponding with ettringite. Aluminium may be present as finely intermixed ettringite or be present in C-S-H (absorbed in the interlayer or substituted Si at the bridging sites) along with sulfate in a ratio corresponding to ettringite.



(a) 18 hours



(b) 24 hours



(c) 48 hours

Figure 4.26: Distribution of aluminium in the various regions of the hydrating matrix from 18–48 hours.

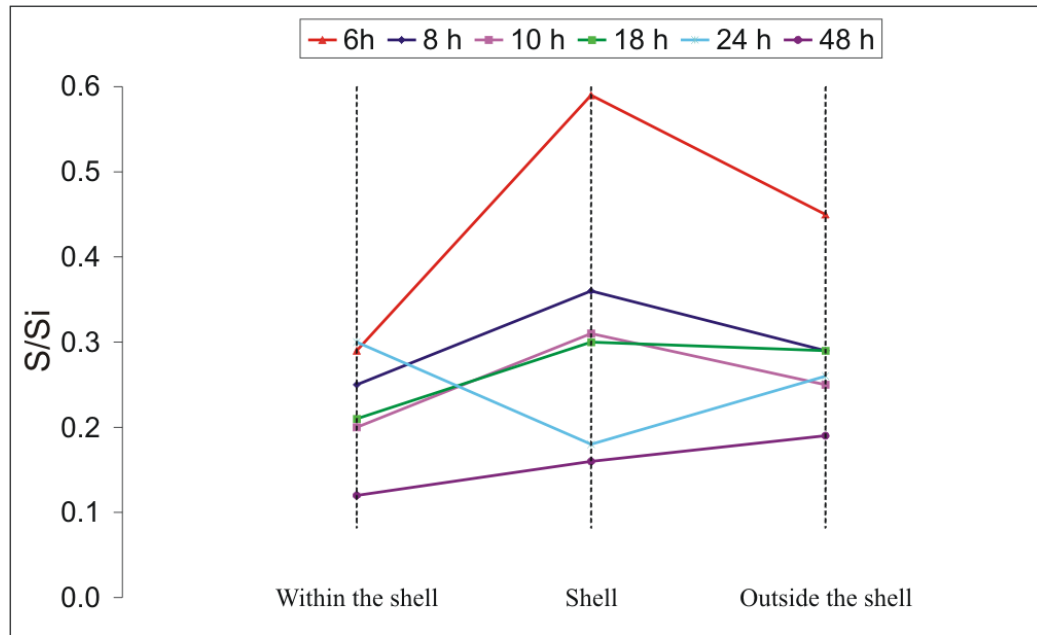
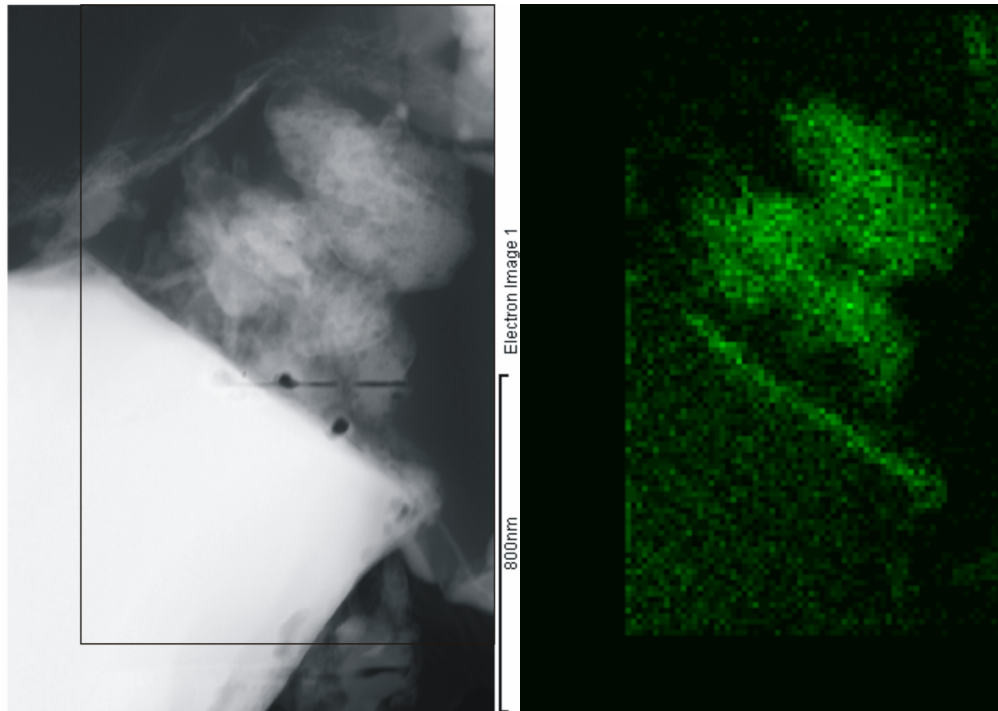
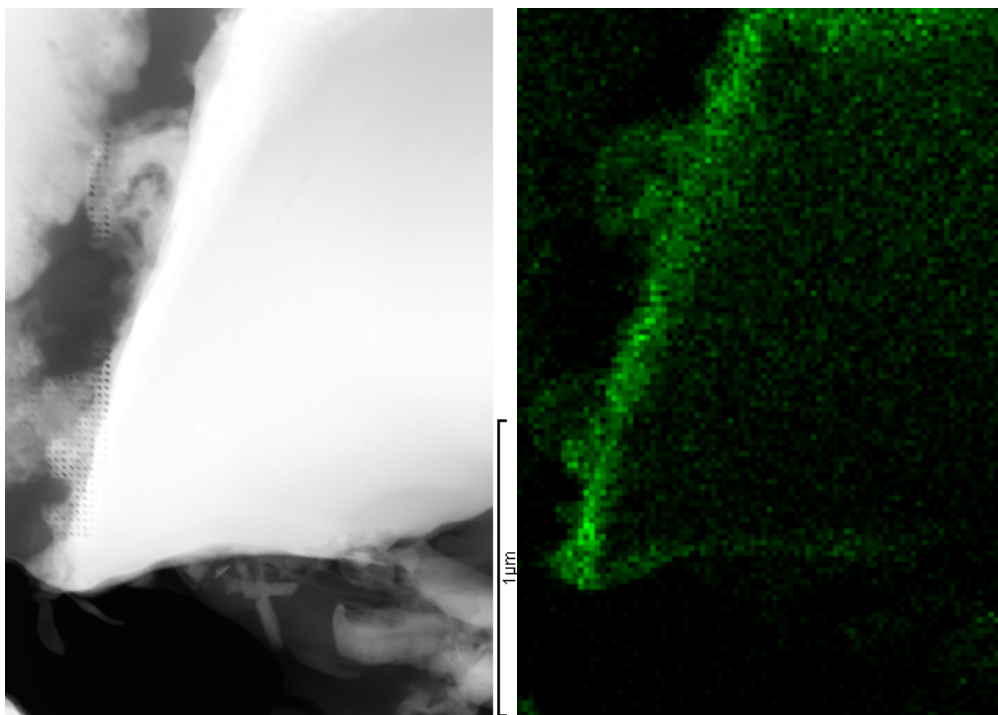


Figure 4.27: Quantitative chemical analysis in TEM shows the variation of S/Si values in the flimsy product, on the shell and in the C-S-H outside the shell. The sulfur concentration increases as we move from the grain towards the shell, where it is maximum, and decreases from the shell towards the outer product. This holds true for all ages before 24 hours, at which renewed growth of ettringite consumes the sulfate on the shell.

Renewed formation of ettringite at 24 hours should in principal be marked by depletion of sulfate in the vicinity. To verify this, S/Si ratios of three different regions, viz., diffuse product, shell and outer product was calculated and plotted for various ages (Figure 4.27). It shows that before 24 hours, the sulfur content is consistently higher in the shell than in any other part of the hydrating matrix. At one day, the formation of ettringite rods consumes most of the sulfur present on the shell resulting in a drastic drop in its concentration. By 48 hours, the shell has given way to outer product and the diffuse product to inner product. Some of the ettringite rods present within the shell have become monosulfate plates (Figure 4.32). The formation of monosulfate from ettringite is a sign of absence of sulfur. Thus now there should be minimum sulfur within the inner product and relatively more sulfur in the outer product. This is also confirmed by Figure 4.27.



(a) Silicate phase (box indicates the mapped region) (b) Sulfur around silicate and on the hydration products



(c) Interstitial phase (d) Sulfur around interstitial phase

Figure 4.28: OPC 2 hours: qualitative maps show that sulfur is well distributed in the matrix, including various anhydrous and hydrated phases.

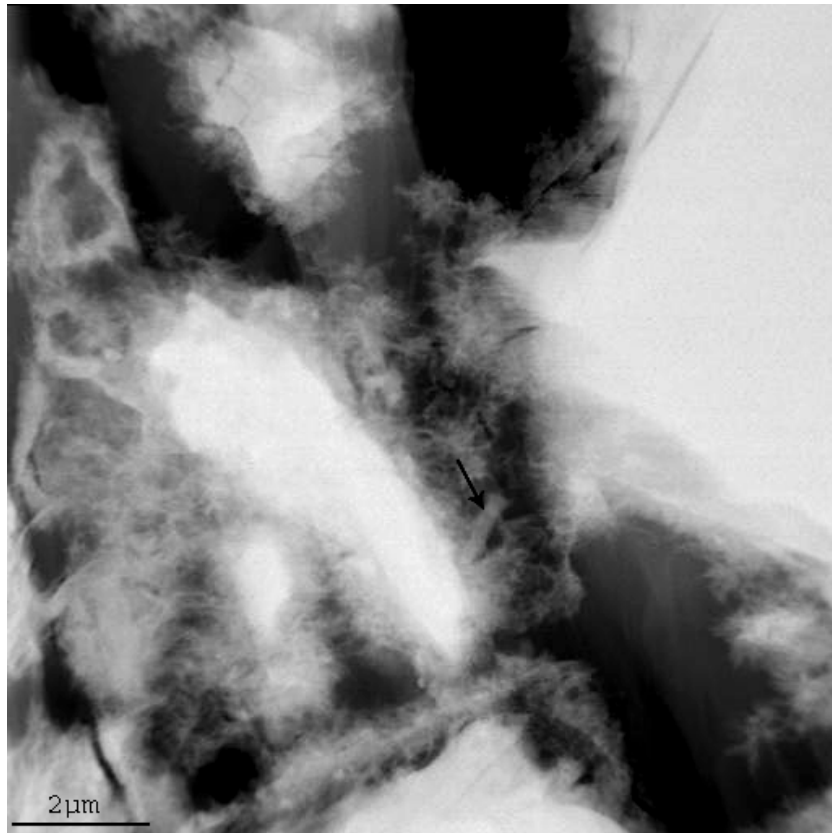


Figure 4.29: OPC 10 hours: ettringite rods (indicated by the arrow) only occasionally seen till 18 hours

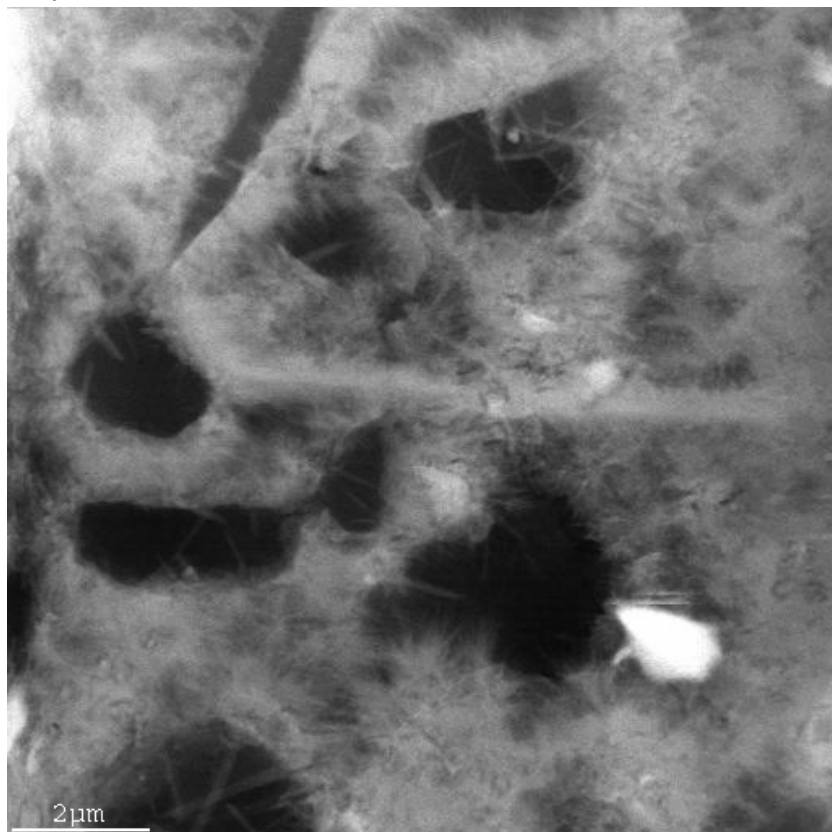


Figure 4.30: Several ettringite needles seen at 24 hours growing from the shell inwards

4.7 Role of ferrites

So far little work has been done to understand the amount of reaction of the ferrite phase in OPC at early ages although they are generally believed to be less reactive than other anhydrous phases in Portland cement, such as alite and tricalcium aluminate.

Chemical analysis in TEM shows that limited amounts of iron is present even at early hours of hydration. Table 4.4 shows the obtained Fe:Ca ratios in the various regions of the hydrating matrix. All the ettringite and monosulfate phases are removed and only the remaining points on hydrated phases (C-S-H) are considered. It is noted that iron is present as early as 6 hours, although in limited amounts. The results show that only limited reaction of the ferrite phase has occurred within the first hours. For all observed ages, since the aluminium and silicate contents are relatively more, the ferrite phase appear to be much less reactive than C_3A and C_3S , as anticipated. Further, from the presented table it can be seen that the average Fe/Ca ratio remains the same at all observed ages. This probably indicates the maximum possible accommodation of iron ions in the matrix. Never was any iron rich hydrate found, hence it is unlikely that FH_3 (equation 3.5 on page 37) is formed at the studied ages.

A significant finding is that while aluminium is well distributed in the matrix, iron is *only* found to be present on or within the shell until 12 hours, with a clear absence outside the shell, except for the very few cases where iron is seen close to C_4AF grains. This is consistent with the findings on shell formation mentioned in section 4.2 that in all observed instances shell is seen to be present only around polyphase grains.

Another crucial question is that of substitution of iron in ettringite and monosulfate phases. Tables 4.2 and 4.3 show the presence of iron in these phases at various ages. It is evident that the substitution begins in between 12 and 18 hours of hydration, with almost 30–40% of Al^{3+} been replaced by Fe^{3+} in some instances. To calculate the average Fe/Al values, only those ettringite and monosulfate phases were considered which have iron in them. The iron substitution seems to be almost the same for the two phases. It may also be noteworthy that the substitution of iron in AFt/AFm phases occurs at about the same time (18 hours) as when iron is found to be present in the matrix, away from the grains or shells. This may

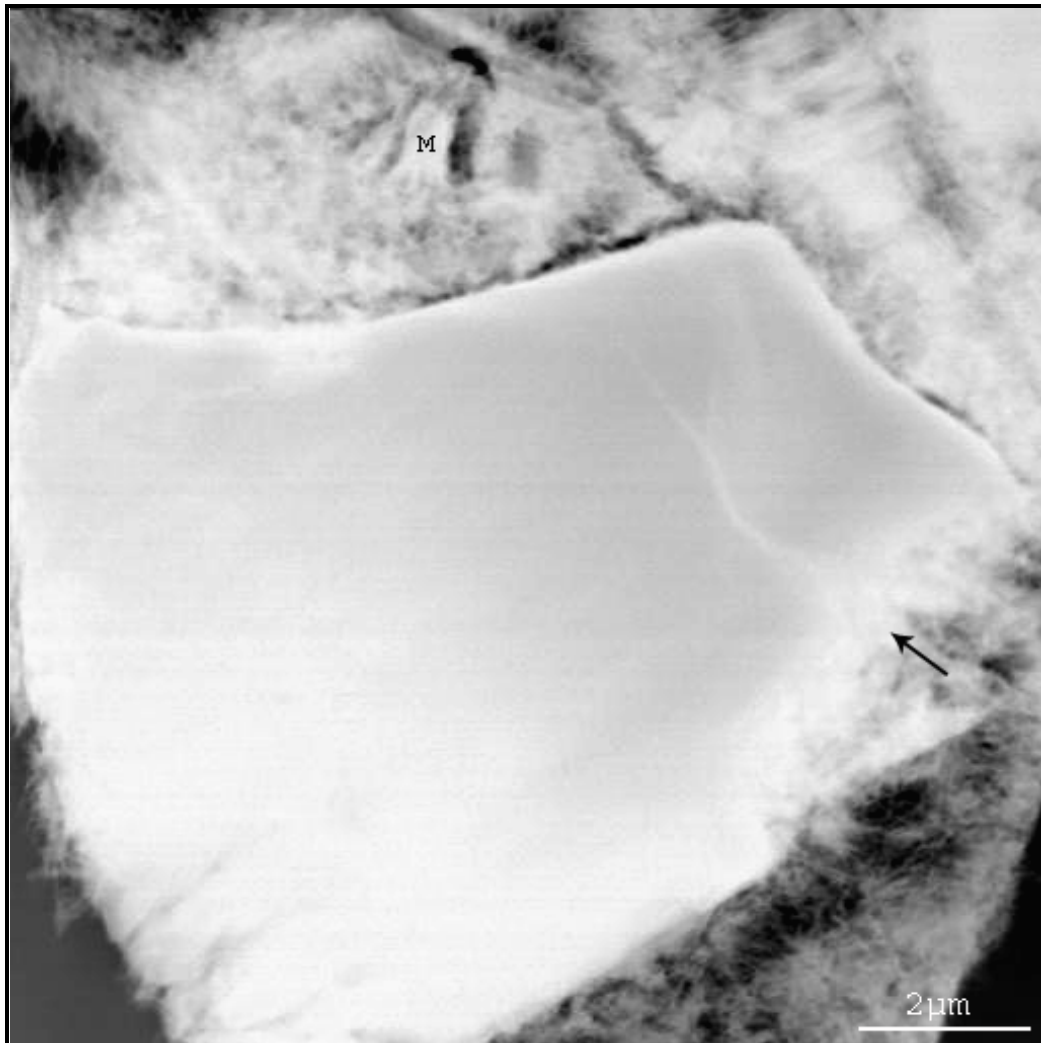
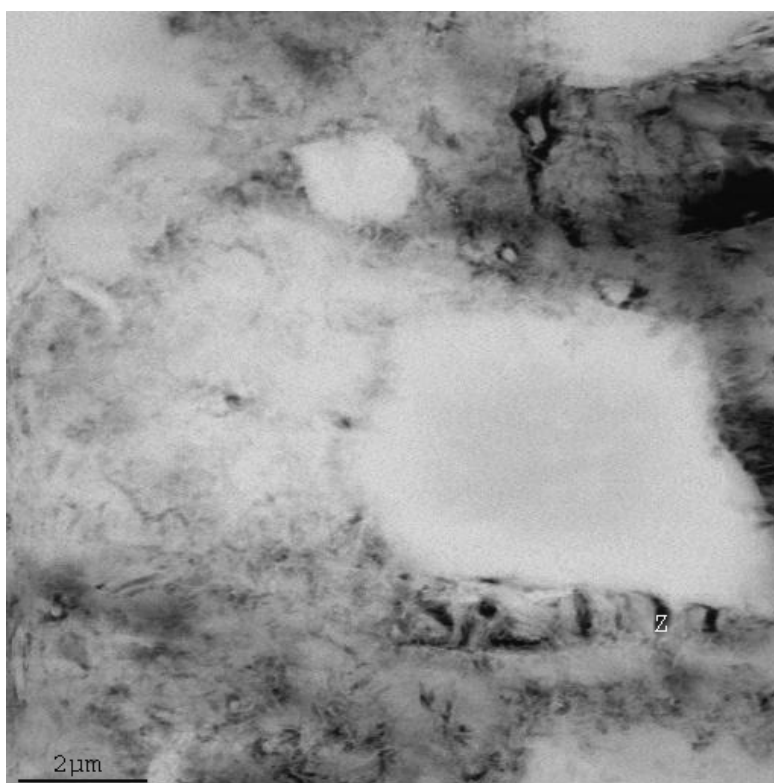
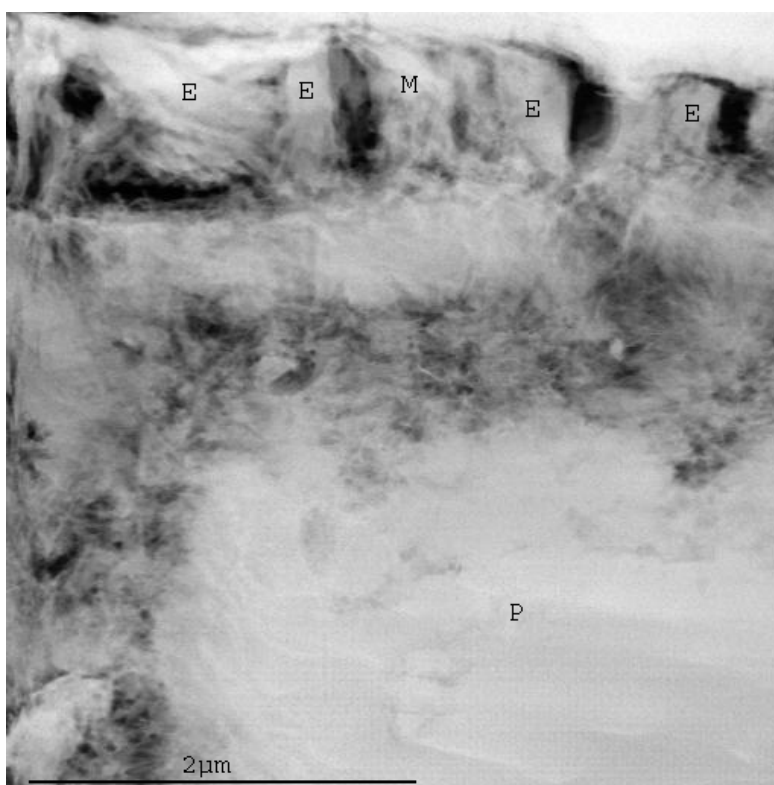


Figure 4.31: OPC 24 hours: seen here is a C_4AF grain just below an alite grain. Note the monosulfate plate (M: $1 \times 0.7 \mu\text{m}^2$) and the partial reaction of the grain (indicated by the arrow). *No shell* is formed around an interstitial phase.

indicate that there is an increased reaction of the ferrite phases at around 18 hours. By 24 hours (Figure 4.31) some parts of a C_4AF grain are seen to have reacted.



(a) The region marked 'Z' is shown below



(b)

Figure 4.32: OPC 48 hours: Formation of monosulfate as a result of reaction of ettringite with the interstitial phases. E → Ettringite, M → Monosulfate, P → Portlandite

Table 4.2: Solid-state substitution of aluminium by iron in ettringite

Substitution of iron in the AFt phases				
Age (h)	$P_{\text{Fe}}/T_{\text{AFt}}$	$(\text{Fe}/\text{Al})_{\text{average}}$	\pm	σ
8	0 / 10	0	\pm	0
10	0 / 05	0	\pm	0
12	0 / 06	0	\pm	0
18	1 / 04	0.43	\pm	0.00
24	8 / 20	0.33	\pm	0.11
48	5 / 10	0.28	\pm	0.08

Table 4.3: Solid-state substitution of aluminium by iron in monosulfate

Substitution of iron in the AFm phases				
Age (h)	$P_{\text{Fe}}/T_{\text{AFm}}$	$(\text{Fe}/\text{Al})_{\text{average}}$	\pm	σ
8	0 / 0	0	\pm	0
10	0 / 0	0	\pm	0
12	0 / 0	0	\pm	0
18	2 / 2	0.37	\pm	0.00
24	0 / 1	undetermined	\pm	
48	4 / 5	0.23	\pm	0.04

P_{Fe}	:	number of particles having iron
T_{AFt}	:	total AFt phases clearly seen
T_{AFm}	:	total AFm phases clearly seen

Table 4.4: Number of points having iron with or without aluminium in them and the average Fe/Ca ratios in various regions

Fe/Ca ratios									
Age (h)	Ip		Shell		Op		Overall		
	Fe/Ca	P_{Fe_T} / T_p	Fe/Ca	P_{Fe_T} / T_p	Fe/Ca	P_{Fe_T} / T_p	Fe/Ca	P_{Fe_T} / T_p	P_{Fe_T} / T_p
6	0.02	03 / 14	0.02	1 / 05	0.00	0 / 013	0.02	04 / 032	
8	U _d	00 / 20	0.07	1 / 27	0.11	2* / 134	0.09	03 / 181	
10	0.03	08 / 28	0.02	7 / 25	0.00	0 / 069	0.03	15 / 122	
12	0.03	04 / 22	0.03	1 / 19	0.08	1* / 027	0.04	06 / 068	
18	0.05	06 / 19	0.04	2 / 26	0.03	6 / 066	0.04	27 [§] / 125	
24	0.05	14 / 42	0.04	6 / 35	0.02	7 / 034	0.04	27 / 111	
48	0.04	05 / 24	U _d	0 / 06	0.04	5 / 044	0.04	10 / 074	
Age (h)	Fe/Ca	P_{Fe} / P_{Fe_T}	Fe/Ca	P_{Fe} / P_{Fe_T}	Fe/Ca	P_{Fe} / P_{Fe_T}	Fe/Ca	P_{Fe} / P_{Fe_T}	P_{Fe} / P_{Fe_T}
6	U _d	0 / 03	U _d	0 / 1	U _d	0 / 0	U _d	00 / 04	
8	U _d	0 / 00	U _d	0 / 1	U _d	0 / 2*	U _d	00 / 03	
10	0.03	7 / 08	0.01	4 / 7	U _d	0 / 0	0.03	11 / 15	
12	0.03	4 / 04	0.03	1 / 1	U _d	0 / 1*	0.03	05 / 06	
18	0.04	3 / 06	U _d	0 / 2	U _d	0 / 6	0.03	15 / 27 [§]	
24	0.05	7 / 14	0.02	3 / 6	0.02	3 / 7	0.04	13 / 27	
48	0.03	2 / 05	U _d	0 / 0	0.08	1 / 5	0.05	03 / 10	

P_{Fe_T} : number of points having iron, irrespective of the presence or absence of aluminium

P_{Fe} : number of points having iron but no aluminium.

T_p : total points in the particular region

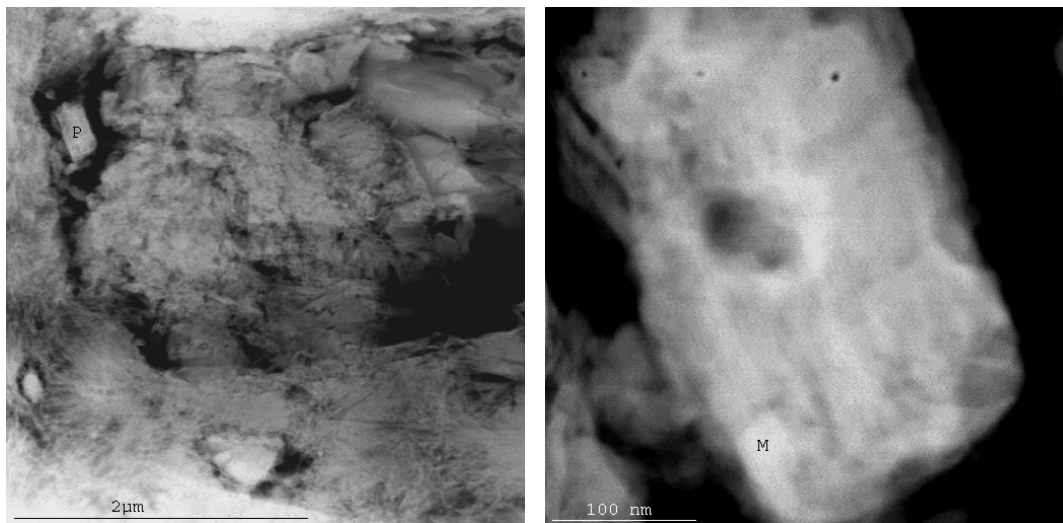
U_d : undetermined

* : points very close ($< 1 \mu\text{m}$) to C_4AF grains

§ : some points could not have been assigned to any particular region, which is why the sum of the points in individual regions is less than the total number of points

4.8 Hydrated phases at nano-scale

Figure 4.33a shows the presence of a portlandite plate in the hydration matrix of a 48 hours old sample. A magnified view of the plate is shown in Figure 4.33b obtained at $\times 170,000$ magnification. The chemical analysis on the phase marked M gives $\text{Ca}:(\text{Al}+\text{Fe})$, $\text{Ca}:\bar{\text{S}}$ and $\bar{\text{S}}:(\text{Al}+\text{Fe}) \sim 5.7, 7$ and 0.7 (ideal value for monosulfate is 0.5). This indicates that the phase is monosulfate ($\sim 50 \times 50 \text{ nm}^2$) which is present in a Ca^{2+} rich matrix (portlandite). This example shows the presence of hydrated phases at nanometer scale. This explains why sometimes chemical analysis results show the presence of alumina and sulfur, for example, in a ratio corresponding to that of ettringite (or monosulfate), but morphologically it is not visible even at moderate magnification.



(a) The magnified view of the portlandite plate (P) is shown on right

(b) M \rightarrow monosulfate

Figure 4.33: OPC 48 hours—small AFm plate ($\sim 50 \times 50 \text{ nm}^2$) having iron, intermixed with or growing on CH at nano-scale.)

Chapter 5

Study of the microstructure and phenomenological study of expansion in OPC, CAC, C \bar{S} blends

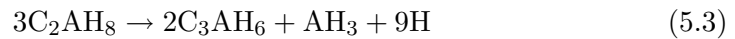
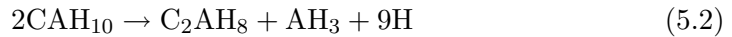
5.1 Literature review of the development of the microstructure

Mixed Binder systems based on combinations of Portland cement, calcium aluminate cement and calcium sulphate are used commercially to produce mixtures having rapid setting and hardening properties, shrinkage compensation etc.

5.1.1 Hydration of pure CAC cements

Unlike OPC, the hydration of CAC cements is strongly dependent on the temperature [182]. From 5 °C onwards the stable hydrates are C₃AH₆ and γ -AH₃. The formation of these hydrates is preceded by the formation of metastable hydrates, CAH₁₀, C₂AH₈ and amorphous phases (equations 5.1–5.3, [182]). These amor-

phous phases have yet to be well characterized, but are assumed to be based on anhydrous alumina and are generally called AH_3 gel. Studies [63] suggest that at early ages they may have compositions closer to CAH_{10} and contain aluminium in fivefold coordination [45]. It is also interesting to note that the ‘conversion’ of the metastable phases to the stable phases may not occur for years, in which case CAH_{10} and C_2AH_8 become the stable hydration products [182].

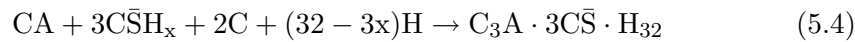


The mechanism of the formation of the hydrates is believed to be the same as in OPC, via through-solution, which involves dissolution of the anhydrous phases, releasing ions in the solution and their later precipitation as hydrates. Scrivener and Capmas [182] reported that the Al^{3+} concentration in the pore solution in the hydration of calcium aluminate cements is nearly the same as that of Ca^{2+} . Lamour and co-workers [124] studied the hydration of CAC cement pastes using Transmission X-ray microscopy and showed the precipitation of Al gel as the primary phase during the first hour of hydration. These results show that in the hydration of CAC cements, Al^{3+} ions have a rich presence and a high degree of mobility in the solution.

5.1.2 Mixture of OPC and CAC

While the setting time for CAC cements is similar to that of pure OPC [182], the setting time of a mixture of OPC and CAC is much shorter [52, 179, 182]. These binary cement mixtures develop strength within a few hours. The long-term strength development is, however, relatively poor. Various techniques [91–94, 218] have been used to study this binary mixture and it is believed that ettringite formation dominates the early age hydration. This is confirmed by SEM studies [92] which showed that needle-type ettringite formed in a 20%CAC–80%OPC paste within the first 30 minutes (equation 5.4 [92]) and was one of the major factors causing quick set. According to some authors [3, 179] setting is affected because

the CA phase in CAC reacts with the sulfate present in OPC rather than letting it to react with the C₃A grains of OPC. This hindering affects the formation of a coating of products around C₃A grains, which is believed to arrest the otherwise rapid reaction of C₃A and helps in a gradual setting. Exploratory studies have also shown that some combinations have excellent resistance to chemical attack [179].



The formation of hydrates depends on the relative proportions of CAC and OPC. For mixture with CAC < ~ 20% (OPC dominant) C-S-H remains the dominant hydrate and aluminium is present in the form of ettringite and C₄AH_x. For such mixes the metastable phases CAH₁₀ and C₂AH₈ are not formed. Similarly mixture with OPC < ~ 20% (CAC dominant) produce the same hydration product as in pure CAC. In between these limits the hydration is not well understood and is believed to involve the formation of aluminosilicate strätlingite (C₂ASH₈) along with other hydrates [182]

5.1.3 CAC+C \bar{S}

Mixtures of CAC and C \bar{S} are considered important in building chemistry, as they are rich in ettringite, a phase with a high capacity to bind water. This makes these mixes an important source to produce products which are rapid drying and rapid hardening [182].

Studies [14, 15] have shown that ettringite and AH₃ gel are the chief hydration products in these mixes. If the calcium sulfate is depleted the ettringite is believed to react with the anhydrous aluminate phase to form monosulfate. The development of hydrates, besides depending on the relative proportions of the two starting anhydrous phases [182], is also known to depend on the type of calcium sulfate used, i.e. hemihydrate, gypsum or anhydrite [123, 179, 182]. In the study of CAC-C \bar{S} mix, Bayoux and co-workers [14, 15] showed that when gypsum or hemihydrate are used, which are more readily soluble than CAC, the solution is rich in Ca²⁺, SO₄²⁻ and deficient in Al³⁺, resulting in the formation of short stubby ettringite crystals. However when anhydrite was used, due to its poorer solubility, the solution is poor in SO₄²⁻ resulting in the formation of long thin needles of

ettringite.

As seen by the different kinds of hydration products formed in this system, the normal conversion reactions in the hydration of pure CAC do not occur.

5.1.4 Ternary blends

Lamberet [123] studied the long term (28 days to 3 years) durability and hydration patterns of ternary mortars. Regarding the microstructure, it was reported that the Portland based systems behave very differently from pure Portland cement and the hydration mechanisms depends on the PC/CAC and CAC/C \bar{S} ratios. The characteristic feature of the mix binders was reported to be the formation of supplementary ettringite and the *delay* in the hydration of silicates.

It was also shown that the Portland rich systems performed better than those rich in CAC-C \bar{S} with regard to carbonation, however the CAC-C \bar{S} rich blends were shown to have maximum resistance to acid media, which was attributed to AH₃, which was believed to act as a diffusion barrier.

The effect of w/c ratio was also brought out as it was shown that the resistance of the mixes to erosion is increased with a decrease in w/c ratio.

5.2 Introduction to the work done

Studies on the microstructures of these binder systems indicate that these microstructures are complex involving much intermixing of phases on the nanometer level. We wish to observe these intermixed phases using TEM, to obtain their chemical composition, morphology, packing etc. and which shall be helpful in better understanding of their influence on the properties of the mixed binder systems.

For the microstructural study of these mix binders a ternary mix M2 which is an OPC dominant system with minor additions of CAC and C \bar{S} (Table 5.1) was prepared at 6 and 16 hours in order to compare its microstructure and chemistry with pure OPC.

Table 5.1: Composition of the ternary mix (M2) studied using TEM

Name of composition	OPC (wt%)	CAC (wt%)	C \bar{S} (wt%)
M2	77.20	6.70 (Secar 51)	16.10 (gypsum)

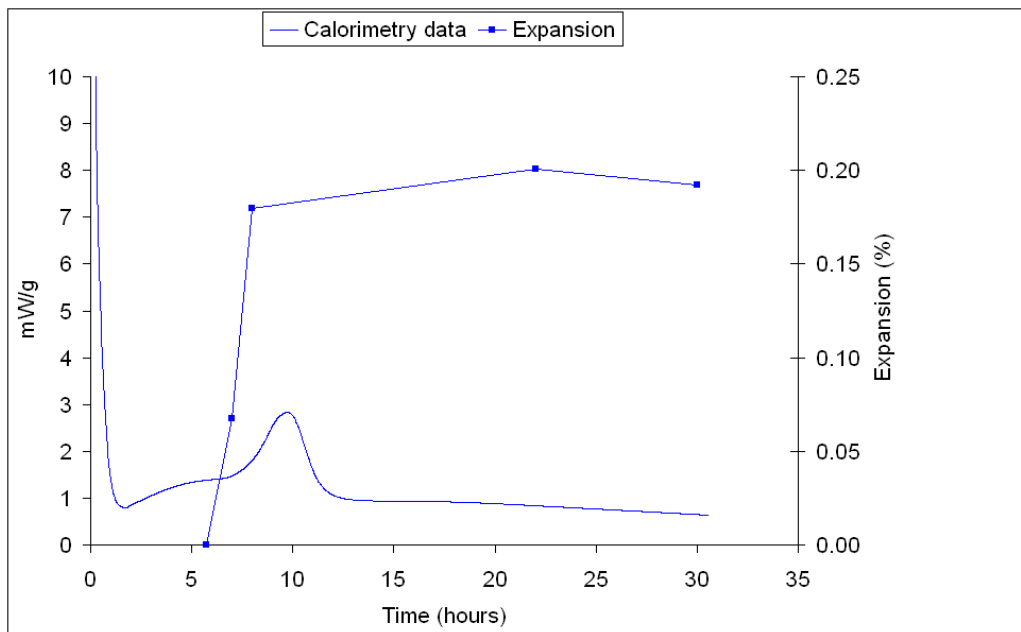


Figure 5.1: The heat of hydration of the ternary mix M2, along with its expansion when cured over water (100 %RH)

5.3 Ternary mix M2

Since M2 is an OPC dominant composition, its microstructure could be expected to be not very different from that of pure Portland. However, added aluminate cement and calcium sulfate could be expected to play an important role in the hydration. For instance this mix was found to be expansive in nature. Figure 5.1 shows the expansion curves along with the heat of hydration.

At **6 hours**, shells of hydration products are seen around most grain (Figure 5.2). Compared with pure OPC at 6 hours, the shell appear broader, however the gap between the shells and the enclosing grain seems to be nearly the same.

Chemical analysis of the composition at **16 hours** shows that similar to pure OPC,

the shells and the hydration products within it are composed of C-S-H, along with the presence of ions such as Al^{3+} , SO_4^{2-} , etc. By 16 hours the microstructure, similar to that of OPC, has evolved considerably with pore space significantly filled by the hydration products. Like in pure OPC, parts of cement grains are seen to have reacted more than the other parts (Figure 5.2). Similarly, striations on cement grains are also observed (Figure 5.3). The shells in M2, however, are broader and more dense than in pure OPC (Figure 5.4).

There are similarities in the morphology of C-S-H seen in M2 and in OPC with differences in their compactness. There is a prominent presence of acicular shaped C-S-H in M2 (Figure 5.5). In all observed instances, the acicular C-S-H (identified by chemical analysis) is found to have a rich presence of magnesium. It is also observed that C-S-H within the shell is relatively more dense than in OPC along with a more prominent presence of fine particles of C-S-H (Figure 5.6). Further, unlike in OPC, *no portlandite* is found in the ternary mix. Another contrasting feature of the microstructure is the *rich presence of ettringite* which are seen as coarse needles in the pore space and as a coating around CAC grains (Figure 5.10 on page 126). This can be expected due to the rich presence of aluminate and sulfate phases. By 16 hours, several *well-developed monosulfate* plates are also seen (Figure 5.11), indicating the limited availability of sulfates. This is unlike the hydration of OPC, where very limited monosulfate is seen as small plates by 18 hours.

In some instances Al gel (confirmed by chemical analysis) is seen in the matrix (Figure 5.11). Along with having aluminium as the major element, small amounts of calcium ($\text{Ca:Al} \sim 0.02$) are also present in it.

5.3.1 Ca:Si ratios

For calculating the calcium and silicate contents of the C-S-H in M2, the same methodology was used as for OPC hydration. All the points corresponding to C-S-H which had the presence or absence of sulfur in them were included while those having aluminium and/or iron were excluded. As shown in later sections, aluminium appears to be largely present as ettringite, although it may also be possible that Al may be absorbed along with sulfate in a ratio corresponding to that of ettringite or monosulfate. Nevertheless, such points have not been included

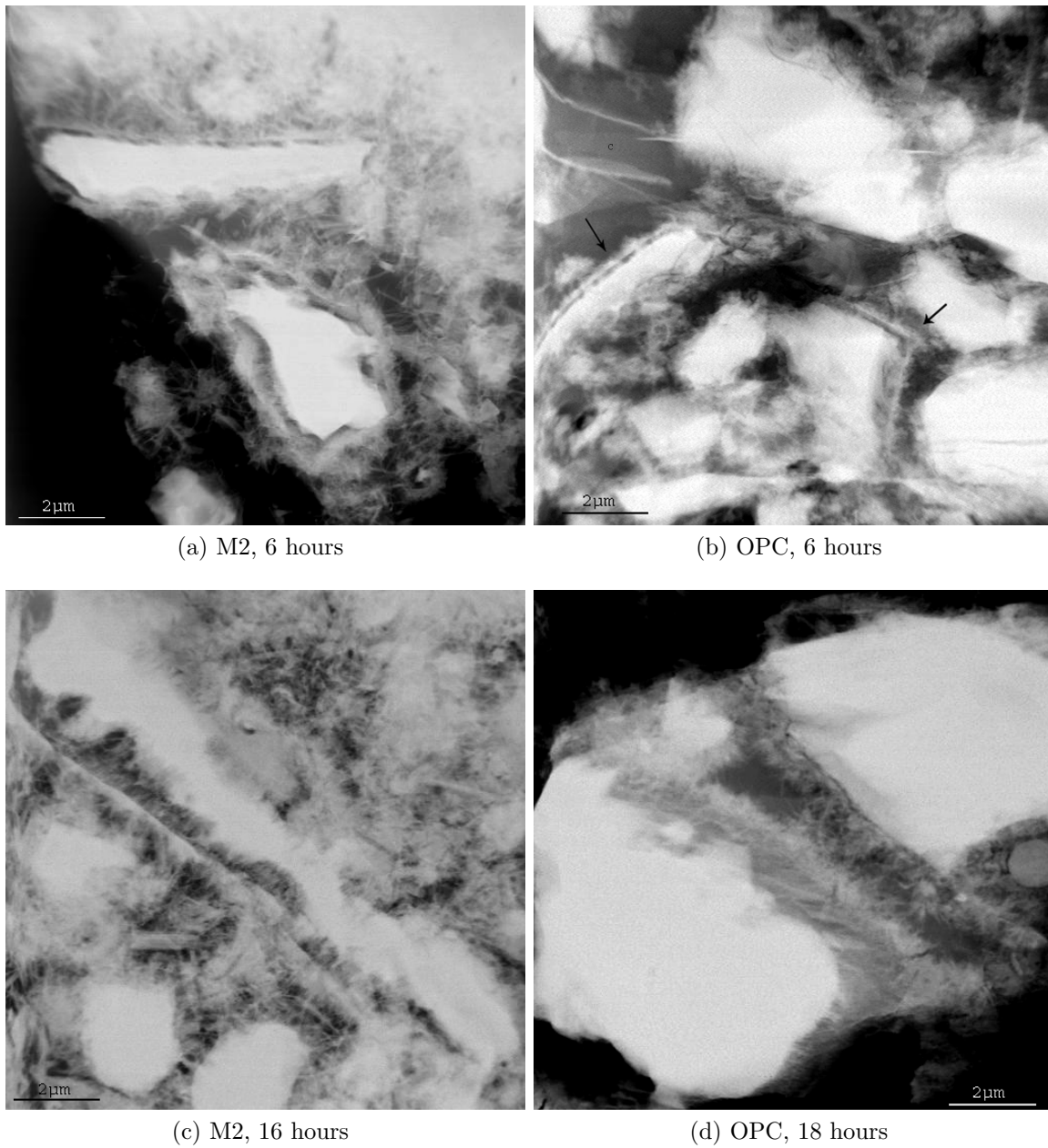


Figure 5.2: Comparing the shell formation in pure OPC and in the ternary mix M2, with OPC as the major phase. The shells in M2 appear broader and denser than in OPC however at 6 hours the gap between the shells and their respective grains remains nearly the same.

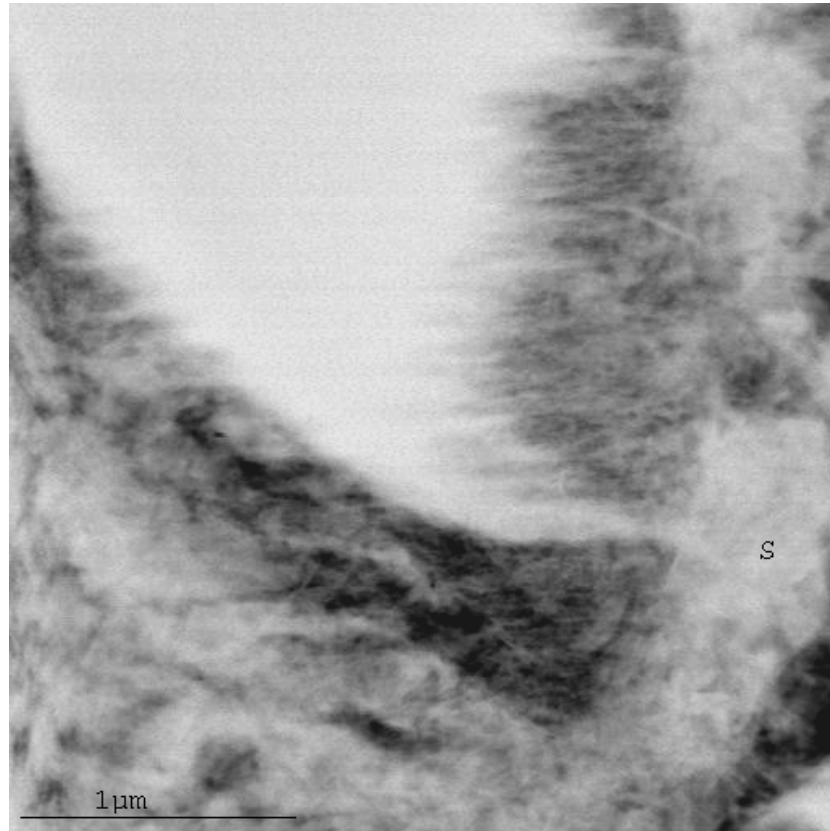


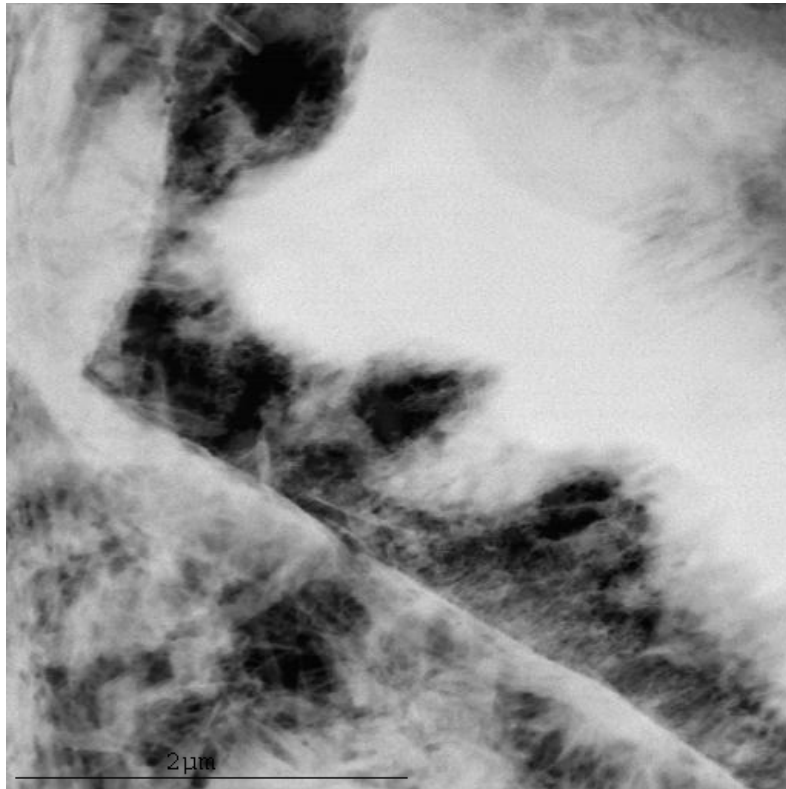
Figure 5.3: M2, 16 hours: similar to OPC, the shells are not empty but filled with C-S-H rich product.

Table 5.2: showing the total number of points taken to calculate Ca/Si ratio in various regions and the number of points among them which have sulfur

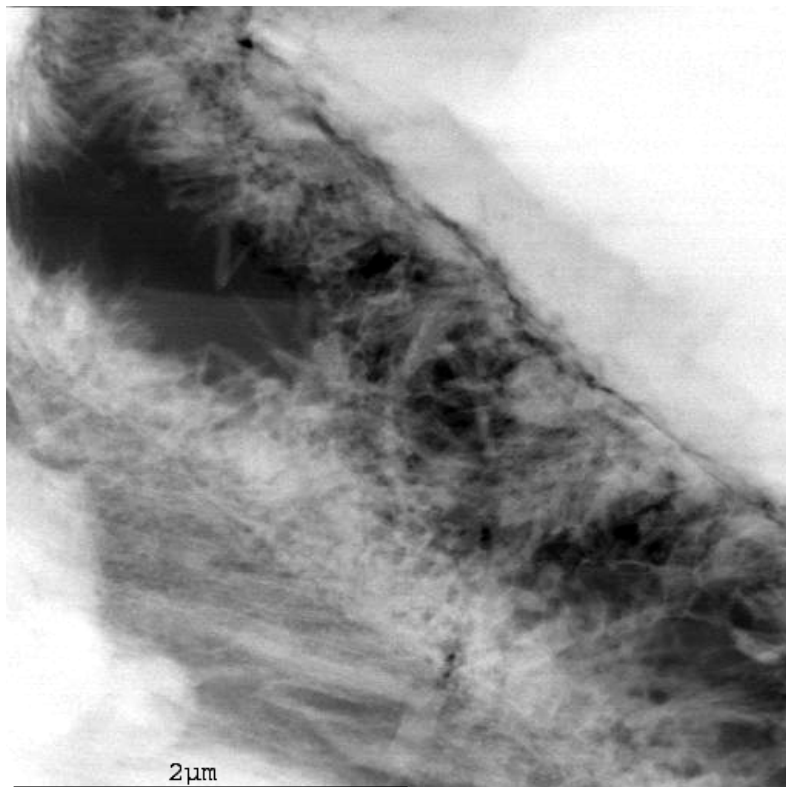
Number of points taken to calculate Ca/Si ratios						
Age (h)	Ip		Shell		Op	
	points having sulfur	total points	points having sulfur	total points	points having sulfur	total points
16	2	7	13	14	12	14

in this calculation.

The number of points taken to calculate Ca:Si ratios is shown in Table 5.2. Again, for the sake of comparison both $(Ca-\bar{S})/Si$ and Ca/Si ratios are presented in



(a) M2, 16 hours



(b) OPC, 18 hours

Figure 5.4: The shell in M2 is seen to be relatively denser and broader than in OPC

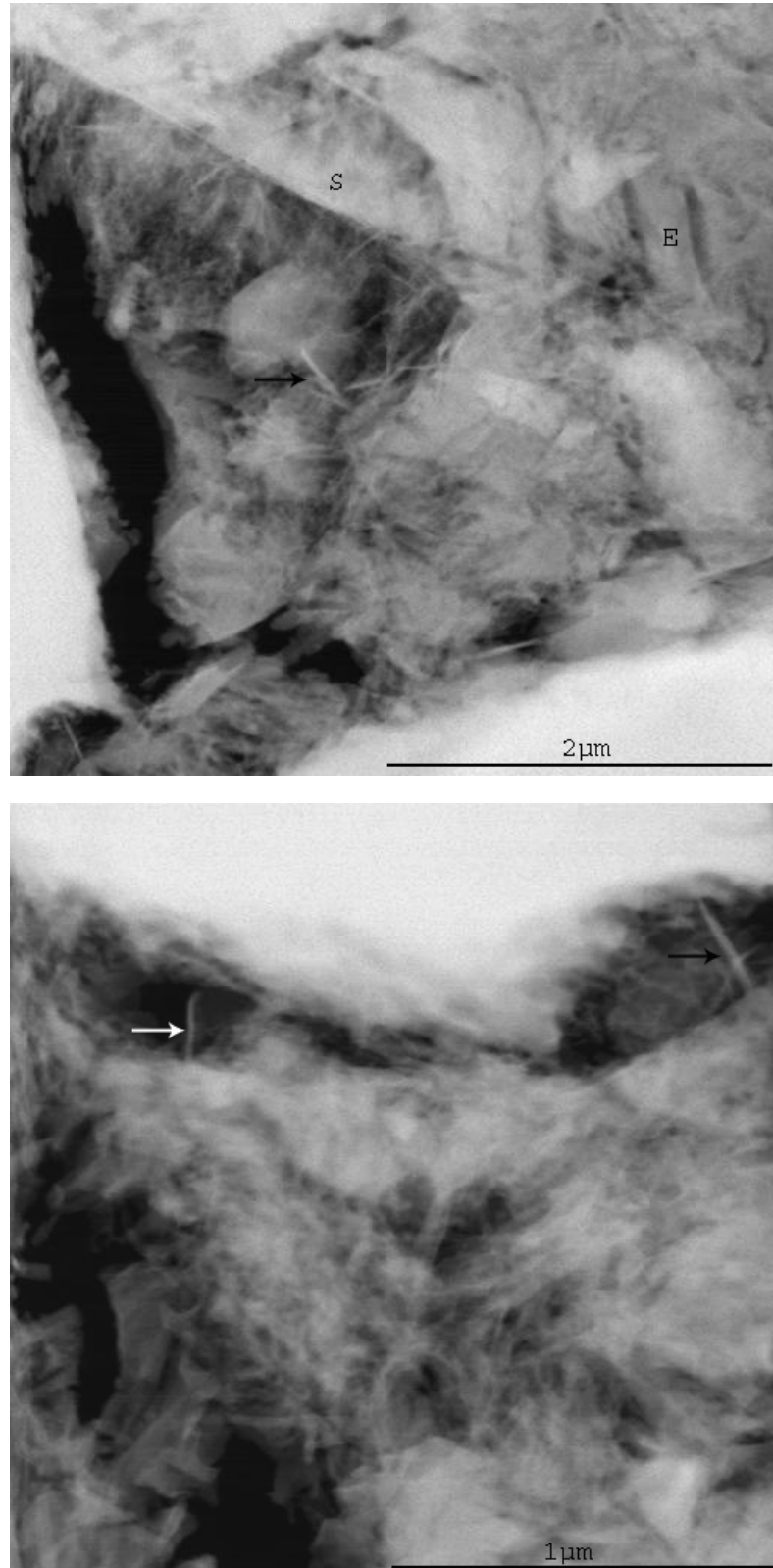
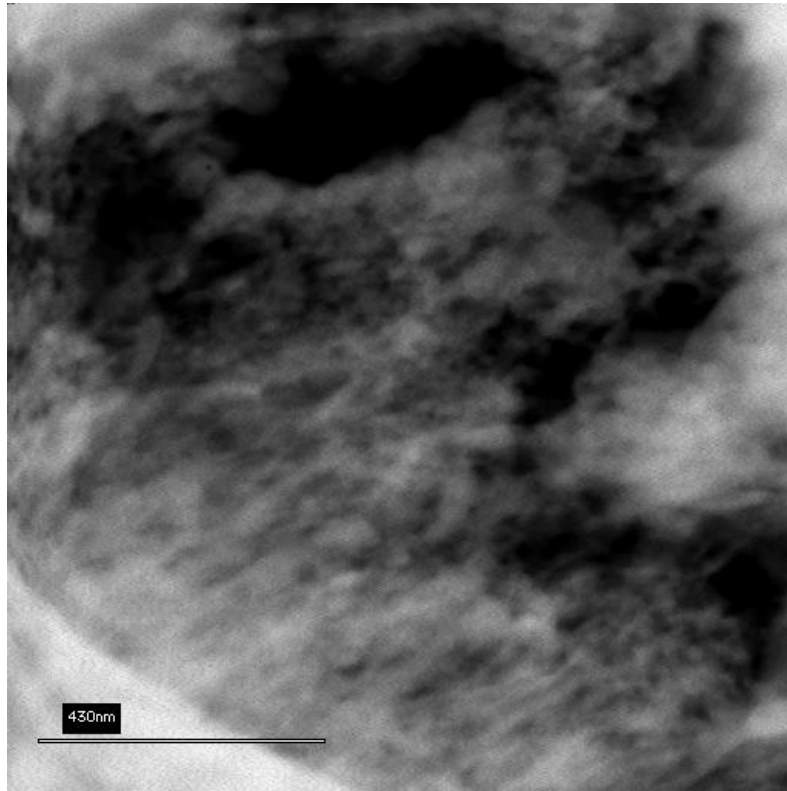
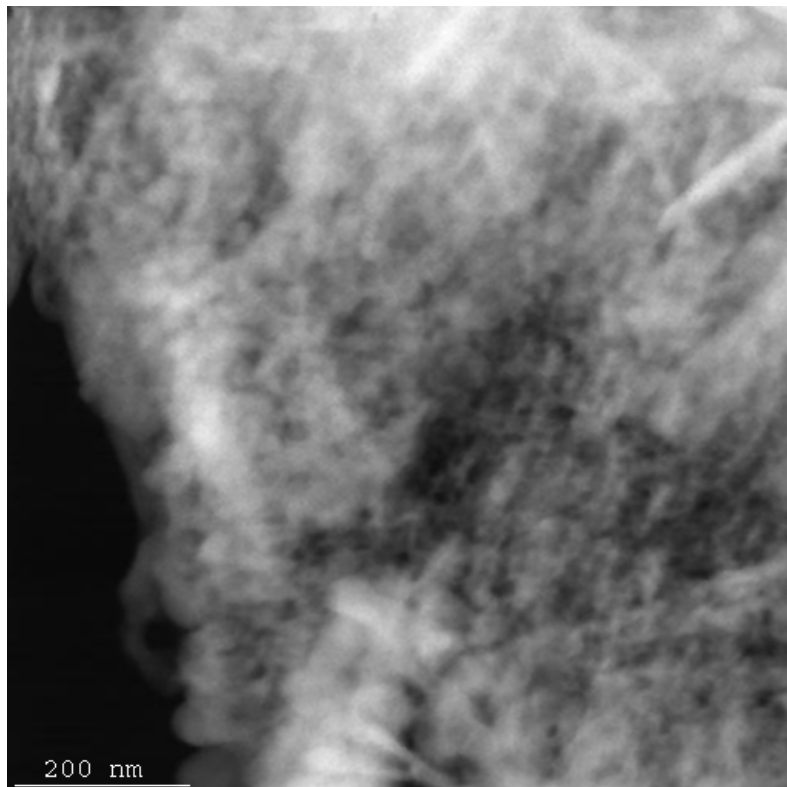


Figure 5.5: M2, 16 hours: a distinguishing feature of the ternary mix is the prominent presence of acicular shape C-S-H (learned from the chemical analysis and marked by arrows). Further, they are only seen within the shell (S). E: ettringite



(a)



(b)

Figure 5.6: M2, 16 hours: high magnification images reveal that C-S-H within the shell is relatively more dense than in OPC with more prominent presence of nanoparticles of C-S-H.

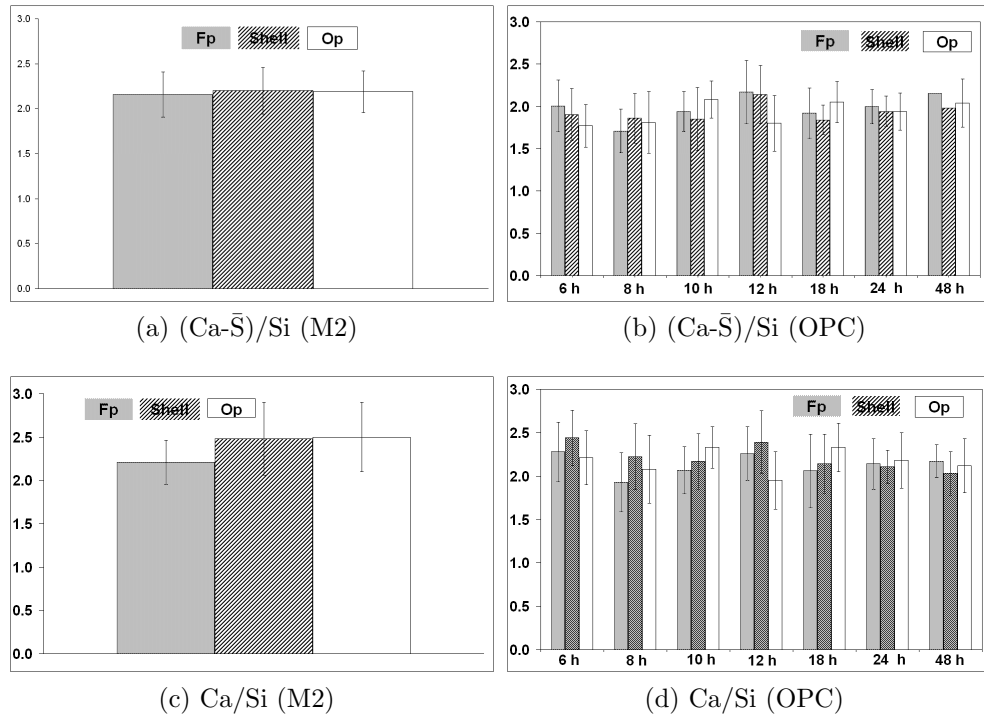


Figure 5.7: M2, 16 hours: seen here are Ca:Si values of C-S-H with and without removing the absorbed sulfur. None of the points included had aluminium and/or iron in them. The ratios are only marginally higher than for pure OPC.

Figure 5.7. It is seen that the values are almost the same as for OPC. Thus the chemistry of C-S-H seems to be unaffected by additions of CAC and CS . This can perhaps be looked in conjunction with the morphology of C-S-H which is also the same as seen in pure OPC.

5.3.2 Role of aluminates

It is interesting to note the distribution of aluminate in the mix at 16 hours. From the images, it is evident that aluminium is present in the form of ettringite, which is present as broad needles and as a coating around CAC grain (Figure 5.10), and as monosulfate plates (Figure 5.11).

However, the obtained chemical analysis reveals that aluminate is also present on

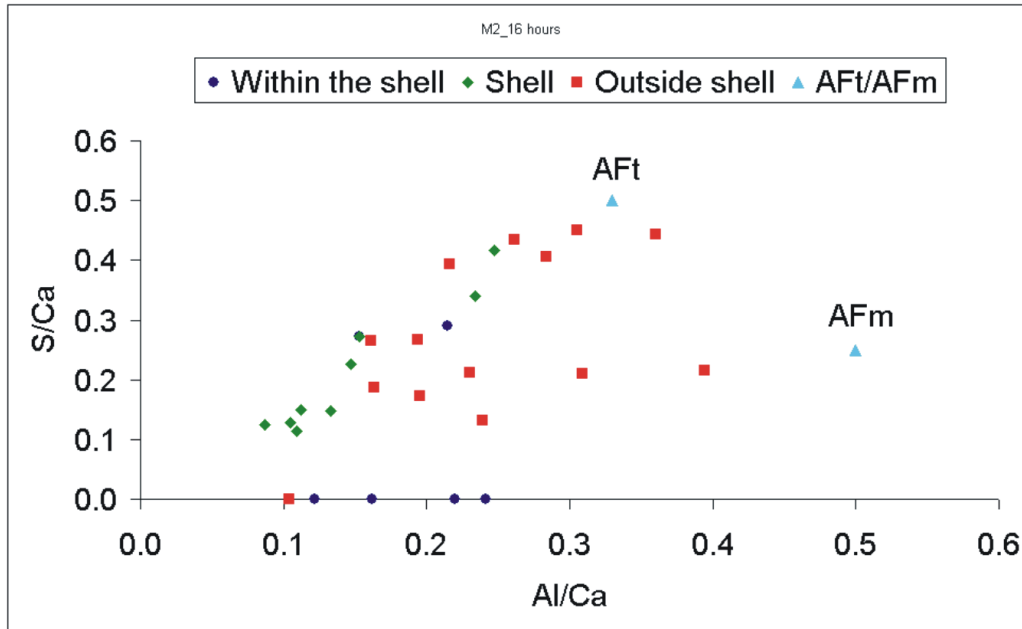


Figure 5.8: M2, 16 hours: distribution of aluminium. It can be present as ettringite and monosulfate finely intermixed with C-S-H, or, some or all of it may be absorbed in the C-S-H, along with sulphate in the ratio corresponding to ettringite or monosulfate.

C-S-H. A plot of the S/Ca : Al/Ca is depicted in Figure 5.8. It suggests that aluminium could be either present as ettringite and monosulfate intermixed with C-S-H at a fine scale, or, some or all of it may be absorbed in the C-S-H, along with sulphate in the ratio corresponding to ettringite or monosulfate.

Another form in which aluminium is seen is the AH_3 phase, normally called as aluminium gel. At low magnifications it is seen as a foam-like product (Figure 5.11a) but higher magnifications image reveal it to have large porosity (Figure 5.11b). It appears almost dark in the dark-field TEM images, suggesting that it has a lower density and/or average atomic number. Similar characteristics of the same phase have also been observed in the binary mix B2 (page 180).

Distribution of sulfate

Average values of the S:Si ratios of the various regions, namely, flimsy product (within the shell), the shell and the outer product were calculated as shown in

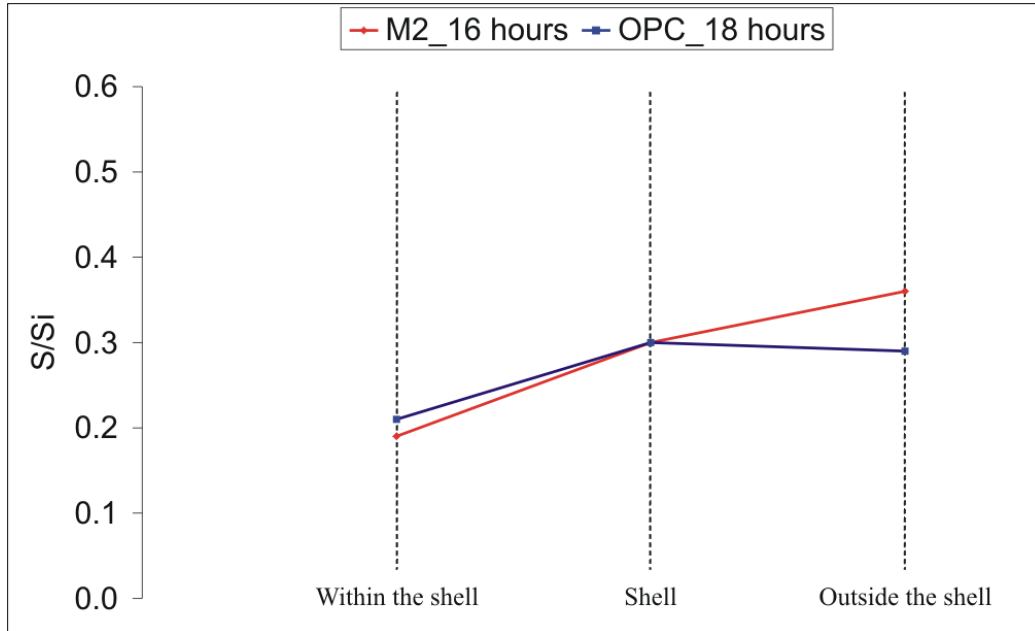


Figure 5.9: The sulfur concentration in M2 increases as one moves from the grain towards the shell. This is in concurrence with the similar results reported in the hydration of OPC.

Figure 5.9. It is interesting to note that the ratios are similar to that seen in OPC and the amount of sulfur present increases as one moves from the surface of the grain towards the shell and beyond. This is principally in concurrence with the findings of the hydration of Portland cement.

5.3.3 Role of ferrites

Like in OPC, some iron is found in the studied mix at 16 hours. It can come from C_4AF in OPC and from the ferrite phases in Secar 51. Since only about 1% of iron oxide is present in Secar (Table 2.2 on page 7), a significant increase in the iron content, compared to that in pure OPC, is not to be expected. This is confirmed by the results shown in Table 5.3. The iron to calcium ratios of the various regions are the same as noted for OPC.

It is interesting to note that iron, like in OPC, is again found to be mostly present within the shell and in very limited amounts outside the shell.

Table 5.3: Number of points having iron with or without aluminium in them and the average Fe/Ca ratios in various regions

Fe/Ca ratios				
	Ip	Shell	Op	Overall
Age (h)	Fe/Ca P_{FeT}/T_p	Fe/Ca P_{FeT}/T_p	Fe/Ca P_{FeT}/T_p	Fe/Ca P_{FeT}/T_p
16	0.06 9 / 22	0.04 3 / 26	0.03 2 / 30	0.05 14 / 78

Age (h)	Fe/Ca P_{Fe}/P_{FeT}	Fe/Ca P_{Fe}/P_{FeT}	Fe/Ca P_{Fe}/P_{FeT}	Fe/Ca P_{Fe}/P_{FeT}
16	0.05 3 / 9	0.02 1 / 3	0.04 1 / 2	0.04 6 / 14

P_{FeT} : number of points having iron, irrespective of the presence or absence of aluminium

P_{Fe} : number of points having iron but no aluminium.

T_p : total points in the particular region

Solid-state substitution in AFt/AFm phases

In order to realize the presence of iron, if any, in the aluminate containing hydrates, all the ettringite and monosulfate phases that were clearly visible were identified. Out of 6 AFm and 13 AFt phases, none of them have any presence of iron in them (Tables 5.4 and 5.5). Thus it can be concluded that solid-state substitution *has not* occurred by 16 hours in the mix M2. This correlates with the reported findings of pure Portland cement, which showed the first instance of solid-state substitution of iron at 18 hours.

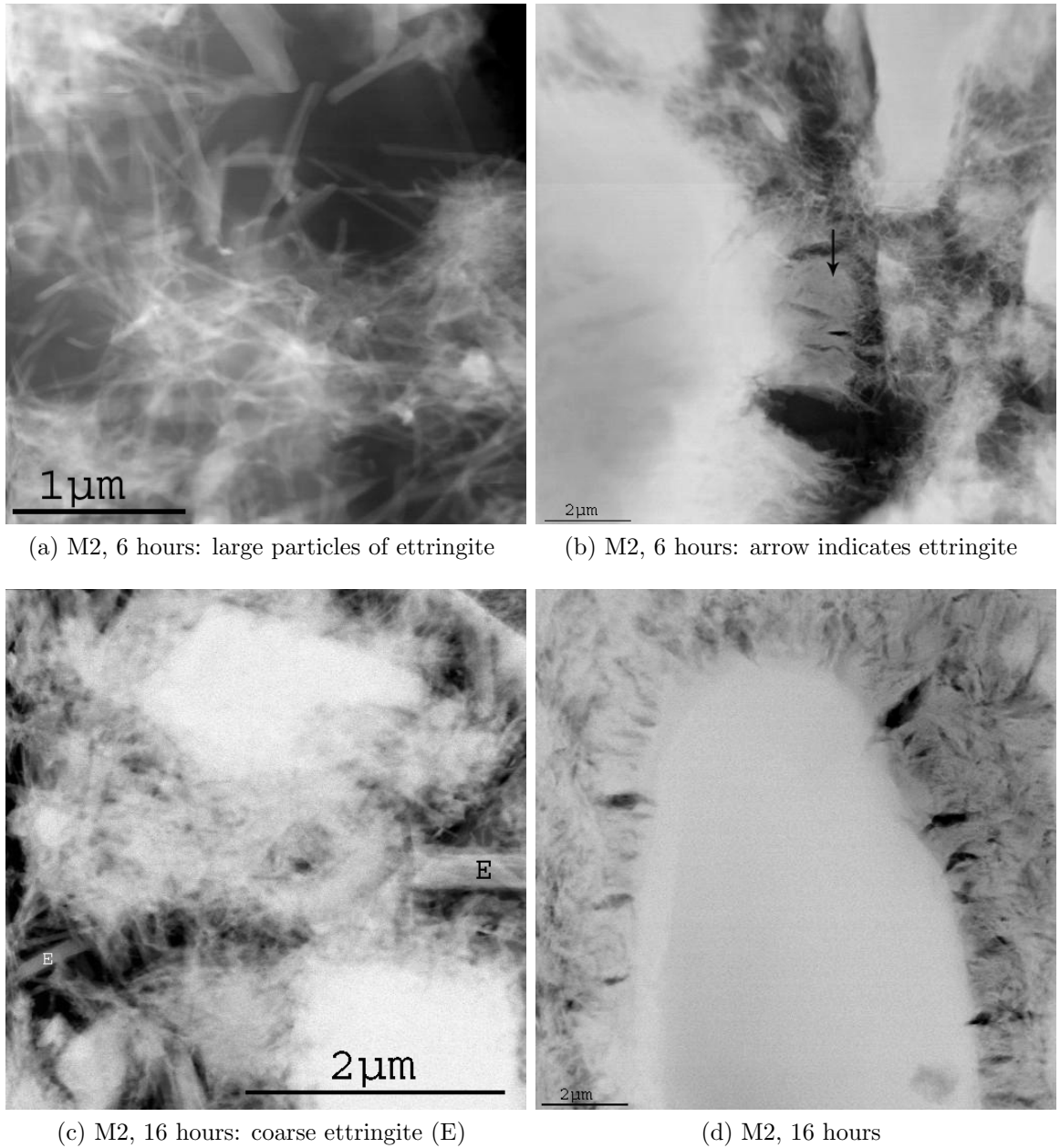
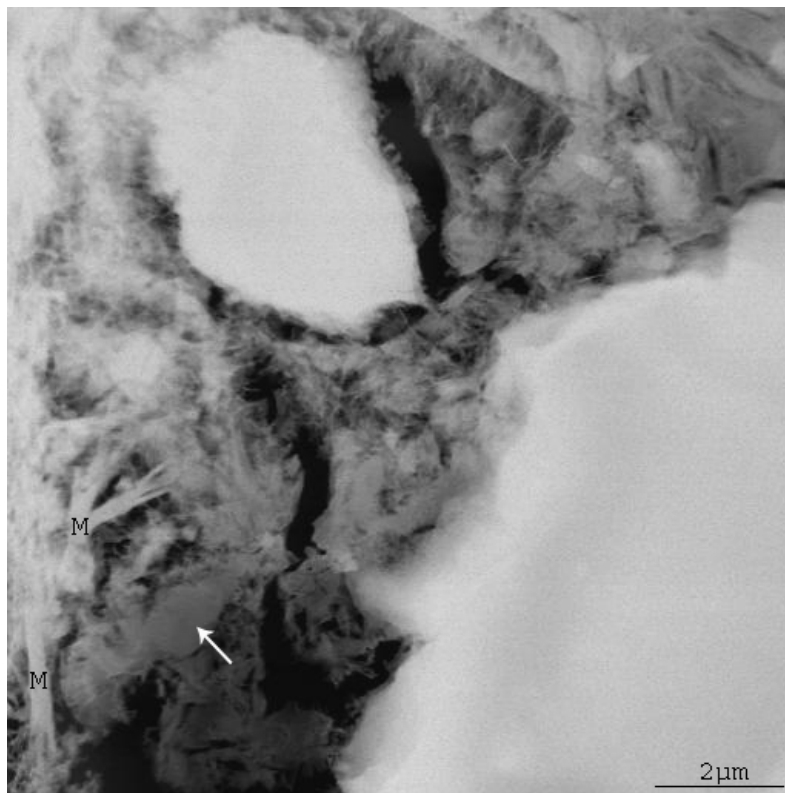
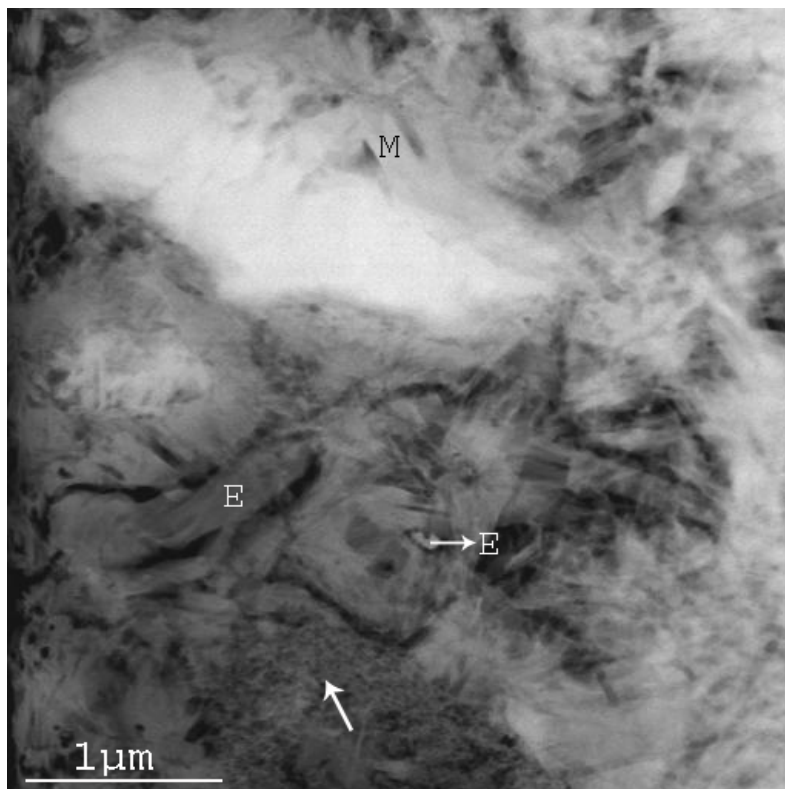


Figure 5.10: Composition M2: ettringite seen as coarse needles in the pore space and as a coating around CAC grains.



(a)



(b)

Figure 5.11: Al gel (indicated by the arrows) seen present in the well developed matrix at 16 hours, along with ettringite (E) and monosulfate (M) phases.

Table 5.4: Solid-state substitution of aluminium by iron in ettringite

Substitution of iron in the AFt phases				
Age (h)	$P_{\text{Fe}}/T_{\text{AFt}}$	$(\text{Fe}/\text{Al})_{\text{average}}$	\pm	σ
16	0 / 13	0	\pm	0

Table 5.5: Solid-state substitution of aluminium by iron in monosulfate

Substitution of iron in the AFm phases				
Age (h)	$P_{\text{Fe}}/T_{\text{AFm}}$	$(\text{Fe}/\text{Al})_{\text{average}}$	\pm	σ
16	0 / 6	0	\pm	0

P_{Fe}	:	number of particles having iron
T_{AFt}	:	total AFt phases clearly seen
T_{AFm}	:	total AFm phases clearly seen

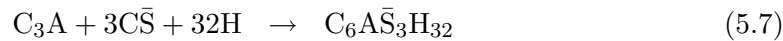
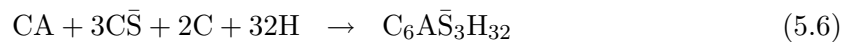
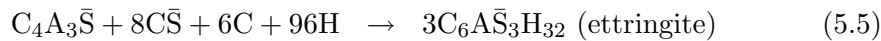
5.4 Expansion in ternary mixes

Recent works [83, 123] have shown that the ternary mixes involving OPC, CAC and CS may also undergo damaging expansion if they contain too much sulfate. This is an important issue in the formulation of blended products which are used for applications such as repair. The amount of expansion seems to depend on the relative proportions of the blended cements. Giroud [83] studied a wide range of blends in order to better define the expansion limit. It was found that the form of expansive destruction changed with the different blends—some samples disintegrated while others cracked, while remaining intact. Still others showed stable expansions with no apparent detrimental effects. Some preliminary observations were made of the evolution of the phases, but no conclusions on the mechanisms of expansion were drawn. In order to study and understand the phenomenon of expansion in these ternary mixes, it is considered useful to review the work done by several authors in the field of expansion in sulfoaluminate cements. This is

presented in the proceeding sections.

5.5 Literature review of the expansion in sulfoaluminate cements

According to ASTM C 845-96 standard [1], the classification of expansive cements covers the three following groups: K, M and S. Type K is produced from anhydrous calcium sulfoaluminate ($4\text{CaO} \cdot 3\text{Al}_2\text{O}_3 \cdot \text{SO}_3$), calcium sulfate, and uncombined calcium oxide. Expansive cement M is produced from calcium aluminate cement and calcium sulfate. Type S cement is produced from tricalcium aluminate (C_3A) and calcium sulfate [119]. Their basic hydration reactions are as follows:



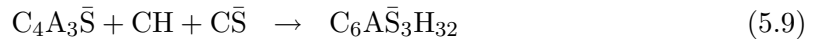
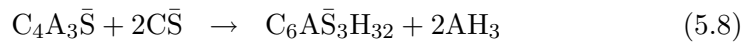
Several theories have been proposed to explain the mechanism of formation of ettringite and the resulting expansion in sulfoaluminate cement pastes. There exist two major schools of thought: the Crystal Growth Theory and the Swelling Theory. According to former, expansion is caused by the growth of ettringite crystals from the surfaces of the expansive particles or from the solution resulting in crystallization pressure and hence expansive forces. The swelling theory states that the expansion is caused by water-adsorption and swelling characteristics of ettringite ‘gel’ which forms by a through-solution mechanism. Work done by several authors in support of the two theories is presented as follows.

5.5.1 The crystal growth theory

Budnikov and Kravchenko [30] studied the phenomenon of expansion in hardened expansive cement pastes. They attributed the formation of crystals as the cause of expansion, and it was believed that expansion occurs when the growth of crystals

moves the obstacles apart. Expansion was said to be dependent on the number of crystallization nuclei in a unit of volume and also on the rate at which crystals grow in the matrix. This was explained as follows: if the number of crystallization nuclei per unit volume is large the expansion will be small, but if the number per unit volume is small, expansion will be large, despite a lesser number of these expansive sites. This is because a large number of nuclei per unit volume would mean the formation of ettringite crystals, though in large amounts, but in a short time span during which the cement would not become sufficiently hardened to provide for expansion. But if the ettringite crystals form late, the expansion will be relatively larger, provided that the cement has gained considerable hardness. The factors thought to influence expansion are the composition of the expansive cement, the fineness of a cement, the temperature of the environment, and the admixture modifying the structures of the newly-formed hydrate.

Nakamura and co-workers [142] studied the expansive behaviour of mixtures involving $C_4A_3\bar{S}$, $Ca(OH)_2$ and $CaSO_4$. They reported that expansion occurred only when ettringite was formed and shrinkage occurred when monosulfate phases were formed. It was reported that the condition of formation of ettringite seemed dependent upon the concentration of SO_4^{2-} ions around the $C_4A_3\bar{S}$ particles, regardless of the presence or absence of $Ca(OH)_2$. It was not explicitly stated how the ionic concentrations were measured, but it is inferred that SO_4^{2-} concentrations referred to the different amounts of sulfate added in the mix. The following stoichiometric reactions were proposed to explain the formation of ettringite:



In the presence of CH, when Ca^{2+} ions are present in abundance, ettringite crystallized as fine grains coating the surface of $C_4A_3\bar{S}$ particles. This coating developed during the process of hydration and began to act on the adjacent particles resulting in expansion. The amount of expansion was shown to increase with the increase in $Ca(OH)_2$ content. However, it was also stated that the expansion was not necessarily dependent upon the amount of ettringite that was formed, but rather on the type of ettringite, referring to fine or coarse ettringite. In the absence of CH no

expansion was produced even though ettringite was formed. In the above stated reaction, when Ca^{2+} ions were relatively scarce, ettringite formed as large crystals in the solution. The authors also studied the mixes involving the pure mixtures of $\text{C}_4\text{A}_3\bar{\text{S}}-\text{Ca}(\text{OH})_2-\text{CaSO}_4$ and ordinary portland cement. In this case expansion was reported to occur even when CH was absent from the pure mixture. This was attributed to the likely supply of CH by the silicate phases present in the cement. Hence $\text{Ca}(\text{OH})_2$ is needed to produce expansion. They also stressed the significance of strength development to expansion since the expansion begins only when the cement obtains considerable hardness.

Along this line, the effects of lime concentration on the mode of formation of ettringite and on the resulting expansion were studied by Okushima and co-workers [153]. In concurrence with previous works [30] formation of ettringite was reported to be the cause of expansion. It was also reported that very little expansion occurs when the relative concentration of lime was low. They also reported that ettringite can form either on the surface of aluminate particles or in the solution. In the case of $\text{C}_4\text{A}_3\bar{\text{S}}$ alone, monosulfate and $\text{Al}(\text{OH})_3$ are produced, and this causes ettringite to crystallize in the solution. But in the presence of lime, $\text{C}_4\text{A}_3\bar{\text{S}}$ hydrates quickly and becomes covered with a fine coating of ettringite crystals without changing the outer shape of the grain. The coating then begins to expand. The formation of ettringite in this manner was attributed to a topochemical (solid to solid) formation. However, as now widely believed, it is unlikely that ettringite can form topochemically, since the crystal structures of ettringite and all other aluminium rich anhydrous phases are totally different. Most likely ettringite is formed via through-solution. Nevertheless, the authors further mentioned that the driving force of expansion is the pressure created by crystal growth from products under compressive stresses. It was also added that the degree of expansion depends on the size of the crystals produced, being larger with the smaller crystals. Using XRD analysis it was shown that ettringite is produced as long as gypsum is available. However, at a certain point of hydration, monosulfate comes into existence just when the concentration of ettringite starts to drop. This probably indicates the monosulfates formation at the expense of ettringite.

Kalousek and Benton [113] in their study of the mechanism of external sulfate attack on cement pastes have attributed expansion to the ettringite crystals that grow in confined sites and which exert expansive forces against the surrounding

walls. They stated that there is no correlation between the amounts of ettringite precipitated and expansion. It is only a part of the increase in the amount of ettringite which is effective in causing expansion, the remainder depositing in voids. This is because as Ca^{2+} , SO_4^{2-} and OH^- diffuse to the original sites of C_3A , ettringite develops expansive stresses against the surrounding walls of the C-S-H gel and, therefore, produce expansion by crystallization pressure. This is because ettringite occupies a volume larger than was occupied by C_3A . This hypothesis is similar to the proposed mechanism of crystal pressures due to small ettringite particles depositing in sub-micron pores in the study of expansion due to delayed ettringite formation.

In the study of the mechanism of expansion in expansive cements some authors [163] assumed the expansive particles C_3A and $\text{C}_4\text{A}_3\bar{\text{S}}$ to be surrounded by a solution of uniform thickness containing dissolved sulfates, calcium hydroxides, and water. It was also assumed that as soon as reaction starts, the surfaces of the expansive particles immediately become covered by ettringite which was thought to be present as a dense coating. Further hydration occurs and increases the thickness of this layer. When the layer exceeds the surrounding solution thickness, it will push other particles apart, resulting in overall expansion. Expansion will continue until either the expansive particles or the dissolved sulfates will deplete. Following these assumptions, a Micromechanical Model was developed to calculate geometrically the final magnitude of expansion [163]. The magnitude was thought to be a function of the final thickness of the ettringite coating and on the number of expansive sites. These two factors are influenced by the chemical composition of individual components, w/c, and the particle- size distribution (PSD) of the expanding particles. The model predicted that there is an optimum PSD resulting in the highest expansion, confirmed later in other experiments [40, 41, 116]. One disadvantage of the model is that it does not say anything about the kinetics of ettringite formation and how it would affect the time of expansion.

Some authors [20, 102] applied the crystal growth theory to study the expansion mechanism of pure $\text{C}_4\text{A}_3\bar{\text{S}}$ particles. It was assumed that a ettringite layer forms on the surfaces of $\text{C}_4\text{A}_3\bar{\text{S}}$ particles which was thought to be made of fine intermeshed crystallites enclosing pores between them. It was proposed that expansion does not start instantaneously but at a critical degree of hydration when the first contact is formed between the expanding spheres. Further hydration produces more

ettringite which will push against other particles, thus producing expansion. The time at which the critical hydration occurs could correspond to the time it takes for the ettringite crystals to grow through the solution surrounding the grains in the micromechanical model.

Ogawa and Roy [152] in their microstructural study of $C_4A_3\bar{S}$ hydration found that at early stages of hydration, ettringite formed as very small irregular particles around $C_4A_3\bar{S}$. Later, these particles changed to needle-like crystals arranged radially around $C_4A_3\bar{S}$ particles enclosing pores between them. Expansion began when reaction zones intersected and mutually exerted pressure. This observation was different from the micromechanical model which assumed the ettringite layer to be dense and without any pores. This could explain why the model calculated smaller expansion strain values compared to the experimental measurements.

Odler and co-workers [150,151] studied the effect of ettringite formation on expansion in a blended mix of Al-bearing compounds, gypsum and tricalcium silicate. They attribute the cause of expansion to the topochemical formation of ettringite. However the capacity of ettringite to cause expansion was found to differ greatly in pastes made with different Al rich compounds serving as Al^{3+} source. It was suggested that this occurs due to the “way” (referring to the topochemical or through-solution mechanisms) ettringite is formed. It was also reported that the expansion increases with increasing amounts of water taken up from the environment while ettringite is formed, although uptake of water was not found to be essential for expansion to occur. Thus they acknowledge the role of the swelling pressures while attributing the primary cause of expansion as the formation of ettringite.

As previously stated, an important realization that has been achieved over the years is that while formation of ettringite could develop crystal pressures and cause expansion, the formation of ettringite itself could not be topochemical [139]. This is so because of the complete dissimilarity between its crystal structure and any of the anhydrous phases. Ettringite is thus widely believed to form only via through-solution mechanism.

Chatterji during investigation of the deterioration of concrete due to $CaCl_2$ [34] inferred that that aggressiveness of latter is due to the crystallization of complex salts of $CaCl_2$, $Ca(OH)_2$ and/or $CaCO_3$. However the reason for pressure generation

due to crystallization of the salts was not clear and the possibility of crystal growth pressure was presented as a conjecture. Future studies by the same author [35,37] showed the existence and destructive nature of crystallization pressures. It was concluded that a porous material may be damaged during crystallization of a solid if crystallization pressures are sufficiently high. It was also noted that the existence of a supersaturated solution in the matrix is a necessary but not sufficient condition for damage.

Scherer and co-workers [70,174,175] further developed the theory of crystal growth in pores to include thermodynamic and kinetic factors influencing crystallization pressure. Similar to the works of Chatterji, they acknowledged that the necessary condition for the occurrence of crystallization pressure is the presence of supersaturation, but that it is not sufficient. It was argued that there must also exist a disjoining force between the crystal and the confining walls. Further, if there is a repulsive force between the crystal and the surrounding surface, then a film of the liquid, few nanometers thin, would exist on the surface of the crystal. The film would feed the crystal with requisite ions for further growth and the crystal will push the walls with a force proportional to this driving force for growth. The existence of this film was inferred from the past works [16,51,196] which showed that crystal subjected to a load continues to grow, adding material in between its surface and the surrounding walls. However it was realized that stresses generated in few pores would be unlikely to cause any significant damage to the body since only a very small volume is affected by the stress. For considerable damage, such as fracture to occur, crystals would need to grow through a region of the body 'comparable in size to the strength controlling flaws' [174]. Therefore the driving force for growth must be sufficient to permit the crystals to pass through fine pores which lead into a percolating network of larger pores. For expansion in DEF for instance it was estimated that ettringite present in pores of few nanometers in size would cause sufficient expansion and crystals present in larger pores would cause much less expansion. The work of Scherer and co-workers allowed *quantification* of the stresses developed by crystallization pressures and help understand the reasons for deterioration in cement based materials, besides other porous materials, more clearly.

5.5.2 The swelling theory

Certain clay minerals are known to imbibe water and swell. High surface area and unsatisfied surface charges are believed to generate attractive force between such clays and water. On similar lines, Mehta [133] based on experimental evidence introduced a hypothesis on the mechanism of expansion caused by formation of fine ettringite crystals. He suggested that the mode of formation of ettringite follows a through-solution mechanism. Second, in the presence of saturated $\text{Ca}(\text{OH})_2$, the rate of hydration of the aluminates decreases significantly. This causes the ettringite crystals to be gel-like and colloidal in size. These colloidal particles due to their large specific surface area will adsorb water molecules. This will generate strong swelling pressures leading to an overall expansion of the system without any change in the crystal lattice of ettringite. In the absence of lime, Mehta adds that the aluminate phase will hydrate rapidly. This will form large, long-lathed ettringite crystals. These crystals will not produce expansion because of their low specific surface area, adsorbing lesser amounts of water molecules to their surfaces.

In studying the hydration of $\text{C}_4\text{A}_3\bar{\text{S}}\text{-C}\bar{\text{S}}\text{H}$ systems with and without quick lime, Mehta [133] examined the microstructural development and came to the same conclusions as those drawn by Okushima et. al. [153] concerning the ettringite crystal sizes. Scanning electron micrographs indicated that while in the presence of lime, ettringite crystals were about $1\ \mu\text{m}$ in length and $1/4\ \mu\text{m}$ in width, in the absence of lime, they were larger, having a length of 6-8 μm and a width of about $0.5\ \mu\text{m}$. Replacing $\text{C}_4\text{A}_3\bar{\text{S}}$ with CA produced similar results. Since ettringite crystals are much coarser than the poorly-crystallized C-S-H gel and the fact that they can be easily identified in SEM, the classification of ettringite as 'gel' remains a subject of controversy between the two schools.

In another experiment Mehta and Hu [134] prepared pure ettringite using $\text{C}_4\text{A}_3\bar{\text{S}}$, C and $\text{C}\bar{\text{S}}$. The size of ettringite formed was found out using SEM and reported to be $1 \times 0.25\ \mu\text{m}^2$. This was referred to as colloidal or microcrystalline, although this may be a point of contention. The amount of water absorbed by these ettringite particles at different relative humidities was observed along with the corresponding volume changes, if any. It was reported that for RH <90% only little water was absorbed, at 90% RH about 1.4% water was absorbed with an expansion of <3%; at 95% RH 9.6% water was absorbed with a large expansion of >12.5%. There was no

difference between the XRD patterns of the ettringite before and after exposure to 95% RH, indicating that the crystal structure of ettringite has remained unchanged due to water gain. This led the authors to assume that water was largely present between the crystals in a surface adsorbed condition. This experiment showed direct evidence of expansion of ettringite due to water absorption.

Mehta and Wang [136] performed other experiments along this line. They observed that blends containing fine ettringite crystals expand significantly more than those containing coarse ettringite crystals. Once more, this characteristic has been attributed to the larger specific surface area of the fine ettringite crystals, adsorbing more water.

Chen and Mehta [38] using Small angle X-ray Scattering found out the surface area of ettringite to be $153 \text{ m}^2/\text{g}$, which is much more than the value of $20 \text{ m}^2/\text{g}$ reported by Okushima and co-workers [153]. Nevertheless the reported values are smaller than the surface area of C-S-H which is believed to be about $300 \text{ m}^2/\text{g}$ [41]. In order to calculate the surface charge, ettringite particle $<75 \mu\text{m}$ in size were separately homogenized with demineralized water and with 10^{-3} M $\text{Ca}(\text{OH})_2$ solution. In water, the zeta potential was found out to be -11.6 mV and in CH solution, -13.4 mV . It is argued [133] that this negative charge would attract the molecules of a polar fluid like water.

According to Dent Glasser [59] any material could produce swelling pressures when immersed in water provided that it (1) is not significantly soluble (2) has sufficient porosity to absorb water (3) is of comparable polarity to water, so that the chemical potential of the absorbed water is lowered (4) is not rigidly cross-linked in three dimensions. Mehta and Wang [136] argue that ettringite fulfills all these four conditions. Besides having a negative charge and therefore lowering the chemical potential of the adsorbed water, ettringite formed in cement paste is insoluble and stable. The agglomerates of ettringite crystals produced are porous. Moreover ettringite has no intercrystalline chemical bonding and is thus not cross-linked.

Similar to Power's [156] mechanism of shrinkage, it is possible that the water adsorbed on the surfaces of ettringite could put the surface in tension (surface tension) and the bulk of the body in compression. This could result in shrinkage. The swelling mechanism, therefore, may be attributed to the decrease in van der Waals forces of interparticle attraction between the ettringite crystals. This could

result in an overall net expansion, compensating for the shrinkage caused by the surface tension of the ettringite crystals.

However it can be argued that if ettringite swells why not C-S-H which is known to be present as a gel at a fine scale. Apparently, no work has been reported which takes into consideration the possible absorption and swelling of C-S-H. However it can be said that perhaps C-S-H would absorb some water and swell but since ettringite has a larger surface area, is believed to carry a negative charge and has a greater affinity towards water, it would absorb and swell more than C-S-H.

5.6 Work done

5.6.1 Mix design

Blended mixes of OPC (*CEM I 52.5*), CAC (*Secar 51*) and C \bar{S} in various proportions (Figures 5.12, 5.15 and 5.19) were mixed with demineralized water and the solution was homogenized using an electrical blender which was employed for a minimum of 10 minutes until a uniform consistency was reached. Thereafter the mixes were placed in moulds of sizes $1 \times 1 \times 4 \text{ cm}^3$ and placed in humidity chamber (100% relative humidity) until demoulded. For each composition 100 g of the dry mix was used and six specimens were prepared. For compositions 6 and 12, anhydrous calcium sulfate was used along with w/c of 0.35, whereas for all other compositions gypsum and w/c=0.42 were used. Gypsum was used instead of anhydrite in order to avoid any possible volumetric changes to the system due to the reaction of anhydrite to form gypsum during the course of hydration.

5.6.2 Curing regimes

Two curing regimes were used in this study. In the first instance, samples after demoulding were kept over a support inside a desiccator filled with de-carbonated water, with its top closed. This provided a humidity close to 100% RH to the hydrating samples.

In the second regime, samples after demoulding were placed inside a bath filled

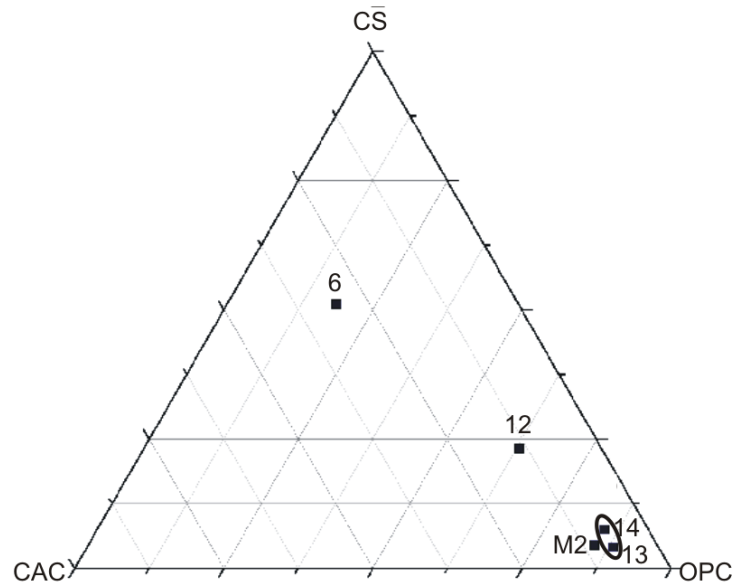


Figure 5.12: A figure showing the studied ternary formulations. Compositions 6 and 12 disintegrate due to high amounts of expansion. Sample M2 which is also expansive in nature was studied in a TEM. For a more detailed study on the phenomenon of expansion, compositions 13, 14 and those lying in between the two (circled) were chosen. The magnified view of the circled region showing the formulations is shown in Figures 5.15 and 5.19

with de-carbonated water. In both cases, the samples were placed in a room with temperature maintained at 20°C.

5.6.3 Experimental techniques

Length measurement

Specimens placed in the 4 cm long mould were primarily used to measure expansion. The expansion was measured only along the length of the samples in the following manner: the ends of the moulds were fitted with a detachable semi-spherical stud of solid metal which bonded with the poured mix during its setting.

Upon demoulding, the sample was placed in between two ends of a pressure sensitive dilatometer, with sockets to fit the spherical ends of the metal studs. In order to measure the amount of expansion, difference between the two readings was taken and divided by the original length of the bar (40 mm). The machine has a least count of 0.001 mm and includes a standard reference cylinder bar which is used to initialize the instrument to zero before each measurement.

The values of expansion presented in the various expansion curves correspond to the average values of 4–6 specimens.

Calorimetry

A part of the original mix was placed in glass tubes which were subsequently sealed and placed inside the calorimeter to obtain the heat evolution with time.

X-ray diffraction

A portion of the original cement paste for each composition was placed in separate cylindrical plastic moulds and cured in identical manner as the specimens for expansion measurement. They were demoulded at the same time as latter and slices cut from these specimens were employed to obtain X-ray diffraction patterns for phase identification.

SEM

Some of the bars used for measuring the expansion were also used for microstructural study in a SEM. The samples were freeze dried at various times, then cut into sections which were subsequently polished for study in SEM.

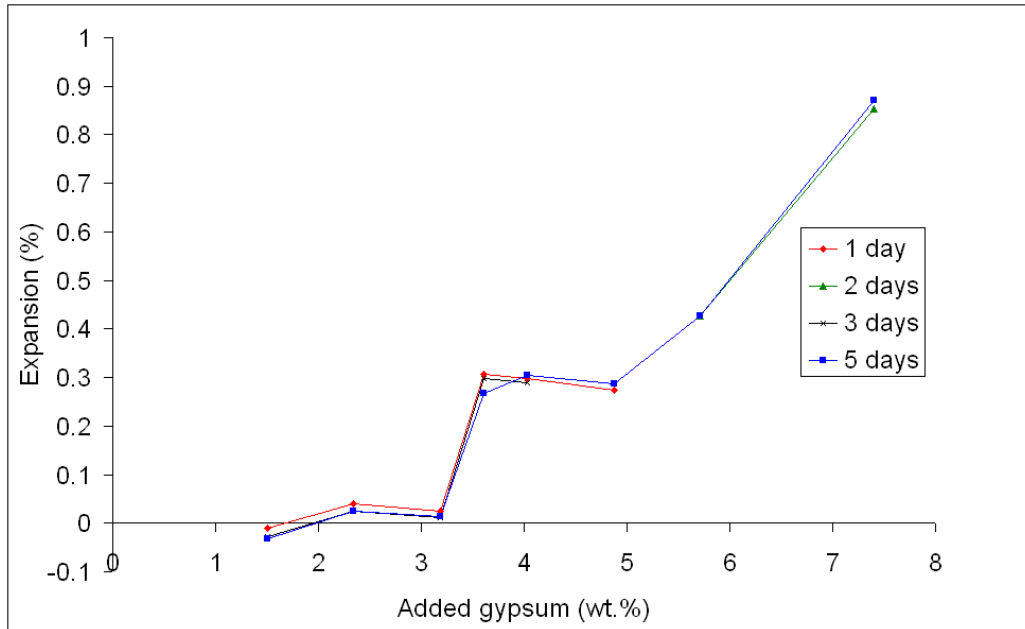


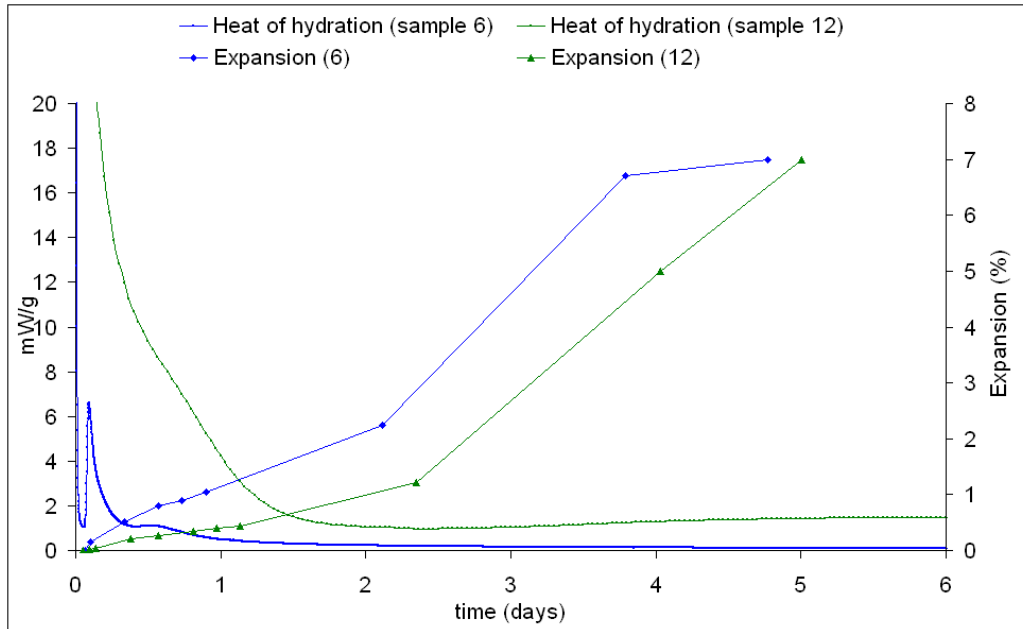
Figure 5.13: The figure shows the percentage of expansion in various compositions as a function of added gypsum. Below 2% of added gypsum there is shrinkage in the mix, indicating that drying has occurred in the specimens. Gypsum when added in excess of 3.3% causes large expansion ($> 0.1\%$).

5.7 Results

5.7.1 Expansion and heat of hydration

Samples 6 and 12 showed rapid setting (within 1.5 hours) after which they were demoulded and kept under water. The specimens showed expansion which continued to increase with time until it resulted in the disintegration of the samples (Figure 5.14). Further, it can be seen that the expansion does not seem to depend on the heat of hydration or in other words on the formation of hydrates. It was realized that composition which have relatively lesser amount of Portland cement tend to expand at a high rate. In order to understand the phenomenon of expansion, it was necessary to study mixes which had a more controlled expansion.

Compositions chosen to make a more detailed study of the phenomenons of expansion were those which had OPC as the major phase namely compositions 13 and 14 in Figure 5.15.



(a) Expansion curves for compositions 6 and 12



(b) Formulation 6



(c) Formulation 12

Figure 5.14: Initial chosen compositions and their results: a high amount of expansion is noted for compositions 6 and 12 (cured under water), which eventually results in their disintegration by 5 days. There seems to be no relationship with the heat of hydration and the expansion

Curing over water

However, even compositions 13 and 14 showed considerable expansion, which varied proportionately with the sulfate content (Figure 5.16). Thus, several other

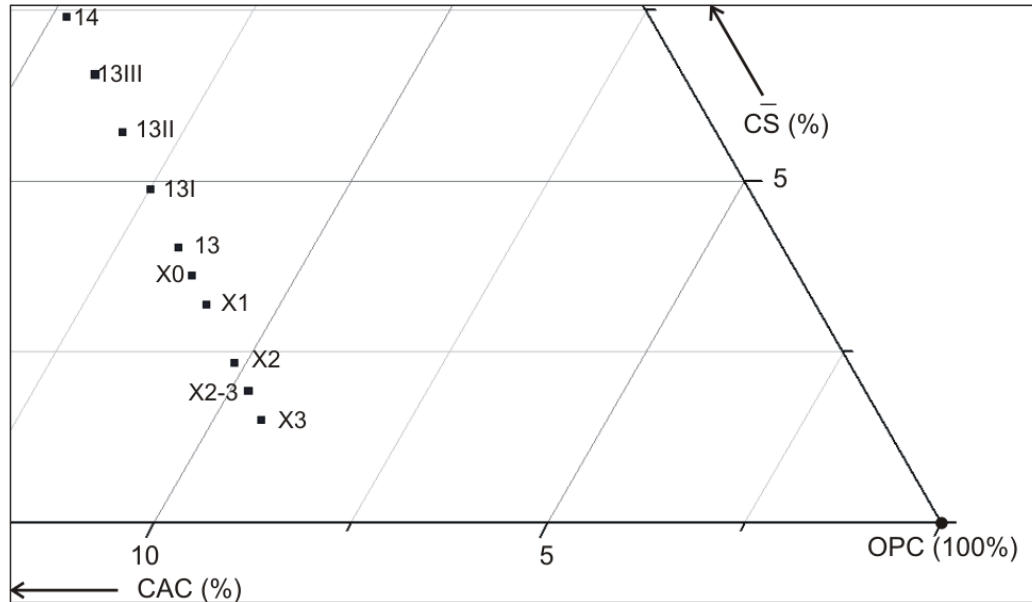


Figure 5.15: Compositions chosen to study the phenomenon of expansion in ternary mixes (magnified view of the circled part of the Triangle in Figure 5.12).

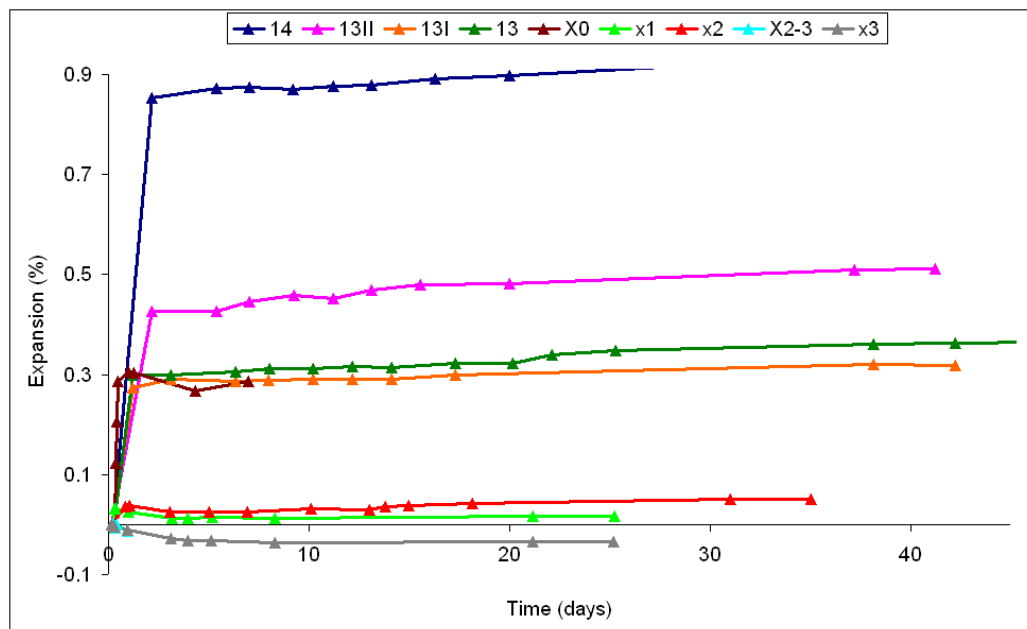


Figure 5.16: Expansion in ternary mixes cured over water (100% RH). Expansion values are average of 4–6 samples for each compositions.

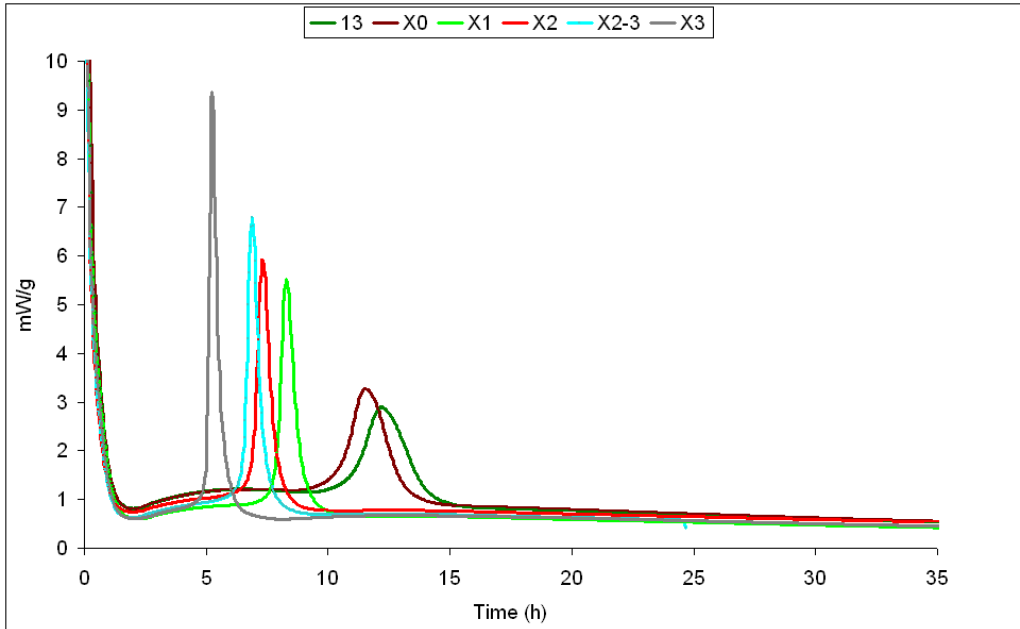


Figure 5.17: Heat of hydration of various ternary mixes. The height of the major peak decreases and its occurrence delayed with the increase in gypsum content.

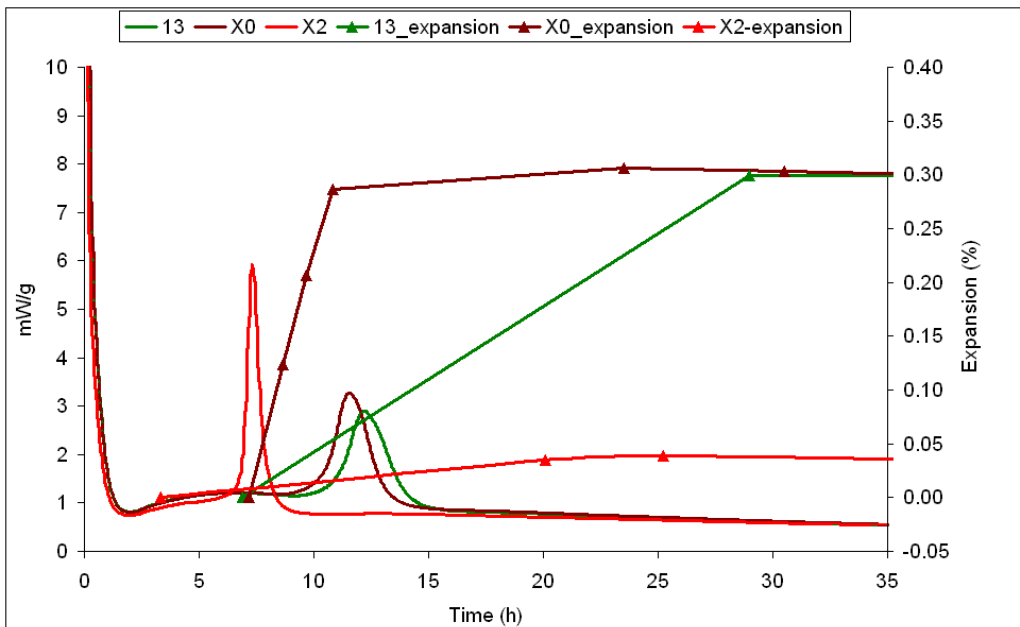


Figure 5.18: Heat of hydration and the expansion curves.

compositions both in between 13 and 14 as well as those lying below 13 were chosen to compare and study their expansive behaviour. These compositions and their designations are shown in Figure 5.15.

The expansion curves of the various mixes are shown in Figure 5.16. It was seen that the maximum expansion for all the observed samples occurred by one day after which the specimens do not expand any further and instead the *length remained constant*.

For all the samples, the amount of expansion increases with the increase in sulfate content. From sample 14 to 13, the amount of expansion for various mixes is observed to decrease gradually, however the expansion for composition X1 is noted to be much less than for 13; shrinkage was observed for sample number X3. Formulations X0 (mean of 13 and X1) was chosen to see if its expansion lies in between that of 13 and X1, which have a significant difference in their expansion. Similarly X2-3 (mean of X2 and X3) was chosen as it lies between two compositions which respectively show limited expansion and shrinkage. As seen from the expansion curves, while X0 expands similar to 13 and not in between the samples 13 and X1, X2-3 shows shrinkage, similar to X3. The relation of expansion with sulfate content is shown in Figure 5.13. It shows that for the studied compositional range, samples having gypsum content < 2 weight% show no expansion, those having gypsum contents of about 2–3% show 0.02–0.05% of expansion, which is slightly above the acceptable limit of 0.02%. However the samples with gypsum content $> 3.3\%$ show expansion in excess of 0.1%.

The heat of hydration of several compositions was studied using calorimetry (Figure 5.17). The curves show the presence of a small shoulder which corresponds to OPC hydration, and is followed by a large peak. This high amount of heat could be liberated as a result of the rapid reaction of the aluminate phase. It is further observed that with the increase in sulfate content the height of the major peak decreases and its occurrence delayed. This is likely due to the retardation of the aluminate phase by gypsum. There appears to be no correlation between the heat of hydration and the amount of expansion.

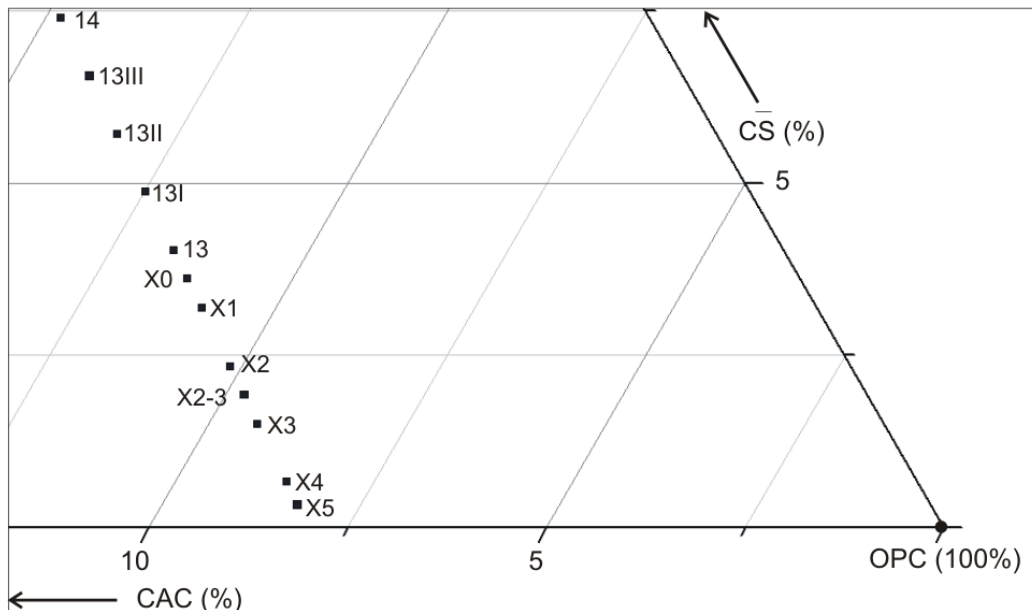


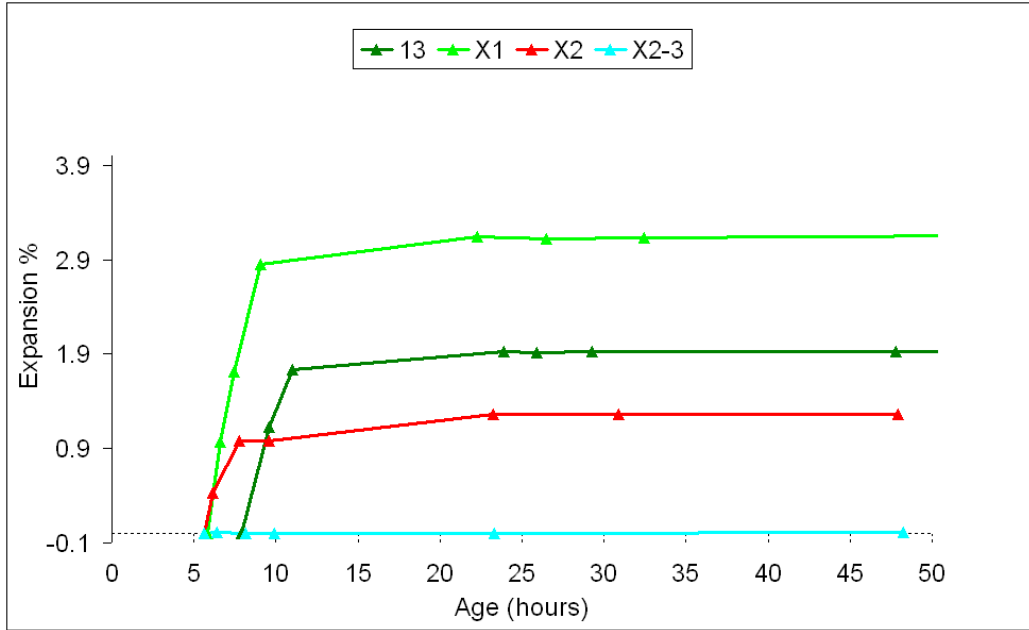
Figure 5.19: Formulations of the ternary mixes studied for the effect on expansion due to curing under water (magnified view of the circled part of the Triangle in Figure 5.12).

Specimens cured under water

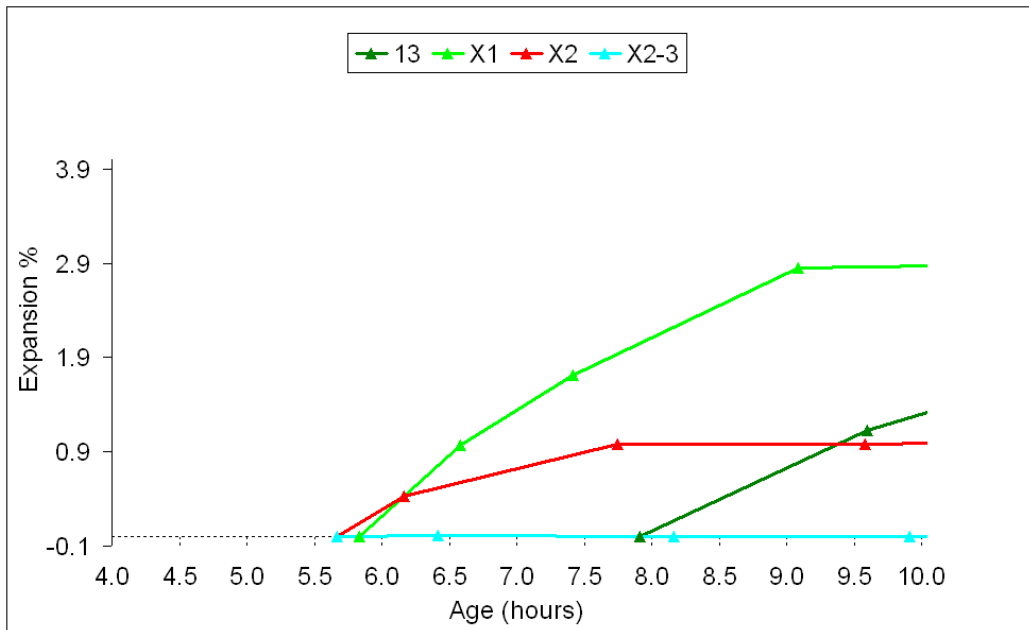
When the same compositions were cured under water it was observed that the rate and amount of expansion is much more than in the case of curing over water. This observation of quicker and higher expansion under water is similar to the results reported in the past regarding expansion in sulfoaluminate cements. In order to see the effect of added sulfate content some more compositions having further lower gypsum additions but the same OPC:CAC ratio were studied (Figure 5.19).

The results are presented in Figures 5.20 and 5.21. It seems that the amount of expansion a specimen incurs depends strongly on the time of demoulding, irrespective of the amount of sulfate present in it.

While sample X4 does not expand at all under same conditions, the sample X5 which has a lower gypsum content shows considerable expansion (Figure 5.21). The only thing separating the two is their demoulding times. Further, different samples of the same composition show higher amounts of expansion as their demoulding time is reduced.

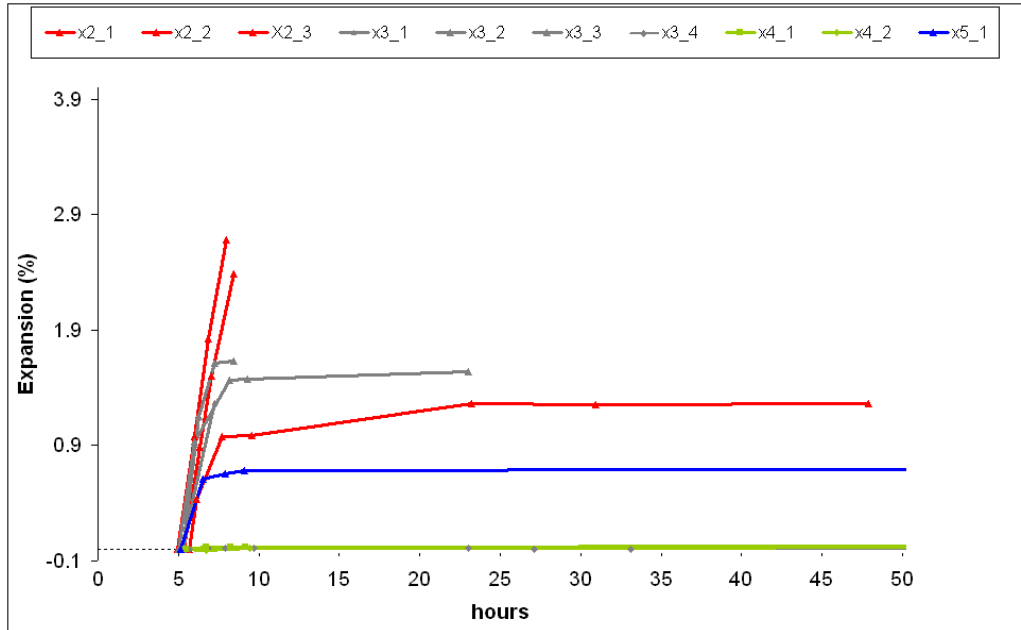


(a)

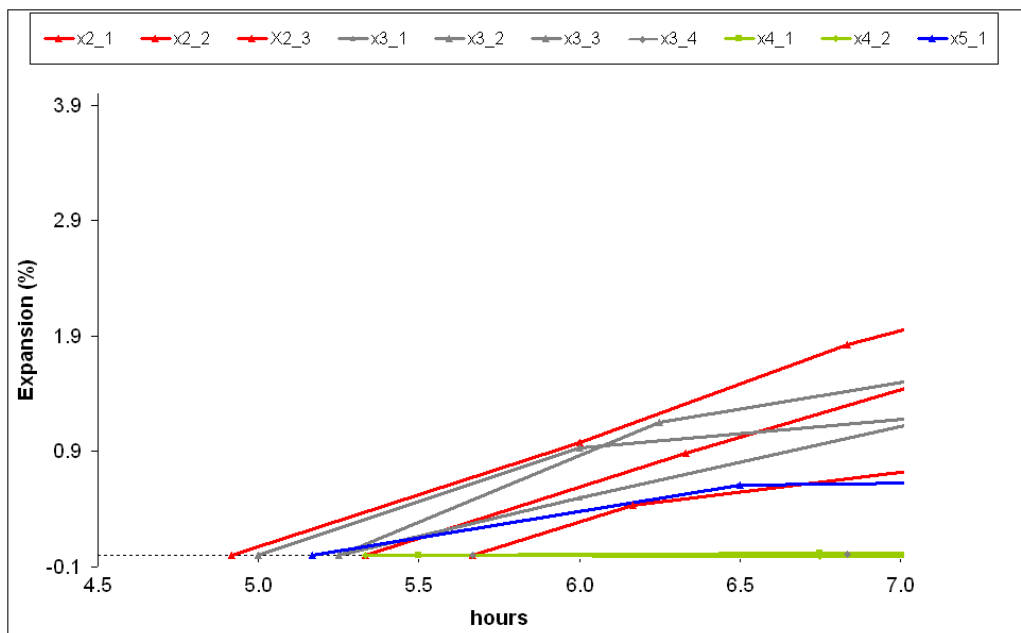


(b) A magnified view of the figure 5.20a above

Figure 5.20: High amounts of expansion for samples cured under water. Note the effect of demoulding time on the amount of expansion. The ‘less expanding’ X1 expands more when demoulded earlier than ‘13’.



(a)



(b) A magnified view of the figure 5.21a above

Figure 5.21: High amounts of expansion for samples cured under water. Note the effect of demoulding time on the amount of expansion. x2_1, x2_2 etc. refer to the samples with same respective compositions but demoulded at different times.

5.7.2 XRD

In order to observe the hydrate phases, particularly ettringite, X-ray diffraction of the various mixes was carried at various hydration times, corresponding to different amounts of expansion. The obtained XRD patterns (Figures 5.22 and 5.23) show the presence of ettringite in all the observed samples. In some of them a small peak corresponding to hemihydrate ($C_3A \cdot 0.5\bar{C}\bar{C} \cdot 0.5CH \cdot 11.5H$) is also seen.

To see if there exists any relationship between the amounts of expansion and the amounts of ettringite and hemihydrate a semi-quantitative analysis of the obtained XRD patterns was made in the following manner. The XRD peaks corresponding to ettringite and hemihydrate at $2\theta \sim 9^\circ$ and 11° respectively were isolated and their backgrounds (noise) removed. Subsequently the areas of the extracted peaks was obtained and plotted against time. Both the steps of background subtraction and peak area calculation were performed by the software upon providing it with the requisite instructions. This is a crude method to obtain the amounts of phases present, involving various errors. Nevertheless it can be used to obtain an estimate on the amounts of phases present. Expansion curves were also plotted on the same graph to compare the amounts of expansion and ettringite, monosulfate phase. Both qualitative and semi-quantitative results show that the amounts of expansion does not depend on the presence or the amount of ettringite. Furthermore, in various mixes ettringite is seen to be present before, at and after the main calorimetry peaks.

Additionally, all the compositions observed by XRD showed absence of gypsum at all observed ages. Thus X-ray diffraction, which shows the presence of crystalline hydrates, fails to clarify the hydration of the mixes corresponding to the peak of the calorimetry curves. It is also observed that non-expanding mixes may have a higher ettringite content than the samples which show expansion and have lower sulfate content (for instance X5 and X4 in Figure 5.23). This suggests that ettringite growth in confined spaces or otherwise is not responsible for expansion in these instances. This effect of demoulding times on expansion is also noted for other mixes as well.

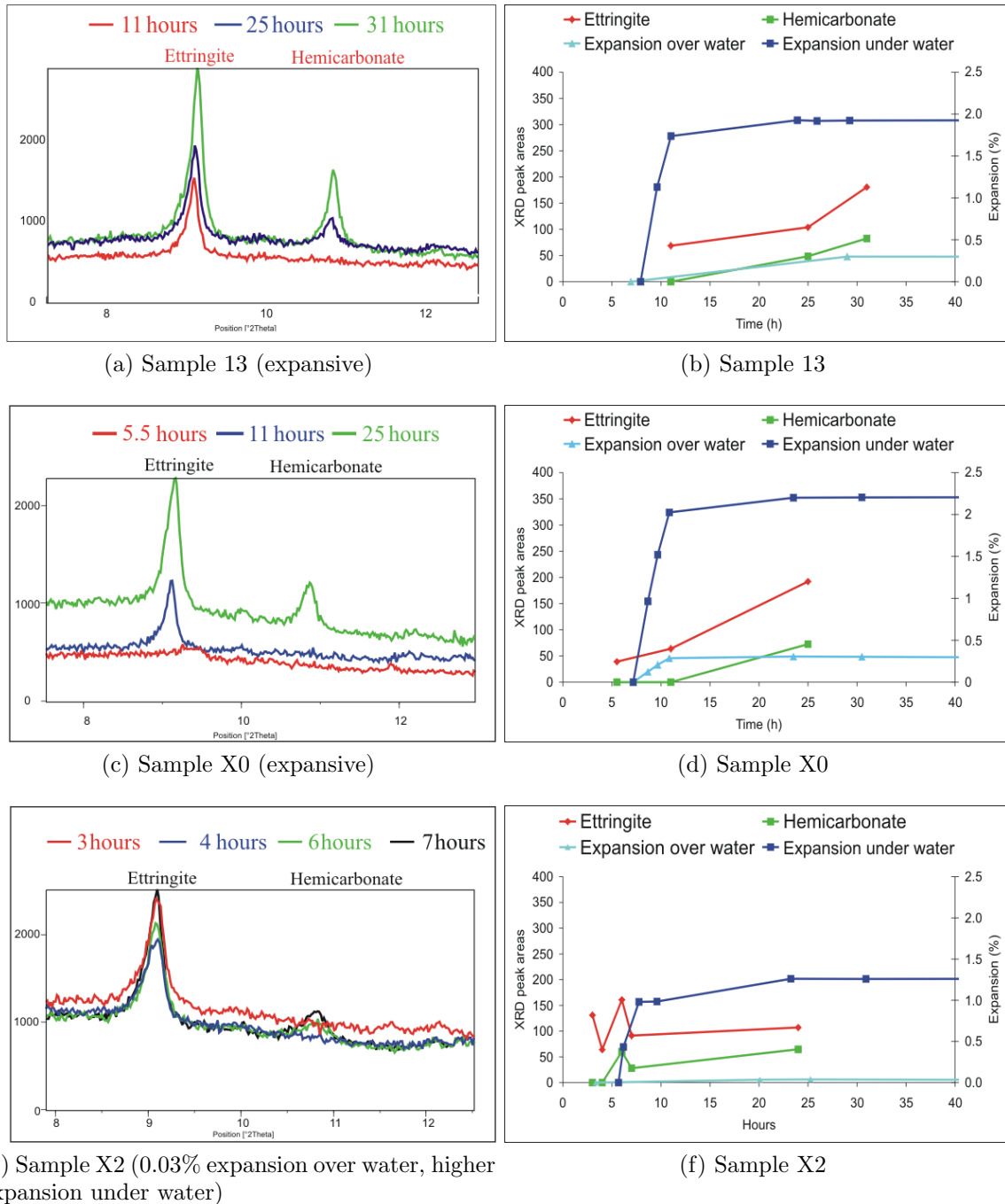
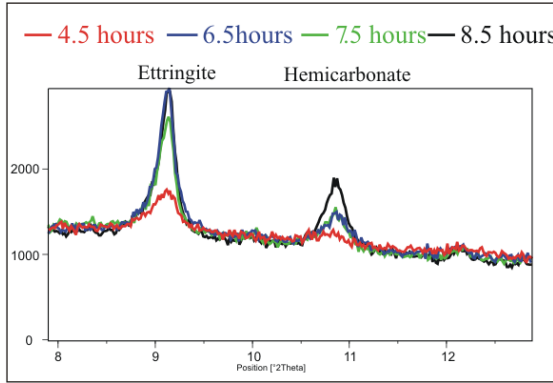
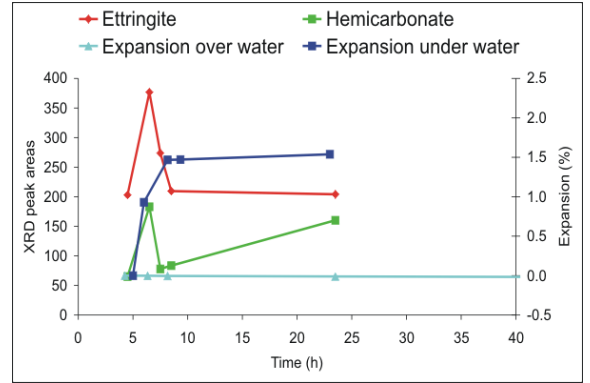


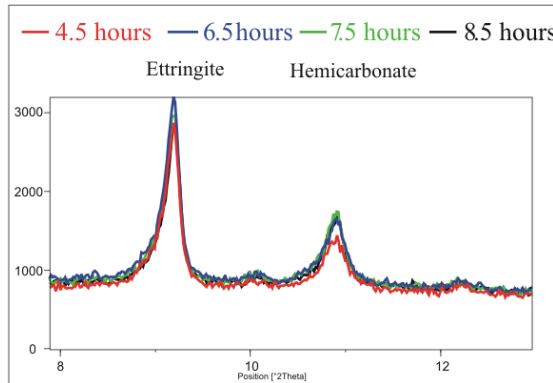
Figure 5.22: XRD patterns of the ternary mixes studied for expansion. Alongside a semi-quantitative analysis is also presented showing the evolution of ettringite and hemicarbonate with time, and the expansion of the mixes. There seems to be no relationship between the amount of expansion and the amount of ettringite or hemicarbonate.



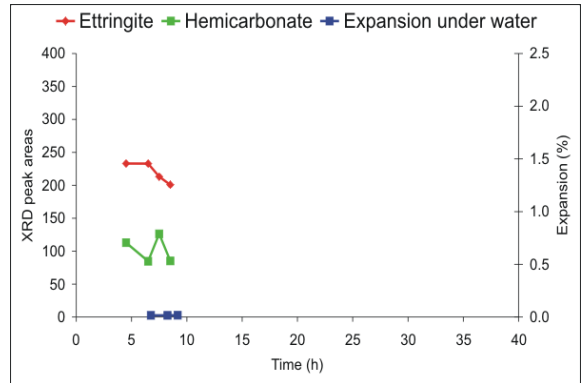
(a) Sample X3 (expansion only under water)



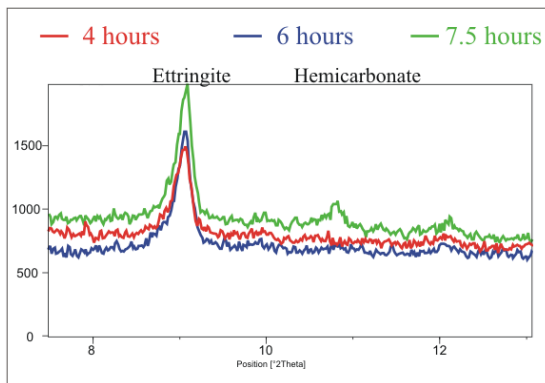
(b) Sample X3



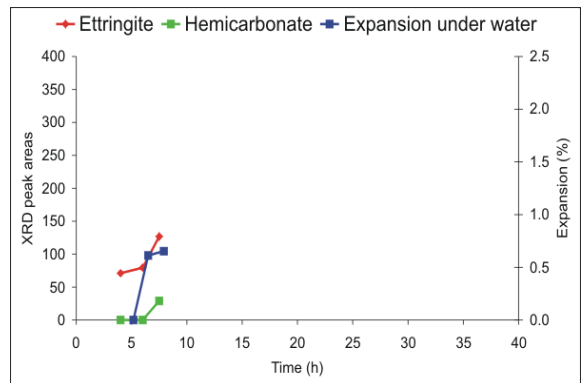
(c) Sample X4 (no expansion)



(d) Sample X4



(e) Sample X5 (expansion only under water)



(f) Sample X5

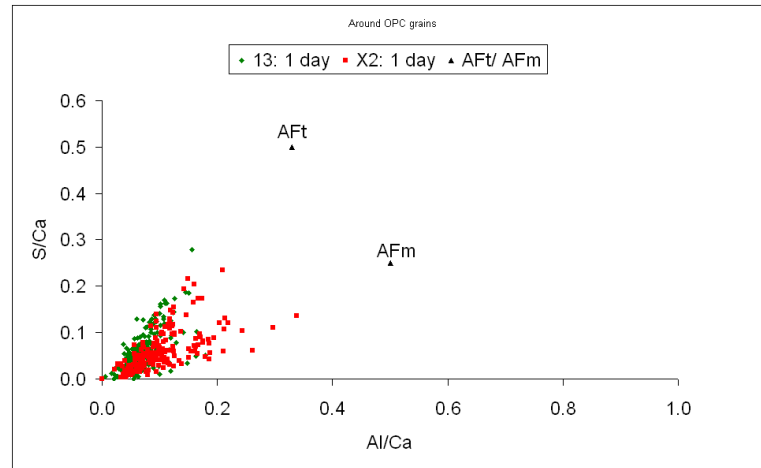
Figure 5.23: The sample X5 appears to have less ettringite than X4 but still expands while X4 does not. X5 is demoulded 90 minutes earlier than X4.

5.7.3 SEM studies

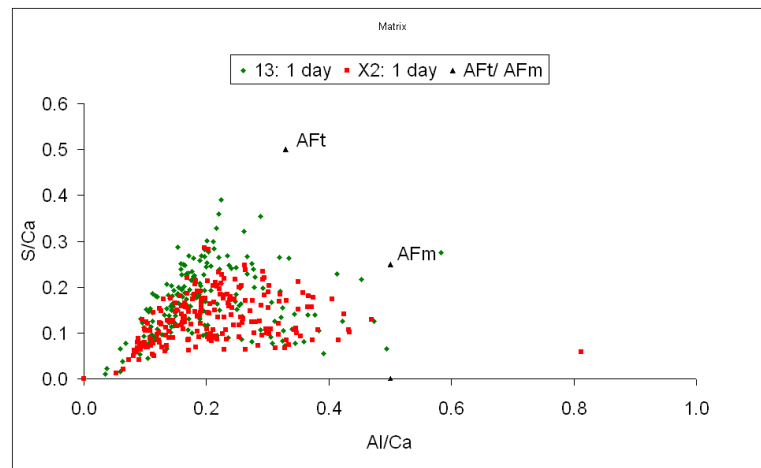
Polished specimens of two compositions cured over water were prepared for study in SEM . Besides imaging, quantitative chemical analysis was done to get an idea on the nature and distribution of hydration products being formed. Chemical analysis on three regions was conducted, namely: hydration products immediately around the CAC grains, around OPC grains and those present in the hydration matrix, away from cement grains. The results of chemical analysis are shown in Figure 5.24.

It is evident that ettringite is predominantly formed around CAC grains in expansive systems, probably very limited amount of ettringite is formed in the hydration matrix and around the OPC grains. Further it is learnt that with the decrease in added gypsum the amount of sulfate (S/Ca ratio) distributed in the hydrating system consistently decreases. This could mean relatively fewer ettringite particles for mixes with lesser gypsum content.

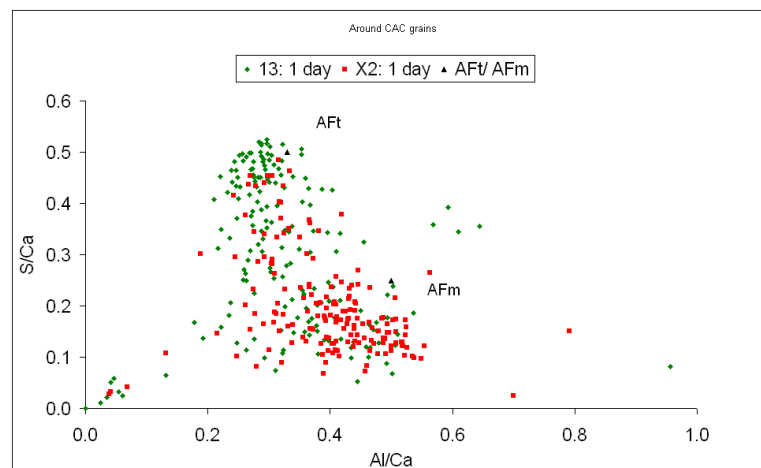
The morphological evidence and the arrangement of ettringite is provided by the SEM images shown in Figure 5.25. It shows the formation of ettringite around CAC grains in the mixes. Figure 5.26 shows the formation of C-S-H rich shell with no ettringite around OPC grains. Comparing the images obtained for compositions 13 (0.3% expansion) and X2 (0.03% expansion) no significant differences in the arrangement and bonding of the ettringite are seen.



(a) around OPC grains



(b) in the matrix



(c) around CAC grains

Figure 5.24: Distribution of ettringite in the ternary mixes. The ettringite is mostly present around the CAC grains. Formulation 13 expands to 0.3 % and X2 only expands to 0.03 % by 1 day, after which no expansion occurs in either of the mixes.

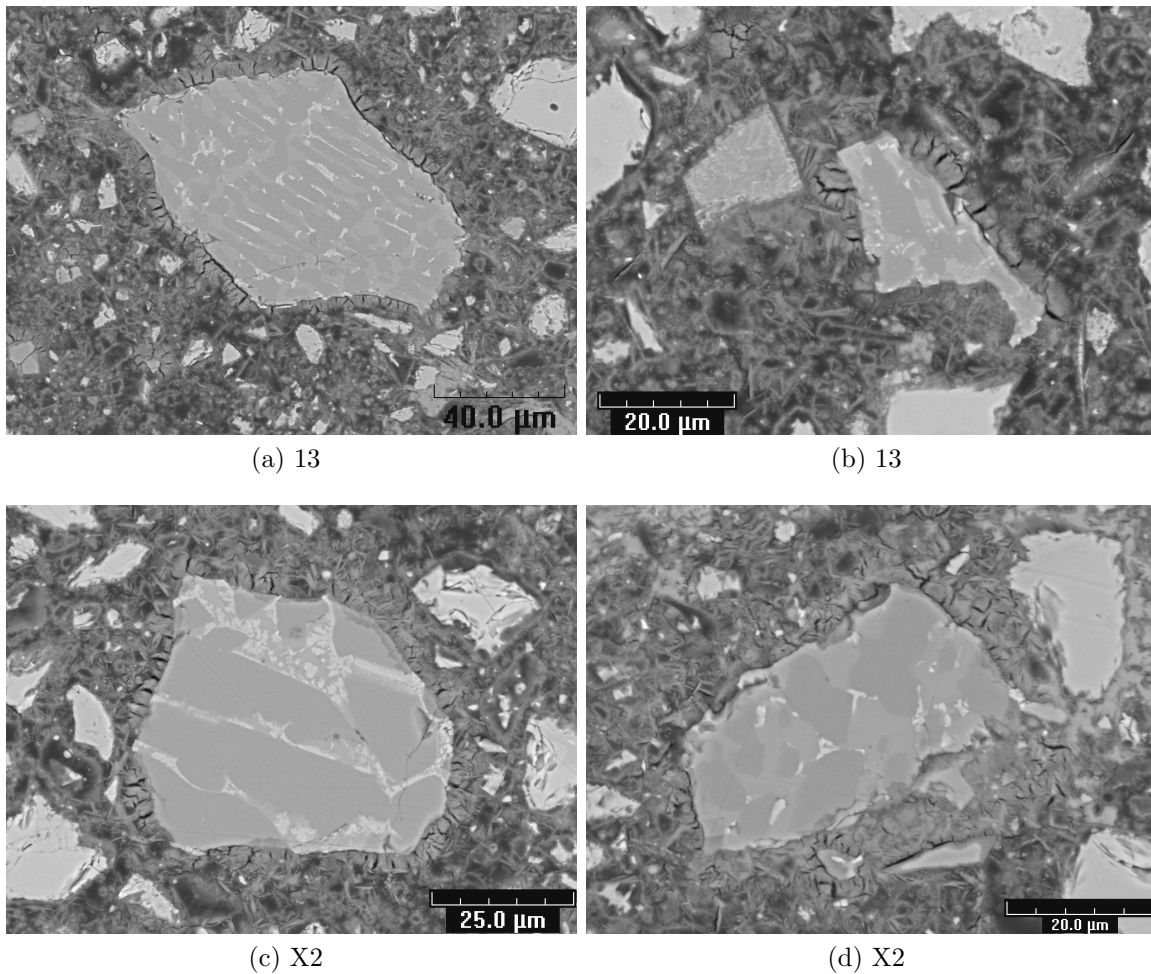


Figure 5.25: The region around CAC grains in ternary mixes 13 and X2 at 1 day. While 13 expands to 0.3 %, X2 only expands to 0.03 % by 1 day. No expansion occurs in either of the mixes after 1 day. There does not appear to be any difference between the two compositions in the distribution of ettringite around CAC grains.

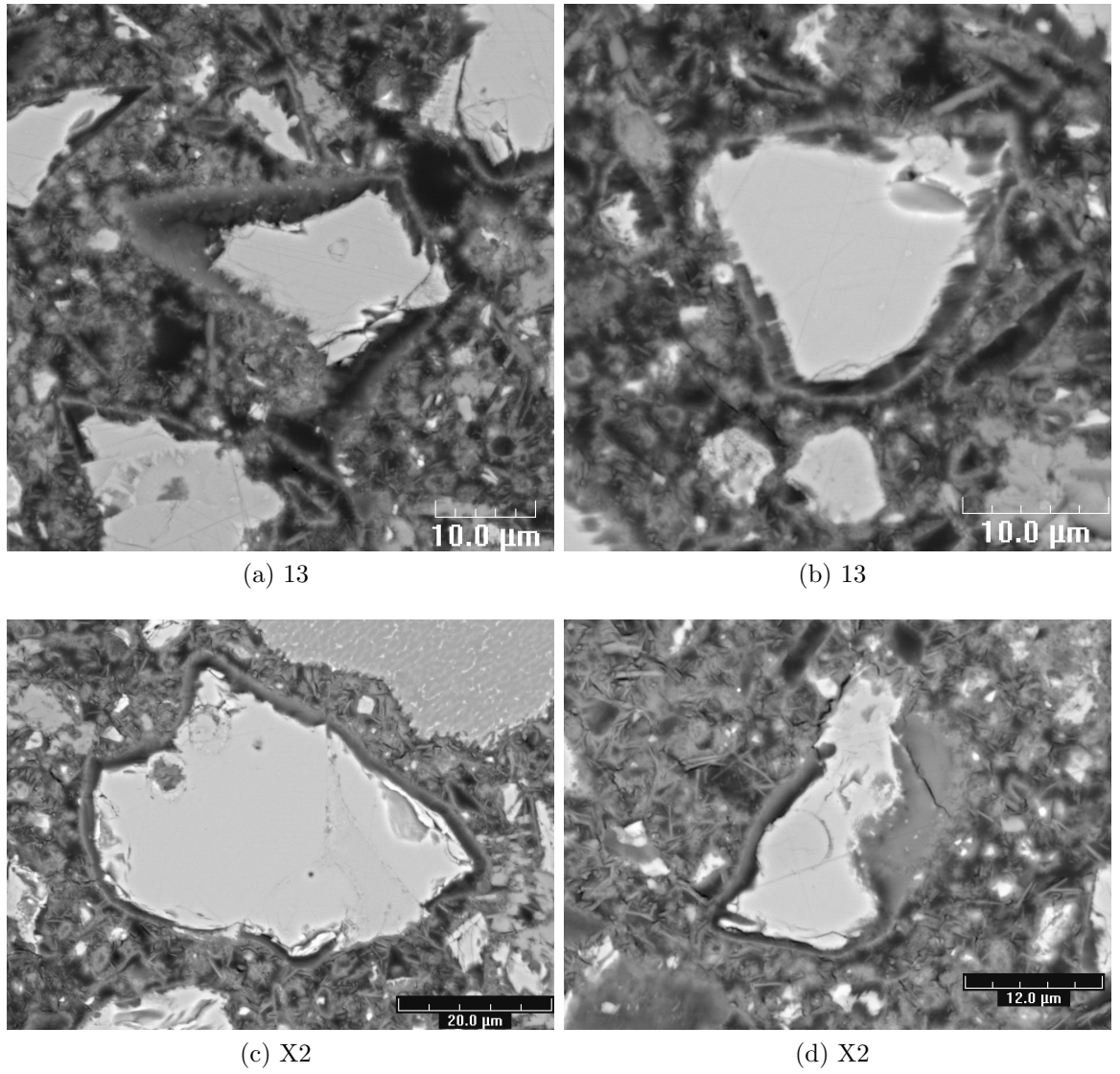


Figure 5.26: The region around OPC grains in ternary mixes 13 and X2 at 1 day.

5.8 Discussion

The cause of expansion in ternary mixes has not been found. However based on the results obtained some conclusions can be drawn.

Samples cured over water (100% RH)

The amount of expansion increases with an increase in the amount of added sulfur. With regard to the sulfur content in the mixes, it is observed that the height of the major peak in the heat of hydration is decreased and its occurrence delayed as the amount of sulfur is increased. This is consistently noted for all observed compositions and is believed to occur due to a more controlled and delayed reaction of the aluminates by sulfates. However there does not appear to be any relationship between the amounts of expansion and the heat of hydration. These results suggest that although amount of expansion is related to the amount of sulfur in the mix, the expansion may not be related to the formation of hydrates.

Data obtained from XRD shows the presence of ettringite in similar amounts in expanding and non-expanding mixes. Ettringite is also seen to be present at times before, during and after the main peak in the calorimetry curves of expanding and non-expanding mixes. Thus no firm conclusions can be drawn.

SEM results show that ettringite is mostly present around CAC grains and probably in limited amounts in the matrix. The morphology and arrangement of ettringite is the same in mixes with very different amounts of expansion. Thus simply the formation of ettringite does not seem to be responsible for expansion. However it is possible that crystallization pressures due to the growth of hydrates in confined spaces may be generated and cause expansion.

It is also important to note that with time the expansion ceases to occur and the length of the cement bars remains constant. This could be related to the development of compressive strength due to OPC hydration. With time the internal expansive forces may or may not decrease. However it is likely that the expansive forces would be difficult to counter by the limited compressive strength developed due to OPC hydration in the mix at early ages. This is why the amount of expansion is relatively large. Nevertheless, the expansive force, unless they remain too

large (like for samples 6 and 12 with uncontrollable expansion), should be balanced by the development of sufficient compressive strength with time.

Samples cured under water

When cured under water the compositions which were not expansive at 100% RH begin to show considerable expansion and those which incurred expansion at 100% RH show a significant increase in expansion. For the same composition the amount of expansion increases with a decrease in demoulding time, although the rate at which expansion occurs remains the same. This is likely to be due to higher expansive forces and/or lower compressive strength, to counter the expansion, due to limited hydration of OPC at early ages.

These results on the relationship of expansion, when cured under water, with demoulding time presents an interesting and perhaps an unexplored front in the subject of expansion in cementitious materials. Apparently it is not possible to explain the relationship using any of the postulates of the crystal growth theory. The only plausible explanation appears to be swelling of hydration products present at the early ages as a result of water absorption, although this swelling is not necessarily related directly to the presence of ettringite. Should this be the case, it appears that swelling pressures are larger, although probably short-lived, and cause higher expansion than pressures generated by the growth of crystals.

In both curing conditions the expansion eventually stops either due to the cessation in the expansive forces or due to the sufficient strength development of the mix due to OPC reaction. This preliminary study reveals the complexity of the phenomenon of expansion in cementitious systems, about which much needs to be learned.

Chapter 6

Heat induced internal sulfate attack (DEF)

6.1 Introduction

Sulfate attack is a phenomenon which leads to degradation of cement or concrete and may also involve loss of strength. Excessive sulfate from an external source such as environment (*external sulfate attack*) or contamination (*internal sulfate attack*) is well known to cause expansion and damage in cement pastes through the formation of ettringite.

More recently it was discovered that in cement paste, which has been subjected to temperatures above about 70°C during curing, internal sulfate attack may occur due to sulfate absorbed on the C-S-H at high temperatures and released on return to room temperature. This leads to the formation of ettringite which cause expansion, but also may form without damage.

6.2 Literature review on delayed ettringite formation

Delayed ettringite formation (DEF), a form of internal sulfate attack, was first implicated as a primary cause of deterioration in heat-cured precast mortars and concrete in the early 1980's [100]. It can be defined as formation of ettringite in a paste, mortar or concrete by a process beginning after hardening is substantially complete, and in which no sulfate comes from outside the cement paste. It can cause damage, which may be apparent only after a period of months or years.

In mortars subjected to high temperature, ettringite is often undetectable immediately after heat curing [64, 100, 125, 219]. However, ettringite does form during subsequent exposure to moisture in all mortars subjected to heat cure, in a delayed way, irrespective of whether the mortars expands or not. Therefore the mere fact of the formation of ettringite in a hardened material can not be justified as a cause for expansion. Further, in heat cured mortars which subsequently expanded, it was observed that gaps around aggregate particles were often fully or partly filled with ettringite or portlandite [64, 100, 110, 125, 186, 219]. This growth of ettringite in the gaps has been claimed as the cause of expansion [62, 100, 138, 149, 219]. However, this proposed hypothesis was put in doubt as it was later reported [66] that empty gaps were observed first at the beginning of expansion and ettringite later deposited in these pre-existing gaps as a product of re-crystallisation, normally referred to as secondary ettringite.

Some authors [125] studied the composition of the inner product C-S-H, formed during heating. It was reported that in mortars which subsequently expanded, EDS analysis of the inner C-S-H immediately after heat curing indicates of an intimate mixture of C-S-H and ettringite, whereas in non-expanding mortars the sulfate and aluminium were reported to be present with the stoichiometry of a mixture of C-S-H and calcium monosulfate. This led the authors to postulate that ettringite may form within the lighter¹ inner C-S-H rims and cause expansion of the paste.

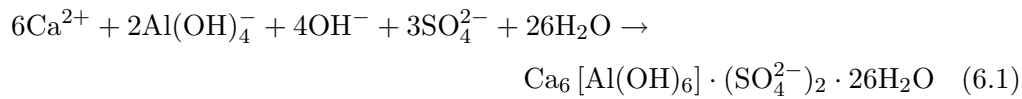
However, subsequent work [64] found that in the lighter inner C-S-H, immediately

¹It refers to a higher grey level as seen in SEM-BSE images. For details on differences in grey levels of C-S-H due to heating see [67]

after heat curing, sulfate is sorbed on the C-S-H and aluminium substitutes for silicon in the C-S-H structure. Upon subsequent storage in water at ordinary temperatures the level of sorbed sulfate drops, while most of the Al that entered the C-S-H stays there. The outer C-S-H gel appears to be intermixed with calcium monosulfate and/or calcium monocarboaluminate. With time as expansion begins, a significant number of microanalyses of outer product C-S-H correspond to a mixture of C-S-H and ettringite. The main reactants are believed to be calcium sulfate from C-S-H, monosulfate, and pore solution. These phases are mixed on a sub-micrometre scale, and the reaction can only occur by dissolution and precipitation.

C-S-H	provides	Ca^{2+} , SO_4^{2-} , OH^- , H_2O
Monosulfate	provides	Ca^{2+} , SO_4^{2-} , OH^- , $\text{Al}(\text{OH})_4^-$, H_2O
Pore solution	provides	H_2O , SO_4^{2-}

These react to form ettringite as per the following equation [207]:



The concentration of the aluminium ion in the solution is extremely low. Most of the ettringite is therefore likely to be formed close to the main source of this constituent, which is the monosulfate. The growth of sub-micrometer ettringite is expected to cause expansion because it forms in a confined space of the outer product [207]. However, this was deduced indirectly from interpretation of the microanalyses in the SEM where the resolution is more than 1 μm . The aim of this part of the work was to try to observe the formation of ettringite in small pores, directly by TEM

6.3 Work done

6.3.1 Cement bar preparation

Cement pastes made of pure OPC at a w/c ratio of 0.35 were placed in moulds of sizes $4 \times 4 \times 16 \text{ cm}^3$ and $1 \times 1 \times 4 \text{ cm}^3$ and cured as per section 6.3.2. The different sized bars were prepared at different dates but from the same cement and at the same w/c.

6.3.2 Curing regime

The cement pastes were prepared and placed in the moulds, sealed with polythene sheets to maintain the w/c ratio, placed in temperature regulated water bath initially at 20°C . The temperature of the water bath was increased linearly from 20°C to 90°C in two hours. The temperature was maintained at 90°C for 12 hours, after which the heating was stopped and the moulds were let to cool inside the tub for the next five hours. Thereafter the samples were demoulded and placed under de-carbonated water for further hydration (Figure 6.1).

6.3.3 Expansion profiles

Their expansion profiles are shown in Figure 6.2. Hydration of shorter bars was stopped at 0.09 % expansion after 70 days and that of longer bars after 191 days at an expansion of 0.25%.

6.3.4 Observations using TEM

Three TEM samples, one at 0.09% and two at 0.25% expansion were prepared.

Low magnification images show the abundant presence of long monosulfate plates (Figure 6.3). However, in some instances at higher magnifications, ettringite needles are seen growing from the nearby monosulfate (Figure 6.4). Additionally, some images (Figure 6.6) show ettringite present in matrix in varying shapes. The significance to the phenomenon of expansion, if any, of possible variations in the

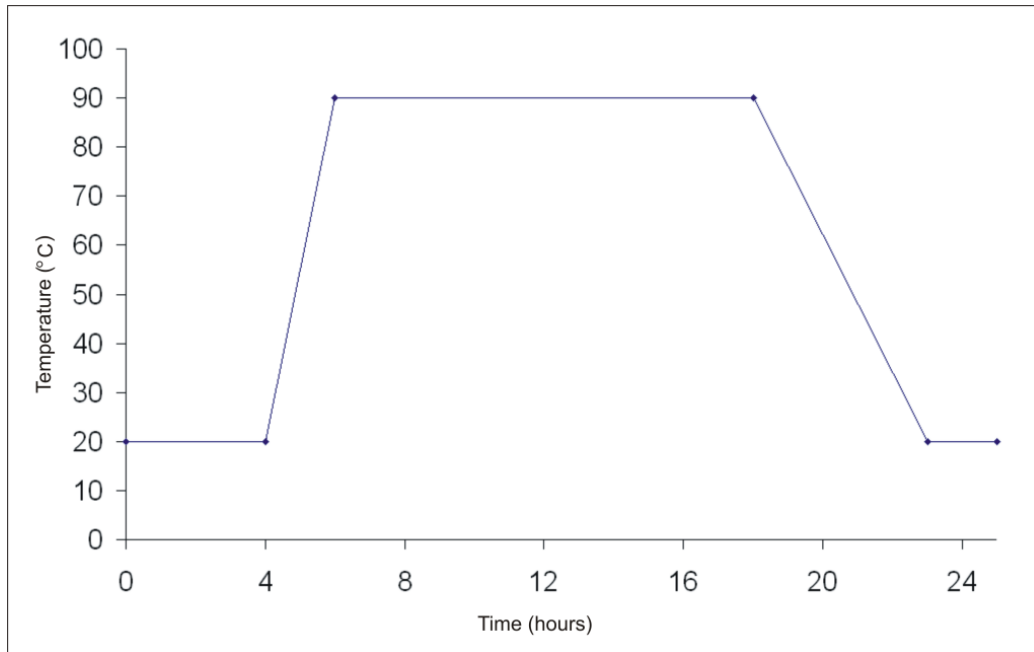


Figure 6.1: Heat curing regime (Adopted from [64])

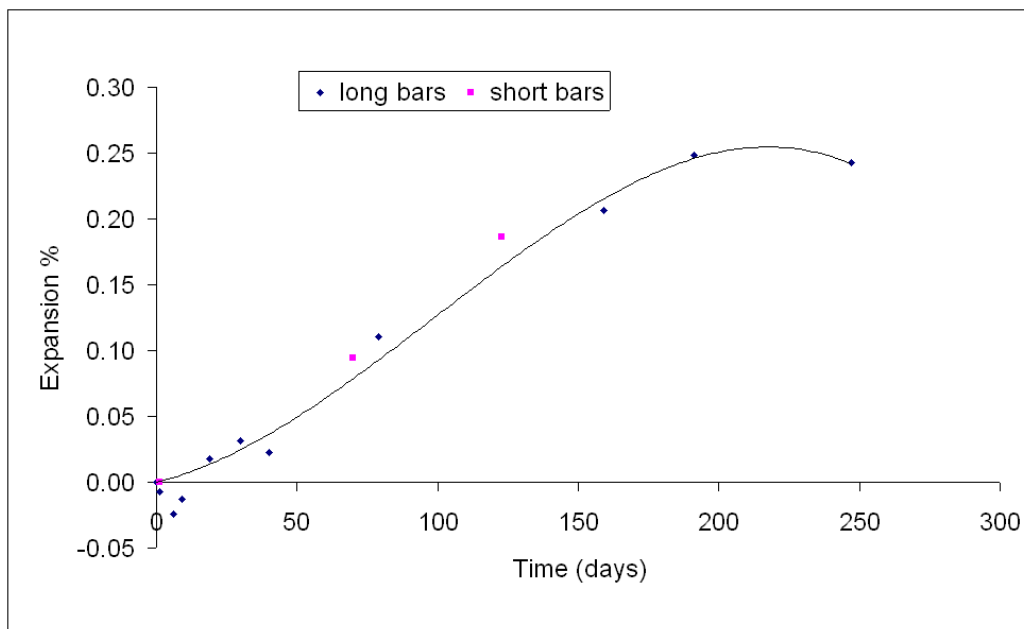


Figure 6.2: Expansion curve for the heat cured cement bars

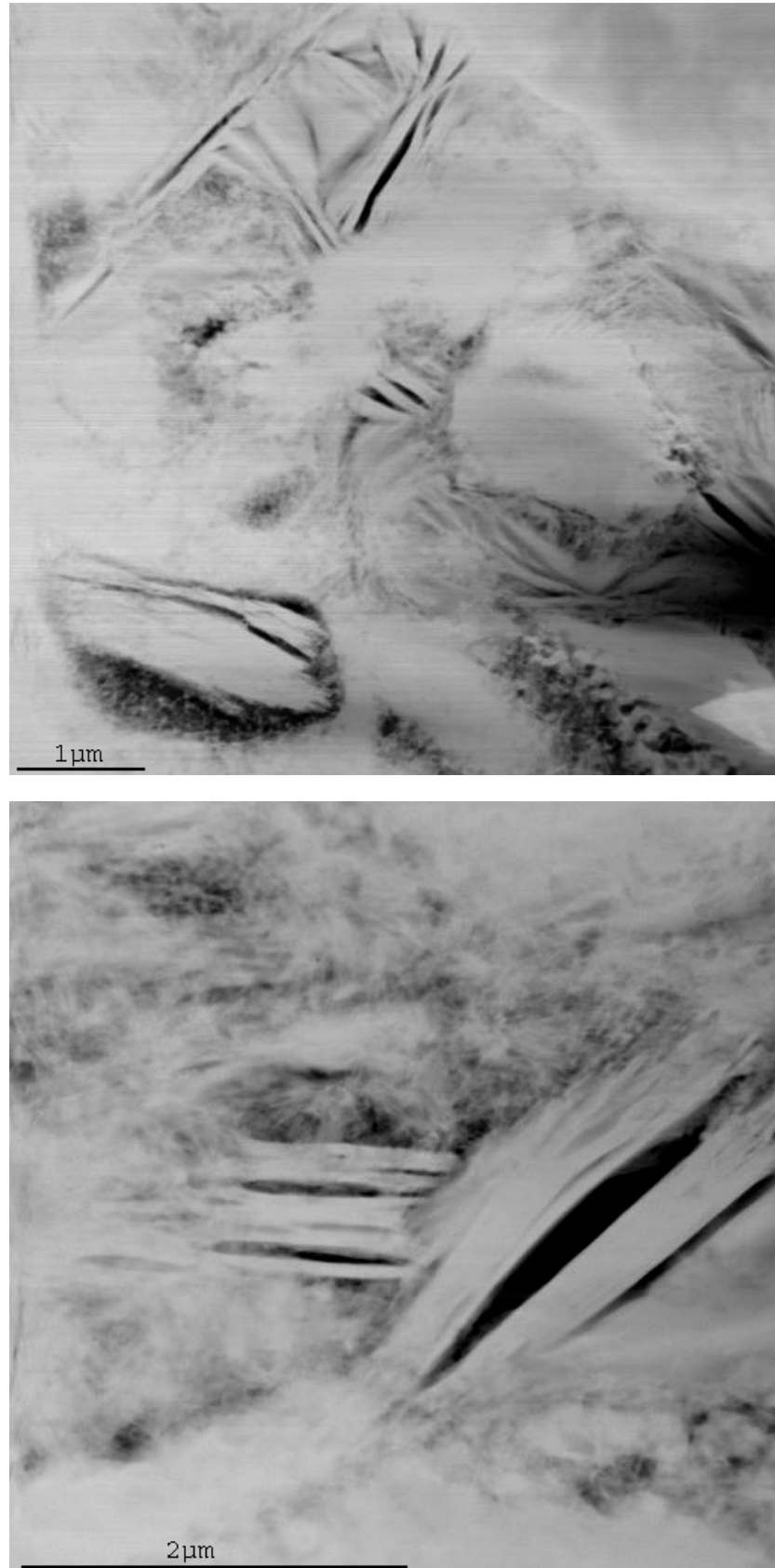
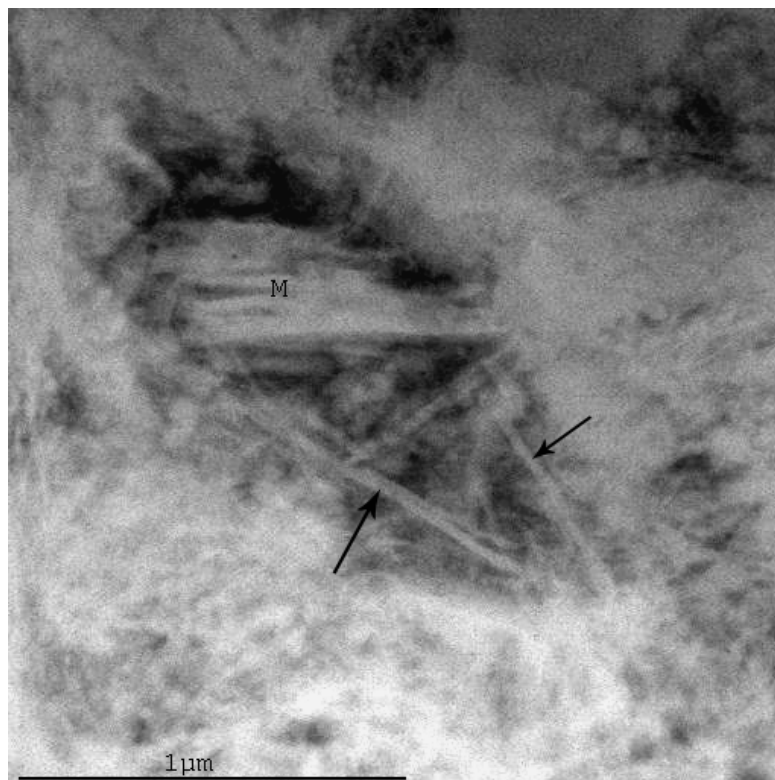


Figure 6.3: Low magnification images reveal the abundant presence of mono-sulfate plates (0.09% expansion at 70 days).



(a) Region marked 'Z' is shown below



(b)

Figure 6.4: Higher magnification images show the presence of ettringite rods (shown by the arrow), probably growing from the adjacent monosulfate plate (M) (0.25% expansion at 191 days).

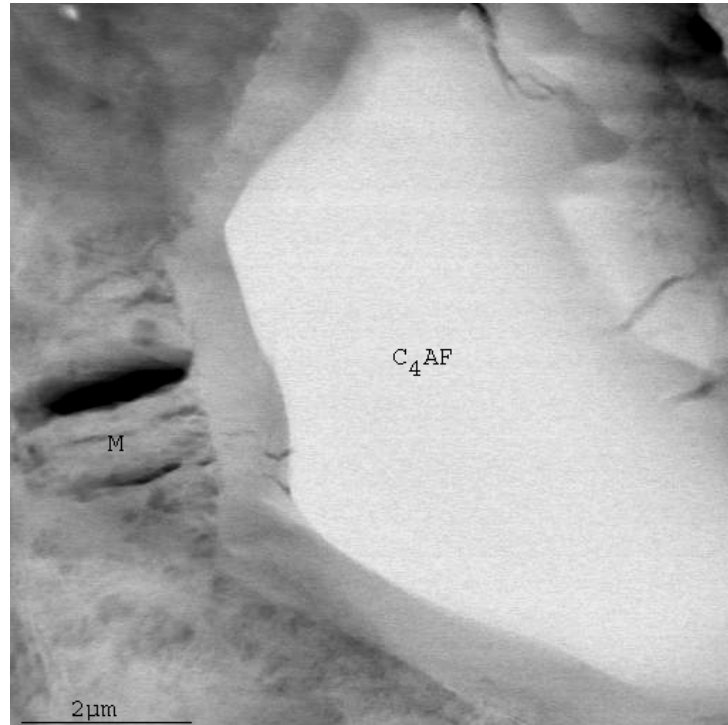


Figure 6.5: Cement paste expanded to 0.25 % (191 days) showing a rim of hydration products around a C_4AF grain along with monosulfate (M). Average of 9 analysis points gives $\bar{S}/Si = 0.47 \pm 0.12$, $Fe/Al = 0.82 \pm 0.28$, $(Al+Fe)/Si = 2.15 \pm 0.36$, $(Al+Fe)/Ca = 0.44 \pm 0.07$

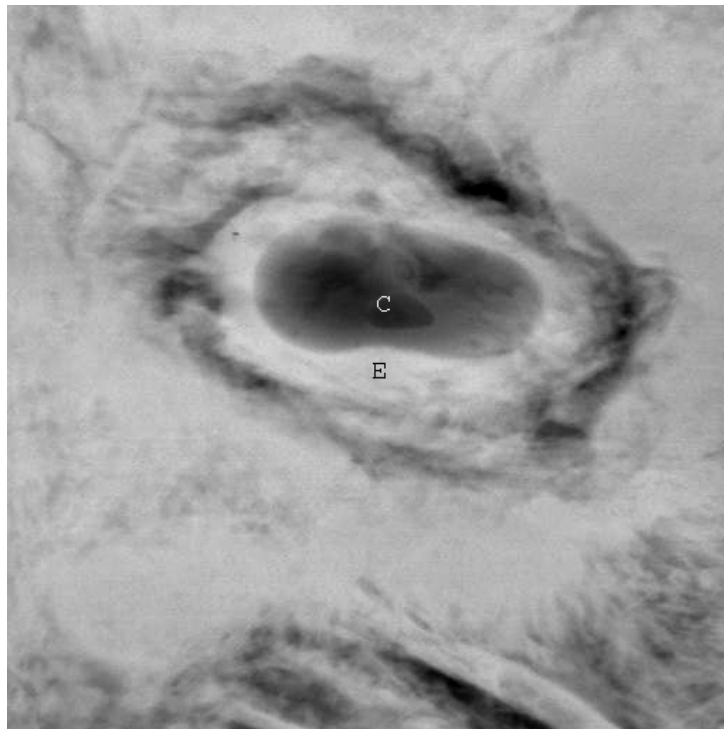


Figure 6.6: Ettringite (E) seen in different shapes (0.25% expansion at 191 days); 'C' refers to carbon-coating.

shape of ettringite is not known. Nevertheless presence of ettringite in the outer product, in some instances, near the monosulfate plates is in line with what is expected.

6.4 Discussion

Observations made using TEM on heat cured cement pastes show the presence of ettringite needles apparently growing from the nearby monosulfate. This observation is in line with what was anticipated. They were, however, not observed in pores of few nanometers in size as expected. This could be due to thick specimens. Further, some ettringite needles of varying shapes were also seen present in the matrix, not necessarily growing from monosulfate. The significance of the shapes of ettringite to expansion is not known.

Chapter 7

Conclusions and future work

7.1 Ordinary Portland cement (at ambient temperature)

Shell formation

- There is already a distinct shell formation at 6 hours.
- The shell is not empty, but filled with more diffuse C-S-H than in other parts of the hydrating matrix.
- In all observed instances till 10 hours, the shell is noted to be formed only around polyphase grains.
- In all observed instances and for all ages, the shell is formed uniquely around the silicate part of the grain.
- At 6 hours, the thickness of the shell is in the range $\sim 0.05\text{--}0.2\ \mu\text{m}$, whereas the separation between the shells and their respective grains is $\sim 0.05\text{--}0.45\ \mu\text{m}$.
- At one day, the shell is seen in its final state with values of the gap and shell thickness in the range $\sim 0.5\text{--}2.5\ \mu\text{m}$ and $0.3\text{--}2.6\ \mu\text{m}$, respectively.

- There is continuity of the shell with the hydration products immediately outside
- There is a filling in from all sides of the region in between the shell and the grain by 48 hours. This results in the formation of inner and outer products.

Sulfates

- Large unreacted gypsum particles are seen until 6 hours but not at 8 hours or thereafter.
- Sulfate ions are well distributed everywhere in the hydrated matrix even at 2 hours.
- Sulfate content is more on the shell than in other region of the micro-structure until before 24 hours.
- At 24 hours, there is a renewed growth of ettringite which are seen growing from the shell inwards. This results in the consumption of sulfate in the shell, thus lowering its concentration there.

Silicates

- C-S-H is seen as early as 2 hours mostly present as a layer of variable thickness around cement grains.
- There is relatively more deposition of hydration products on silicates than on interstitial phases at 2 hours.
- C-S-H often has a granular appearance within the shell.
- Ca/Si ratio of pure C-S-H phase is almost the same (about 2) for all the regions and for all the ages until 48 hours.

Interstitial phases

- Aluminium is well distributed in the hydrating matrix.
- Iron is mostly found to be present on and within the shell.

- Ettringite is formed around both silicate and interstitial phases, indicating its formation via through-solution mechanism.
- Solid-state substitution of aluminium with iron both in ettringite and mono-sulfate occurs in between 12 and 18 hours.

Cement grains

- Some parts of the grains react more than the others. This indicates a preferential reactivity of cement grains.
- There is presence of striations on the surface of cement grains, which are 20–25 nm apart. Alite is the principal phase seen to exhibit this behaviour.

7.2 Blended cements involving OPC, CAC and $\overline{\text{CS}}$

7.2.1 Microstructural study

Ternary mix M2 (OPC as the major component)

- The hydration of OPC in ternary mixes in terms of shell formation and associated microstructural features is relatively unaffected by minor additions of CAC and gypsum.
- The amount of ettringite at any given time is more in the studied ternary binders than in pure OPC.
- The microstructure is compact and pore space well filled by 16 hours.
- Fine particles of C-S-H are seen, but only within the shell, similar to OPC. There is a significant presence of acicular shape C-S-H.
- The average Ca:Si ratio of C-S-H is nearly the same as for OPC, indicating no effect on C-S-H composition.
- Aluminium is well distributed in the matrix

- Iron is predominantly present within the shell, as in OPC hydration. The percentage of points having iron and the Fe:Ca ratio are the same as for OPC.
- No solid-state substitution of iron in AFt and AFm phases has occurred by 16 hours.

7.2.2 Phenomenon of expansion in ternary mixes

- The amount of expansion increases with increase in gypsum content.
- There is no relationship between the heat of hydration and the amount of expansion. However the height of the major peak in the heat of hydration is decreased and its occurrence delayed with the increase in gypsum content in the mixes.
- Most of the ettringite is formed around CAC grains in identical manner in expansive and non-expansive cements.
- For samples kept over water (100% RH), expansion occurs for all samples having gypsum content > 2 weight%. The expansion could be due to the development of crystallization pressures as a result of possible growth of hydrates in confined spaces.
- For the samples cured under water, expansion seems to depend on the demoulding time. Significant expansion occurs even in samples having 0.3 weight% gypsum content, when demoulded at early ages. The expansion could be due to the swelling of hydration products, although this swelling is not necessarily related directly to the presence of ettringite.

7.3 Expansion in heat-cured cement pastes (DEF)

Cement pastes cured to 90 °C and subsequently cooled to 20 °C showed expansion with time. This confirms the results reported in past that expansion not only

occurs in heat-cured mortars and concrete but also in pure cement pastes. This indicates towards the existence of the crystallization pressures believed to be due to the formation of ettringite during late hydration. Subsequently, TEM specimens were prepared to find evidence of the existence of ettringite needles in the outer product as generally believed. In some instances this was found to be true and ettringite needles are seen to grow, apparently, in association with a nearby monosulfate plates.

7.4 Future work

From the obtained results some more information is obtained on the phenomenon of shell formation. However its cause is still not clear. Attempts need to be made to study hydration of alite to compare its apparent shell formation with that of OPC. It is seen that sulfates in conjunction with the interstitial phases play a significant role in the development of the microstructure. Thus it seems appropriate that additions of Portland cement or alite with sulfates need to be studied. Further work in this direction could have the potential to alter the alite in clinker to gypsum ratio in the production of cement, possibly resulting in favourable financial impacts on the cement industry and society.

Much needs to be learned about the phenomenon of expansion in blends of OPC, CAC and $\text{C}\bar{\text{S}}$. Thin sections of expansive cements could be studied in TEM to observe if ettringite is present in fine pores which may cause expansion. Regarding the high expansion while curing under water, probably some innovative experiments need to be done since conventional techniques fail to provide any clear answers. For instance, pure commonly occurring hydrates, such ettringite, C-S-H, etc., can be prepared and placed under water to see their relative affinities for water and any associated expansion. It is possible that some phenomenon other than crystal or swelling pressures is responsible for expansion.

Appendix A

Binary mixes of OPC, CAC and CAC, $\text{C}\bar{\text{S}}$

Two binary mixes, one involving OPC, CAC and the other CAC with $\text{C}\bar{\text{S}}$ were studied. The mix F15 has OPC and CAC (Secar 51) in the weight ratio of 7:3, while B2 is composed of CAC (Fondu) and $\text{C}\bar{\text{S}}$ (anhydrite) in the ratio of 1:1. For F15 a 14 day old specimen and for B2 one specimen each at 1 and 7 days was prepared.

During the study of the binary mixes, precise quantitative chemical analysis could not have been obtained, thus only qualitative and semi-quantitative results are presented. Monosulfate phases, for instance, in the binary mixes were identified based on the $\bar{\text{S}}/\text{Al}$ ratio which was found to lie in the range 0.23–0.56, ideal values of $\bar{\text{S}}/\text{Al}$ for monosulfate being 0.50 and for ettringite 1.50. Only one phase was observed to have a S:Al ratio of 1.78 (Mix B2, Figure A.3) and is believed to be ettringite.

A.1 F15 (CAC: $\text{C}\bar{\text{S}}$)

This is the same formulation as studied by Lamberet [123] for long term (28 days–3 years) durability studies. At the observed ages, the microstructure was shown to be dense. While ettringite was absent, AFm was found to be present and thought

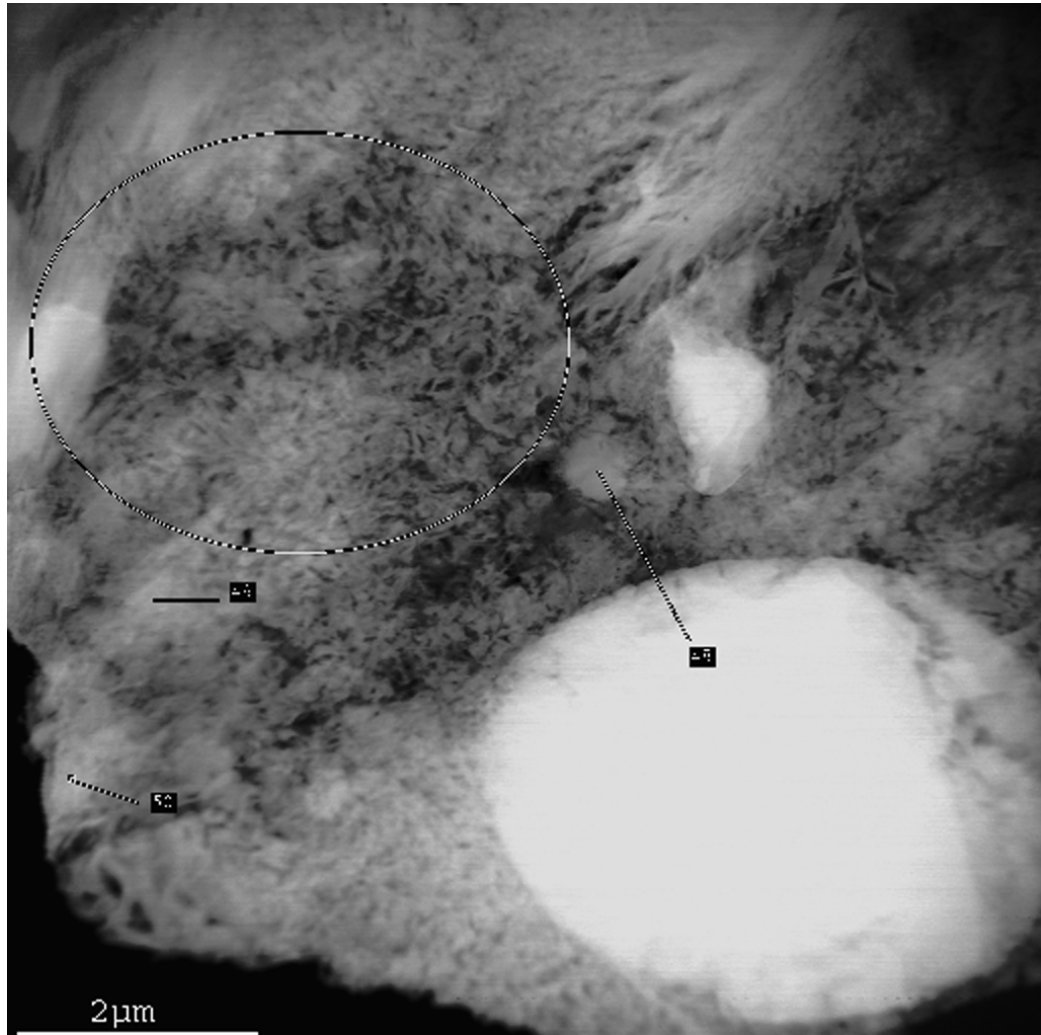


Figure A.1: Typical low-magnification image of F15 at 14 days. The big grain is a silicate phase

to exist as a solid-solution between C_4AH_{13} , monocarboaluminate, hemicarbonate and monosulfate. Portlandite was found to be absent.

In this study, from the obtained chemical analysis ¹ all the analysed hydration products are found to be rich in calcium and silicon. Aluminium is noted to be present in all of them and in a wide distribution, ranging from few at. wt. % to amounts double that of Si. 97% of the analysed points corresponding to hydration

¹It may be of some interest to note that the hydrates of this mix (F15) were much more resistant to electron-beam damage in the TEM than those of pure OPC

products have iron in very small amounts whereas 32% points have sulfur as well, in amounts relatively more than iron. No portlandite is found in the mix at the observed age.

The microstructure of the binary mix, as seen in TEM, at 14 days is found to be dense and compact (Figure A.1). However, there are significant differences in the morphologies of C-S-H in pure OPC and F15. In OPC there are mainly two morphologies of C-S-H namely foil-like, representing the inner product, and fibrous with poor compactness, representing the outer product. In F15, on the other hand, there seems to be little or no diversity in the C-S-H morphology. C-S-H appears like well developed flakes which seem to be well bonded with each other providing a uniformly densified matrix (Figure A.2).

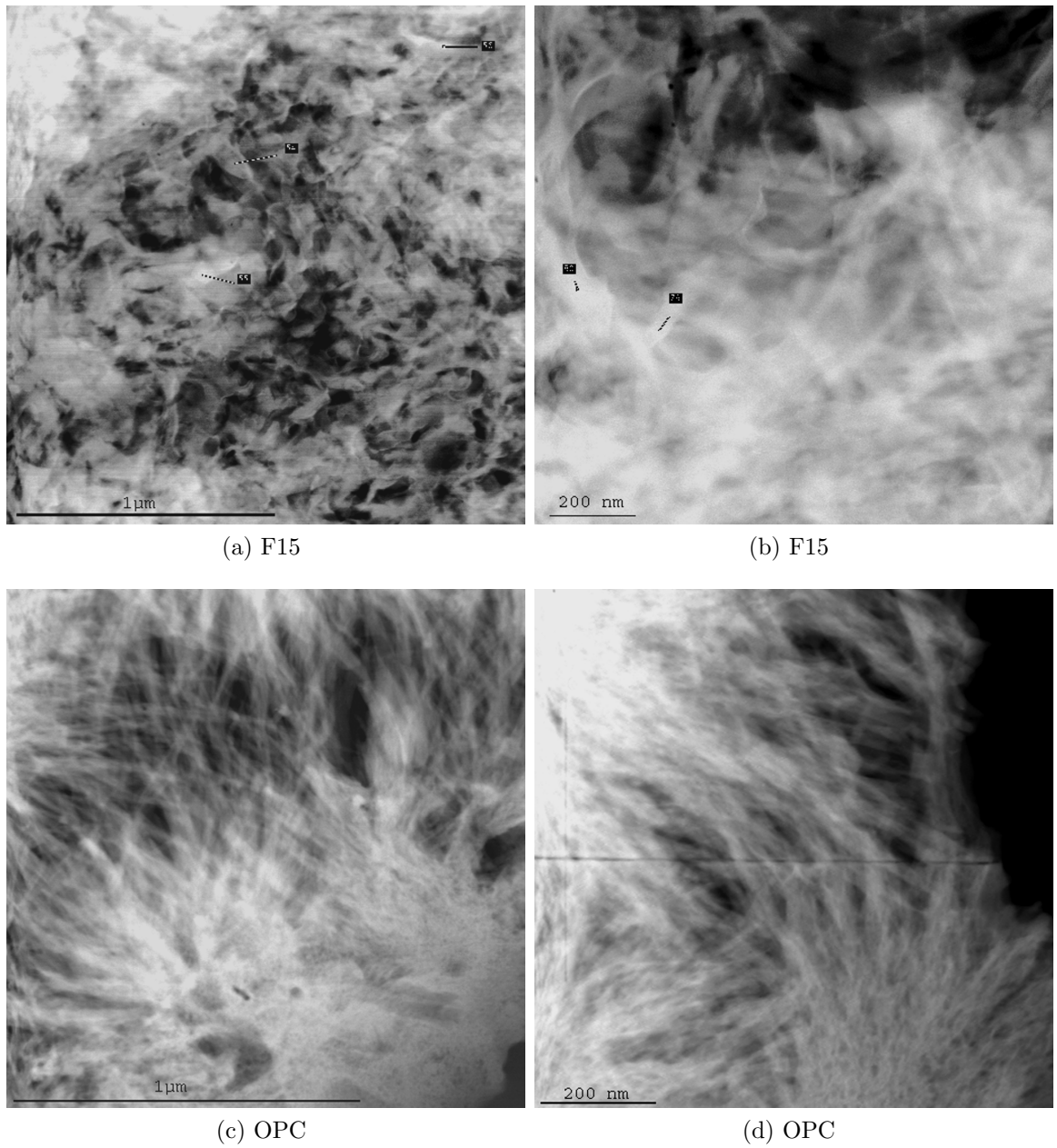


Figure A.2: Comparing the morphologies of C-S-H in pure OPC and F15 at 14 days, seen at different magnifications

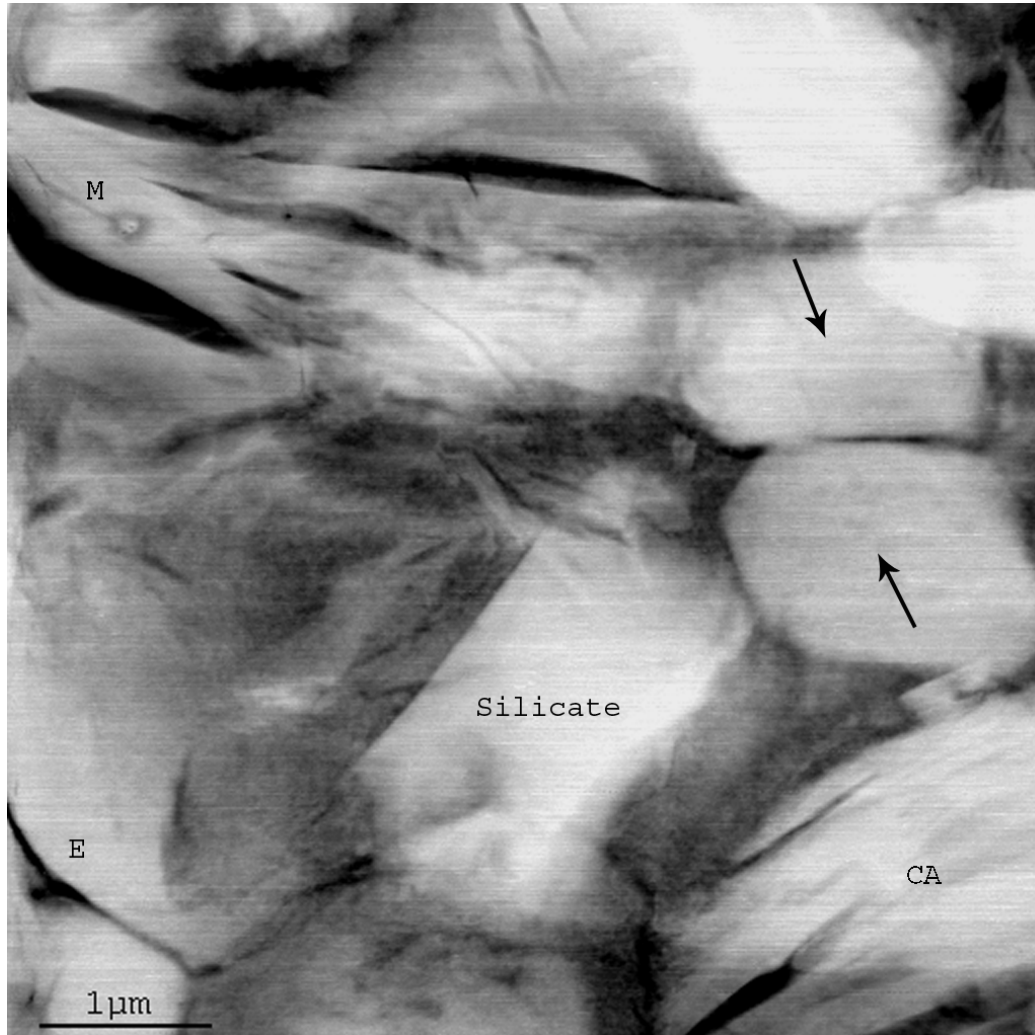


Figure A.3: B2, 1 day: monosulfate (M), ettringite (E), CA, $\text{C}\bar{\text{S}}$ (shown by arrows) and anhydrous silicate grains. Alumina gel is seen deposited around the grains

A.2 B2 (CAC: $\text{C}\bar{\text{S}}$)

For this study Fondu has been used as the calcium aluminate cement with hemihydrate calcium sulfate ($\text{CaSO}_4 \cdot 0.5\text{H}_2\text{O}$), in the ratio 1:1. One sample each at 1 and 7 days was studied in TEM and emphasis is given to understand the growth and distribution of aluminate rich hydrated phases along with other phases. It is important to understand how the two phases, CAC and $\text{C}\bar{\text{S}}$, react in context of

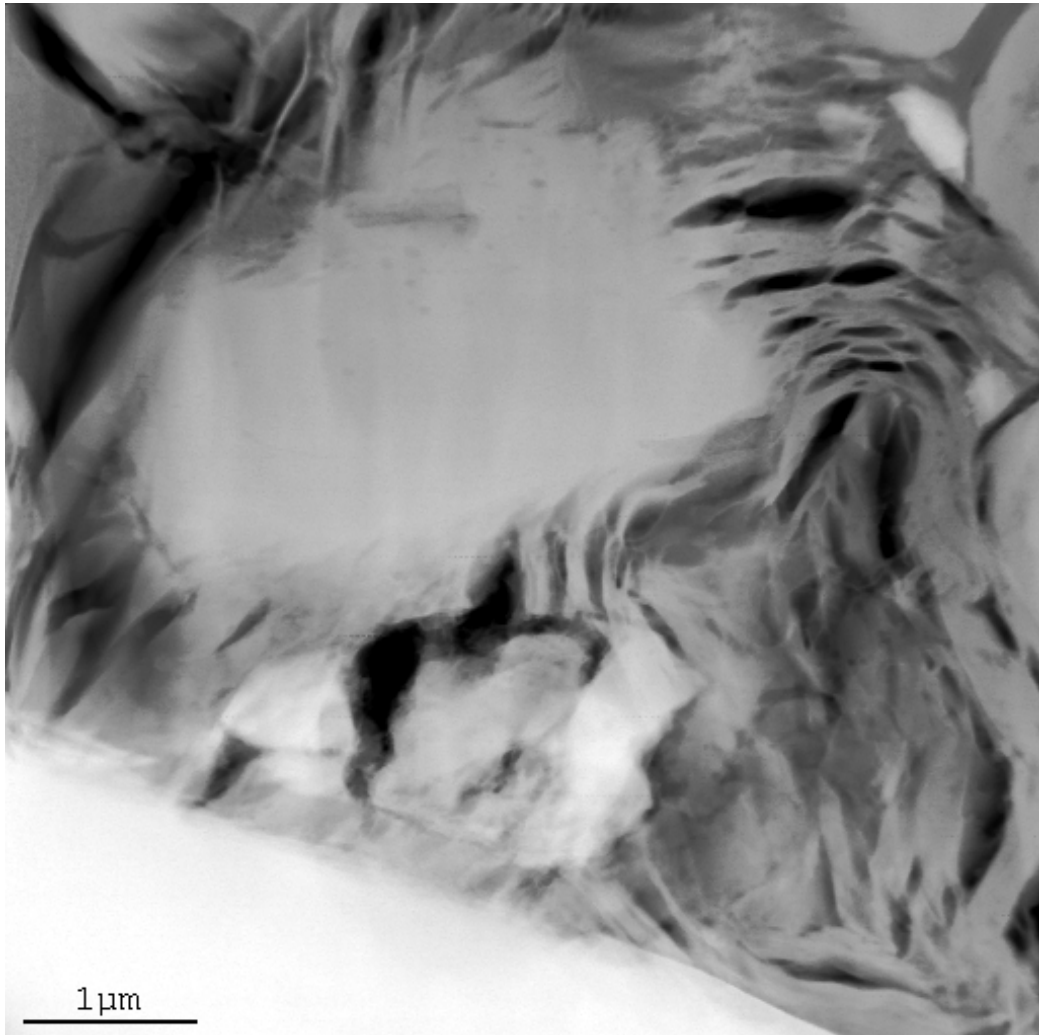


Figure A.4: B2, 7 day: calcium sulfate grain in the centre with monosulfate plates around

understanding the microstructure of the ternary mixes involving Portland cement.

Due to a higher density of aluminate and ferrite phases they appear brighter in the dark-field images than calcium sulfate grains. The C \bar{S} grains are generally round shaped while aluminoferrites have an approximate rectangular cross-section. Thus it is fairly easy to visually identify the individual phases, besides confirming their identity by chemical analysis. Even at 7 days large unreacted phases are seen, indicating a slow reaction of the mix.

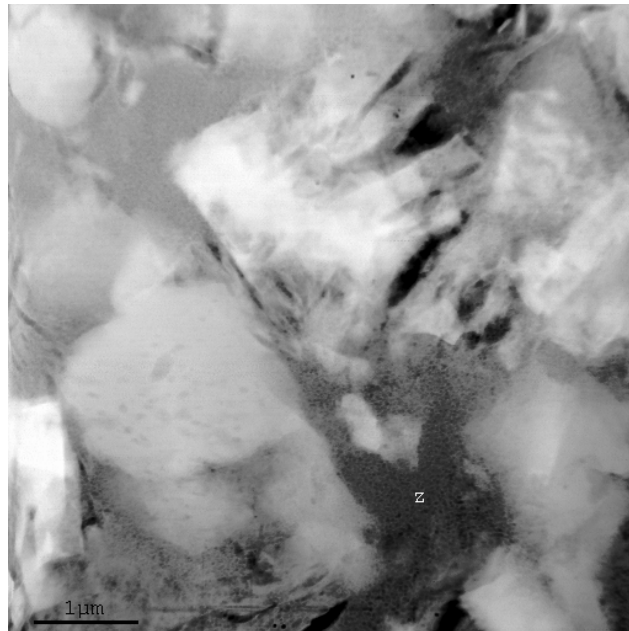
With regard to the hydrated phases, monosulfate, Al gel and some ettringite are seen to present. While at 1 day, monosulfate is seen present in the pore space as long plates (Figure A.3), at 7 days monosulfate is seen growing from the calcium sulfate grains in large numbers (Figure A.4). The growth of monosulfate on calcium sulfate and not on aluminates is interesting to note.

In the chemical analysis of alumina gel a small amount of calcium is always found, besides aluminium as the major element. This is explained by the high magnification image (Figure A.5b) which shows the presence of fine particles which are likely to be either CaO or Ca(OH)₂. It is also apparent that Al gel is highly porous and has a low atomic number and/or density; from the images it also looks amorphous.

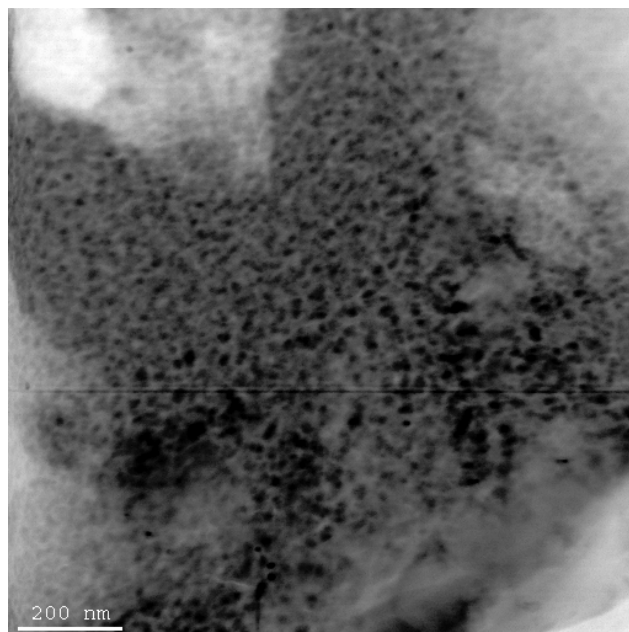
A.2.1 Discussion

The hydration matrix of the binary mix B2 is rich in aluminium. This can be concluded due to the significant presence and wide distribution of aluminate hydrates, such as monosulfate and Al gel, in the matrix.

An observation of interest is the apparent growth of monosulfate platelets from the $\bar{C}\bar{S}$ grain. The molar ratio of \bar{S} :Al at the time of mix can be estimated to be about 0.5 (taking CA as the main phase of Fondu, Table 2.3 on page 7). This corresponds well with the formation of monosulfate which has the same \bar{S} :Al ratio of 0.5. However the abundant presence of monosulfate around calcium sulfate and much less elsewhere seem to respectively indicate of the high affinity of Al³⁺ ions by $\bar{C}\bar{S}$ phase and of the low mobility of SO₄²⁻ ions in the mix.



(a) B2, 7 days: magnified view of Al gel (region marked 'Z') is shown below



(b) Magnified view of alumina gel

Figure A.5: Alumina gel is seen to have the presence of fine calcium rich particles. It is seen to be highly porous with a low average atomic number and/or density.

Appendix B

Effect of specimen thickness on chemical analysis

B.1 Introduction

It is known that chemical analysis in an electron microscope involves the acquisition of the emitted characteristic X-rays of the respective elements present in the specimen by the X-rays detectors. The microscope consequently estimate their relative amounts and presents the chemical spectrum of the analysed region. However, these emitted X-rays can be absorbed by the specimen if it is ‘too’ thick and may lead to an inaccurate estimate of the elements present in the sample. This is one of the problems in doing chemical analysis in a SEM which generally involves the study of bulk samples [213, Chapter 35].

The advantage in a TEM is the small thickness of the specimen which avoid any such absorptions. However it is possible that the specimen is thin enough for it to be transparent to the electrons resulting in image formation, but may still be too thick for obtaining good chemical analysis.

To this end, the following work was done to get an estimate on the effect of X-ray absorption on TEM specimens.

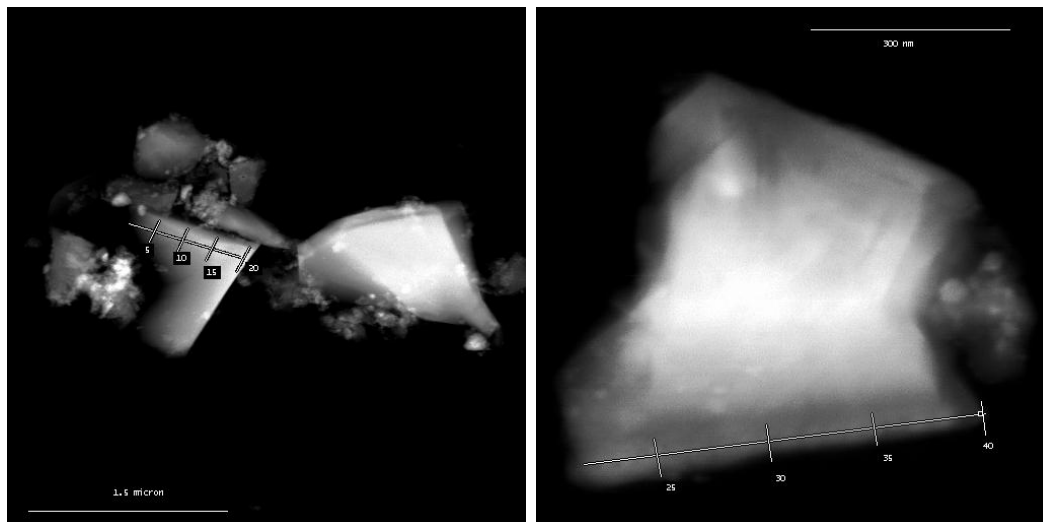


Figure B.1: Pure alite particles with Ca:Si ratio as 3. The lines on the images correspond to the path along which chemical analysis was carried and the numbers on the line constitute the X-axis of the graph in Figure B.2.

B.2 Work done

Pure alite was taken in powder form, dissolved in highly pure acetone and a drop of this mixture placed on a carbon coated copper mesh TEM grid. After allowing the grid to dry for several hours, the specimen was placed in the TEM. Several particles of alite are seen in the microscope, which have various thicknesses. A relative estimate of the thickness can be gauged by the amount of brightness of a particular region of a particle. Since dark-field imaging is employed, the darker the phase appears on the image, the thinner it is and vice-versa.

Quantitative EDS analysis was carried out along a line at regular distance along the direction of increasing specimen thickness (Figure B.1). Consequently a graph of the obtained atomic percentages of calcium, silica and Ca:Si ratio (which is normalized by multiplying the original values with 10) is plotted against the number of points, which indirectly represent the specimen thickness (Figure B.2).

It can be seen that the points which appear almost dark in the image, and are thus quite thin, show Ca:Si as nearly 3.0, which is the ideal value for alite, but as the specimen starts to get thicker the ratio of Ca and Si increases steadily (points which

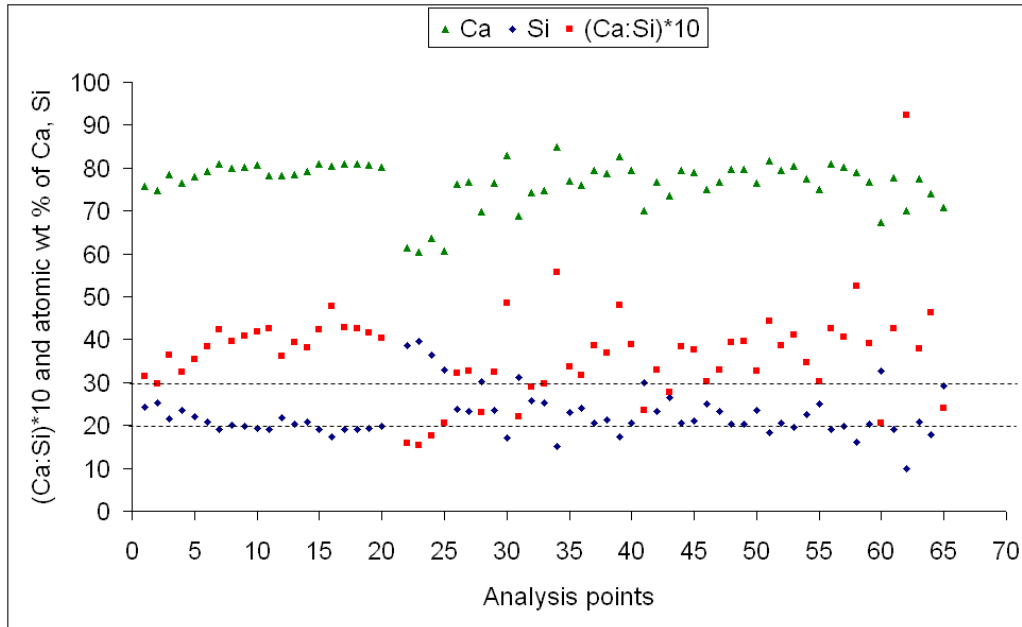


Figure B.2: The graph showing the variation of calcium and silica contents in alite, along with normalized Ca:Si ratios with specimen thickness.

have the ratio as 2 correspond to belite). From the atomic% values it is further learned that this increase is due to a corresponding decrease in the value of Si. This is because silica is a lighter element than calcium and its characteristic X-rays are absorbed by the specimen as it gets thicker. Thus the following conclusions can be drawn from these observation.

- The transmission electron microscope used in this project gives accurate quantitative chemical analysis and thus its results are reliable.
- With an increase in specimen thickness the characteristic X-rays of lighter elements in the specimen stand in danger of being absorbed, which may lead to their underestimation in the analysis.

Bibliography

- [1] *ASTM C 845-96, Standard specification for expansive hydraulic cement.*
- [2] <http://ciks.cbt.nist.gov/garboz/cell1994/node4.htm>.
- [3] AMATHIEU, L., BIER, T. A., AND SCRIVENER, K. L. *Calcium Aluminate Cements*. IOM, Communications, London, 2001, ch. Mechanisms of set acceleration of Portland cement, pp. 303–317.
- [4] ANDERSEN, M. D., JAKOBSEN, H. J., AND SKIBSTED, J. Incorporation of aluminum in the calcium silicate hydrate (C-S-H) of hydrated portland cements: A high-field ^{27}Al and ^{29}Si MAS NMR investigation. *Inorg. Chem.* *42*, 7 (2003), 2280–2287.
- [5] ANDERSEN, M. D., JAKOBSEN, H. J., AND SKIBSTED, J. Characterization of white portland cement hydration and the C-S-H structure in the presence of sodium aluminate by ^{27}Al and ^{29}Si MAS NMR spectroscopy. *Cement and Concrete Research* *34*, 5 (2004), 857–868.
- [6] ANDERSEN, M. D., JAKOBSEN, H. J., AND SKIBSTED, J. A new aluminium-hydrate species in hydrated portland cements characterized by ^{27}Al and ^{29}Si MAS NMR spectroscopy. *Cement and Concrete Research* *36*, 1 (2006), 3–17.
- [7] BAILEY, J. E., AND HAMPSON, C. J. The microstructure and chemistry of tricalcium aluminate hydration [and discussion]. *Philosophical Transactions of the Royal Society of London. Series A, Mathematical and Physical Sciences* *310*, 1511 (1983), 105–111.
- [8] BARBARULO, R., PEYCELON, H., AND PRENE, S. The role of C-S-H and temperature in delayed ettringite formation. In *International RILEM TC*

- 186-ISA Workshop on Internal Sulfate attack and delayed ettringite formation* (Villars, Switzerland, 2002), pp. 155–166.
- [9] BARRET, P., BETRANDIE, D., AND MENETRIER, D. Comparative study of C-S-H formation from supersaturated solutions and C_3S solution mixtures. In *Proceedings of 7th International Congress on Chemistry of Cement* (Paris, 1980), vol. II, pp. 261–266.
- [10] BARRET, P., AND MENETRIER, D. Filter dissolution of C_3S as a function of the lime concentration in a limited amount of lime water. *Cement and Concrete Research* 10, 4 (1980), 521–534.
- [11] BARRET, P., MENETRIER, D., AND BERTRANDIE, D. Cinétique d'hydratation des aluminates et silicates de calcium en relation avec les mécanismes du durcissement dans les ciments. *Revue Internationale Des Hautes Temperatures Et Des Refractaires* 14 (1977), 127–133.
- [12] BARRET, P., MENETRIER, D., AND BERTRANDIE, D. Mechanism of C_3S dissolution and problem of the congruency in the very initial period and later on. *Cement and Concrete Research* 13, 5 (1983), 728–738.
- [13] BARRET, P., MENETRIER, D., BETRANDIE, D., AND REGOURD, M. In *Proceedings of 7th International Congress on Chemistry of Cement* (Paris, 1980), vol. Volume II, p. 279.
- [14] BAYOUX, J. P., BONIN, A., MARCDARGENT, S., AND VERSCHAEVE, M. *Calcium Aluminate Cements*. E & FN Spon, London, 1990, ch. Study of the hydration of properties of aluminous cement and calcium sulfate mixes.
- [15] BAYOUX, J. P., TESTUD, M., AND ESPONOSA, B. Thermodynamic approach to understanding the $CaO - Al_2O_3 - SO_3$ system. In *Proceedings of the 9th International Conference on Chemistry of Cement* (New Delhi, 1992), vol. 4.
- [16] BECKER, G. F., AND DAY, A. L. Note on the linear force of growing crystals. *Journal of Geology* XXIV, 4 (1916), 313–333.
- [17] BENSTED, J., AND VARMA, S. P. Studies of ettringite and its derivatives. *Cement Technology* 2 (1971), 73–76.

- [18] BENSTED, J., AND VARMA, S. P. Ettringite and its derivatives. II. chromate substitution. *Silicates Industriels* 37, 12 (1972), 315–318.
- [19] BENTUR, A. Effect of gypsum on the hydration and strength of C₃S pastes. *Journal of the American Ceramic Society* 59, 5-6 (1976), 210–213.
- [20] BENTUR, A., AND ISH-SHALOM, M. Properties of type K expansive cement of pure components II. proposed mechanism of ettringite formation and expansion in unrestrained paste of pure expansive component. *Cement and Concrete Research* 4, 5 (1974), 709–721.
- [21] BIRCHALL, J. D., AND THOMAS, N. L. The mechanism of retardation of setting of OPC by sugars. In *Proceedings of the British Ceramic Society* (1984), vol. 35, pp. 305–315.
- [22] BONEN, D., AND DIAMOND, S. Interpretation of compositional patterns found by quantitative energy dispersive X-ray analysis for cement paste constituents. *Journal of the American Ceramic Society* 77, 7 (1994), 1875–1882.
- [23] BROUGH, A. R., DOBSON, C. M., RICHARDSON, I. G., AND GROVES, G. W. In situ solid-state NMR studies of Ca₃SiO₅: hydration at room temperature and at elevated temperatures using ²⁹Si enrichment. *Journal of Materials Science* V29, 15 (1994), 3926–3940.
- [24] BROWN, P., BARRET, P., DOUBLE, D. D., FROHNSDORFF, G., JOHANSEN, V., PARROT, L. J., POMMERSHEIM, J. M., REGOURD, M., SCRIVENER, K. L., TAYLOR, H. F. W., AND YOUNG, J. F. The hydration of tricalcium aluminate and tetracalcium aluminoferrite in the presence of calcium sulfate. *Matériaux et Constructions* 19, 110 (1986), 137–147.
- [25] BROWN, P. W. Early hydration of tetracalcium aluminoferrite in gypsum and lime-gypsum solutions. *Journal of the American Ceramic Society* 70, 7 (1987), 493–496.
- [26] BROWN, P. W. Effects of particle size distribution on the kinetics of hydration of tricalcium silicate. *Journal of the American Ceramic Society* 72, 10 (1989), 1829–1832.

- [27] BROWN, P. W., FRANZ, E., FROHNSDORFF, G., AND TAYLOR, H. F. W. Analyses of the aqueous phase during early C₃S hydration. *Cement and Concrete Research* 14, 2 (1984), 257–262.
- [28] BROWN, P. W., HARNER, C. L., AND PROSEN, E. J. The effect of inorganic salts on tricalcium silicate hydration. *Cement and Concrete Research* 16, 1 (1986), 17–22.
- [29] BRYDSON, R., RICHARDSON, I. G., MCCOMB, D. W., AND GROVES, G. W. Parallel electron energy loss spectroscopy study of Al-substituted calcium silicate hydrate (C-S-H) phases present in hardened cement pastes. *Solid State Communications* 88, 2 (1993), 183–187.
- [30] BUDNIKOV, P. P., AND KRAVCHENKO, I. V. Expansive cement. In *Proceedings of the 5th International Symposium of the Chemistry of Cement* (Tokyo, 1968), pp. 319–330.
- [31] BUHLERT, R., AND KUZEL, H. J. The replacement of Al³ by Cr³ and Fe³ in ettringite. *Zement Kalk-Gips* 24, 2 (1971), 83–85.
- [32] BYE, G. C. *Hydration of Portland Cement, Portland Cement, Composition, production and properties*, second ed. Thomas Telford, London, 1999.
- [33] CARPENTER, A. B., CHALMERS, R. A., GARD, J. A., SPEAKMAN, K., AND TAYLOR, H. F. W. Jennite, a new mineral. *American Mineralogist* 51 (1966), 56.
- [34] CHATTERJI, S. Mechanism of the CaCl₂ attack on portland cement concrete. *Cement and Concrete Research* 8, 4 (1978), 461–467.
- [35] CHATTERJI, S. Mechanism of expansion of concrete due to the presence of dead-burnt cao and mgo. *Cement and Concrete Research* 25, 1 (1995), 51–56.
- [36] CHATTERJI, S., AND JEFFERY, J. W. Studies of early stages of paste hydration of cement compounds, I. *Journal of the American Ceramic Society* 45, 11 (1962), 536–543.
- [37] CHATTERJI, S., AND THAULOW, N. Unambiguous demonstration of destructive crystal growth pressure. *Cement and Concrete Research* 27, 6 (1997), 811–816.

- [38] CHEN, S.-S., AND MEHTA, P. K. Zeta potential and surface area measurements on ettringite. *Cement and Concrete Research* 12, 2 (1982), 257–259.
- [39] CLAYDEN, N. J., DOBSON, C. M., GROVES, G. M., HAYES, C. J., AND RODGER, S. A. Hydration of tricalcium silicate followed by solid-state ^{29}Si NMR spectroscopy. *J. Chem. Soc., Chem. Commun.* (1984), 1396–1397.
- [40] COHEN, M. *Micromechanics of expansive mechanisms in expansive cement concretes*. PhD thesis, Stanford University, 1981.
- [41] COHEN, M. Theories of expansion in sulfoaluminate - type expansive cements: Schools of thought. *Cement and Concrete Research* (1983), 809–818.
- [42] COLLEPARDI, M., BALDINI, G., PAURI, M., AND CORRADI, M. Tricalcium aluminate hydration in the presence of lime, gypsum or sodium sulfate. *Cement and Concrete Research* 8, 5 (1978), 571–580.
- [43] COLLEPARDI, M., MONOSI, S., MORICONI, G., AND CORRADI, M. Tetra-calcium aluminoferrite hydration in the presence of lime and gypsum. *Cement and Concrete Research* 9, 4 (1979), 431–437.
- [44] CONG, X., AND KIRKPATRICK, R. J. ^{17}O and ^{29}Si MAS NMR study of $\beta\text{C}_2\text{S}$ hydration and the structure of calcium-silicate hydrates. *Cement and Concrete Research* 23, 5 (1993), 1065–1077.
- [45] CONG, X., AND KIRKPATRICK, R. J. Hydration of calcium aluminate cements: A solid-state ^{27}Al NMR study. *Journal of the American Ceramic Society* 76, 2 (1993), 409–416.
- [46] CONG, X., KIRKPATRICK, R. J., YARGER, J. L., AND MCMILLAN, P. F. The structure of calcium-silicate hydrate: NMR and Raman spectroscopic results. In *2nd International Conference on NMR Spectroscopy of Cement-based Materials* (Bergamo, 1996).
- [47] CONSTANTINIDES, G., AND ULM, F.-J. The effect of two types of C-S-H on the elasticity of cement-based materials: Results from nanoindentation and micromechanical modeling. *Cement and Concrete Research* 34, 1 (2004), 67–80.

- [48] COPELAND, L. E., BODOR, E., CHANG, T. N., AND WEISE, C. H. Reactions of tobermorite gel with aluminates, ferrites, and sulfates. *J. Res. Dev. Lab., Portland Cem. Assoc.* 9 (1967), 61–74.
- [49] COPELAND, L. E., AND KANTRO, D. L. Hydration of Portland cement. In *Proceedings of 5th International Congress of Chemistry of Cement* (Tokyo, 1969), vol. II, pp. 387–421.
- [50] CORDES, S. *Einsatz von Sekundärneutralteilchen - Massenspektrometrie bei der Untersuchung der Anfangshydratation von Tricalciumsilicat*. PhD thesis, Technische Universität Clausthal, 1995.
- [51] CORTE, A. E. Vertical migration of particles in front of a moving freezing plane. *Journal of Geophysical Research* 67, 3 (1962), 1085–1090.
- [52] COTTIN, B. F. Hydration of calcium silicates and aluminates mixes. In *Proceedings of the 7th International Congress on the Chemistry of Cement* (Paris, 1980), vol. 5, pp. 113–118.
- [53] COURAULT, A. C. *Simulation expérimentale des C-S-H dans les betons modernés: étude de la composition et des propriétés à l'équilibre dans les milieux complexes*. PhD thesis, Université de Bourgogne, Dijon, France, 2000.
- [54] DALGLEISH, B. J., AND IBE, K. Thin-foil studies of hydrated portland cement. *Cement and Concrete Research* 11, 5-6 (1981), 729–739.
- [55] DAMIDOT, D., AND NONAT, A. *Hydration and setting of cement*. E&FN Spon, 1992, p. 23.
- [56] DAMIDOT, D., AND NONAT, A. C₃S hydration in diluted and stirred suspension: (II) properties of C-S-H precipitated during the two kinetic steps. *Advances in Cement Research* 6, 22 (1994), 83–91.
- [57] DAMIDOT, D., AND NONAT, A. C₃S hydration in diluted and stirred suspensions: (I) study of the two kinetic steps. *Advances in Cement Research* 6, 21 (1994), 27–35.
- [58] DAMIDOT, D., NONAT, A., AND BARRET, P. Kinetics of tricalcium silicate hydration in diluted suspensions by microcalorimetric measurements. *Journal of the American Ceramic Society* 73, 11 (1990), 3319–3322.

- [59] DENT GLASSER, L. S. A reply to P.K. Mehta's discussion of "osmotic pressure and the swelling of gels". *Cement and Concrete Research* 10, 1 (1980), 125–126.
- [60] DENT GLASSER, L. S., LACHOWSKI, E. E., MOHAN, K., AND TAYLOR, H. F. W. A multi-method study of C₃S hydration. *Cement and Concrete Research* 8, 6 (1978), 733–739.
- [61] DIAMOND, S. Cement paste microstructure - an overview at several levels. In *Conference Proceedings at University of Sheffield, Cement Concrete Association* (1976), pp. 2–30.
- [62] DIAMOND, S. Delayed ettringite formation – processes and problems. *Cement and Concrete Composites* 18, 3 (1996), 205–215.
- [63] EDMONDS, R. N., AND MAJUMDAR, A. J. The hydration of monocalcium aluminate at different temperatures. *Cement and Concrete Research* 18, 2 (1988), 311–320.
- [64] FAMY, C. *Expansion of heat cured mortars*. PhD thesis, Imperial College, London, 1999.
- [65] FAMY, C., SCRIVENER, K. L., ATKINSON, A., AND BROUGH, A. R. Effects of an early or a late heat treatment on the microstructure and composition of inner C-S-H products of portland cement mortars. *Cement and Concrete Research* 32, 2 (2002), 269–278.
- [66] FAMY, C., SCRIVENER, K. L., AND BROUGH, A. R. Role of microstructural characterisation in understanding the mechanism of expansion of expansion due to delayed ettringite formation. In *International RILEM TC 186-ISA Workshop on Internal Sulfate attack and delayed ettringite formation* (Villars, Switzerland, 2002), pp. 167–172.
- [67] FAMY, C., SCRIVENER, K. L., AND CRUMBIE, A. K. What causes differences of c-s-h gel grey levels in backscattered electron images? *Cement and Concrete Research* 32, 9 (2002), 1465–1471.
- [68] FAUCON, P., CHARPENTIER, T., NONAT, A., AND PETIT, J. C. Triple-quantum two-dimensional ²⁷Al magic angle nuclear magnetic resonance

- study of the aluminium incorporation in calcium silicate hydrates. *Journal of the American Chemical Society* 120, 46 (1998), 12075–12082.
- [69] FELDMAND, R. F., AND RAMACHANDRAN, V. S. The influence of $\text{CaSO}_4 \cdot 2\text{H}_2\text{O}$ upon the hydration character of $3\text{CaO} \cdot \text{Al}_2\text{O}_3$. *Magazine of Concrete Research* 18, 57 (1966), 185–196.
- [70] FLATT, R. J. Salt damage in porous materials: how high supersaturations are generated. *Journal of Crystal Growth* 242, 3-4 (2002), 435–454.
- [71] FUJII, K., AND KONDO, W. Estimation of thermochemical data for calcium silicate hydrate C-S-H. *Journal of the American Ceramic Society* 66, 12 (1983), C-220–C-221.
- [72] FUKUHARA, M., GOTO, S., ASAGA, K., DAIMON, M., AND KONDO, R. Mechanisms and kinetics of C_4AF hydration with gypsum. *Cement and Concrete Research* 11, 3 (1981), 407–414.
- [73] FULLMANN, T., WALENTA, G., BIER, T., ESPINOSA, B., AND SCRIVENER, K. L. Quantitative rietveld phase analysis of calcium aluminate cements. *World Cement Research* (1999), 1–6.
- [74] GARD, J. A., MOHAN, K., TAYLOR, H. F. W., AND CLIFF, G. Analytical electron microscopy of cement pastes: I, tricalcium silicate pastes. *Journal of the American Ceramic Society* 63, 5-6 (1980), 336–337.
- [75] GARRAULT-GAUFFINET, S., AND NONAT, A. Experimental investigation of calcium silicate hydrate (C-S-H) nucleation. *Journal of Crystal Growth* 200, 3-4 (1999), 565–574.
- [76] GARTNER, E. M., AND GAIDIS, J. M. *Materials Science of Concrete I*. American Ceramic Society, Westerville, Ohio, USA, 1989, p. 95.
- [77] GARTNER, E. M., AND JENNINGS, H. M. Thermodynamics of calcium silicate hydrates and their solutions. *Journal of the American Ceramic Society* 70, 10 (1987), 743–749.
- [78] GARTNER, E. M., YOUNG, J. F., DAMIDOT, D. A., AND JAWED, I. *Structures and Performance of Cements*, 2nd ed. Spon Press, New York, USA, 2002, ch. 3.

- [79] GAUFFINET, S. *Etude expérimentale et par simulation numérique de la cinétique de croissance et de la structure des hydrosilicates de calcium, produits d'hydratation des silicates tricalcique et dicalcique*. PhD thesis, University of Dijon, France, 1998.
- [80] GAUFFINET, S., FINOT, E., LESNIEWSKA, E., AND NONAT, A. Observation directe de la croissance d'hydrosilicate de calcium sur des surfaces de silice et de silice par microscopie à force atomique. *Comptes Rendus de l'Académie des Sciences - Series IIA - Earth and Planetary Science* 327 (1998), 231–236.
- [81] GAUFFINET, S., FINOT, E., AND NONAT, A. Experimental study and simulation of C-S-H nucleation and growth. In *Proceedings of 2nd RILEM Workshop on Hydration and Setting : Why does cement set? An interdisciplinary approach* (Dijon, France, 1997).
- [82] GAUFFINET-GARRAULT, S., FINOT, E., LESNIEWSKA, E., AND NONAT, A. Study of C-S-H growth on C₃S surface during its early hydration. *Materials and Structures* 38, 4 (2005), 435–442.
- [83] GIROUD, G. Expansion des mélanges ternaires (PC, CAC, C \bar{S}). Diploma project, École Polytechnique Fédérale de Lausanne, Switzerland, February 2005.
- [84] GREENBERG, S. A., AND CHANG, T. N. Investigation of the colloidal hydrated calcium silicates. II. solubility relationships in the calcium oxide-silica-water system at 25°C. *J. Phys. Chem.* 69, 1 (1965), 182–188.
- [85] GREENBERG, S. A., CHANG, T. N., AND ANDERSON, E. Investigation of colloidal hydrated calcium silicates. I. solubility products. *J. Phys. Chem.* 64, 9 (1960), 1151–1157.
- [86] GRIMMER, A. R. *Applications of NMR to Cement Science*. Gordon and Breach, London, 1994, p. 77.
- [87] GROVES, G. W. Portland cement clinker viewed by transmission electron microscopy. *Journal of Material Science* 16 (1981), 1063–1070.
- [88] GROVES, G. W., SUEUR, P. J., AND SINCLAIR, W. Transmission electron microscopy and microanalytical studies of ion-beam-thinned sections

- of tricalcium silicate paste. *Journal of the American Ceramic Society* 69, 4 (1986), 353–356.
- [89] GRUTZECK, M., BENESI, A., AND FANNING, B. Silicon-29 magic angle spinning nuclear magnetic resonance study of calcium silicate hydrates. *Journal of the American Ceramic Society* 72, 4 (1989), 665–668.
- [90] GRUTZECK, M. W., AND RAMACHANDRAN, A. R. An integration of tricalcium silicate hydration models in light of recent data. *Cement and Concrete Research* 17, 1 (1987), 164–170.
- [91] GU, P., AND BEAUDOIN, J. J. A conduction calorimetric study of early hydration of ordinary portland cement/high alumina cement pastes. *Journal of Materials Science* 32, 14 (1997), 3875–3881.
- [92] GU, P., BEAUDOIN, J. J., QUINN, E. G., AND MYERS, R. E. Early strength development and hydration of ordinary portland cement/calcium aluminate cement pastes. *Advanced Cement Based Materials* 6, 2 (1997), 53–58.
- [93] GU, P., FU, Y., AND BEAUDOIN, J. J. A study of the hydration and setting behaviour of OPC – HAC pastes. *Cement and Concrete Research* 24, 4 (1994), 682–694.
- [94] GU, P., YAN, F., PING, X., AND BEAUDOIN, J. J. Electrochemical behaviour of portland-cement/high-alumina-cement systems at early hydration times. *Journal of Materials Science Letters* 12, 22 (1993), 1771–1773.
- [95] HADLEY, D. W. *The nature of the paste-aggregate interface*. PhD thesis, Purdue University, 1972.
- [96] HADLEY, D. W., DOLCH, W. L., AND DIAMOND, S. On the occurrence of hollow-shell hydration grains in hydrated cement paste. *Cement and Concrete Research* 30, 1 (2000), 1–6.
- [97] HALL, C. E. *Introduction to Electron Microscopy*. McGraw-Hill, New York, 1953.
- [98] HEAD, M. K., WONG, H. S., AND BUENFELD, N. R. Characterisation of ‘hadley’ grains by confocal microscopy. *Cement and Concrete Research* 36, 8 (2006), 1483–1489.

- [99] HEIDENREICH, R. D. *Fundamentals of Transmission Electron Microscope*. Interscience, New York, 1964.
- [100] HEINZ, D., LUDWIG, U., AND RUDIGER, I. Delayed ettringite formation in heat treated mortars and concretes. *Concrete Precasting Plant and Technology* 11 (1989), 56–61.
- [101] HENDERSON, E., AND BAILEY, J. E. The compositional and molecular character of the calcium silicate hydrates formed in the paste hydration of $3\text{CaO} \cdot \text{SiO}_2$. *Journal of Materials Science* 28, 13 (1993), 3681–3691.
- [102] ISH-SHALOM, M., AND BENTUR, A. Properties of type K expansive cement of pure components I. hydration of unrestrained paste of expansive component – results. *Cement and Concrete Research* 4, 4 (1974), 519–532.
- [103] JAWED, I., GOTO, S., AND KONDO, R. Hydration of tetracalcium aluminoferrite in presence of lime and sulfates. *Cement and Concrete Research* 6, 4 (1976), 441–453.
- [104] JELENIĆ, I., PANOVIĆ, A., AND BEZJAK, A. Hydration and strength development in alite- C_3A -CH-quartz pastes containing readily soluble alkalis. *Cement and Concrete Research* 10, 3 (1980), 463–466.
- [105] JELENIĆ, I., PANOVIĆ, A., HALLE, R., AND GACESA, T. Effect of gypsum on the hydration and strength development of commercial portland cements containing alkali sulfates. *Cement and Concrete Research* 7, 3 (1977), 239–245.
- [106] JENNINGS, H. M. *Advances in Cement Technology*. Pergamon, Oxford, U.K., 1983, ch. The developing microstructure in Portland cement, pp. 349–396.
- [107] JENNINGS, H. M. Aqueous solubility relationships for two types of calcium silicate hydrate. *Journal of the American Ceramic Society* 69, 8 (1986), 614–618.
- [108] JENNINGS, H. M. A model for the microstructure of calcium silicate hydrate in cement paste. *Cement and Concrete Research* 30, 1 (2000), 101–116.

- [109] JENNINGS, H. M., DALGLEISH, B. J., AND PRATT, P. L. Morphological development of hydrating tricalcium silicate as examined by electron microscopy techniques. *Journal of the American Ceramic Society* 64, 10 (1981), 567–572.
- [110] JOHANSEN, V., THAULOW, N., JAKOBSEN, U. H., AND PALBOL, L. Heat cured induced expansion. In *3rd Beijing International Symposium Cement and Concrete* (1993).
- [111] KALOUSEK, G. L. Analysing SO₃-bearing phases in hydrating cements. *Mater. Res. Stand.* 5 (1965), 292–304.
- [112] KALOUSEK, G. L., AND ADAMS, M. Hydration products formed in cement pastes at 25 to 150°C. In *Proceedings of the Journal of American Concrete Institute* (September 1951), no. 48, pp. 77–90.
- [113] KALOUSEK, G. L., AND BENTON, E. Mechanism of seawater attack on cement pastes. In *Proceedings of the Journal of American Concrete Institute* (February 1970), vol. 67, pp. 187–192.
- [114] KANARE, H., AND GARTNER, E. M. *Cement Research Progress*. American Ceramic Society, 1984, ch. 13. Optimum Sulfate in Portland Cement, pp. 213–251.
- [115] KANTRO, D. L., BRUNAUER, S., AND WEISE, C. H. Development of surface in the hydration of calcium silicates. II. extension of investigations to earlier and later stages of hydration. *Journal of Physical Chemistry* 66, 10 (1962), 1804–1809.
- [116] KERDEGARI, A. *The Role Of Gypsum In Portland Cement And Expansive Cement*. PhD thesis, Dept. of Civil Engineering, Stanford University, Stanford, California., 1978.
- [117] KJELLEN, K. O., AND JUSTNES, H. Revisiting the microstructure of hydrated tricalcium silicate—a comparison to portland cement. *Cement and Concrete Composites* 26, 8 (2004), 947–956.
- [118] KLEPEIS, S. J., BENEDICT, J. P., AND ANDERSON, R. Specimen preparation for transmission electron microscopy of materials. In *MRS Symposium Proceedings* (Pittsburgh, Pennsylvania, 1988), vol. 115, p. 179.

- [119] KONIK, Z., MALOLEPSZY, J., ROSZCZYNIANSKI, W., AND STOK, A. Production of expansive additive to portland cement. *Journal of the European Ceramic Society* 27, 2-3 (2007), 605–609.
- [120] KUZEL, H. J. Ersatz von Al^{3+} durch Cr^{3+} und Fe^{3+} in $3\text{CaO} \cdot \text{Al}_2\text{O}_3 \cdot \text{CaCl}_2 \cdot n\text{H}_2\text{O}$ und $3\text{CaO} \cdot \text{Al}_2\text{O}_3 \cdot \text{CaSO}_4 \cdot n\text{H}_2\text{O}$. *Zement Kalk-Gips* 21, 12 (1968), 493–499.
- [121] LACHOWSKI, E. E., MOHAN, K., TAYLOR, H. F. W., LAWRENCE, C. D., AND MOORE, A. E. Analytical electron microscopy of cement pastes: III, pastes hydrated for long times. *Journal of the American Ceramic Society* 64, 6 (1981), 319–321.
- [122] LACHOWSKI, E. E., MOHAN, K., TAYLOR, H. F. W., AND MOORE, A. E. Analytical electron microscopy of cement pastes: II, pastes of portland cements and clinkers. *Journal of the American Ceramic Society* 63, 7-8 (1980), 447–452.
- [123] LAMBERET, S. *Durability of ternary binders based on Portland Cement, Calcium Aluminate Cement and Calcium Sulfate*. PhD thesis, École Polytechnique Fédérale de Lausanne, Switzerland, 2005.
- [124] LAMOUR, V., MONTEIRO, P., LUCERO, A., DENBEAUX, G., JOHNSON, L., AND MEYER-ILSE, W. Study of early-age hydration of calcium aluminate cements through transmission X-ray microscopy. <http://www.als.lbl.gov/als/compendium/AbstractManager/uploads/99050.pdf>.
- [125] LEWIS, M. C., AND SCRIVENER, K. L. Microstructural effects of elevated temperature curing and delayed ettringite formation. In *Material Research Society Symposium Proceedings* (Boston, 1995).
- [126] LOCHER, F. W. Hydration of pure Portland cements. In *Proceedings of 7th International Congress on Chemistry of Cement* (Paris, 1980), vol. IV, pp. 49–54.
- [127] MACPHEE, D. E., LACHOWSKI, E. E., AND GLASSER, F. P. Polymerisation effects in C-S-H: implications for portland cement hydration. *Advances in Cement Research* 1 (1988), 131–137.

- [128] MARCHESE, B. A discussion of the paper “studies on the hydration of tricalcium silicate pastes. I. scanning electron microscopic examination of microstructural features”. *Cement and Concrete Research* 4, 3 (1974), 481–483.
- [129] MASSAZZA, F., AND DAIMON, M. Chemistry of hydration of cements and cementitious systems. In *Proceedings of 9th International Congress on Chemistry of Cement* (New Delhi, India, 1992), vol. I, pp. 383–446.
- [130] MÉNÉTRIER, D. *Contribution à l'étude cinétique de la formation des hydrates dans les solutions aqueuses obtenues à partir du ciment alumineux*. PhD thesis, University of Dijon, Dijon, France, 1977.
- [131] MÉNÉTRIER, D., AND BARRET, P. *Cement Research Progress*. American Ceramic Society, 1982, ch. 12. Research in France: 1977–1981, pp. 223–267.
- [132] MÉNÉTRIER, D., JAWED, I., SUN, T. S., AND SKALNY, J. ESCA and SEM studies on early C₃S hydration. *Cement and Concrete Research* 9, 4 (1979), 473–482.
- [133] MEHTA, P. K. Mechanism of expansion associated with ettringite formation. *Cement and Concrete Research* 3, 1 (1973), 1–6.
- [134] MEHTA, P. K., AND HU, F. Further evidence for expansion of ettringite by water adsorption. *Journal of the American Ceramic Society* 61, 3-4 (1978), 179–181.
- [135] MEHTA, P. K., AND MONTEIRO, P. J. M. *Concrete: Microstructure, Properties and Materials*. McGrawHill, New York, 2006.
- [136] MEHTA, P. K., AND WANG, S. Expansion of ettringite by water adsorption. *Cement and Concrete Research* 12, 1 (1982), 121–122.
- [137] MIDGLEY, H. G., AND ROSAMAN, D. The composition of ettringite in set Portland cement. In *Proceedings of 4th International Symposium on Chemistry of Cement* (Washington, 1962), vol. III-S2, pp. 259–262.
- [138] MIELENZ, R. C., MARUSIN, S. L., HIME, W. G., AND JUGOVIC, Z. T. Investigation of prestressed concrete railway ties distress. *Concrete International* 17 (1995), 62–68.

- [139] MIN, D., AND MINGSHU, T. Formation and expansion of ettringite crystals. *Cement and Concrete Research* 24, 1 (1994), 119–126.
- [140] MINARD, H. *Etude intégrée des processus d'hydratation, de coagulation, de rigidification et de prise pour un système C₃S-C₃A-sulfates-alcalins*. PhD thesis, University of Bourgogne, Dijon, France, 2003.
- [141] NACHBAUR, L., NKINAMUBANZI, P.-C., NONAT, A., AND MUTIN, J.-C. Electrokinetic properties which control the coagulation of silicate cement suspensions during early age hydration. *Journal of Colloid and Interface Science* 202, 2 (1998), 261–268.
- [142] NAKAMURA, T., SUDOH, G., AND AKAIWA, S. Mineralogical composition of expansive cement clinker rich in SiO₂ and its expansibility. In *Proceedings of the 5th International Symposium on the Chemistry of Cement* (1968), vol. V, pp. 351–365. Supplementary paper IV-74.
- [143] NEGRO, A., AND STAFFIERI, L. The hydration of calcium ferrites and calcium aluminoferrites. *Zement-Kalk-Gips* 32, 2 (1979), 83–88.
- [144] NONAT, A. The structure and stoichiometry of C-S-H. *Cement and Concrete Research* 34, 9 (2004), 1521–1528.
- [145] NONAT, A., LECOQ., X., AND GAUFFINET, S. Calcium hydroxide concentration in solution: parameter determining the kinetics of the early hydration of tricalcium silicate and the characteristics of the products. In *Proceedings of 10th International Congress on Chemistry of Cement* (Gothenburg, Sweden, 1997), vol. 2, p. 55.
- [146] ODLER, I. Interaction between gypsum and the C-S-H phase formed in C₃S hydration. In *Proceedings of 7th International Congress on Chemistry of Cement* (Paris, 1980).
- [147] ODLER, I. *Leas Chemistry of Cement and Concrete*, 4th ed. Arnold Press, London, UK, 1998, ch. 6, p. 245.
- [148] ODLER, I., AND ABDUL-MAULA, S. Possibilities of quantitative determination of the AFt-(ettringite) and AFm-(monosulphate) phases in hydrated cement pastes. *Cement and Concrete Research* 14, 1 (1984), 133–141.

- [149] ODLER, I., AND CHEN, Y. On the delayed expansion of heat cured portland cement pastes and concretes. *Cement and Concrete Composites* 18, 3 (1996), 181–185.
- [150] ODLER, I., AND COLAN-SUBAUSTE, J. Investigations on cement expansion associated with ettringite formation. *Cement and Concrete Research* 29, 5 (1999), 731–735.
- [151] ODLER, I., AND GASSER, M. Mechanism of sulfate expansion in hydrated portland cement. *Journal of the American Ceramic Society* 71, 11 (1988), 1015–1020.
- [152] OGAWA, K., AND ROY, D. M. $C_4A_3\bar{S}$ hydration, ettringite formation, and its expansion mechanism: II. microstructural observation of expansion. *Cement and Concrete Research* 12, 1 (1982), 101–109.
- [153] OKUSHIMA, M., KONDO, R., MUGURUMA, H., AND ONO, Y. Development of expansive cement with calcium sulphoaluminous cement clinker. In *Proceedings of the 5th International Symposium on the Chemistry of Cement* (Tokyo, 1968), pp. 419–438.
- [154] POELLMANN, H., KUZEL, H. J., AND WENDA, R. Solid solution of ettringites part I: incorporation of OH^- and CO_3^{2-} in $3CaO \cdot Al_2O_3 \cdot 32H_2O$. *Cement and Concrete Research* 20, 6 (1990), 941–947.
- [155] POMMERSHEIM, J., AND CHANG, J. Kinetics of hydration of tricalcium aluminate in the presence of gypsum. *Cement and Concrete Research* 18, 6 (1988), 911–922.
- [156] POWERS, T. C. Mechanism of shrinkage and reversible creep of hardened cement paste. In *Proceedings of the International Conference on the Structure of Concrete*, Cement and Concrete Association (London, U.K., 1965).
- [157] PRATT, P. L., AND GHOSE, A. Electron microscope studies of portland cement microstructures during setting and hardening. *Phil. Trans. R. Soc. A310* (1983), 93–103.
- [158] RAMACHANDRAN, V. S., AND BEAUDOIN, J. J. Hydration of C_4AF + gypsum: study of various factors. In *Proceedings of 7th International Congress on Chemistry of Cement* (Paris, 1980), vol. II, pp. 25–30.

- [159] RAYMENT, D. L., AND MAJUMDAR, A. J. The composition of the C-S-H phases in portland cement pastes. *Cement and Concrete Research* 12, 6 (1982), 753–764.
- [160] REGOURD, M., THOMASSIN, J. H., BAILLIF, P., AND TOURAY, J. C. Study of the early hydration of Ca_3SiO_5 by X-ray photoelectron spectrometry. *Cement and Concrete Research* 10, 2 (1980), 223–230.
- [161] REIMER, L. *Springer series in Optical Sciences, Transmission Electron Microscopy, Physics of image formation and microanalysis*, vol. 36. Springer Verlag, 1984.
- [162] REIMER, L. *Springer series in Optical Sciences, Scanning Electron Microscopy, Physics of image formation and microanalysis*, vol. 45. Springer Verlag, 1998.
- [163] RICHARDS, C. W., AND HELMUTH, R. A. Expansive cement concrete micromechanical models for free and restrained expansion. Tech. Rep. Technical Report TR 191, Department of Civil Engineering, Stanford University, Stanford, California., 1977.
- [164] RICHARDSON, I. G. The nature of C-S-H in hardened cements. *Cement and Concrete Research* 29, 8 (1999), 1131–1147.
- [165] RICHARDSON, I. G. The nature of the hydration products in hardened cement pastes. *Cement and Concrete Composites* 22, 2 (2000), 97–113.
- [166] RICHARDSON, I. G. Tobermorite/jennite- and tobermorite/calcium hydroxide-based models for the structure of C-S-H: applicability to hardened pastes of tricalcium silicate, β -dicalcium silicate, portland cement, and blends of portland cement with blast-furnace slag, metakaolin, or silica fume. *Cement and Concrete Research* 34, 9 (2004), 1733–1777.
- [167] RICHARDSON, I. G., AND GROVES, G. W. Models for the composition and structure of calcium silicate hydrate (C-S-H) gel in hardened tricalcium silicate pastes. *Cement and Concrete Research* 22, 6 (1992), 1001–1010.
- [168] RICHARDSON, I. G., AND GROVES, G. W. The incorporation of minor and trace elements into calcium silicate hydrate (C-S-H) gel in hardened cement pastes. *Cement and Concrete Research* 23, 1 (1993), 131–138.

- [169] RICHARDSON, I. G., AND GROVES, G. W. Microstructure and microanalysis of hardened ordinary portland cement pastes. *Journal of Materials Science* 28, 1 (1993), 265–277.
- [170] RIETVELD, H. M. A profile refinement method for nuclear and magnetic structures. *Journal of applied crystallography* 2 (1969), 65–71.
- [171] RODGER, S. A., AND GROVES, G. W. Electron microscopy study of ordinary portland cement and ordinary portland cement-pulverized fuel ash blended pastes. *Journal of the American Ceramic Society* 72, 6 (1989), 1037–1039.
- [172] RODGER, S. A., GROVES, G. W., CLAYDEN, N. J., AND DOBSON, C. M. Hydration of tricalcium silicate followed by ^{29}Si NMR with cross-polarization. *Journal of the American Ceramic Society* 71, 2 (1988), 91–96.
- [173] ROGERS, D. E., AND ALDRIDGE, L. P. Hydrates of calcium ferrites and calcium aluminoferrites. *Cement and Concrete Research* 7, 4 (1977), 399–409.
- [174] SCHERER, G. W. Crystallization in pores. *Cement and Concrete Research* 29, 8 (1999), 1347–1358.
- [175] SCHERER, G. W. Stress from crystallization of salt. *Cement and Concrete Research* 34, 9 (2004), 1613–1624.
- [176] SCHWIETE, H., AND IWAI, T. The behaviour of the ferritic phase in cement during hydration. *Zement-kalk-Gips* 17, 9 (1964), 379–386.
- [177] SCHWIETE, H., LUDWIG, U., AND JAGER, P. Investigations in the system $3\text{CaO} \cdot \text{Al}_2\text{O}_3 - \text{CaSO}_4 - \text{CaO} \cdot \text{H}_2\text{O}$. In *Symposium on Structure of Portland Cement paste and concrete*. Highway research board, Washington, 1966, pp. 353–367.
- [178] SCHWIETE, H. E., AND NIEL, E. M. G. Formation of ettringite immediately after gaging of a portland cement. *Journal of the American Ceramic Society* 48, 1 (1965), 12–14.
- [179] SCRIVENER, K. *Advanced Concrete Technology*. Elsevier Ltd., 2003, ch. Calcium Aluminate Cements, pp. 2/1–2/31.

- [180] SCRIVENER, K. L. *The development of microstructure during the hydration of Portland cement*. PhD thesis, University of London, 1984.
- [181] SCRIVENER, K. L. A study of the microstructure of two old cement pastes. In *Proceedings of 8th International Congress on Chemistry of Cement* (Rio de Janeiro, 1986), vol. III, pp. 389–393.
- [182] SCRIVENER, K. L., AND CAPMAS, A. *Lea's Chemistry of Cement and Concrete*. Arnold, 1998, ch. Calcium Aluminate Cements, pp. 709–778.
- [183] SCRIVENER, K. L., FULLMANN, T., GALLUCCI, E., WALENTA, G., AND BERMEJO, E. Quantitative study of portland cement hydration by X-ray diffraction/rietveld analysis and independent methods. *Cement and Concrete Research* 34, 9 (2004), 1541–1547.
- [184] SCRIVENER, K. L., AND PRATT, P. L. Microstructural studies of the hydration of C_3A and C_4AF independently and in cement paste. In *British Ceramic Society* (1984), vol. 35, pp. 207–209.
- [185] SCRIVENER, K. L., AND WIEKER, W. Advances in hydration at low, ambient and elevated temperatures. In *Proceedings of 9th International Congress on Chemistry of Cement* (New Delhi, India, 1992), vol. I, pp. 449–482.
- [186] SKALNY, J., JOHANSON, V., THAULOW, N., AND PALOMO, A. DEF: as a form of sulfate attack. *Matériaux et Constructions* 46, 244 (1996), 5–29.
- [187] SKALNY, J., AND TADROS, M. E. Retardation of tricalcium aluminate hydration by sulfates. *Journal of the American Ceramic Society* 60, 3-4 (1977), 174–175.
- [188] STADE, H., AND WIEKER, W. Zum aufbau schlecht geordneter calciumhydrogensilicate. *i. bildung und eigenschaften einer schlecht geordneten calciumhydrogendisilicatphase*. *Zeitschrift für Anorganische und Allgemeine Chemie* 466 (1980), 55–70.
- [189] STADELMANN, C., TRETTIN, R., WIEKER, W., AND RAMM, M. Studies of the hydration of Ca_3SiO_5 by ESCA- and krypton-adsorption-measurements. *Cement and Concrete Research* 15, 1 (1985), 145–150.

- [190] STEIN, H. N. Some characteristics of the hydration of $3\text{CaO} \cdot \text{Al}_2\text{O}_3$ in the presence of $\text{CaSO}_4 \cdot 2\text{H}_2\text{O}$. *Silicates Industriels* 28 (1963), 141.
- [191] STEIN, H. N., AND STEVELS, J. M. Influence of silica on the hydration of $3\text{CaO} \cdot \text{SiO}_2$. *Journal of Applied Chemistry* 14 (1964), 338–346.
- [192] STEVIE, F. A., GIANNUZZI, L. A., AND PRENITZER, B. I. *Introduction to Focused Ion Beams: instrumentation, theory, techniques, and practice*. 2005.
- [193] STRUBLE, L. J. Synthesis and characterization of ettringite and related phases. In *Proceedings of the 8th International Congress on Chemistry of Cement* (Rio de Janeiro, Brasil, 1986), vol. 6, pp. 582–588.
- [194] SUN, G. K., AND YOUNG, J. F. *Handbook of analytical Techniques in Concrete Science and Technology*. Noyes Publication, Park Ridge New Jersey, USA, 2000, pp. 629–657.
- [195] SUN, G. K., YOUNG, J. F., AND KIRKPATRICK, R. J. The role of al in C-S-H: NMR, XRD, and compositional results for precipitated samples. *Cement and Concrete Research* 36, 1 (2006), 18–29.
- [196] TABER, S. The growth of crystals under external pressure. *Am. J. Sci.* 41 (1916), 532–556.
- [197] TADROS, M. E., JACKSON, W. Y., AND SKALNY, J. Study of the dissolution and electrokinetic behaviour of tricalcium aluminate. In *Proceedings of international conference on collids and surfaces, Puerto Rico* (Academic press, New York, 1976), M. Kerker, Ed., vol. IV, pp. 211–223.
- [198] TADROS, M. E., SKALNY, J., AND KALYONCU, R. S. Early hydration of tricalcium silicate. *Journal of the American Ceramic Society* 59, 7-8 (1976), 344–347.
- [199] TAMAS, F. D., SARKAR, A. K., AND ROY, D. M. Hydraulic cement: their structure and properties. *Cement and Concrete association* (1976), 55.
- [200] TAMAS, F. D., AND VERTES, A. A Mossbauer study on the hydration of brownmillerite ($4\text{CaO} \cdot \text{Al}_{12}\text{O}_3 \cdot \text{Fe}_2\text{O}_3$). *Cement and Concrete Research* 3, 5 (1973), 575–581.

- [201] TANG, F. J., AND GARTNER, E. M. Influence of sulphate source of portland cement hydration. *Advances in Cement Research* 1, 2 (1988), 67.
- [202] TAYLOR, H. F. Proposed structure for calcium silicate hydrate gel. *Journal of the American Ceramic Society* 69, 6 (1986), 464–467.
- [203] TAYLOR, H. F. W. Chemistry of cement hydration. In *Proceedings of 8th International Congress on Chemistry of Cement* (Rio de Janeiro, Brazil, 1986), vol. I, pp. 82–110.
- [204] TAYLOR, H. F. W. *Advances in Cement Manufacture and Use*. Engrg. Found., New York, 1989, p. 295.
- [205] TAYLOR, H. F. W. *Cement Chemistry*, second ed. Thomas Telford, London, 2004.
- [206] TAYLOR, H. F. W., BARRET, P., BROWN, P. W., DOUBLE, D. D., FROHNSDORFF, G., JOHANSEN, V., MÉNÉTRIER-SORRENTINO, D., ODLER, I., PARROTT, L. J., POMMERSHEIM, J. M., REGOURD, M., AND YOUNG, J. F. The hydration of tricalcium silicate. *Materials and Structures* V17, 6 (1984), 457–468.
- [207] TAYLOR, H. F. W., FAMY, C., AND SCRIVENER, K. L. Delayed ettringite formation. *Cement and Concrete Research* 31, 5 (2001), 683–693.
- [208] TAYLOR, H. F. W., MOHAN, K., AND MOIR, G. K. Analytical study of pure and extended portland cement pastes: I, pure portland cement pastes. *Journal of the American Ceramic Society* 68, 12 (1985), 680–685.
- [209] TAYLOR, H. F. W., MOHAN, K., AND MOIR, G. K. Analytical study of pure and extended portland cement pastes: II, fly ash- and slag-cement pastes. *Journal of the American Ceramic Society* 68, 12 (1985), 685–690.
- [210] THOMASSIN, J. H., REGOURD, M., BAILLIF, P., AND TOURAY, J. C. Etude de l'hydratation initiale de C_3S par spectrométrie de photoélectrons. *C.R. Hebd. Seances Acad. Sci., Ser. C* 288, 3 (1979), 93–95.
- [211] WILLIAMS, D. B., AND CARTER, C. B. *Transmission Electron Microscopy, Basics* I. Plenum Press, New York, 1996.

-
- [212] WILLIAMS, D. B., AND CARTER, C. B. *Transmission Electron Microscopy, Diffraction II*. Plenum Press, New York, 1996.
- [213] WILLIAMS, D. B., AND CARTER, C. B. *Transmission Electron Microscopy, Spectrometry IV*. Plenum Press, New York, 1996.
- [214] WILLIAMSON, R. B. Solidification of portland cement. *Progress in Materials Science* 15, 3 (1972), 189–286.
- [215] WU, Z.-Q., AND YOUNG, J. F. Formation of calcium hydroxide from aqueous suspensions of tricalcium silicate. *Journal of the American Ceramic Society* 67, 1 (1984), 48–51.
- [216] YOUNG, J. F. Investigations of calcium silicate hydrate structure using silicon-29 nuclear magnetic resonance spectroscopy. *Journal of the American Ceramic Society* 71, 3 (1988), C-118–C-120.
- [217] YOUNG, J. F., TONG, H. S., AND BERGER, R. L. Compositions of solutions in contact with hydrating tricalcium silicate pastes. *Journal of the American Ceramic Society* 60, 5-6 (1977), 193–198.
- [218] ZHANG, X., YANG, Y., AND ONG, C. K. Study of early hydration of OPC – HAC blends by microwave and calorimetry technique. *Cement and Concrete Research* 27, 9 (1997), 1419–1428.
- [219] ZHANG, Z. *Delayed ettringite formation in heat-cured cementitious systems*. PhD thesis, Purdue University, USA, 1999.

Index

A

Aluminates 36, 99, 122
 AFm 49
 crystal structure 49
 in CAC, C \bar{S} blend 178
 solid-state substitution .. 50, 108,
 128
 AFt 47
 crystal structure 48
 solid-state substitution .. 48, 108,
 128
 basic reactions 37
 distribution
 M2 123
 OPC 100, 101
 hydration 55
 second burst of hydration ... 77, 78

C

C-S-H 37
 at 2 hours of hydration 91
 atomic structure 39
 Ca:Si 46, 81, 122
 chemical composition 45
 classifications 38, 39
 morphology
 in OPC, CAC blend 176
 outside the shell 86
 shell 85

 within the shell 83
 polymerization 41
 presence of aluminium .43, 100, 101
 sorption of sulfate 45
Calorimetry 7
 expansive cements 141, 143
Cement grains
 preferential reactivity 70
 ridges on the surface 76, 94
Chemical analysis
 basic concept 15
 challenges in TEM 78
 effect of specimen thickness 181
 spatial resolution 17
 formula 17
Conclusions 167

E

Electron-matter interaction 12
 electron scattering 12, 14
 interaction cross-section 14
 formula 15
 various signals 13
Expansion in cements
 DEF 157
 literature review 158
 results obtained 160, 163
 in blends of OPC, CAC and C \bar{S} 128
 discussion 155

- OPC + CAC + $C\bar{S}$
 curing over water 141
 curing under water 145
 the crystal growth theory 129
 the swelling theory 135
- F**
-
- Ferrites 37, 105, 124
 basic reactions 37
 Fe:Ca ratios 109, 125
 hydration 56
 solid-state substitution 108, 128
- I**
-
- Imaging
 contrast and brightness 10
 resolution 11
 formula 11
- Introduction 1
- M**
-
- Materials used 6
 CAC cements 7
 OPC 6
- Mix binder systems 111
 hydration of CAC and $C\bar{S}$
 CAC+ $C\bar{S}$ 173
 literature review 113
 hydration of CAC cements
 literature review 111
 hydration of OPC and CAC
 literature review 112
 OPC+CAC 173
 hydration of OPC, CAC and $C\bar{S}$
 Ca:Si 122
 literature review 114
 role of aluminates 123
 shell formation 117
- N**
-
- Nano-scale
 hydrates 110
 particulate morphology of C-S-H 82,
 83
- S**
-
- SEM 18
 Backscattered electrons 19
 general formula 20
 chemical analysis 20
 ettringite in expansive mixes ... 152
 ray-diagram 19
 Secondary electrons 19
- Shell formation
 from 6–48 hours 69
 around different grains 71
 around polyphase grain 73, 74
 belites within 78
 blends of OPC, CAC and $C\bar{S}$.. 117
 Ca:Si 81, 122
 hydration product within 75, 76
 inception 72
 literature review 59
 morphology 84, 85, 117
- Silicates
 C-S-H
 polymerization 41, 101
 presence of aluminium ... 43, 100,
 101
 basic reactions 36
 belites at 24 hours 78
 growth of ettringite 94

- theories of hydration 50
- Sulfates 99, 123
- distribution
- M2 (16 hours) 124
- OPC (2 hours) 103
- OPC (6–48 hours) 102
- gypsum till 6 hours (OPC) 95
- role in OPC (literature review) .. 57

T

- TEM 20
- bright and dark field . 21, 24, 27, 28
- chemical analysis 29
- contrast 21
- diffraction 23
- mass-thickness con..... 21
- Z-contrast 23
- OPC hydration (review) 63
- ray diagram 22
- specimen preparation
- Focussed Ion Beam 31, 33, 89
- mechanical polishing 30
- STEM 24
- dark and bright field 27, 28
- operation 25

X

- X-ray diffraction 8
- Bragg's equation 8
- of the expansive mixes 149, 150

Prakash Chandra Mathur

prakash.mathur@gmail.com
Avenue d'Ouchy 60,
1006 Lausanne, Switzerland
+41 (0) 21 693 73 67

Work experience

2002–2006 : Assistant at the Laboratory of Construction Materials (EPFL)

2001 : Diploma project in Civil engineering and Microtechnique (EPFL)

1999 : Summer internship at a hot-mix plant in India

Education

2002–2007 : Ph.D in Material Science from EPFL, Switzerland

1997–2001 : B.Tech in Civil engineering from IIT Delhi, India

Skills

Softwares : \LaTeX , Corel, Mathematica, Adobe Photoshop

Languages : English, French (basic) and Hindi

Personal details

Marital status : Single

Date of birth : October 11, 1978